Étude de processus métaboliques non enzymatiques vers une compréhension de l'origine de la vie

Elodie Chevallot-Béroux

UNIVERSITÉ DE STRASBOURG

ÉCOLE DOCTORALE DES SCIENCES CHIMIQUES

Laboratoire de Catalyse Chimique
Institut de Science et d'Ingénierie Supramoléculaires (ISIS)

THÈSE présentée par :

Elodie CHEVALLOT-BEROUX

Soutenue le : 28 Novembre **2019**

Pour obtenir le grade de : **Docteur de l'université de Strasbourg**

Discipline/ Spécialité : Chimie/Chimie Catalytique

Non-enzymatic metabolic processes to understand the origin of life

THÈSE dirigée par :
Pr. Joseph MORAN Directeur de thèse, université de Strasbourg

RAPPORTEURS :
Pr. Robert PASCAL Rapporteur, Université de Montpellier
Pr. Pierre STRAZEWSKI Rapporteur, Université Claude Bernard Lyon 1

AUTRES MEMBRES DU JURY :
Pr. Petra HELLWIG Examinateur, Université de Strasbourg

Dédicace

Comme symbole de ces années qui nous sépare de ton départ,

À ce scientifique qui m'aura inspiré,

À mon Papi.

Remerciements

Mes plus grands remerciements vont à Joseph MORAN, mon directeur de thèse, qui m'a accueilli dans son laboratoire il y a maintenant presque 3 ans et demi et m'a donné la chance de pouvoir travailler sur l'imposant sujet de recherche « l'origine de la vie ». La communication n'a pas toujours été facile à mes débuts, mais Joseph a toujours su répondre présent à mes demandes, afin de m'aiguiller dans mes recherches et de toujours trouver les mots pour me redonner confiance dans mon travail. Cette thèse m'a apportée des connaissances scientifiques, mais j'ai aussi beaucoup appris sur moi-même et développé des connaissances annexes qui me seront utiles pour ma vie future ; c'est pour tout cela que je remercie Joseph.

Mon sujet de recherche a souvent été liés à d'autres, de par sa vastitude, et je souhaiterais chaleureusement remercier tous mes collègues de laboratoire : Kamila, je ne te remercierais jamais assez pour tous tes travaux de relecture que tu as fait pour moi lors de mes trois ans de thèse, ainsi que toute l'aide scientifique que tu m'as apporté depuis mes débuts ; Sreejith, je sais que nos débuts auront été difficiles, mais tu as accepté de m'accorder ton amitié, et je te remercie pour ça ; Jan, qui est arrivé au laboratoire comme mon sauveur, je te remercie de nouveau pour toutes les méthodes de travail et ta gentillesse que tu as partagé avec moi lors de cette dernière année, j'ai tant appris ; Paul, pour nos discussions sur de très nombreux sujets, et tes références Wikipédia toujours bienvenues.

Je remercie aussi tous mes autres collègues de laboratoire, Vuk, pour tous ces bons moments passés ensemble, et le plus Français de tous ; Ed, pour nos discussions matinales ; Anton, pour ton passage éclair mais intense, Jing, Shaofei, Florent, Abijith et Capucine, pour avoir participer à l'ambiance du laboratoire ; et pour finir Nathalie, pour ta gentillesse et le soutien que tu nous apportes au laboratoire.

Le meilleur pour la fin, comme on dit hein, Lucas. Nous avons fait nos débuts ensemble, et ce fut le début d'une longue amitié. Tu as été là pour tous mes moments difficiles, à supporter mes crises existentielles, tu as su être à l'écoute (presque tout le temps) de mes histoires, et nous avons partagé bien plus que nos thèses. Je te souhaite tout le meilleur pour la suite de ta vie, ton intérêt pour tout un tas de choses est une qualité hors norme, même si parfois déstabilisante, et je suis énormément reconnaissante que l'on t'est placé sur mon

chemin. Merci pour tout Lulu, tu as été ma force, mon divertissement, mon conseillé, et le meilleur partenaire de paillasse durant ces trois ans ! De nouveau, Merci !

J'aimerais aussi remercier ma famille proche, car on sait tous qu'une thèse est aussi difficile pour nous que pour notre entourage. Moumoune et Papou, de m'avoir toujours soutenu, encouragé et écouté, malgré les difficultés à comprendre mon charabia. Rassurez-vous, mon statut étudiant est presque fini ! Nanon, pour nos conversations presque quotidiennes toujours fortes intéressantes, et pour tous nos week-ends partagés. Notre relation a tellement évolué durant ces dernières années, tu es aujourd'hui une motivation, une confidente et une source de joie pour moi, merci d'être là Sœurette ! Je remercie bien évidemment ma grande famille, mes grands-mères, mon grand-père, mes oncles et tantes, mes cousins et cousines, vous faites tous parti de moi, vous m'avez permis d'être la personne que je suis aujourd'hui.

De plus, j'aimerais remercier tous mes amis, qui sont pour moi une deuxième famille. Vous avez fait de ces trois ans un pur bonheur, et je ne vous remercierais jamais assez pour tout ce que vous m'apportez dans ma vie : rire, larmes de joie, ragots en tout genre, week-ends, apéros, shopping, sport… Alors merci à Ninou, Gab, Xav et Joris, Fafou, Elo, Dada, Blandine, Alice et Vlad, Zelie, Thomas, Alex et Franck… Que nos moments passés ensemble soient encore nombreux et toujours aussi festifs !

Ami ou famille, tu fais partie des deux, et mes remerciements ne seront surement pas à la hauteur de tout ce que tu m'as apportés durant ces trois (huit) ans ! Alors merci Boris d'avoir toujours été là pour moi, tu es mon meilleur ami, mon plus grand amour et bien plus encore. Tu me donnes la force d'avancer et tu me ralentis dans mes excès, tu fais partie de mon équilibre. Notre vie ensemble ne fait que commencer !

Finalement, j'aimerais aussi remercier Pr. Robert PASCAL, Pr. Pierre STRAZEWSKI ainsi que Pr. Petra HELLWIG d'avoir accepté d'évaluer mon manuscrit et de faire partie de mon jury de soutenance.

Table of contents

REMERCIEMENTS 7

TABLE OF CONTENTS 11

LIST OF ABBREVIATIONS 17

RESUME 19

PART I – GENERAL INTRODUCTION 35

1. LITERATURE REVIEW 37

1.1. ABIOGENESIS 37
1.1.1. HISTORICAL ATTEMPTS TO EXPLAIN THE ORIGIN OF LIFE 38
1.1.1.1. Spontaneous generation 38
1.1.1.2. Primordial soup hypothesis and proteinoid microsphere 38
1.1.1.3. The RNA world 39
1.1.1.4. LUCA 40
1.1.2. HYPOTHETICAL CRADLE OF LIFE 41
1.1.3. CONTROVERSIES 43
1.2. METABOLIC ORIGINS OF LIFE 46
1.2.1. AN ENERGETIC PERSPECTIVE 46
1.2.2. A METABOLIC PERSPECTIVE 47
1.2.3. A PHYLOGENETIC PERSPECTIVE 49
1.2.4. PRIMITIVE METABOLIC PROCESSES 53

2. THE WOOD-LJUNGDAHL PATHWAY 54

2.1. OVERVIEW 54
2.2. ENZYMES AND MECHANISM 55

3. TRICARBOXYLIC ACID CYCLES 57

3.1. INTRODUCTION 57
3.2. THE RTCA CYCLE BIOCHEMISTRY 58
3.2.1. REDUCTIVE CARBOXYLATIONS 59
3.2.2. ATP-DEPENDENT CARBOXYLATIONS 59
3.2.3. REDUCTIONS 61
3.2.4. DEHYDRATIONS-HYDRATIONS 62
3.2.5. RETRO-ALDOL CLEAVAGE 63
3.3. THE TCA CYCLE BIOCHEMISTRY 64
3.3.1. DECARBOXYLATION 64
3.3.2. ALDOL ADDITION 65
3.3.3. OXIDATIONS 65
3.3.4. DECARBOXYLATIVE OXIDATION 66

3.4. THE GLYOXYLATE CYCLE 67

4. THIOESTERS 69

4.1. A THIOESTER WORLD 70
4.2. MAIN ROUTES FOR BIOLOGICAL THIOESTER FORMATION 72
4.2.1. RTCA CYCLE 72
4.2.2. TCA CYCLE 73
4.2.3. GLYCOLYSIS 74

5. GENERAL PERSPECTIVE OF THIS THESIS 75

PART II – THE REVERSE TRICARBOXYLIC ACID CYCLE THE RTCA CYCLE 77

1. INTRODUCTION 79

2. PREVIOUS STUDIES ON THE RTCA 80

3. OUR STUDY – ATP INDEPENDENT REACTIONS 82

3.1. REDUCTION REACTIONS 83
3.2. DEHYDRATIONS REACTIONS 85
3.3. EFFECT OF COMPARTMENTALIZATION 88
3.4. HYDRATION REACTION 88
3.5. COMBINED REACTIONS 90
3.6. LIMITATIONS 91

4. CONCLUSION & PERSPECTIVES 94

PART II – THE WOOD-LJUNGDAHL PATHWAY 95

1. INTRODUCTION 97

2. PREVIOUS STUDIES ON THE W-L PATHWAY 98

3. FE^0 AS A CATALYST FOR CO_2 FIXATION 100

3.1. EFFECT OF PHYSICAL PARAMETERS 100
3.2. MECHANISTIC CONSIDERATIONS 102

4. PHYSICAL STUDIES ON IRON POWDER FOR CO_2 FIXATION 104

5. ELECTROCHEMISTRY ON IRON WIRE 107

5.1. PREVIOUS ELECTROCHEMICAL STUDIES ON CO_2 REDUCTION TO ACETATE AND PYRUVATE 107
5.2. FE^0 WIRE AS THE CATALYST 108

5.3. Fe oxide as the catalyst 114

6. IRON OXIDES AS THE TRUE CATALYSTS FOR CO_2 FIXATION 115

6.1. Recent updates 115
6.2. Effect of different iron oxides 116

7. CONCLUSION & PERSPECTIVES 122

PART IV - THIOESTERS 123

1. INTRODUCTION 125

2. FORMATION OF THIOESTERS FROM KETO-ACIDS 128

2.1. Thioester formation under thermal conditions 131
2.2. Thioester formation under photochemical conditions 136
2.3. Different keto-acids and thiols 141
2.4. Multiple ketoacids in one pot 144

3. THIOESTER FORMATION FROM A COMPLEX KETOACID-GENERATING REACTION NETWORK 145

3.1. Introduction of the network 145
3.2. Formation of thioesters from the network 147

4. CONCLUSION & PERSPECTIVES 152

PART V – EXPERIMENTAL PART 153

1. THE REVERSE TRICARBOXYLIC ACID CYCLE 155

1.1. General information 155
1.2. Materials 155
1.3. Analytical method for GC-MS analysis 156
1.4. Formation of rTCA intermediates 164
1.4.1. General procedure: Fe^0 / Zn^{2+}/ Cr^{3+}reactions 164
1.4.2. Metal screens 164
1.4.3. Reactions in micellar solutions 165
1.4.4. Portion-wise reagent addition 165
1.4.5. Reaction with oxalosuccinic acid 166
1.5. Experimental data 167
1.5.1. GC-MS chromatograms of authentic samples 167
1.5.2. Metal-promoted malate dehydration screen. 181
1.5.3. Metal-promoted isocitrate dehydration screen. 182
1.5.4. Metal-promoted aconitate hydration screen. 183
1.5.5. Reduction selectivity screen. 184
1.5.6. Non-enzymatic reaction of the rTCA cycle. 185

2. THE W-L PATHWAY 200

2.1. GENERAL INFORMATION 200
2.2. MATERIALS 201
2.2.1. CHEMISTRY 201
2.2.2. ELECTROCHEMISTRY 202
2.3. ANALYTICAL METHODS 203
2.3.1. PRODUCT IDENTIFICATION 203
2.3.2. NMR SAMPLE PREPARATION 204
2.4. SYNTHETIC PROCEDURES 205
2.4.1. FOR METAL-PROMOTED CO_2 FIXATION REACTIONS 205
2.4.2. ELECTROCHEMISTRY 205
2.5. EXPERIMENTAL DATA 207
2.5.1. IRON OXIDES SCREENS IN CO_2 FIXATION REACTIONS 207
2.5.2. ELECTROCHEMISTRY DATA 208
2.5.3. DATA OBTAINED FROM A COLLABORATION WITH HARUN TUEYSUEZ 209

3. THIOESTERS 211

3.1. GENERAL INFORMATION 211
3.2. MATERIALS 212
3.3. ANALYTICAL METHOD 213
3.3.1. GC-FID ANALYSIS 213
3.3.2. LCMS ANALYSIS 215
3.3.3. GC-MS ANALYSIS 219
3.4. FORMATION OF THIOESTERS UNDER PREBIOTIC CONDITIONS 220
3.4.1. GENERAL PROCEDURES FOR THIOESTER FORMATION 220
3.4.2. THIOESTER FORMATION FROM A NON-ENZYMATIC REACTION NETWORK 221
3.5. EXPERIMENTAL DATA 222
3.5.1. GC-FID CHROMATOGRAMS OF AUTHENTIC SAMPLES 222
3.5.2. LC-MS OF AUTHENTIC SAMPLES 225
3.5.3. THIOESTERS FORMATION UNDER VARIOUS CONDITIONS 231
3.5.3.1. GC-Fid chromatograms of thioester under various conditions 232
3.5.3.2. LC-MS chromatograms of thioester under various conditions 242
3.5.3.1. NMR spectra of thioester under various conditions 248
3.5.4. THIOESTER FORMATION FROM A NON-ENZYMATIC REACTION NETWORK 252
3.5.4.1. GC-Fid chromatograms of thioester from network 253
3.5.4.2. LC-MS chromatograms of thioester from network 255
3.5.4.3. GC-MS chromatograms of thioester from network 258

GENERAL CONCLUSION 266

REFERENCES 270

APPENDIX – OXIDATION PROJECT 280

List of Abbreviations

ACS	acetyl CoA synthase
ADP	adenosine diphosphate
AMP	adenosine monophosphate
ATP	adenosine triphosphate
BC	before Christ
cm	centimeter
CO	carbon monoxide
CO_2	carbon dioxide
CoA	Coenzyme A
CODH	carbon monoxide dehydrogenase
CoFeSP	corrinoid iron sulfur protein
Compd	compound
conc	concentrated
CTAB	cetrimonium bromide
Da	Dalton
dd	doublet of doublet
DMF	dimethylformamide
DSS-Na	sodium 3-(trimethylsilyl)-1-propanesulfonate
DTBP	di-*tert*-butyl peroxide
E^0	standard electrode potential
ECF	ethylchloroformate
equiv.	equivalent
EtOAc	ethyl acetate
EtOH	ethanol
$FAD/FADH_2$	Flavin adenine dinucleotide
Fig.	figure
FT-IR	Fourier-transform infrared spectroscopy
g	grams
G3P	glycerol 3-phosphate
GAPDH	glyceraldehyde 3-phosphate dehydrogenase
GC-MS	gas chromatography mass spectrometry
GTP/GDP	guanosine-5′-tri/diphosphate
Hz	hertz
kJ	kilo joule
LUCA	Last Universal Common Ancestor
M	molar
MCF	methylchloro-formate
MDH	malate dehydrogenase
MeOH	methanol
mg	milligram
MHz	mega hertz
min	minute
mL	milliliter
mM	millimolar
mmol	millimole
$NAD^+/NADH$	nicotinamide adenine dinucleotide
$NADP^+/NADPH$	nicotinamide adenine dinucleotide phosphate
nm	nanometer
NMR	nuclear magnetic resonance
OGC	oxalosuccinate synthetase
OGDC	oxoglutarate dehydrogenase complex
PC	pyruvate carboxylase
PDC	pyridinium dichromate
PEP	phosphoenol-pyruvate
PEPC	phosphoenolpyruvate carboxylase
ppm	part per million
q	quartet
RNA	Ribonucleic Acid
rpm	revolution per minute
rTCA	reverse/reductive tricarboxylic acid
s	singlet
SD	standard deviation
SDC	sodium dodecyl sulfate
SDH	succinate dehydrogenase
SEM	scanning electron microscope
SHE	standard hydrogen electrode
SCE	saturated calomel electrode
t	triplet
TCA	tricarboxylic acid
TEAB	tetraethylammonium bromide
THF	tetrahydrofuran
TPGS	DL-α-Tocopherol methoxypolyethylene glycol succinate
TPP	thymine pyrophosphate
UV	ultraviolet
V	volt
w/w	weight by weight
W-L	Wood-Ljungdahl
XRD	X-ray diffraction
µL	microliter
%	percent
˚C	degree Celsius

Résumé

Étude de processus métaboliques non enzymatiques vers une compréhension de l'origine de la vie

1. Introduction

Au travers des sept dernières décennies, chimistes et biologistes ont proposé différentes approches afin de comprendre l'un des plus grand mystère toujours non résolu, l'origine de la vie.[1] Au travers de diverses découvertes, comme la très connue expérience de Miller-Urey, deux hypothèses majeures se sont détachées – une origine génétique ou une origine métabolique de la vie.[2,3] La première hypothèse repose sur l'émergence d'un matériel génétique, capable de catalyser sa propre réplication, qui serait à l'origine de la vie.[2] De nombreux scientifiques soutiennent cette hypothèse, rendue plus forte récemment par la découverte des ribozymes, molécules de l'ARN ayant des propriétés catalytiques, similaire à l'action des protéines ; mais la complexité de l'ARN – ou des ribozymes - suscite des doutes sur son émergence précoce dans les conditions semblables à celle trouvées sur Terre à cette période, appelée conditions prébiotiques.[4] A contrario, une origine métabolique propose la formation de premiers réseaux biochimiques, menant vers une biochimie primitive, dans un ordre respectant la complexité des matériels et des indices trouvés dans les organismes autotrophes.[3] Ainsi, les enzymes, responsables de la majorité des réactions métaboliques dans la biologie actuelle, ainsi que le matériel génétique, seraient apparues plus tard, de par leurs complexités structurales. Dans cette hypothèse, un réseau complexe de réactions chimiques pourrait avoir émerger à partir de simples métabolites utilisés dans des combinaisons de réactions non-enzymatiques cataboliques et/ou anaboliques, dans des conditions prébiotiques.[5]

Les précédentes recherches effectuées par les chimistes sur les origines de la vie étaient concentrées principalement sur la synthèse d'intermédiaires intéressants dans la biologie, sans avoir une vue d'ensemble de la biochimie du vivant.[6] En effet, la vie construit toutes ses molécules à partir du dioxyde de carbone, pourtant très peu de recherches se sont

intéressées à son utilisation comme matériel de départ. On peut citer comme exemple les organismes autotrophes, qui utilisent seulement six voies métaboliques pour construire leurs matériels nécessaires à leurs fonctionnements à partir du CO_2, et ce depuis presque 4 milliards d'années.[7] Parmi elles, on trouve la voie de l'acétyle CoA (aussi appelée voie Wood-Ljungdahl) et le cycle du rTCA (également appelé le cycle de Krebs inverse), tous deux très intéressants car considérés comme primitifs et permettant la synthèse de précurseurs chimiques universels pour toute la biochimie.[8] Les deux premiers chapitres de cette thèse traiteront en détail les expériences menées afin de proposer une possible explication à leurs apparitions dans des conditions prébiotiques.

Plus récemment, à la lumière de nos précédentes recherches, il a été découvert au laboratoire la formation d'un réseau complexe de réactions chimiques permettant la synthèse de dizaines métabolites simplement à partir de deux métabolites - le glyoxylate et le pyruvate – en synthèse monotope.[9] Suite à cette surprenante découverte, nous avons voulu nous intéresser à la synthèse de thioesters, qui ont un rôle important dans la biologie, en tant qu'intermédiaires dans la biosynthèse (permet la synthèse de l'ATP par hydrolyse), et qui permettent une conservation du flux d'énergie biologique (de liaison C-C à C-S à phosphoanhydride).[10] Par conséquence, les thioesters ont sûrement eut un rôle important dans la chimie prébiotique.[11] Une étude a été menée afin de reproduire deux principales voies biochimiques, de manière prébiotique et non-enzymatique, la décarboxylation oxydante d'alpha-céto-acides et l'oxydation d'aldéhydes, permettant la synthèse de thioesters. Cette étude fera l'objet du dernier chapitre de cette thèse, et sera mise en relation avec le réseau complexe de réactions chimiques afin d'élargir le réseau de molécules et sa complexité.

2. Résultats et discussions

a. Le cycle du rTCA

En raison de sa propriété autocatalytique et de sa place centrale en biochimie, le cycle de la rTCA a été suggéré comme étant une voie métabolique qui s'est probablement développée très tôt dans l'émergence de la vie. Dans notre recherche à promouvoir un métabolisme primitif sans enzyme, nous nous sommes tout d'abord intéressés aux étapes du cycle du rTCA ne nécessitant pas l'utilisation de l'ATP : les étapes de réductions, de déshydrations et d'hydratations (Fig 1; étapes C, D, E, H, I et J).

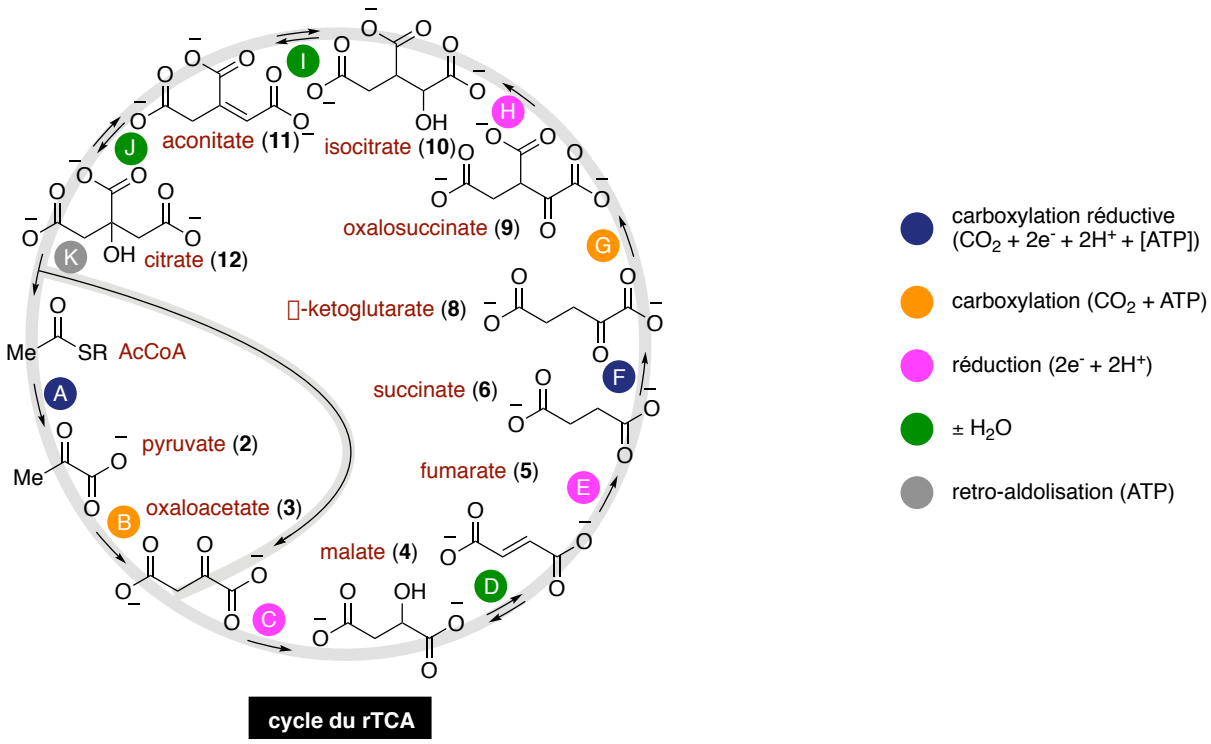

Fig 1. Les réactions du cycle du rTCA

Ces étapes sont catalysées par des enzymes dans la biologie, qui ont pour la plupart un métal dans leur centre actif. Nous avons fait le pari que des catalyseurs beaucoup plus simples, comme des métaux seuls, ou des ions métalliques très simples, pourraient reproduire les actions des différentes enzymes. Des précédents travaux ont essayé de démontrer la plausibilité de cette hypothèse, comme l'équipe de Scot Martin qui a montré la faisabilité par voie photochimique des réactions de réductions non-enzymatique du rTCA [12]; mais aucun d'eux n'ont démontré la possibilité de réactions multi-étapes sous un même set de conditions. Pour ce faire, nous avons réalisé des expériences d'exploration

systématique (screening) couplées à une méthode analytique haut débit (dérivatisation et injection GC-MS) afin de tester le plus de conditions possibles très rapidement (ions métalliques, températures, pH, agents réducteurs…), dans des combinaisons semblables aux conditions possibles sur la Terre à cette période.

Nous avons découvert que le fer métallique (Fe^0) en présence d'ions métalliques est capable de réaliser les six étapes du cycle du rTCA ne nécessitant pas d'ATP (Fig 1 ; étapes C, D, E, H, I et J). En effet, Fe^0 a été choisi pour ces propriétés de réducteur, mais aussi pour sa compatibilité avec les deux autres ions métalliques, Zn^{2+} et Cr^{3+}, permettant respectivement les étapes de déshydrations et d'hydratation. Toutes ces expériences ont été mené en milieu aqueux acide (1M HCl), à des températures variantes entre 40 °C et 140 °C, nécessaire à l'activation du Cr^{3+} (Table 1). Les rendements des réductions (entrées 1, 2 et 3) sont tous très intéressants, sans produit hors cycle observé. Les rendements des déshydratations/hydratations seuls sont très faibles, dû à l'équilibre des produits (entrées 4, 7, 8, 9 et 10). Mais combinée à une réaction irréversible, cela permet d'obtenir le produit final, favorisant l'équilibre vers la production du produit déshydraté (entrée 5). Les rendements ont pu être augmenté en utilisant des micelles, pouvant mimer le phénomène de compartimentalisation dans la roche sous l'océan (entrée 6).

Finalement, les deux séquences de trois réactions successives ont été réalisé, avec ou sans micelle, permettant d'obtenir la formation des différents intermédiaires, avec de très faibles proportions de produits hors cycle (entrées 11, 12 et 13).

Il a été aussi démontré que ces réactions sont majoritaires face aux réactions hors-cycle (entré 14), importante critique pouvant affaiblir la plausibilité de cette hypothèse du cycle rTCA à l'origine d'une chimie prébiotique.

Table 1. Les réactions du cycle du rTCA qui sont favorisées par des métaux/ions

Entrée	Substrat (0.1 mmol)	Conditions[a]				L'espèce détecté après la réaction dans le mélange (%)[‡]										
						Cycle de marche								Hors cycle		
		Fe^0 (equiv.)	Zn^{2+} (equiv.)	Cr^{3+} (equiv.)	Micelles	2	4	5	6	8	10	11	12	15	16	17
Réduction																
1	3	10	-	-	-		90	10								
2[b]	5	10	-	-	-		15	20	65							
3[c]	9	10	-	-	-				2		98					
Hydration/Déshydration																
4[d]	5	-	-	-	-		77	23								
5[d]	4	10	10	-	-		94	4	2							
6[e]	4	10	10	-	oui		82	7	11							
7[d,f]	10	-	1	-	-						51	49				
8[d,f]	11	-	1	-	-						12	88				
9[g]	11	-	-	6	-							67	33			
10[g]	12	-	-	6	-							23	77			
Séquence en trois étapes																
11[e]	3	10	15	4	oui		52	3	41					4		
12[h]	9	5	10	6	-						65	30	2		3	
13[h]	9	5	10	6	oui				5		72	21	2			
Réduction compétitive																
14[c]	2+3+5 8+11	10	15	6	oui	20	6	18	4	20		28		2	2	<1

[‡] Les valeurs rapportées ont été déterminées par GC-MS après une procédure dérivatisation et représenter la moyenne d'au moins deux courses. Les composés 3 et 8 n'ont pas été détecté par cette méthode et sont ainsi omis. [a]Sauf indication contraire: 1 M HCl in H_2O, 16 h, 140 °C. [b]3 h, 140 °C. [c]3 h, 40 °C. [d]48 h, 140 °C. [e]20 °C, 24 h. [f]Réaction dans 1 M H_2SO_4 in H_2O, 16 h, 140 °C. [g]1 h, 20 °C, 24 h, 140 °C. [h]Cycle thermique: 16 h, 140 °C; 10 h, 20 °C; 16 h, 140 °C.

La réalisation de ces deux séquences de trois réactions successives du cycle du rTCA supporte l'hypothèse de son émergence très tôt dans l'échelle de la vie. Cependant, cette étude n'a pas pour objectif d'affirmer que ces ions (Zn^{2+} et Cr^{3+}) sont nécessairement les catalyseurs du cycle du rTCA non-enzymatique, mais apparaissent plus comme une preuve du concept que des métaux simples pourraient être à l'origine d'une chimie prébiotique.[13]

b. Étude de la fixation du CO_2

Nous nous sommes ensuite intéressés à la voie Acétyle CoA (aussi connue comme la voie de Wood-Ljungdahl), une des seules voies chimiques linéaires utilisées par les organismes autotrophes pour fixer le CO_2.[14] Avec l'aide d'enzymes contenant des métaux de transition et des cofacteurs, elle donne lieu à la réduction d'une première molécule de CO_2 en monoxyde de carbone (CO), puis d'une deuxième molécule de CO_2 en groupe méthyle (-CH_3) et finalement, à la combinaison des deux molécules résultantes pour former un groupe acétyle (CH_3CO^-).[15] Les groupes acétyles peuvent réagir encore une fois avec le CO_2 et deux électrons pour former du pyruvate, le précurseur commun à tous les sucres, permettant ainsi la première réaction du cycle du rTCA (Fig 1, étape A).

Au laboratoire, il a été récemment démontré que le fer métallique pouvait agir en tant que réducteur du CO_2 en acétate et pyruvate en solution aqueuse, sous différentes températures et pressions.[16] Le fer métallique permettrait de reproduire l'action des enzymes et cofacteurs que la voie de l'acétyle CoA utilise pour diviser le gaz H_2 en deux protons et deux électrons, qui sont alors utilisés pour réduire le CO_2. Un premier mécanisme a été proposé (Fig 2), avec des réactions se produisant à la surface du métal, permettant la synthèse de différents intermédiaires qui sont observés lors des expériences.

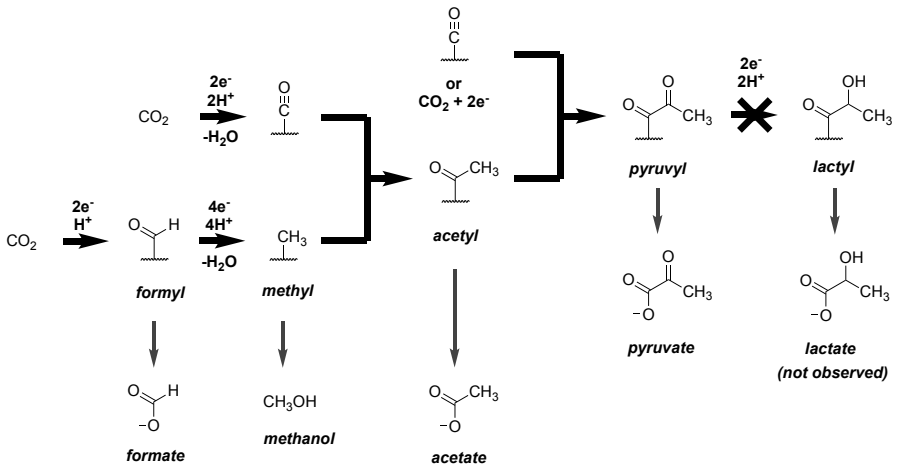

Fig 2. Mécanisme proposé pour la formation des différents intermédiaires à la surface du fer métallique

Pour une meilleure compréhension du mécanisme, et pour permettre la formation d'acétate et pyruvate en plus grande quantité, nous avons mené différentes expériences. Tout d'abord, une collaboration avec un laboratoire d'Allemagne (Dr. Tueysuez, Institut Max-Planck de Müllheim) nous a permis de recueillir des informations sur la morphologie et la structure du fer avant et après réaction dans le réacteur sous pression. Des comparaisons ont été faites entre différents échantillons, par des études SEM (Fig 3), XRD et FT-IR, nous indiquant que le fer réagit avec le CO_2 et se transforme en $FeCO_3$ (réduction de la taille des particules, changement de la structure cristalline et 3 bandes d'absorption caractéristiques des ions carbonates dans le spectre IR). Malheureusement, cela ne nous a pas permis d'acquérir plus d'information sur le mécanisme de réaction, ne permettant pas l'observation de diffèrent intermédiaires à la surface du métal ni même d'oxyde de fer formé lors de la réduction du CO_2.

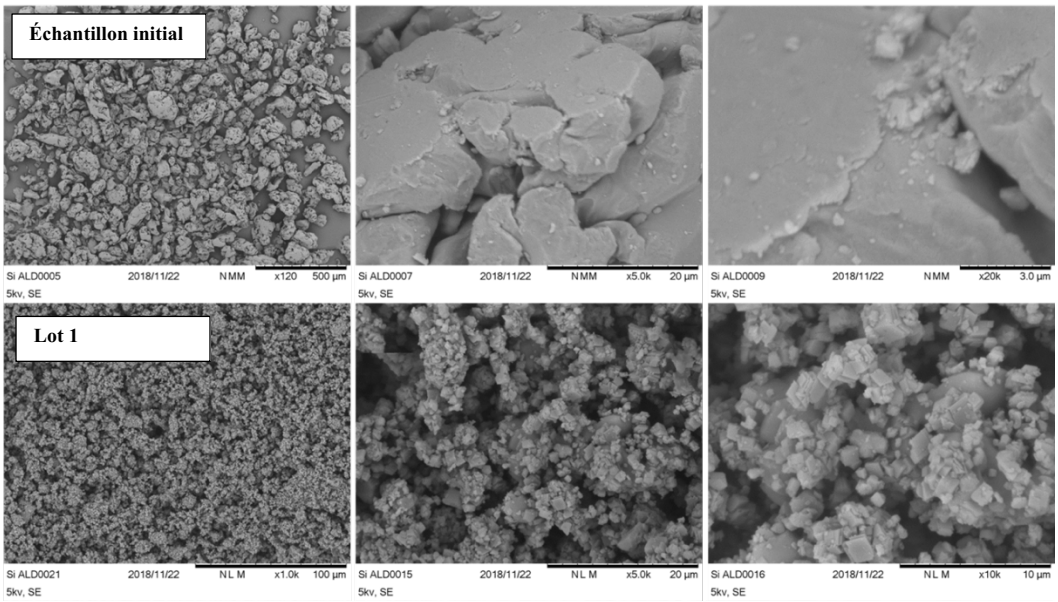

Fig 3. Images SEM d'échantillons de fer métallique avant réaction (Échantillon initial) et après réaction (Lot 1)

Par la suite, nous avons travaillé en collaboration avec deux laboratoires spécialisés en électrochimie (laboratoires du Pr. Ruhlmann et du Pr. Hellwig). Des électrodes de fer pur ont été utilisées comme électrodes de travail, et différents potentiels (-0,44V à -1,5V/ESH afin de rester dans le domaine d'immunité du Fe^0) ont été appliqués en présence de CO_2 (apport constant d'un flux de CO_2 dans le soluté). Lors des premières expériences, des

concentrations élevées et très variées pour chaque intermédiaire ont été retrouvé en solution, sans relation entre les expériences ou les potentiels appliqués. Une hypothèse que les oxydes de fer produits in-situ, plutôt que le fer métallique lui-même, soient les catalyseurs responsables de la réduction du CO_2 a alors été émise, ce qui pourrait expliquer l'irrégularité des résultats. Devant l'incapacité de répéter ces résultats malgré diverses tentatives, nous avons conclu à la non possibilité de reproduire notre expérience sous pression par voie électrochimique à l'aide d'un fil de fer. Si les oxydes de fer sont nécessaires à la réaction, les potentiels nécessaires aux réductions du CO_2 sont trop bas pour pouvoir les conserver à la surface du fil de fer, ceux-ci sont rapidement réduit à la surface de la cathode, expliquant ainsi notre incapacité de reproduire cette réaction en appliquant un potentiel.

A la suite de ces résultats, une nouvelle hypothèse a été formulée sur le mécanisme responsable de la réduction du CO_2 dans nos expériences : en effet, le fer métallique ne serait pas responsable de la réduction du CO_2, mais permettrait la réduction de l'eau, formant de l'hydrogène H_2, et s'oxyderait alors en un oxyde de fer. L'hydrogène permettrait la réduction du CO_2, et l'oxyde de fer formé serait alors utilisé comme catalyseur, permettant la formation d'acétyle et de pyruvyle à sa surface. Cette hypothèse a été confirmée par une étude de différents oxydes de fer, Fe^{2+} et Fe^{3+}, en présence d'un mélange de CO_2 et H_2 : les concentrations en acétyle et pyruvyle se sont révélées plus importante lors de l'utilisation de magnétite (Fe_3O_4). Toutefois, la formation d'acétyle et pyruvyle a aussi été observé lors de pressurisations avec CO_2 seul, nous incitant à repenser le mécanisme. Une possible oxydation supplémentaire de Fe^{2+} en Fe^{3+} est envisagé, permettant de réduire soit l'eau, soit directement CO_2. Le mécanisme de cette réaction reste controversé, des expériences supplémentaires sont nécessaires afin de comprendre ces résultats. Cependant, le fer semble être un bon catalyseur pour la formation d'acétyle et pyruvyle, intermédiaires cruciaux dans la création d'un métabolisme.

c. Thioester formation

Toujours dans l'optique de reproduire des voies biologiques sans enzyme, nous nous sommes intéressés à la formation de thioesters à partir du pyruvate, un céto-acide biologique qui est le précurseur biosynthétique de sucres et de plusieurs acides aminés, par une décarboxylation oxydante.[17] Cette réaction est connue en synthèse organique, mais requiert des solvants organiques ou de complexes oxydants organiques.[18] Différents résultats ont été obtenus à partir du pyruvate, mais aussi différents céto-acides (intermédiaires appartenant au cycle de Krebs et intéressants pour la biochimie) sous différentes conditions (thermal ou photochimique, différents thiols), décrits ci-dessous (Table 2).

Nous avons trouvé que des conditions identiques à de récents travaux favorisant un cycle de réactions cataboliques ressemblant au cycle de Krebs (TCA), permettrait de promouvoir la synthèse de thioesters (peroxodisulfate ($S_2O_8^{2-}$) comme oxydant, FeS comme catalyseur, 70°C) (Méthode A).[19] Le thiol *N*-acetylcysteamine a été utilisé comme modèle, sa structure étant le fragment réactif de la Coenzyme A, le principal réactif en biochimie pour la synthèse de thioesters. Ces conditions ont été testées sur différents céto-acides (entrées 1, 4 et 5), mais aussi sur un aldéhyde (entrée 7) et deux acides alpha hydroxylés (entrées 7 et 8), montrant sa large gamme d'action. Un autre thiol et un disulfure ont aussi été testé, afin de confirmer la réactivité des céto-acides dans ses conditions (entrées 2 et 3). Par la suite, nous avons cherché à adapter ces conditions à des composés sensibles à la chaleur (décarboxylation de l'oxaloacétate à 70°C), utilisant des conditions photochimiques permettant une synthèse plus douce (Méthode B). L'utilisation de lumière UV-A permettant la formation de radicaux sulfates à partir de $K_2S_2O_8$, et nous permet d'accéder à la formation de thioesters sans apport thermique. On observe une meilleure conversion pour le céto-acide sensible ralentissant faiblement la décarboxylation du produit (entrées 5 et 5'). Puis, le sel $KHSO_4$ a été utilisé en substitut du fort oxydant $K_2S_2O_8$, qui permettrait une meilleure intégration dans un système plus complexe, produisant le même radicaux sulfates (Méthode C). Les rendements obtenus sont globalement plus faibles, mais cette méthode est douce et innovante. Finalement, l'ion ferrique ($Fe(ClO_4)_3$) connu pour sa réactivité en photochimie à produire des radicaux OH en milieu aqueux, a été testé, mais n'a montré qu'une faible efficacité (Méthode D).

Table 2. Formation de thioesters à partir de céto-acides biologiques et aldéhydes

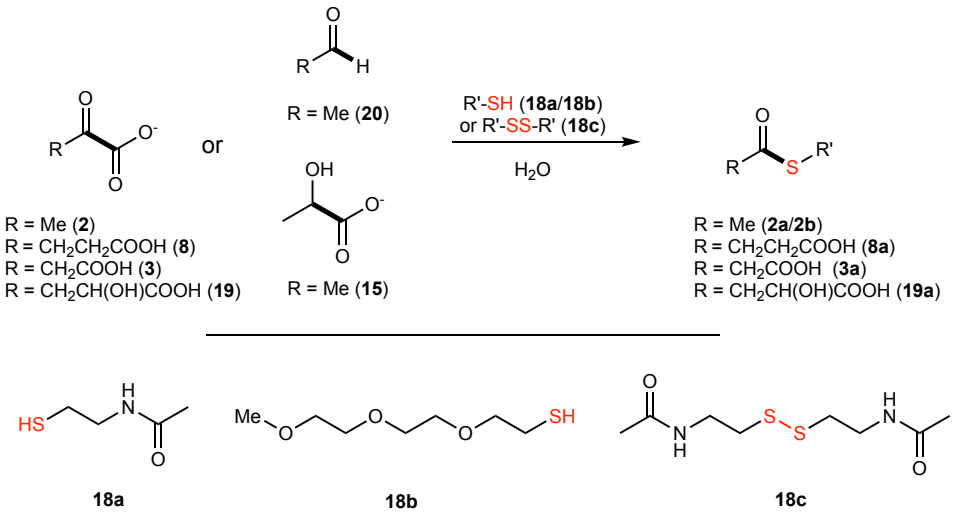

18a **18b** **18c**

Entrée	Substrat *(0.5 mmol)*	Thiol. *(0.1 mmol)*	Produit	Rendement produit (%) ± DS			
				Méthode A[a]	Méthode B[b]	Méthode C[c]	Méthode D[d]
1	Pyruvate **2**	**18a**	**2a**	26.6 ± 0.7	31.2 ± 0.4	22.1 ± 0.4	5.1 ± 0.1
2	Pyruvate **2**	**18b**	**2b**	14.6 ± 0.1	24.1 ± 0.6	17.6 ± 1.0	5.6 ± 0.2
3	Pyruvate **2**	**18c**[e]	**2a**	32.9 ± 0.8	31.9 ± 1.7	4.9 ± 0.2	0.5 ± 0.1
4	α-ketoglutarate **8**	**18a**	**8a**	9.5 ± 1.9	24.5 ± 1.8	13.1 ± 0.9	/
4'			**19a**	11.4 ± 0.5	3.8 ± 0.2	< 0.5	/
5	Oxaloacetate **3**	**18a**	**3a**	6.7 ± 0.4	23.6 ± 1.6	7.9 ± 1.6	/
5'			**2a**	2.6 ± 0.3	2.4 ± 0.3	< 0.5	/
6	Hydroxyketoglutarate **19**	**18a**	**19a**	2.0 ± 0.1	9.9 ± 0.8	3.5 ± 0.2	/
7	Acetaldehyde[f] **20**	**18a**	**2a**	14.7 ± 1.4	12.9 ± 2.1	19.6 ± 1.6	1.7 ± 0.2
8	Lactate **15**	**18a**	**2a**	3.6 ± 0.1	3.5 ± 0.2	0 ± 0.0	0.8 ± 0.1

[a]$K_2S_2O_8$ (2.0 equiv), FeS (0.5 equiv) dans H_2O, 3 h, 70 °C. [b]$K_2S_2O_8$ (2.0 equiv), FeS (0.5 equiv) dans H_2O, 6 h, UV-A. [c]$KHSO_4$ (3 M) dans H_2O, 6 h, UV-A. [d]$Fe(ClO_4)_3$ (2.0 equiv) dans H_2O, 6 h, UV-A. [e]0.05 mmol de disulfure ont été utilisés, le rendement calculé est basé sur 0.1 mmol de thiol [f]1.0 mmol de substrat ont été utilisé.

Puis, nous avons voulu intégrer ces conditions aux récents résultats publiés par notre laboratoire, sur la création d'un de réactions chimiques permettant la synthèse de presque tous les intermédiaires du cycle de Krebs, ainsi que d'autres céto-acides, seulement à partir du pyruvate et du glyoxylate (70 °C, Fe^{2+}, 3 h).[9] A partir des céto-acides formés, combiné avec l'ajout de nos conditions et du thiol, nous pourrions alors produire divers thioesters, à partir seulement de deux métabolites. Nos résultats sont présentés ci-dessous (Table 3).

Dans un premier temps, nous avons reproduit le réseau complexe réactionnel, puis additionné nos réactifs (thiol et additifs) et soumis ce mélange à nos conditions photochimique (entrée 1). A la suite de cette séquence réactionnelle, nous avons retrouvé de nombreux céto-acides observés précédemment, mais nous avons aussi observé la formation en très faible concentration des thioesters voulus (thioacetate **2a**, succinyl thioester **8a** et malyl thioester **19a**). Les thioesters ont aussi été observés lors de l'ajout depuis le départ du thiol, et soumis à nos conditions thermal (entrées 2 et 3). Par la suite, nous avons testé diverses combinaisons, la formation du réseau réactionnel en condition photochimique en une ou deux additions (entrées 4, 5, 6, 7 et 8), ainsi que la combinaison thermal et photochimique avec l'ajout depuis le départ du thiol (entrées 9 et 10), mais seule la formation du thioacétate a été observé, provenant du pyruvate n'ayant pas réagi. Cette absence d'observation des autres thioesters lors de ces réactions peut être expliquée par les très faibles concentrations produites des céto-acides, les concentrations des thioesters formées à partir de celles-ci sont peut-être trop faibles pour être détectées par notre méthode d'analyse.

Table 3. Formation de thioesters à partir d'un réseau réactionnel non-enzymatique

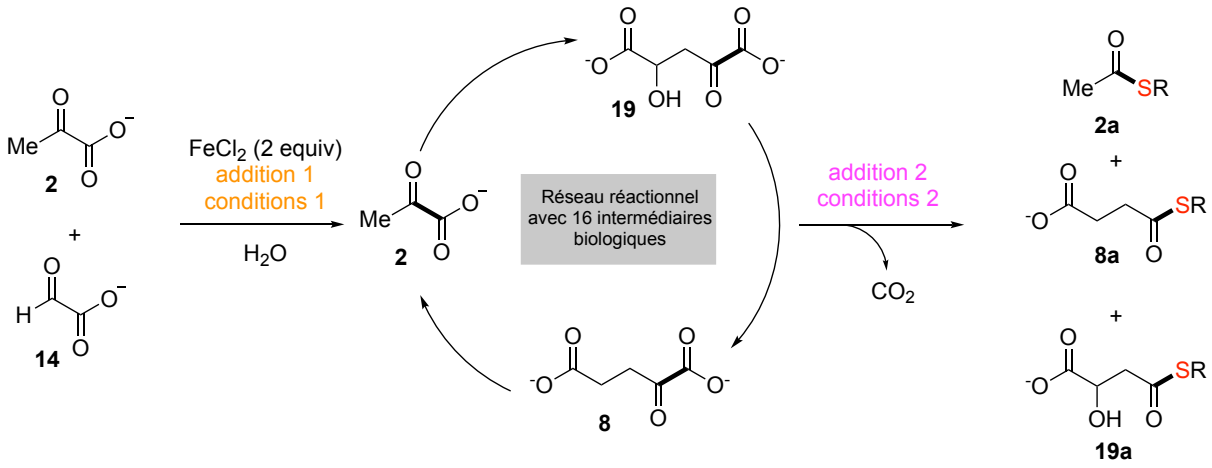

Entry	Pyruvate **2** equiv	addition 1 (equiv)	conditions 1	addition 2 (equiv)	conditions 2	Concentration (mM) Thioacetate **2a**	Succinyl thioester **8a**	Malyl thioester **19a**
1	2		70 °C, 1 h	Thiol **18a** (1) $KHSO_4$ (3 M)	UVA, 3 h	0.11 ± 0.01	0.19 ± 0.04	0.06 ± 0.00
2	2	Thiol **18a** (1)	70 °C, 1 h	$K_2S_2O_8$ (2)	70 °C, 3 h	1.41 ± 0.11	0.11 ± 0.01	3.60 ± 0.30
3	2	Thiol **18a** (1)	70 °C, 3 h	$K_2S_2O_8$ (2)	70 °C, 3 h	1.11 ± 0.14	0.11 ± 0.02	3.63 ± 0.28
4	1	Thiol **18a** (1) $KHSO_4$ (3 M)	UVA, 3 h	-	-	0.06 ± 0.05	-	-
5	1	Thiol **18a** (1) $KHSO_4$ (3 M)	UVA, 6 h	-	-	0.16 ± 0.02	-	-
6	2	Thiol **18a** (1) $KHSO_4$ (3 M)	UVA, 3 h	-	-	0.11 ± 0.05	-	-
7	2	Thiol **18a** (1) $KHSO_4$ (3 M)	UVA, 6 h	-	-	0.31 ± 0.05	-	-
8	2	Thiol **18a** (1)	UVA, 1 h	$KHSO_4$ (3M)	UVA, 3 h	0.22 ± 0.02		
9	2	Thiol **18a** (1)	70 °C, 1 h	$KHSO_4$ (3M)	UVA, 3 h	0.12 ± 0.01	-	-
10	2	Thiol **18a** (1)	70 °C, 1 h	$KHSO_4$ (3M)	UVA, 6 h	0.15 ± 0.01	-	-

[a]Déterminé par analyse GC-FID après extraction avec de l'acétate d'éthyle. [b]Déterminé par analyse LCMS. Pour les expériences du réseau réactionnel 0.5 µL au lieu de 0.1 µL sont injectés, la valeur résultante calculée à l'aide des courbes d'étalonnage a ensuite été divisé par 5.

En conclusion, nous avons mis en place différentes méthodes permettant la synthèse de thioesters à partir de céto-acides, d'acides alpha hydroxylés ou encore d'aldéhydes, et de thiols ou disulfure. L'optimisation des conditions thermal et photochimiques a été effectué, avec l'utilisation de différents additifs permettant l'ajustement à la sensibilité des réactifs utilisés.

Finalement, nous avons réussi à intégrer nos conditions de formation de thioesters à un réseau réactionnel complexe dans des conditions prébiotiques plausibles. Ainsi, à partir de seulement deux simples métabolites et d'un thiol, nous sommes capables de former une multitude de céto-acides, intéressantes pour la biochimie, qui peuvent par la suite réagir pour former des thioesters, molécules réactives et permettant une conservation de l'énergie. Ces résultats sont en attente de publication.

3) Conclusion générale

Ces dernières années, il a été prouvé au laboratoire que le cycle de Krebs inverse, ainsi que la voie de l'Acétyle CoA, peuvent être effectués sans enzyme et uniquement avec des catalyseurs inorganiques en milieu aqueux. Ces résultats nous ont poussé vers une recherche de complexité, nous amenant à la découverte d'un réseau complexe de réactions, ressemblant dans ces suites de réactions au métabolisme, à partir seulement de deux simples métabolites et d'ions métalliques. Ces recherches ont pu être combinées à notre découverte de conditions permettant la synthèse de thioesters, de façon thermale ou photochimique. Grâce à cette association, un mélange d'intermédiaires plus ou moins complexes peut être généré à partir de très simples métabolites, dans des conditions qui semblent plausible sur la Terre il y a 3,5 milliards d'années. L'origine de la vie, et plus particulièrement du métabolisme peut être étudiée sous un nouvel angle grâce à ses résultats. Le but n'est plus de créer des intermédiaires intéressants pour la biochimie dans des conditions prébiotiques, mais de relier ces travaux à un ensemble plus important, et proche de ce que la biologie utilise, à partir du seul CO_2. De nouvelles pistes afin d'élargir encore ce réseau protométabolique et non-enzymatique sont étudiées au laboratoire, l'histoire n'en est qu'à ses débuts.

PART I – General Introduction

1. Literature Review

The origin of life has been one of the most fascinating mysteries from generation to generation. Believers or rationalists, scientists or laypeople, have dedicated time to this curiosity for decades, and yet the origin of life remains one of the most challenging questions of all times.

Diverse hypotheses emerged from these investigations: from a religious point of view, the emergence of life can only be a divine act, which cannot be explained by the laws of science. For some fatalists, it could have been a chance event, explained for example by the *panspermia hypothesis*, which speculates that life was transported to Earth from somewhere else in the Universe. However, this does not definitively explain life's origin and shifts the problem to a different location instead. Finally, the origin of life could also have been a deterministic event, which - following the laws of nature and physical principles - occurred on Earth and eventually gave rise to known living forms.[1] For a scientific study of the origin of life, only the latter part will be described in this manuscript.

1.1. Abiogenesis

Abiogenesis is defined as "the creation of organic molecules by forces other than living organisms" (from Biology Dictionary). It is generally thought to have proceeded gradually, with increasing complexity, rather than have been a one-off event.[20] The study of abiogenesis is a combination of biology, biophysics, geochemistry and biochemistry, in order to determine how primitive chemical reactions gave rise to life. The above definition took a very long time to be formulated, and here we will retrace its history.

1.1.1. Historical attempts to explain the origin of life

1.1.1.1. Spontaneous generation

In 300 BC, Aristotle, believed that certain forms of life could have arisen from non-living matter (bees from flowers, mice from dirty hay). He proposed the formation of some living organisms from decaying organic substances and named this theory the *spontaneous generation*. It was accepted until the 17th century, when new evidence was discovered disproving it: in 1668, Redi showed that no maggots appeared in meat when flies were prevented from laying eggs. The concept of biogenesis appeared as a result of this experiment: *omne vivum ex ovo* (Latin for "every living thing from an egg"). Later, in 1861, Pasteur put an end to the *spontaneous generation* theory with his fermentation experiments, demonstrating that bacteria and fungi did not spontaneously appear in sterile and nutrient rich media, but only from other bacteria and fungi.[21]

A revolutionary theory of evolution through natural selection was first proposed by Wallace in some of Darwin's writings in 1858, which were used later by Darwin to support his own theories.[22] Unfortunately for Wallace, the honors of this scientific theory of evolution go to Darwin - in a letter to Hooker he speculated that life could have originated in a "warm little pond" that contained all sorts of nutrients.[23]

1.1.1.2. Primordial soup hypothesis and proteinoid microsphere

Miller and Urey, in 1952, were the first ones to perform an experiment mimicking the chemical environment thought to have been present on the early Earth.[24] This famous experiment, supporting the "soup" theory proposed in 1924 by Oparin as the hypothetical set of conditions present on the early Earth, demonstrated the production of amino acids from a highly reducing mixture of gases and electrical sparks.[25] This way, the spontaneous generation had its comeback. The Miller-Urey experiment, which is today generally no longer considered a plausible model for the origin of life,[26] was nevertheless the first proof that organic molecules could be spontaneously formed from inorganic precursors.

In 1958, these results inspired Fox, who observed the formation of peptide structures from amino acids in high temperature reactions, which were compatible with prebiotic conditions (conditions on the early Earth before life existed). These peptides could react further, to form polypeptides, named "proteinoid microspheres".[27] Although nowadays all these experiments have only historical value, they were among the first attempts to support the hypothesis of the origin of life being a deterministic event.

1.1.1.3. The RNA world

Building on these experiments, in 1960 Orò reported the synthesis of adenine, a building block of nucleic acids, from an aqueous solution of ammonium cyanide at a temperature below 100 °C.[28] Orgel was the first to argue that RNA-like polymers could have acted as catalysts and enable chemistry between small building blocks, allowing for the development of metabolism.[29] Twenty years later, new properties of RNA were discovered, when Cech and Altman showed the unexpected catalytic activity of RNA in biological reactions, in combination with genetic information storage.[30,31] In light of this evidence, it appeared possible that RNA could have initiated the origin of life. Life in its complexity would not have emerged without basic genetic information: the genetics-first origin of life hypothesis was born. This new hypothesis was so thought-provoking that it gained the support of Nobel laureate Walter Gilbert, who coined the well-known phrase "The RNA world" in 1986. It refers to a hypothetical stage in the origin of life on Earth, where proteins were not yet engaged in biochemical reactions, and used the catalytic activity of RNA instead, in a very primitive self-replicating system.[2] In the following years, many more studies followed. In 1988, Ferris showed RNA polymerization catalyzed by clay. In 1991, Eschenmoser proposed a prebiotic nucleoside synthesis, giving more and more support to the RNA World hypothesis.[32,33]

1.1.1.4. LUCA

In 1859, Darwin was the first one to hypothesize a single progenitor for all life forms.[34] A century later, thanks to advances in genetics and bacterial taxonomy, Woese found that different species have surprisingly few common basic features and processes (genetic code, similar biochemical pathways…). He updated Darwin's hypothesis, proposing an ancient group of organisms with genetics common with the three domains: Bacteria, Archaea and Eukarya.[35] In 2010, Theobald published results providing evidence for the monophyly of all life, a phenomenon known as the Last Universal Common Ancestry (LUCA), where one type of organism was imagined to be at the base of the phylogenetic tree of all life forms that we see on Earth today.[36]

Recently, new studies showed that LUCA is the common ancestor of bacteria and archaea only, and eukaryotes arises from prokaryotes (Fig 4), but information about where and how LUCA lived is still missing.[37] In 2016, Martin described the plausible physiology and habitat of LUCA using a phylogenetic approach. His interpretation of his results were consistent with a theory of an autotrophic origin of life involving the Wood-Ljungdahl pathway in a hydrothermal setting, in an environment rich in H_2, CO_2 and iron.[38]

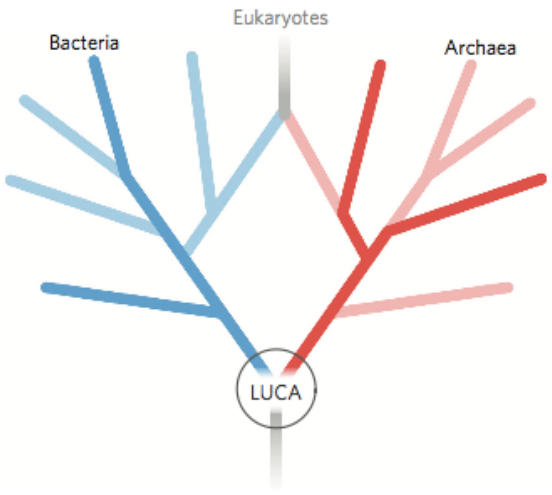

Fig 4. Phylogeny of the Last Universal Common Ancestor (LUCA). Taken with permission from reference 21.

1.1.2. Hypothetical cradle of life

Deep-sea exploration in the late 1970s, based on the observations of water temperature anomalies, revealed a submarine hydrothermal activity (hydrothermal vents, Fig 5) and a presence of animal communities.[39,40] The hot mineral-rich chimneys inspired research on early life, since the hydrothermal vent setting combines reactive gases, dissolved elements, and thermal and chemical gradients which differ along the chimney. In a similar vein, Russell and co-workers speculated that sulfide structures grown in the laboratory could simulate hot springs (100-200 °C), and could be used as culture chambers and flow reactors to investigate conditions under which life could have developed.[41]

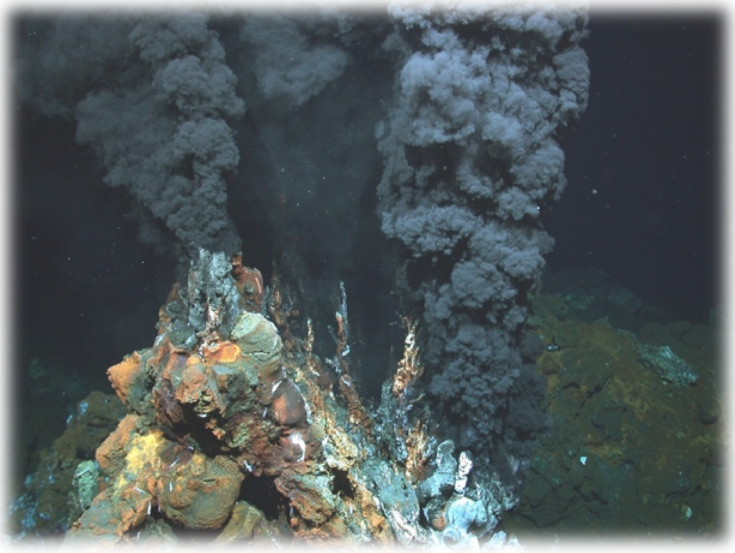

Fig 5. Picture of black smockers.

Based on geochemical and biological observations, Wachtershäuser proposed in 1988 the iron-sulfur world scenario: energy for carbon fixation of an autocatalytic metabolism could be provided by a redox process between ferrous iron and hydrogen sulfide, both present in a hydrothermal vent. The iron sulfide mineral formed could act as a binding surface for organic compounds.[42] This hypothesis was radically different from the prebiotic soup or "RNA world" theories for the origin of life. This new concept was based on biochemical retrodiction, meaning that the primitive biochemistry can be inferred from the organization of known biochemical networks. In the following years, experimental efforts from

Wachtershäuser and Russel were focused on producing evidence to defend this hypothesis (later called "metabolism first") by trying to mimic primitive pathways of CO_2 fixation in an alkaline hydrothermal-like environment.[3,43–45]

A summary of all hypotheses is presented as a timeline in Fig 6:

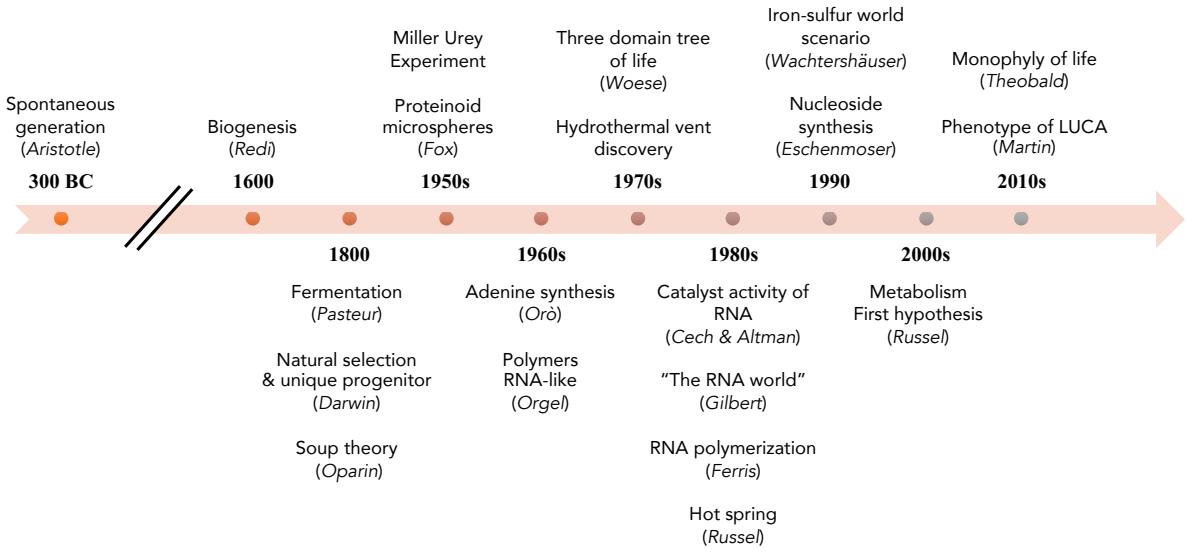

Fig 6. Timeline summarizing Origin of Life research.

1.1.3. Controversies

The "Metabolism First" hypothesis, with a relatively simple surface chemistry proposed, became a strong competitor to the "RNA World" hypothesis, which requires complex genetic material from the early beginning. This gave rise to a debate over which of the two origin of life approaches provides the strongest evidence. A comparison of both these hypotheses is summarized in Table 4.

Table 4. Main features of "The RNA World" and "Metabolism First" approaches

Feature	"The RNA World"	"Metabolism First"
Continuity in chemistry	✗	✓
Darwinian evolution from the beginning	✓	✗
Predetermined selectivity	✓	✗
Requires pre-existing chemical complexity	✓	✗
Robust chemistry	✗	?
Requires homochirality from the beginning	✓	✗

In this thesis, I will present experiments based on the "Metabolism First" hypothesis. Several arguments supporting this choice are presented below.

The major argument in favor of the "Metabolism First" approach is the necessity to make a connection between prebiotic chemistry on the early Earth and primitive life.[46] In other words, the organization of the chemical reactions leading to a primitive life should be

similar enough to today's biochemical networks, at least to a general extent, e.g. by using similar intermediates. This chemistry would not be enzymatic but driven by Earth-abundant minerals. It could require more steps or more complicated transformations, but it must maintain a continuity, such that it could later explain why biochemistry is the way it is and why it uses the pathways or metabolites that it does. In the case of the "RNA world", the potentially prebiotic nucleotide syntheses described to date have no connection to known biochemistry, even if they potentially conform with the early Earth geochemical models.[6]

The second argument against the "RNA World" hypothesis concerns the attempts to show that RNA and its components can be synthetized in the laboratory under what is considered to be geologically relevant conditions.[4] The experimental conditions proposed for these syntheses are unlikely to occur without human intervention[47], as there are multi-step sequences involved that often need different settings or conditions, or even purifications between steps.[48] Moreover, the use of substantial quantities of reactants such as cyanoacetylene or cyanamide, remains highly geochemically doubtful.[6]

Another argument is based on a recent computational study, which demonstrated that autocatalytic metabolic replicators are needed to enable metabolic networks, even if enzymes and genes are present.[49] This means that RNA, even though it carries genetic information and offers a catalytic function, is no longer enough to be at the origin of life. On the other hand, the advantage of enzymes and RNA-like molecules is that their large size can allow for high selectivity in the catalysis of chemical reactions, whereas the selectivity of mineral catalysts for specific reactions remains unclear. A counterargument to this could be that an autocatalytic network stabilized by a constant input of building blocks could be maintained in operation despite low yields of individual reactions or the loss of products.[50–52]

The last argument in favor of the "Metabolism First" scenario is that it requires only simple materials: small and often achiral molecules (mass < 500 Da). In contrast, the "RNA World" involves long polymers of structurally complex nucleotides (mass > 5 000 Da), with multiple chiral centers. In a prebiotic environment, with extreme conditions and a limited number of building block types at our disposal, a robust system is required to create life over

a long period of time, therefore big and specific molecules do not seem to be the best candidates.

Following the above historical outline, the "genetics first" scenario does not seem to be a viable model for origin of life scenario and cannot explain the complexity we observe today. That is why on the following pages our attention will be focused on the metabolic origin of life scenario, to give context to the experimental research presented in this thesis. Through this study, we would like to explore whether primitive proto-metabolic pathways could have emerged before the existence of genetic materials.

1.2. Metabolic origins of life

Nowadays, life on Earth is complex and heterogeneous, with diverse functions and reactions that are fundamental to the nature of the living state. To understand the origin of life, conceptually simple models can be useful. Here, I present a list of essential functions and main biochemical pathways of primitive species, introduced by an energetic study, in order to choose suitable metabolic patterns that could conform with the geochemical conditions of the early Earth.[5]

1.2.1. An energetic perspective

It is generally agreed that the emergence of life was initiated by some autocatalytic cyclic chemical system, to enable the exponential growth of intermediates by successive reactions.[53] Some years ago, the concept of dynamic kinetic stability (DKS) was proposed to support the existence of a common link between the nature of self-replicating chemical and biological systems.[54] This DKS is related to Darwin's principle, which prone the survival of the most stable organism. But, within a physico-chemical context, living systems are thermodynamically unstable, requiring external energy source to maintain the far-from-equilibrium state essential to life.[55] For life emergence, the self-organizing system required must be protected from a fast decay of species to deactivated products, toward the equilibrium state. [56] Every species must be located in a free energy well and protected by kinetic barriers, to avoid conversion to equilibrium, achieved by a free energy exceeding the level of the transition state of the reaction. The kinetic barrier of the reverse of the activation reaction must be high enough so that the energy carrier can be involved in irreversible processes.

The concept of DKS therefore serves to link the kinetics of a simple model for the emergence of life on track towards a complex biological system. This theory stipulates that stable replicating systems, with irreversible reactions, whether chemical or biological, tend to evolve so as to increase their stability. The protometabolic system is maintained in a far-from-equilibrium state, driving by a high enough free energy source, so their DKS increased.

DKS is the driving force of biological evolution, leading to the emergence of new function and later complexity, toward the search for greater stability.[57]

Thus, life on Earth appears to have emerged through the spontaneous emergence of a simple chemical reaction system, initially fragile, which complexified, through the dissipation of an high energy flux, and evolved towards complex replicating systems exhibiting greater DKS.[58]

1.2.2. A metabolic perspective

In order to identify the metabolic processes that are of interest to the origin of life, a classification of the nutritional processes of today's life should be first established. One way is to answer the following two questions:[5]

The first question is whether the organism's metabolism is self-sufficient or whether it depends on other organisms to survive and reproduce. If an organism can exist with only inorganic inputs, producing the necessary biomolecules for its survival and reproduction from its surroundings, this organism is called autotrophic. On the other hand, if an organism relies on other organisms to produce the necessary biomolecules for it to survive, this organism is called heterotrophic. On the early Earth, only inorganic materials, including H_2 and CO_2, were likely widely available in a continuous, sustainable manner. This is a major reason why the metabolisms of autotrophic organisms are often used as models for early biochemistry.[59,60]

The second question is biochemical and considers the source of energy an organism uses for its metabolism. Certain organisms release energy from the oxidation of molecules synthetized or consumed, their metabolism is thereby oxidative. This process needs a source of molecular oxygen as an electron acceptor, or atmospherically generated oxidants, such as nitrites, nitrates or oxidized sulfur species. Other organisms obtain energy from the reduction of molecules or from reductively forming C-C bonds. Their metabolism can be classified as reductive. This process needs reductants, such as dihydrogen, hydrogen sulfide or another source of electrons (Fig 7). The really early Earth's atmosphere was mostly described as a strongly reducing and volatile-rich, generated from the Moon-forming impact on the early Earth,[59] which support the hypothesis of an earliest reductive metabolism. At the very least,

anabolic (reductive) processes would have unavoidably been required to generate organic compounds from CO_2.

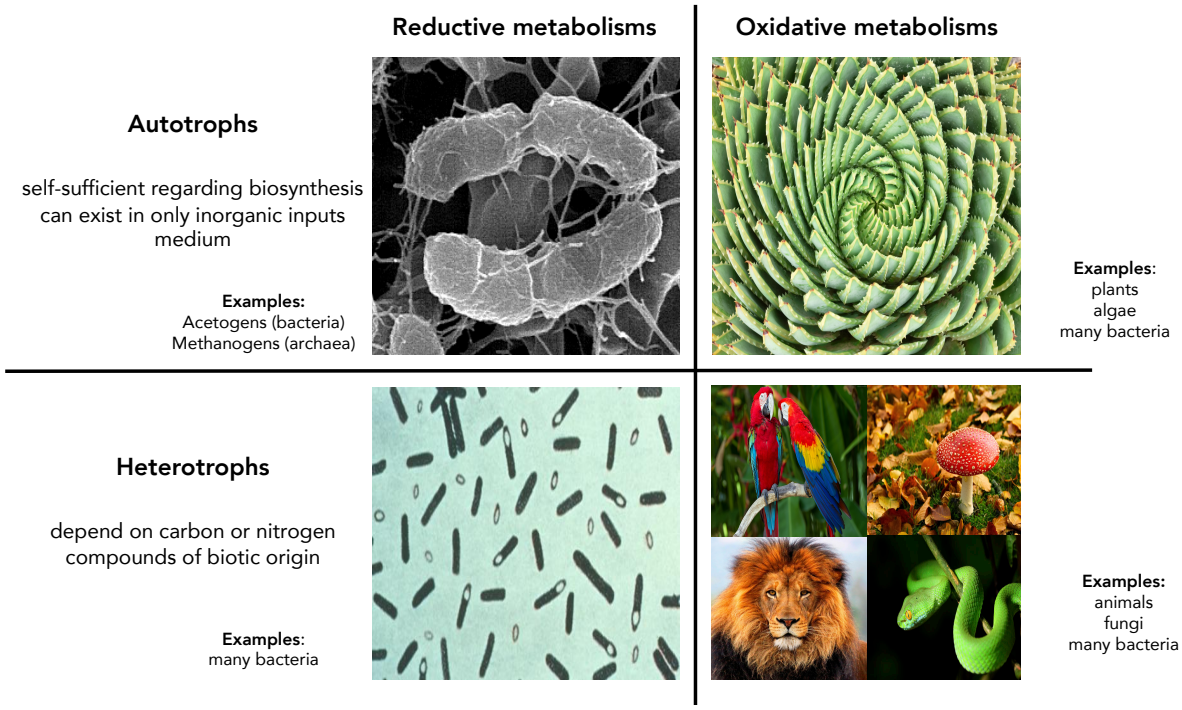

Fig 7. Conceptual divisions within metabolic organization.

However, the net metabolic character of any ecosystem or biosphere is neither net anabolic or catabolic but exists in a steady state. Therefore, the early metabolism cannot consist only of anabolic pathways, but also requires catabolic pathways (oxidative) to keep the network operational far from equilibrium.[61] A similar hypothesis about a synchronistic evolution of autotrophy and heterotrophy has been postulated, which are supposedly inherent to each other.[62] To summarize this section, the proto-metabolic networks that led to life most probably involved a combined synthesis (anabolism) and breakdown (catabolism) of intermediates to generate a far from equilibrium assembly, each powered by different irreversible reactions. The spontaneous complexification and diversification, which characterizes the evolution of life, can only be achieved under out-of-equilibrium conditions, so should be its emergence.[63] Later evolution enabled the selection and diversification into all extant organisms.[64]

1.2.3. A phylogenetic perspective

Once the nature of metabolic reactions of ancient life forms is established, the type of reactions that occurs within them requires further discussion. Through phylogenetics, the study of evolutionary relationships within biology, insights into which pathways may have been operating in ancient life and which are more recent inventions may, in principle, be obtained. As far as we can infer from extant biology, life has always built its biomass from CO_2. In nature, there are seven known CO_2 fixation pathways used by autotrophs.[65,66] One of these is used in photosynthesis (the Calvin-Benson reductive pentose phosphate cycle), which is thought to be a later evolutionary development.[67] Chemoautotrophs, which are autotrophic organisms that synthetize all necessary organic compounds from CO_2, use at least one of the other six pathways, which function with energy sources other than light. Among these pathways, the one that stands out above all others is the reductive Tricarboxylic Acid Cycle (rTCA cycle), also known as the reverse Krebs cycle, the reverse citric acid cycle or the Arnon cycle.[5,65] The rTCA cycle (operating anti-clockwise in Fig 8) was discovered for the first time by Arnon and co-workers in 1966 in deep-branching organisms, such as *Chlorobium thiosulfatophilum* bacterium, which use CO_2 as a building block.[68] In organisms, the rTCA cycle uses a reducing source of electrons such as H_2, H_2S or Fe^{2+} directly from the environment. It was later recognized as a plausible candidate for the earliest CO_2-fixation pathway by Hoffman and co-workers in 1980.[69] Succinate is the precursor to various co-factors and α-ketoglutarate is the precursor to various amino-acids, such as glutamate used by biology for transamination.

This reductive cycle also exists in an oxidative, catabolic form. The oxidative *Krebs cycle* (operating clockwise in Fig 8), also known as the TCA or the *citric acid cycle*, is the most popular catabolic pathway in human metabolism, discovered in 1937.[70] It is found in heterotrophic organisms, which acquire complex molecules such as sugars and fats from other organisms and break them down to produce smaller building blocks and energy through this cycle. The phylogenetic data are not conclusive about whether this TCA at its origin was oxidative, reductive or both,[61] that is why both will be presented all over this manuscript, with a main focus on the rTCA cycle.

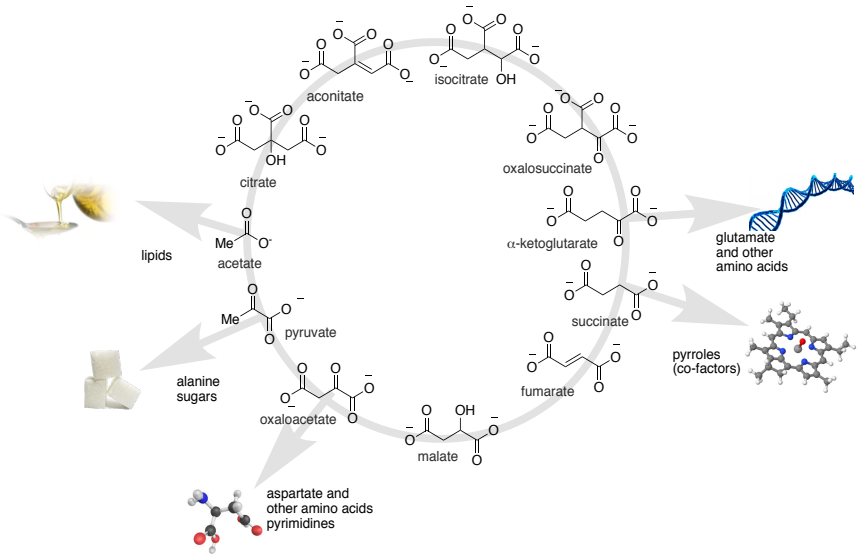

Fig 8. The (reverse) Tricarboxylic Acid, (r)TCA, cycle and its metabolites.

The hypothetical prebiotic rTCA cycle is a network of eleven reactions and eleven carboxylic acids, and it contains the five standard universal precursors (acetate, pyruvate, oxaloacetate, succinate, and α-ketoglutarate) to the most important anabolic reactions in biochemistry (Fig 8). Acetate, or acetyl when it is bound to a co-factor, is the biosynthetic precursor to lipids. Pyruvate is the precursor to sugars and various amino acids. Oxaloacetate is the precursor to various amino acids and pyrimidines. The rTCA, in addition to its key role in biosynthesis in those organisms that use it, is topologically an autocatalytic network involving a relatively small number of reactions.[8] Starting from acetate, a complete turn of the cycle would generate two molecules, oxaloacetate and acetate, and the cycle can start again from acetate. In this case, an overall yield of greater than 50% is required to make the cycle self-amplify. However, it has been pointed out that without enzymatic activity, as there were no enzymes on the early Earth, parasitic reactions could easily happen, bringing the net yield below such a threshold. As a consequence, the cycle would not survive if side reactions exclude more than half of the cycle's products, then the concentration of the cycle components would decline exponentially to zero.[50] As a solution, it has been proposed that a feeder pathway could be combined with the rTCA, to enable a constant input of one of the cycle's intermediates. The overall yield of the cycle could decrease below 50%, but the cycle would persist thanks to the constant supply of material (Fig 9). This is more realistic for a

prebiotic scenario, as long as the yield of individual reactions is > 0%, the cycle is, in principle, sustainable. Multiple feeder reactions are also possible.

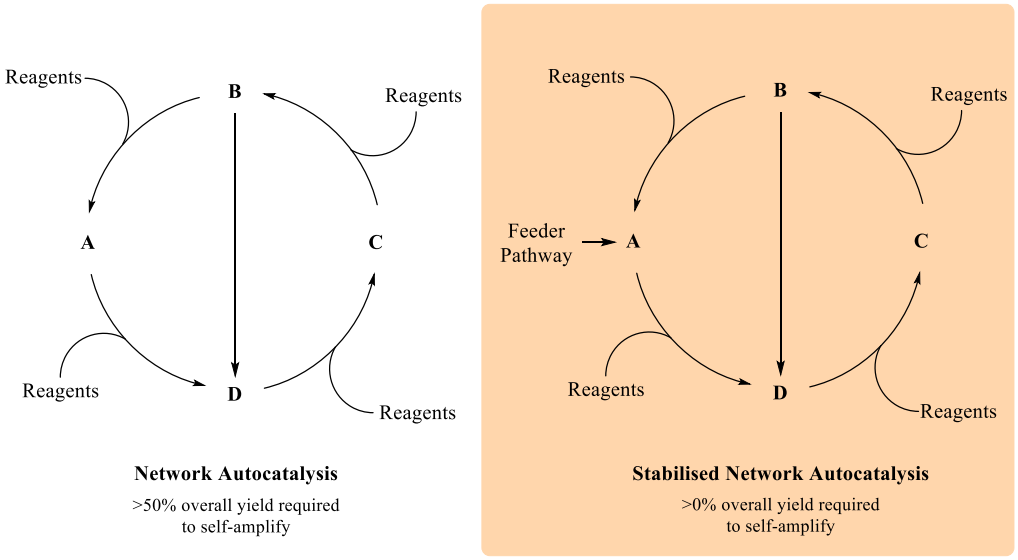

Fig 9. Autocatalytic reaction networks.

One good candidate for the feeder pathway would be the Wood-Ljungdahl (W-L) pathway, serving as a linear and simple "acetate feeder" for the rTCA cycle.[5] A phylogenetic study that analyzed evolutionarily conserved genes across all domains of life showed that among the six known pathways of CO_2 fixation, only the enzymes of the W-L pathway are present in LUCA.[38] In addition to acetate generation, the organisms using this pathway are able to accumulate energy from the overall exergonic chemistry of this process.[71] Thus, a combined W-L pathway with the rTCA cycle has been proposed to be at the origin of the first non-enzymatic stabilized autocatalyzed network: while the W-L pathway provides a constant input of acetate from CO_2, the rTCA builds up the precursors for more evolved biochemistry (Fig 10).

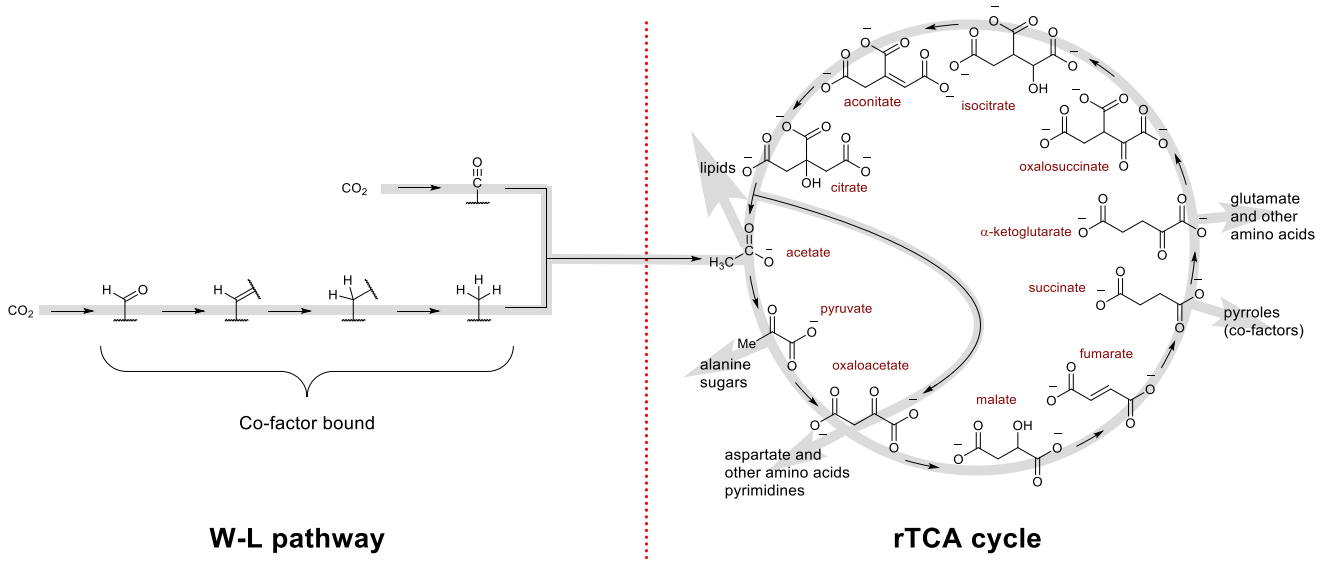

Fig 10. A stabilized autocatalytic network: combination of the W-L pathway and the rTCA cycle.

A hybrid has been proposed, combining the W-L pathway and a linear version, called the "horseshoe" part, of the rTCA cycle. This simpler version, as shown below (Fig 11), has the same chemical intermediates as the rTCA cycle, except that its final product is α-ketoglutarate and it does not proceed further.[44] This version would have predated the complete rTCA cycle, but it remains a hypothesis. The simplified version has less reactions, and the remaining ones are simpler; but it loses its autocatalytic property.

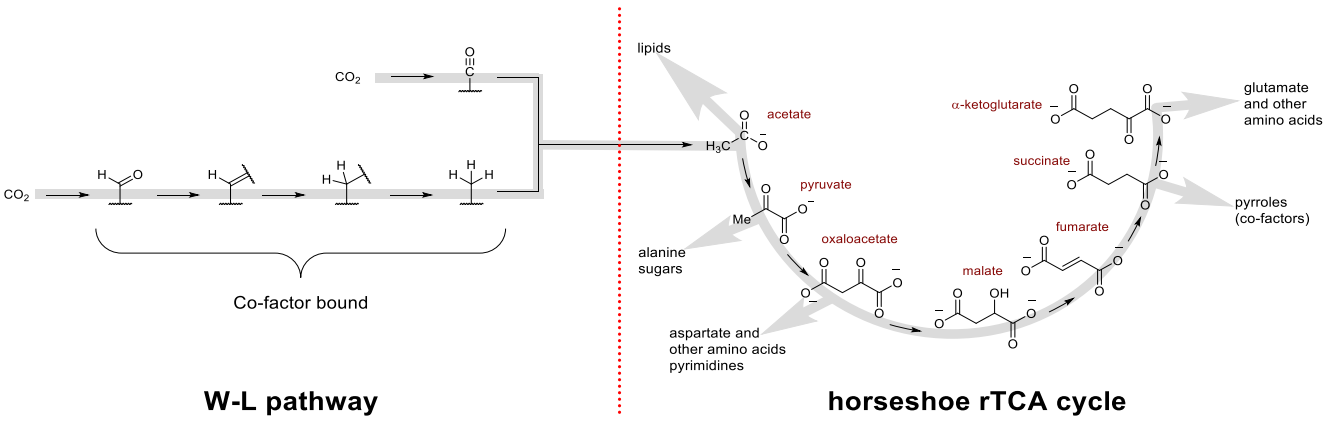

Fig 11. A hybrid of the W-L pathway and the horseshoe fragment of the rTCA cycle.

1.2.4. Primitive metabolic processes

The two carbon fixation pathways mentioned above, the W-L pathway and the rTCA cycle, will be described in more detail in the further part of this thesis, with the assumption that they enable the organization of a proto-metabolic network which gave rise to a primitive life on the early Earth. Furthermore, thioester formation from the TCA cycle intermediates will also be studied, to expand the core carbon, hydrogen and oxygen-based network to more complex molecules and to open new routes of metabolic pathways. Applying both the biochemistry and geochemistry knowledge is essential here, to satisfy the requirements of biologists as well as chemists, as bridging the gap between both these disciplines is necessary to understand the origin of life mystery.

2. The Wood-Ljungdahl pathway

2.1. Overview

It has been suggested that the W-L pathway is the most ancient of the six known CO_2 fixation pathways.[7,72] It is found in both methanogens and acetogens, which use the most ancient forms of energy metabolism, employing the same intermediates but different co-factors for methyl synthesis. Compared to the other five carbon fixation pathways that are cyclic and autocatalytic, the W-L pathway is shorter and linear, it enables acetyl synthesis from CO_2 and involves enzyme/cofactors, most of which contain transition metals (Fig 12).[68] Like the other pathways, it reduces CO_2 using electron sources found in the environment, most often H_2. The mechanism of this endergonic CO_2 reduction by H_2 is complex and proceeds via electron bifurcation. It explains the reduction of CO_2 with electrons coming from H_2, even though the reaction is energetically unfavorable.[73]

The W-L pathway enables the synthesis of acetate by the assembly of two CO_2 molecules: one reduced to a methyl group, and the other one to CO.[15] Moreover, this process contributes to energy production by creating ion concentration gradients that are used to drive adenosine 5'-triphosphate (ATP) synthesis.[74] In acetogens, the pathway is important for biosynthesis and energy metabolism (Fig 12, black arrows), while in methanogens it is only used for the latter (Fig 12, grey arrows).[75]

From a biosynthetic standpoint, the overall function of the W-L pathway is to produce acetyl CoA, the precursor to lipids, and pyruvate, the precursor to sugars and some amino acids.

2.2. Enzymes and mechanism

The mechanism and enzymology of the W-L pathway is now well-known (Fig 10).[15] The first step comprises a reversible two-electron reduction of CO_2 to a formyl group (Fig 10, Step I) and is carried out by an enzyme called *formate dehydrogenase*, when a suitable reductant such as H_2 is available.[75] In anaerobic organisms, this enzyme contains oxygen sensitive metal centers such as tungsten (W), molybdenum (Mo) or iron (Fe). With the aid of tetrahydrofolate (H_4F) or tetrahydromethanopterin (H_4MPT), the formyl moiety undergoes a dehydration and further reductions to become a methyl group (Fig 12, Step II).[76]

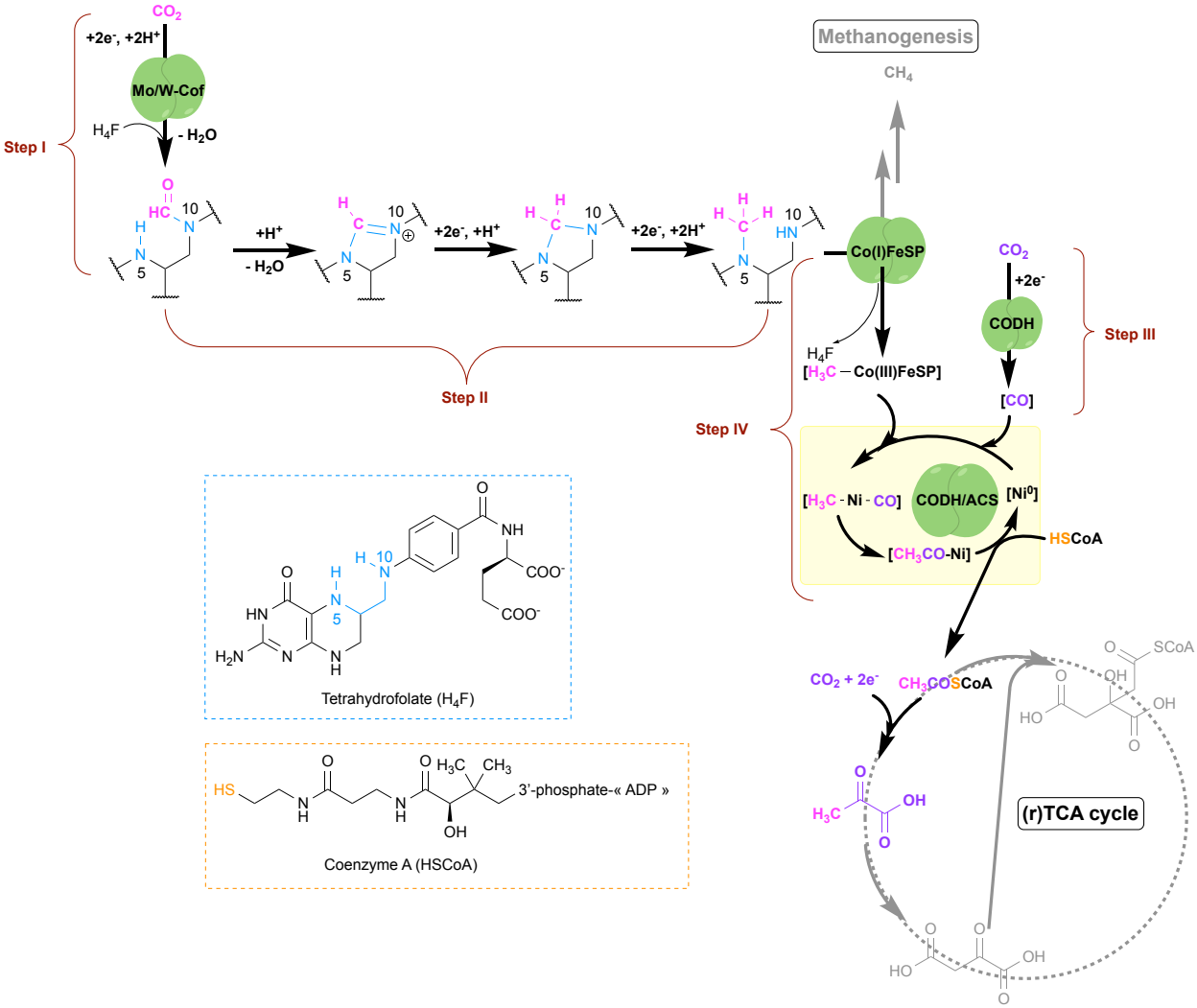

Fig 12. The metalloenzymes and cofactors of the W-L pathway.

In acetogenesis, a Ni-containing metalloenzyme called *carbon monoxide dehydrogenase* (CODH) catalyzes in parallel a second reversible reduction of CO_2 to CO (Fig 10, Step III). Thanks to a mediator enzyme, called *corrinoid iron sulfur protein* (CoFeSP), the methyl group is transferred from its organic co-factor to the reduced active site of a Ni-based enzyme named *acetyl CoA synthase* (ACS), joined by the second pathway (Figure 10, Step IV).[77] Here, CO and methyl group combine to form an acetyl-Ni species (Fig 10, yellow field), which is then trapped by coenzyme A (HSCoA) (Fig 10, Step V), a thiol, to produce acetyl CoA ($CH_3COSCoA$), a thioester.[15] Much of the acetyl CoA produced undergoes a further enzyme-catalyzed reductive carboxylation to furnish pyruvate (Fig 10, Step V). In methanogen organisms, methane (CH_4) can be intercepted from the CoFeSP through further steps (Fig 10, grey arrows).

3. Tricarboxylic Acid cycles

3.1. Introduction

The known biological enzymatic TCA cycle contains five standard universal precursors of biosynthesis; acetate, pyruvate, oxaloacetate, succinate and α-ketoglutarate, which makes it the central pathway for all universal metabolism, as a link to other known metabolic pathways (Fig 13). The complete cycle is found in organisms in either of two opposite forms: the oxidative TCA cycle that has a net catabolic function, and the reductive TCA (rTCA) cycle that has a net anabolic function. They both comprise 13 intermediates, most of which are carboxylic acids, and a few thioesters. Six different types of reactions are needed to perform the cycle: reductive carboxylation/oxidative decarboxylation, hydration/dehydration, reduction/oxidation, hydration/dehydration, thioesterification/hydrolysis and retro aldol/aldol. For some biochemists, the thioesterification step could be excluded from the primitive form of the cycle.[19] Both cycles, the rTCA and the TCA will be presented in the following part, although more focus will be made on the rTCA cycle. To conclude this section, a brief introduction to the glyoxylate cycle, a variation of the TCA cycle, will be presented.

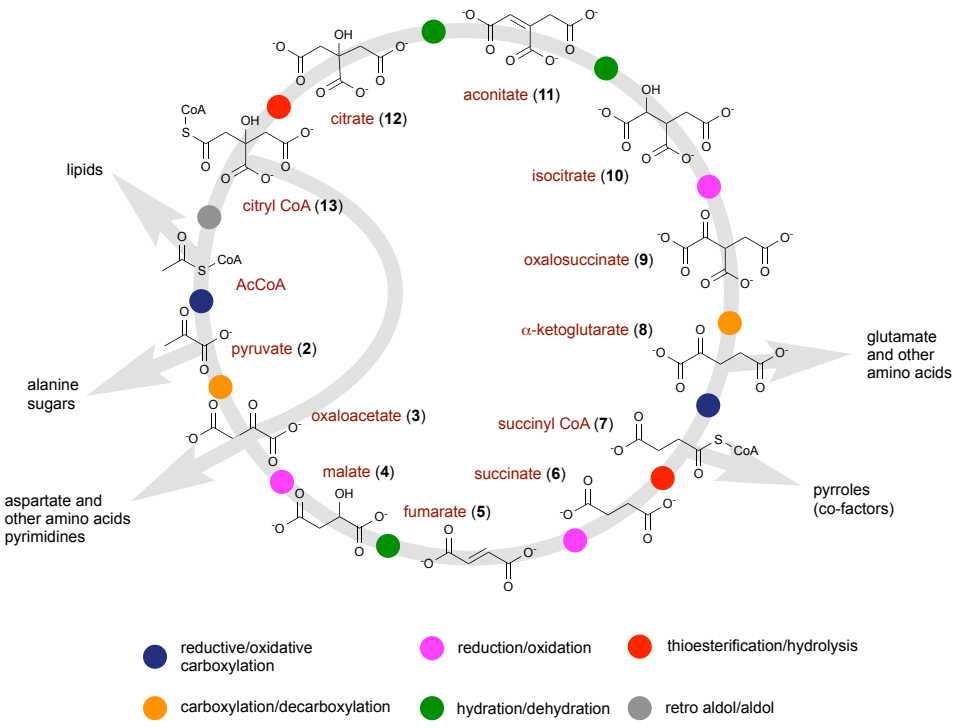

Fig 13. The TCA cycle.

3.2. The rTCA cycle biochemistry

Of the 12 different reactions observed in the cycle (thioesters formation will be explained later, part 4), four C-C bond forming reactions (two reductive carboxylations and two ATP-dependent carboxylations) and one C-C bond-breaking reaction (a retro-aldol reaction) are involved. The rest of the reactions are reductions and reversible hydrations/dehydrations. The specific mechanisms and enzymes involved in these specific reactions have recently been reviewed and will be discussed in detail in the following section.

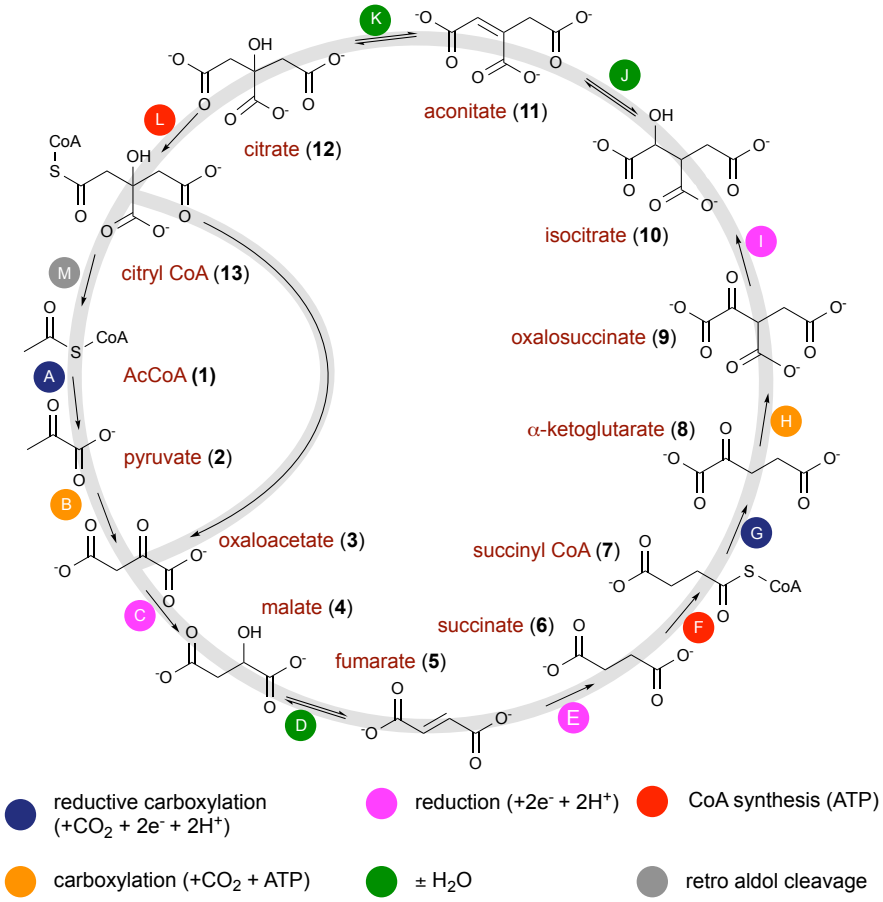

Fig 14. The rTCA cycle.

3.2.1. Reductive carboxylations

There are two reductive carboxylations within the rTCA cycle: the reaction of acetyl-CoA (**1**) to pyruvate (**2**) and from succinyl-CoA (**7**) to α-ketoglutarate (**8**). These two steps are catalyzed by a ferredoxin-dependent enzyme, which contains in its center a [4Fe-4S] cluster mediating electron transfer, and a thiamine pyrophosphate (TPP).[78] The TPP can react with the coenzyme A bound to the acyl group, leading to an enamine in its resonance form.[79] These enzymatic reactions are supposed to be oxygen sensitive, even if similar enzymes have been found in aerobic organisms.[80] The ketoacid is finally formed thanks to the addition of CO_2, which is reduced by a low potential electron donor, such as ferredoxin (Scheme 1). Even though the mechanism is not well understood, it is believed to work in the opposite way than the oxidative decarboxylation, described later.

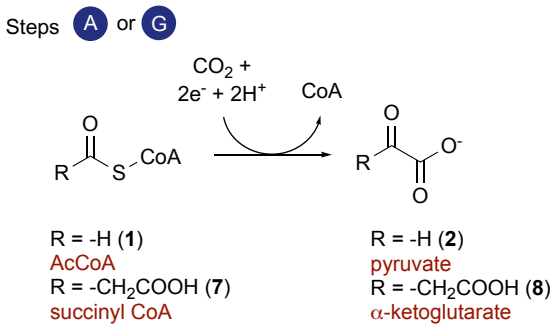

Scheme 1. Reductive carboxylation.

3.2.2. ATP-dependent carboxylations

The conversion of pyruvate (**2**) to oxaloacetate (**3**) is a two-step process (Scheme 3): First, pyruvate is converted to phosphoenolpyruvate (PEP) catalyzed by an enzyme called *pyruvate-phosphate dikinase*. This mechanism is reversible and consumes one molecule of ATP. The enzyme is also found in the gluconeogenesis pathway, where PEP is the starting material for sugar synthesis. Then, *phosphoenolpyruvate carboxylase* (PEPC) catalyzes the irreversible addition of bicarbonate to PEP to form oxaloacetate, using Mg^{2+} or Mn^{2+} as a cofactor. The mechanism proceeds in two major steps (Scheme 2).[81]

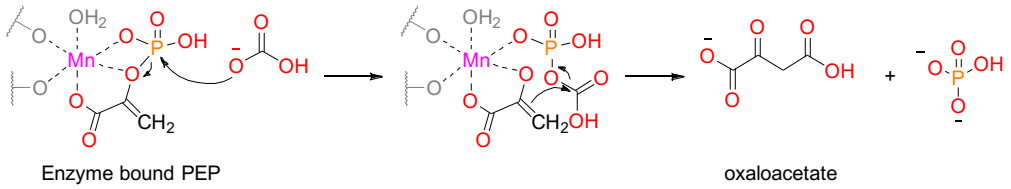

Scheme 2. Mechanism of irreversible addition of bicarbonate to PEP.

In some organisms, only one enzyme, called *pyruvate carboxylase* (PC) is required to catalyze the irreversible carboxylation of pyruvate to oxaloacetate. This enzyme contains a biotin prosthetic group, and requires also ATP and Mg^{2+} or Mn^{2+}.

There is a close relationship between the mechanism of *pyruvate carboxylase* and the enzyme called *oxalosuccinate synthetase* (OGC), responsible for α-ketoglutarate (**8**) carboxylation to oxalosuccinate (**9**): the reaction involves a biotin protein and ATP in the presence of Mn^{2+}.[82,83]

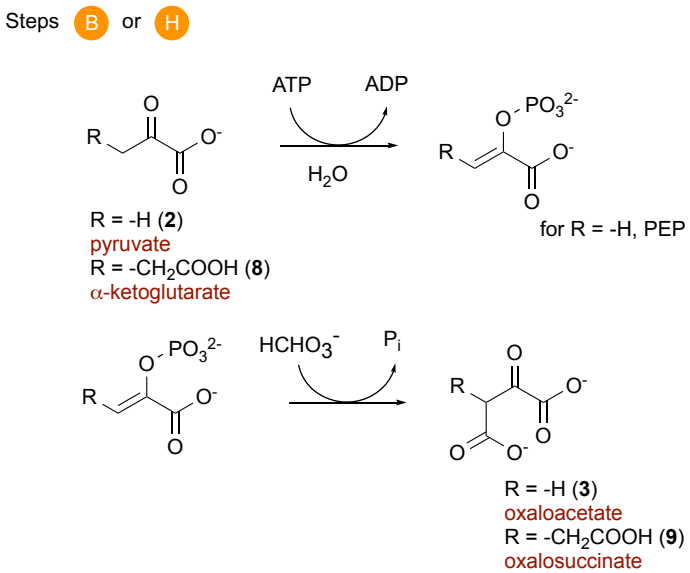

Scheme 3. ATP-dependent carboxylation.

3.2.3. Reductions

There are two different kinds of reductions observed in the rTCA cycle. The first is an α-ketoacid reduction performed by *dehydrogenase* enzymes through oxidation of an electron acceptor, usually NADPH (Scheme 4). It is found in the reduction of oxaloacetate (**3**) to malate (**4**). Particularly, the *isocitrate dehydrogenase*, which is involved in oxaloacetate reduction, catalyzes a two-step process: the carboxylation of α-ketoglutarate (**8**) to oxalosuccinate (**9**) followed by its reduction to isocitrate (**10**).[84]

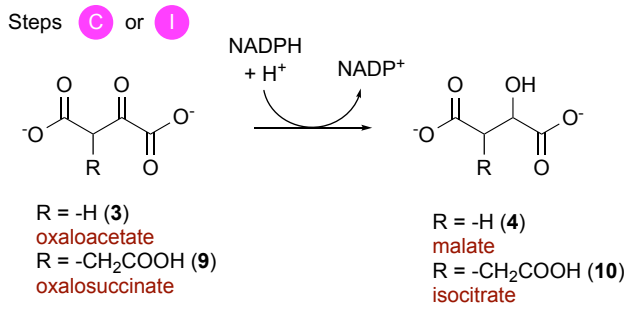

Scheme 4. α-ketoacid reduction.

The second type of reduction in the rTCA cycle is an alkene reduction performed by *fumarate reductase*, which converts fumarate (**5**) to succinate (**6**) (Scheme 5). These enzymes can be divided into two classes depending on the electron acceptor: the enzyme transfers electrons from a quinol, and is thus involved in the production of ATP; or the enzyme transfers electrons from NADH, which is done by certain autotrophs that operate the rTCA cycle.[85,86]

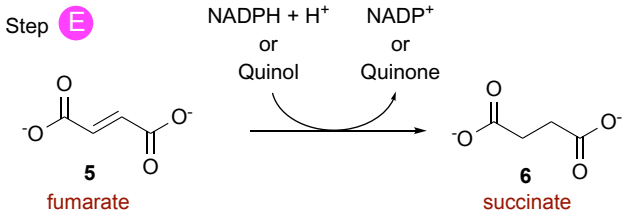

Scheme 5. Alkene reduction.

3.2.4. Dehydrations-Hydrations

An enzyme called *aconitase*, which can be found in the mitochondria of organisms using the rTCA cycle, is responsible for the dehydration of isocitrate (**10**) to aconitate (**11**), followed by the hydration of aconitate to citrate (**12**) (Scheme 6).[87]

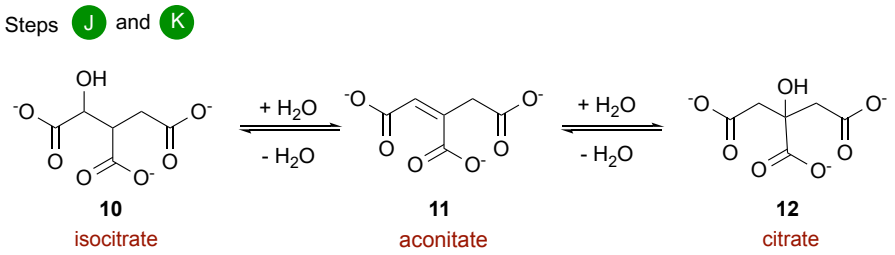

Scheme 6. Dehydration and hydration sequence starting from isocitrate.

The mechanism of this enzymatic reaction is now well-understood: the - OH and - COO^- groups of citric acid are bound to the Lewis-acidic FeS clusters in the enzyme active site. One proton is caught by a base, followed by a rearrangement, and so aconitate adopts the citrate mode. Then, there is a rotation to the isocitrate mode, followed by a hydration – this time on the opposite face of the intermediate. Isocitrate is finally obtained through this overall reversible process (Scheme 7).[88]

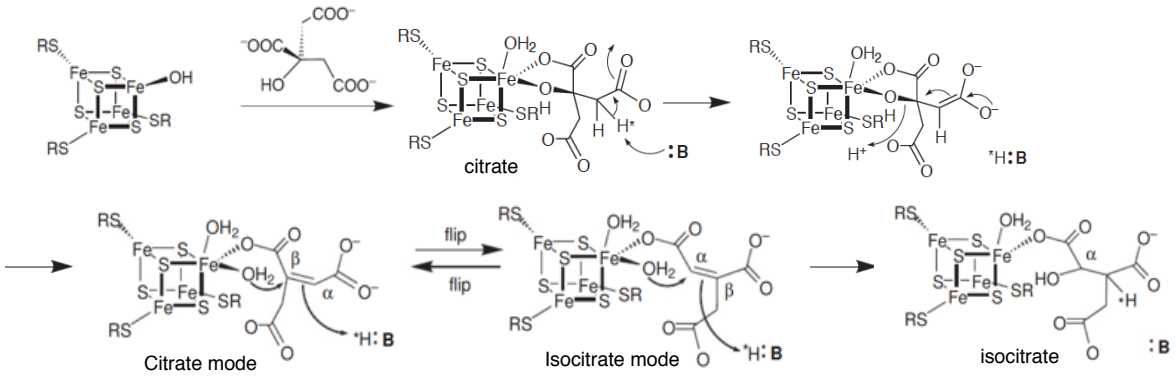

Scheme 7. Mechanism of citrate-isocitrate isomerization

Another enzyme, called *fumarase*, enables the dehydration of malate (**4**) to fumarate (**5**) (Scheme 8). This enzyme is found in the cytosol and is also used by the urea cycle pathway and in amino acid anabolism.[89]

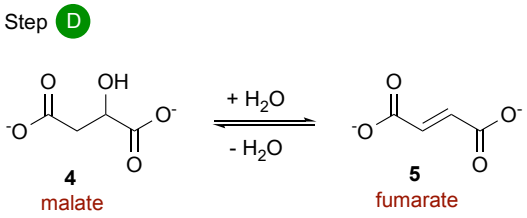

Scheme 8. Dehydration of malate.

3.2.5. Retro-aldol cleavage

In some organisms, the *ATP-citrate lyase* is found to catalyze both thioester synthesis and retro-aldol cleavage steps, in which acetyl-CoA (**1**) and oxaloacetate (**3**) are produced from citrate (**12**) and CoA, going through citryl-CoA (**13**). These two steps include the hydrolysis of ATP to ADP and phosphate.[90] Other organisms use a two-enzyme *Citryl-CoA synthetase/Citryl-CoA lyase* tandem, to perform these reactions one by one. This final reaction of the rTCA cycle is complex but needed to achieve the autocatalytic property of the full cycle.

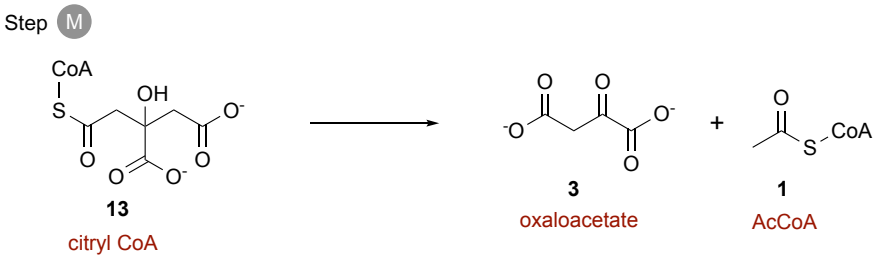

Scheme 9. Retro-aldol cleavage of citryl CoA.

3.3. The TCA cycle biochemistry

A catabolic pathway, such as the TCA cycle, cannot exist in isolation: to break something down, it has first to be made, and so some anabolic route to its intermediates was required before it could exist in its modern form. In other words, the TCA cycle has to emerge after a metabolite-generating reaction network, even if the lag in time is only on the timescale of a chemical reaction. In contrast to the rTCA cycle, the TCA cycle contains only one C-C bond forming reaction (an aldol addition) and four C-C bond breaking reactions (two oxidative decarboxylations that generate energy-rich thioesters and two decarboxylations that generate ATP), the rest being oxidations and the same reversible hydrations/dehydrations as in the rTCA cycle (described in the previous part).

3.3.1. Decarboxylation

The decarboxylations of oxaloacetate (**3**) and oxalosuccinate (**9**) are catalyzed by enzymes called *decarboxylases* (Scheme 10). These enzymes use the free energy of decarboxylation to pump Na^+ ions across the membrane, which provides energy for ATP synthesis.[91] In the case of oxaloacetate, the enzyme uses Zn^{2+} to stabilize the enolate form of pyruvate, coming from the decarboxylation assisted by biotin, until a proton adds.

In the case of α-ketoglutarate (**8**) formation, oxalosuccinate is an intermediate in a two-step reaction starting from isocitrate (**10**) and catalyzed by *isocitrate dehydrogenase* (IDH). Isocitrate undergoes first oxidation and then decarboxylation, which is described later (3.3.3. Oxidations).[84]

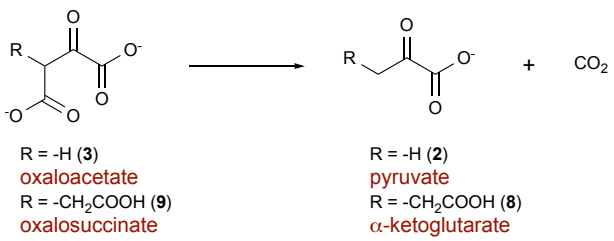

Scheme 10. Decarboxylations within the TCA.

3.3.2. Aldol addition

The aldol addition is the first step of the TCA cycle. It enables the formation of one molecule of citrate (**12**) from the reaction of acetyl CoA (**1**) and oxaloacetate (**3**), catalyzed by *citrate synthase* (Scheme 11).[92]

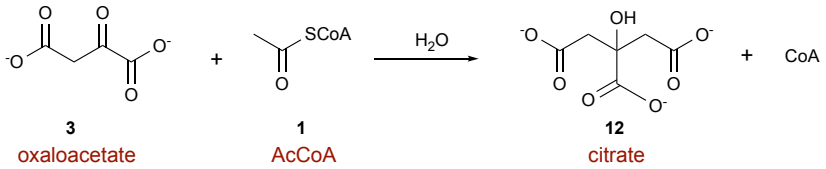

Scheme 11. The aldol condensation.

3.3.3. Oxidations

Analogously to reductions in the rTCA cycle, there are two kinds of oxidations in the TCA cycle. The enzyme *succinate dehydrogenase* (SQR) catalyzes the oxidation of succinate (**6**) to fumarate (**5**) (Scheme 12). This alkane oxidation occurs with the reduction of ubiquinone to ubiquinol, and FAD as hydride acceptors.[93]

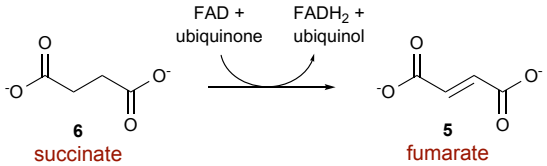

Scheme 12. Alkane oxidation.

The other type are alcohol oxidations. *Malate dehydrogenase* (MDH) is the enzyme responsible for the reversible oxidation of malate (**4**) to oxaloacetate (**3**) (Scheme 13). The reaction occurs through the oxidation of one hydroxyl group on malate and reduction of NAD^+. The same mechanism of the hydride ion transfer to NAD^+ is observed in *lactate dehydrogenase*.[94] A similar oxidation of isocitrate (**10**) to oxalosuccinate (**9**) is catalyzed by *isocitrate dehydrogenase*, which requires the availability of NAD^+ or $NADP^+$ and Mg^{2+}/Mn^{2+}.[84]

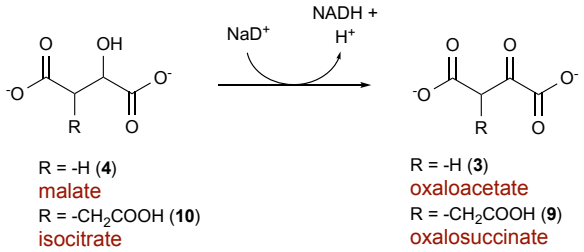

Scheme 13. Alcohol oxidation.

3.3.4. Decarboxylative oxidation

Pyruvate dehydrogenase is an enzyme that functions as a component of a bigger one called *pyruvate dehydrogenase complex* (PDC). PDC transforms pyruvate (**2**), NAD^+ and CoA into acetyl-CoA (**1**), CO_2 and NADH (Scheme 14).

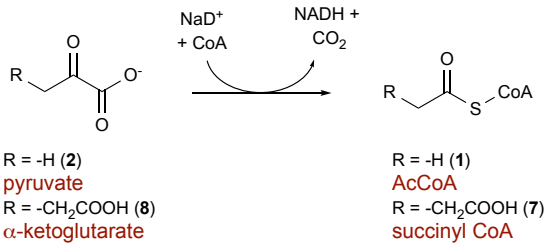

Scheme 14. Oxidative decarboxylation of ketoacids to thioesters.

The conversion requires the coenzyme thiamine pyrophosphate (Scheme 15).[95] *α-Ketoglutarate dehydrogenase* works on α-ketoglutarate (**8**) to convert it to succinyl-CoA (**7**), in a similar way to *pyruvate dehydrogenase*—these two enzymes are structurally related.[96]

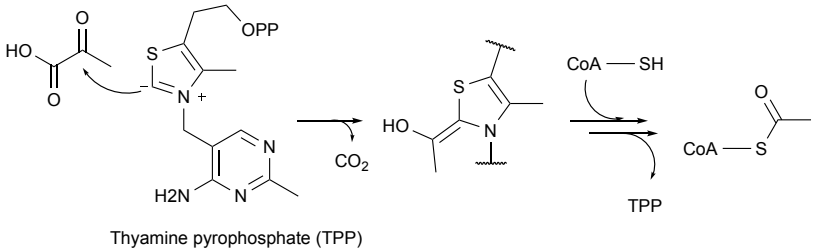

Scheme 15. Mechanism of oxidative decarboxylation.

3.4. The Glyoxylate cycle

The glyoxylate cycle is an anabolic pathway, found mainly in plants and bacteria.[97] The cycle converts acetate to succinate and uses five of the eight enzymes associated with the TCA cycle: *citrate synthase*, *aconitase*, *succinate dehydrogenase*, *fumarase* and *malate dehydrogenase*. The difference is that isocitrate is converted into glyoxylate and succinate, then glyoxylate is condensed with acetate giving malate. The glyoxylate cycle bypasses the oxidative decarboxylation steps in the TCA cycle, allowing simple carbon to be used in gluconeogenesis.[98]

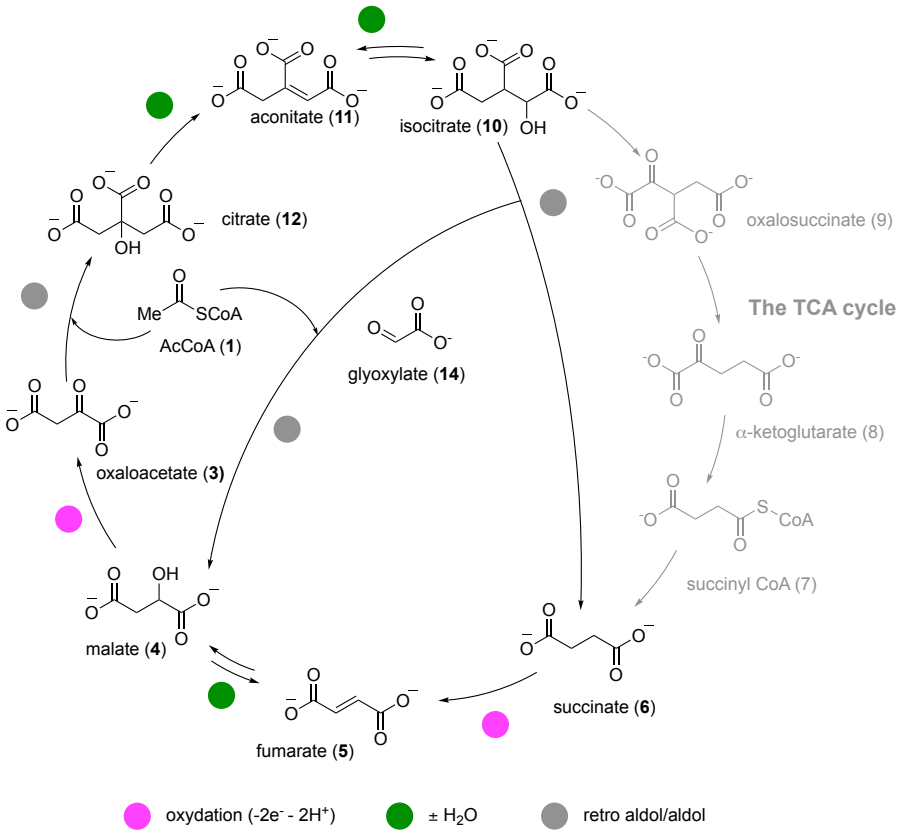

Fig 15. The glyoxylate cycle.

The first specific step in the glyoxylate cycle is the retro-aldol cleavage step, in which glyoxylate (**14**) and succinate (**6**) are produced from isocitrate (**10**). This step requires the presence of the enzyme *isocitrate lyase*. This reaction of the glyoxylate cycle is needed to achieve the autocatalytic property of the full cycle.

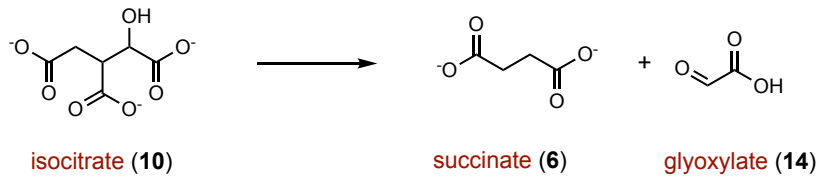

Scheme 16. Retro aldol cleavage of isocitrate.

The aldol addition is the second step specific to the glyoxylate cycle. It enables the formation of one molecule of malate (**4**) from the reaction of acetyl CoA (**1**) and glyoxylate (**14**), made from the previous retro aldol cleavage catalyzed by *malate synthase* (Scheme 17).

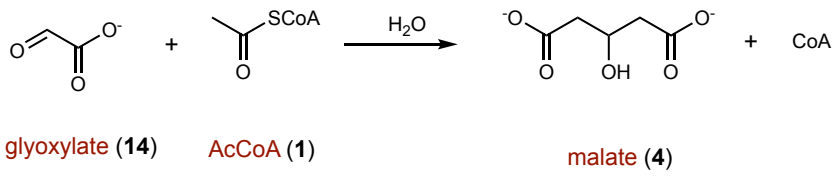

Scheme 17. The aldol condensation.

4. Thioesters

Thioesters are compounds with the functional group R-S-CO-R', formed by the dehydrating condensation of carboxylic acids with thiols. In biology, the most well-known ones are the derivatives of coenzyme A, which contains phosphate (Fig 16). In core catabolic pathways, like the TCA cycle, thioesters are formed by the oxidation of α-ketoacids or aldehydes, and their hydrolysis supplies energy for the production of ATP. In biochemistry, thioesters are common intermediates in many biosynthetic reactions, such as fatty acids formation and degradation.

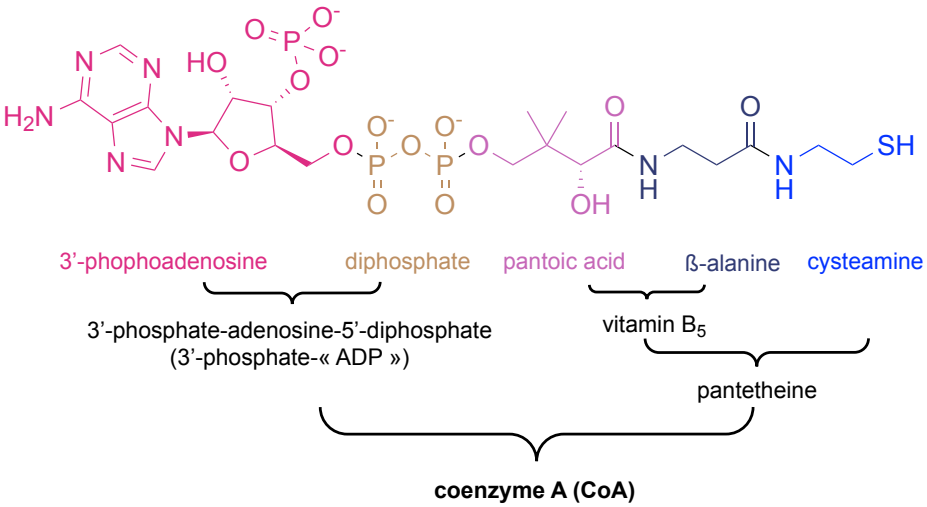

Fig 16. Structure of the coenzyme A.

4.1. A thioester world

The concept of a "thioester world" was first introduced by De Duve, in 1998.[11] He proposed the emergence of protometabolism as a set of chemical reactions that would then generate the RNA world and later enable the production of protein enzymes that led to a biological metabolism. Considering the important role of thioesters in present-day metabolism, he hypothesized that thioesters carried out key functions also in protometabolism and provided a link between the two. The early thioester formation is supported by the geochemically plausible hydrogen sulfide rich environment proposed as prebiotic setting.[99] The thioester-based protometabolism would have been fueled by the free energy of hydrolysis of the thioester bond (ΔG= -36 kJ/mol for AcCoA hydrolysis).[100] However, a question arises concerning phosphate incorporation into prebiotic chemistry, as it is an essential component and building block of the genetic material, that also participates in the metabolic functions in all living systems (ATP, ΔG= -30 kJ/mol for hydrolysis).[101,102,103] Using computational systems biology approaches, Segrè and co-workers showed that a phosphate-independent biochemical network exists within the larger network of all known biochemical reactions within the biosphere. The reactions within this network rely on thioester chemistry, leading to a rich and complex organized biochemistry.[17] This analysis suggests that it may be possible to access a broad spectrum of key biomolecules and a large connected reaction network, using only simple prebiotic materials, without the requirement for ATP (Fig 17).

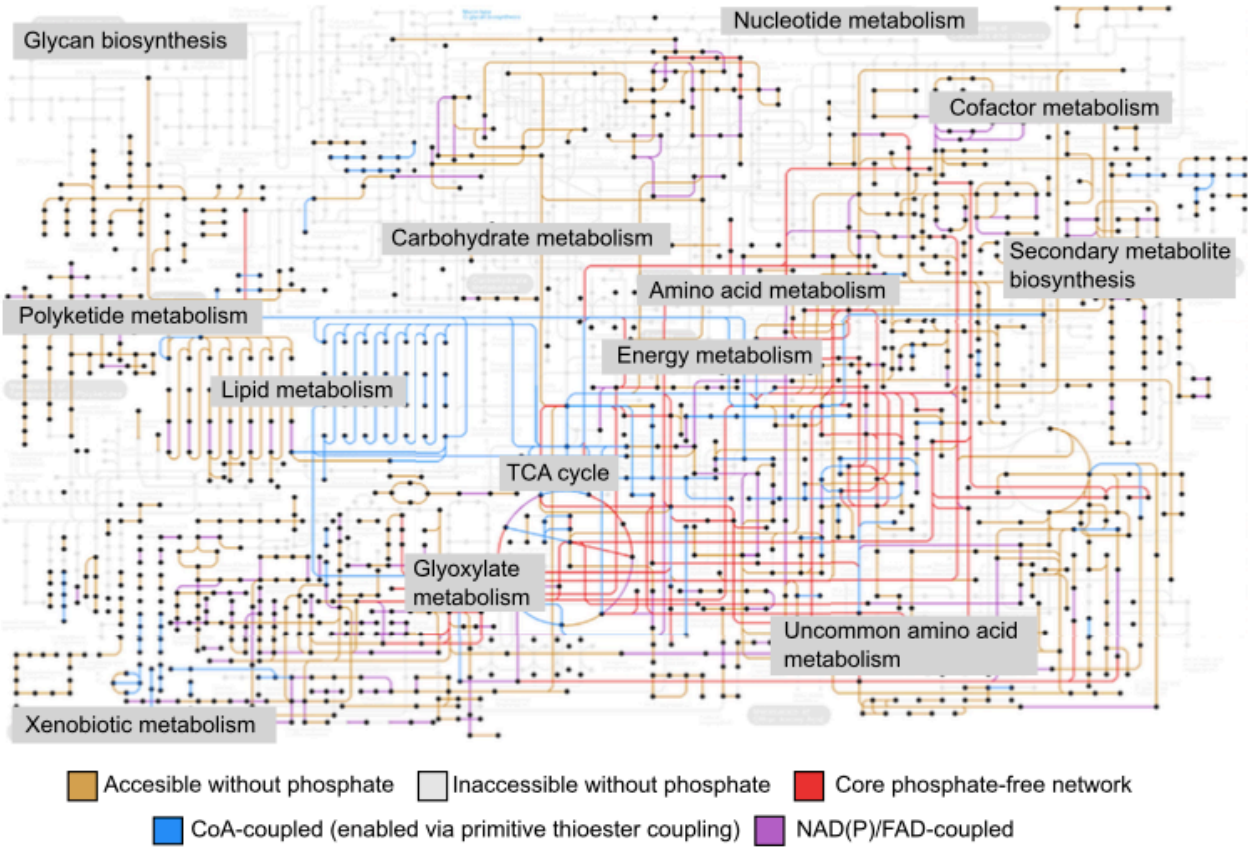

Fig 17. Hypothetical phosphate-free metabolism. Taken with permission from reference [17].

Using the same algorithms as in their study from 2018, in combination with different environmental parameters (temperature, pH, redox potential and availability of molecular precursors), the same team speculated about a biochemical convergence to an organo-sulfur-based protometabolism, organized around the rTCA cycle and driven by thioester and redox reactions.[104] In light of these results, an introduction of biological thioester formation will be presented in the following sections.

4.2. Main routes for biological thioester formation

As it was previously the case with the TCA cycles, a reductive or an oxidative route to thioesters can be observed in biochemistry, with different mechanisms. These two different routes will be presented in the following sections, in the context of the rTCA and the TCA cycles. Glycolysis will also be shortly introduced, to provide a future perspective to the experimental investigations described in this thesis.

4.2.1. rTCA cycle

Two conversions of a carboxylic acid to a thioester are observed within the rTCA. One is the formation of succinyl CoA (**7**) from succinate (**6**), by an enzyme called *succinate-CoA ligase* (Scheme 18). This enzyme requires the presence of CoA and a nucleoside triphosphate, either GTP or ATP, which reacts to form GDP or ADP and an inorganic phosphate molecule.[105] This critical step is important not only for the rTCA cycle, but also for porphyrin, heme and ketone body biosynthesis.

The second thioester synthesis within the rTCA cycle is the formation of citryl CoA (**13**) from citrate (**12**) by *citrate CoA ligase*, which also requires ATP and CoA (Scheme 18).[106] This product is crucial in biochemistry, since it undergoes a retro-aldol cleavage and generates the precursor for fatty acid biosynthesis, acetyl CoA.

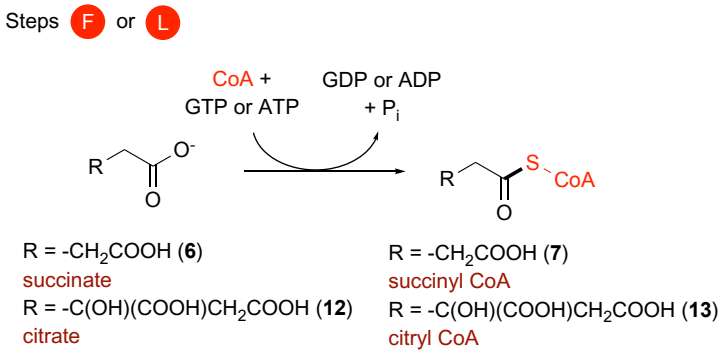

Scheme 18. Thioester synthesis within the rTCA cycle.

4.2.2. TCA cycle

Within the TCA cycle, thioesters are produced by a mechanism depending on electron transfer and involving the oxidative decarboxylation of α-ketoacids (Scheme 19).[11] The *pyruvate dehydrogenase complex* (PDC), combining three different enzymes, converts pyruvate (**2**) into acetyl-CoA (**1**), for which it requires NAD^+ (as electron acceptor) and thiol CoA.[107] This reaction proceeds in three steps: the decarboxylation of the ketoacid, the reduction of NAD^+ to NADH and the transfer of the decarboxylated ketoacid to CoA which forms the end product.

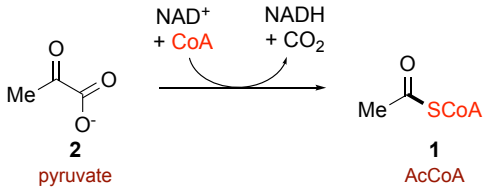

Scheme 19. Thioester synthesis from pyruvate

The second thioester, succinyl-CoA (**7**), is made from α-ketoglutarate (**8**) through the same process, by *oxoglutarate dehydrogenase complex* (OGDC).[108] This reaction is followed by hydrolysis of the thioester to succinate (**6**), which releases energy and is coupled to the production of ATP (Scheme 20).

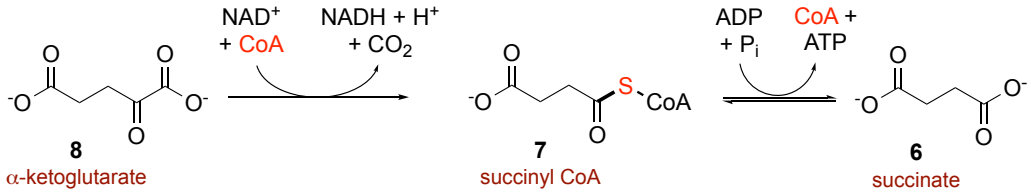

Scheme 20. Thioester synthesis from α-ketoglutarate followed by its hydrolysis.

4.2.3. Glycolysis

A mechanism similar to the one shown in the above section can be found in glycolysis, involving an aldehyde instead of an α-ketoacid. The NAD-dependent oxidation of glyceraldehyde-3-phosphate to 1,3-bisphosphoglycerate is the central reaction for energy retrieval in this pathway. It is carried out by an enzyme called *glyceraldehyde-phosphate dehydrogenase* (GAPDH).[11] In this mechanism, a cysteine residue in the active site of the GAPDH first reacts with the aldehyde, which is subsequently oxidized to a thioester (Fig 18).[109] Then, the phosphorylation can take place thanks to the much higher reactivity of the thioester species, compared to the carboxylic acid.

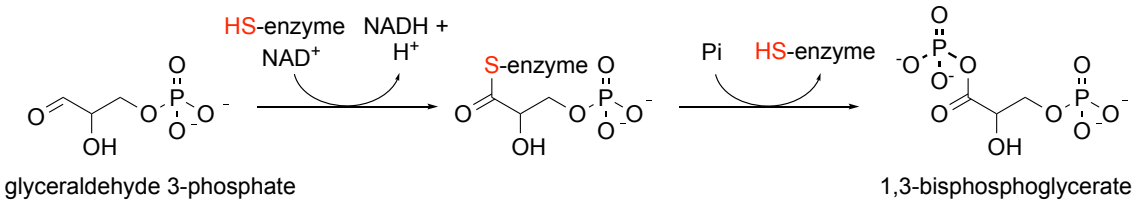

Fig 18. Thioester synthesis in glycolysis.

5. General perspective of this thesis

Within this thesis, I will describe my experimental efforts, carried out within a larger team, to perform some key metabolic reactions without enzymes, using simple aqueous, inorganic conditions, to identify a plausible protometabolism that might have operated at the origin of life. The evidence for non-enzymatic protometabolic pathways was scarce when I joined the laboratory, but since then, more chemical evidence for non-enzymatic protometabolism has emerged. Firstly, I will introduce our first success to reproduce non-enzymatically sequences of the rTCA cycle, which will be followed by the connection with a non-enzymatic W-L pathway. The last chapter will present our recent findings in prebiotic thioester synthesis, as well as its incorporation into a large network providing many intermediates and precursors to biochemistry.

Part II – The reverse TriCarboxylic Acid cycle
The rTCA cycle

1. Introduction

Due to its autocatalytic nature and its central place in biochemistry, it has been suggested that the rTCA cycle could have occupied an important role in prebiotic chemistry, which could have led to the development of early life thanks to its interesting biological intermediates.[5] As we showed in the previous section, the biological rTCA cycle is regulated by ten distinct enzymes; to be a prebiotic plausible hypothesis, it would need to be enabled by much simpler structures, as predicted by a study on the evolution of promiscuous enzymes catalyzing similar steps.[110] An observation of these enzymes showed us that many of them rely on metal-based co-factors in their active sites, this may provide us a clue on its primordial structure. This raises a fascinating question: at a prebiotic stage, could simpler inorganic catalysts have acted as proto-enzymes, which could later have evolved to their final structures once more complex organic molecules became available?

For many years, scientists have already raised the possibility of non-enzymatic reactivity: In 1974, Hartman was among the first to speculate on the emergence of a non-enzymatic metabolism based on the TCA cycle that would have evolved from a simple environment, involving the fixation of CO_2 and N_2 and requiring clays and transition state metals.[111] Later, in 1988, Wachtershäuser hypothesized a prebiotic sulfur-based analog of the rTCA cycle catalyzed by FeS minerals, with the required reducing power obtained from the oxidative formation of FeS_2.[3] In 2004, Smith and Morowitz argued that a primordial non-enzymatic metabolism, biology-resembling rTCA cycle, could be a most-favored pathway in the presence of mineral or surface catalysis, or even without specific mineral catalysis.[8] Some older experiments on hydration and dehydrations reactions of closely related substrates to those of the rTCA cycle have already demonstrated the possibility to achieve some enzymatic steps without enzymes, using only acid, base or metal ion catalyst.[112–114]

2. Previous studies on the rTCA

In parallel with theoretical hypotheses, some experimental searches for prebiotic analogue of specific reaction of the rTCA cycle (Fig 19) were reported: In 1975, Tabushi and co-workers discovered a similar biogenetic-type reaction, the reductive CO_2 fixation of acetyl-CoA to pyruvate, using a simple catalyst modelling ferredoxin activity, known as Schrauzer's complex ($(FeS_4C_4Ph_4)_2$). This non-enzymatic reaction was novel, but gave only a low yield, and required organic solvents (THF-MeOH-H_2O). In 2000, Cody and co-workers explored the potential catalytic role of iron sulfide at 250 °C and elevated pressure. In presence of formic acid, as a source of reactive carbon, pyruvate formation have been observed, with less than 1% yield.[115] A more synthetic organic variant, using electrochemistry with DMF solvent, has been proposed by Lopushanskaja to produce pyruvic acid from acetyl chloride with 60 % yield.[116]

Cody and other co-workers also looked at the non-enzymatic decomposition of citric acid in H_2O at 200 °C. From this, many biology-like decomposition reactions were observed, such as retro-aldol to acetic and oxaloacetic acid, but also parasite reactions, such as decarboxylation to 3-oxo-pentanedioic acid.[117]

In 2006, Martin and his team performed photochemical experiments on the five reduction steps in the rTCA cycle, and they found out that three of them can occur at the surface of the mineral ZnS: reduction of oxaloacetate to malate with 75 % conversion, of fumarate to succinate with 95 %, and the carboxylation of a-ketoglutarate to oxalosuccinate with 2.5 % yield.[12] The in-situ generated ZnS colloidal particles, upon irradiation by UV light, produced electrons which enable the reduction reactions of the rTCA cycle. Later, Su and co-workers examined the oxidation-reduction effect of a prebiotic $FeS/S/FeS_2$ redox system between several pairs of α-hydroxy acids and α-keto acids.[118] At high temperature, a bi-dimensional catalytic system has been discovered, which could operate with FeS and either S^0 in oxidative direction or H_2S in reductive direction. This system could promote the interconversion between pyruvate-lactate and oxaloacetate-malate, moreover to provide a possible pathway for the development of primordial redox biochemistry.

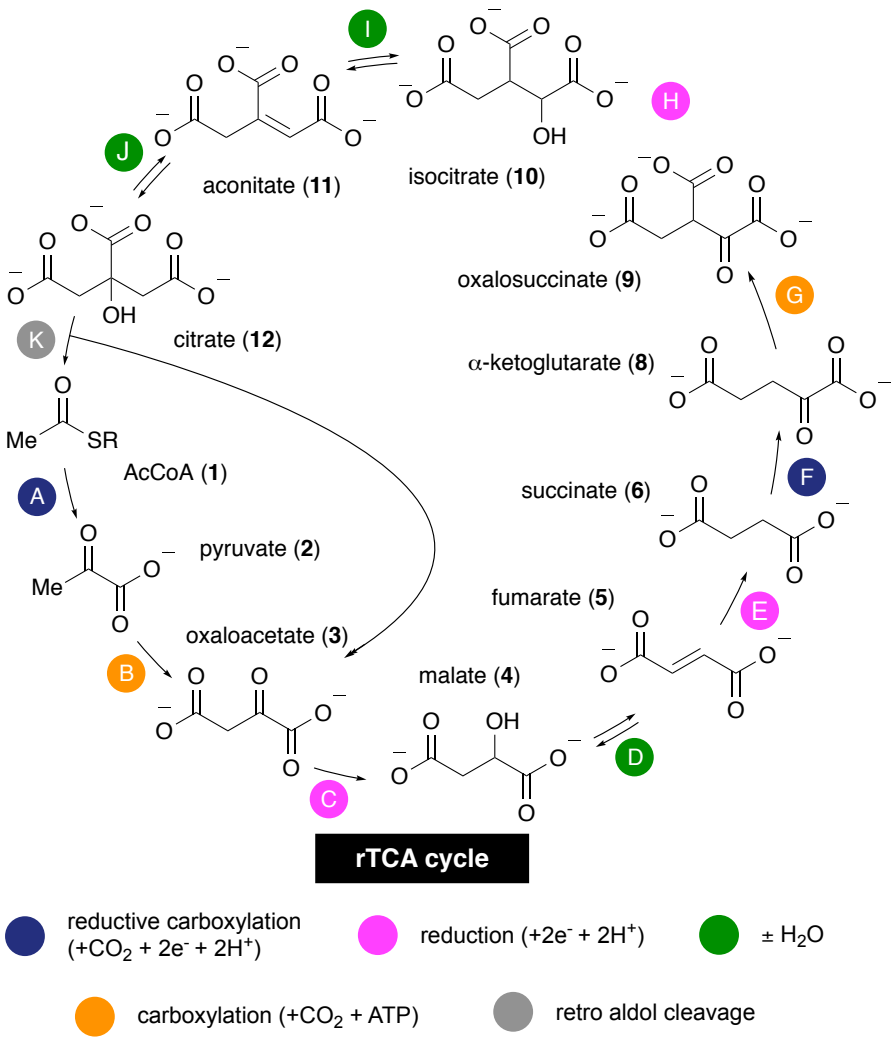

Fig 19. rTCA cycle

3. Our study – ATP independent reactions

From the previous section, only individual reactions of the rTCA cycle, all reduction reactions, have been demonstrated without enzymes. To be a plausible hypothesis for life's emergence, the rTCA reactions, or at least a sequence of reactions, need to be promoted in a continuous manner, ideally under a common set of conditions. Herein, I will introduce my research, accomplished through team work, on chemical conditions to promote all the ATP independent steps of the rTCA cycle, with plausible conditions found on early Earth. Then, I will describe our efforts to combine all of them to achieve a one-pot synthesis, to be the most relevant for life's emergence.

Parts of this chapter have been published as: Muchowska, K., B., Varma, S., J., Chevallot-Beroux, E., Lethuillier-Karl, L., Li, G., Moran, J. Metals promote sequences of the reverse Krebs cycle, *Nat. Eco. & Evo.* **1**, 1716-1721 (2017).

3.1. Reduction reactions

Our initial consideration was a search for a viable reducing agent for step C and H, corresponding to ketone reduction, along with step E, corresponding to alkene reduction (Table 5). The ketone reductions are thought to be challenging as prebiotic processes due to the rapid spontaneous decarboxylation, either oxaloacetate **3** to pyruvate **2** or oxalosuccinate **9** to α-ketoglutarate **8**.[119] Moreover, the non-enzymatic reducing system could also reduce pyruvate **2** or α-ketoglutarate **8** to off-cycle products, respectively lactate **15** and α-hydroxyglutarate **16**, and the cycle could then go no further.

Starting from different known and required reduction potentials (-0.17 V for oxaloacetate and -0.03 V for fumarate), an abiotic environment capable of driving the reduction reactions of the rTCA cycle would seem to require a reducing agent with a reduction potential lower than -0.17 V. In light of this, simple inorganic reducing agents, such as Fe^0, Ni^0, Zn^0, Mn^0, Mo^0, MoO_2 and $Na_2S_2O_4$ have been tested, at various temperatures and across pH ranges. Some potential reducible rTCA intermediates have been selected for a first investigation: pyruvate **2**, oxaloacetate **3**, fumarate **5**, α-ketoglutarate **8** and aconitate **11**. Based on the results, many metals are capable of reduction steps in acidic conditions, but only Ni^0 and Fe^0 are minimizing off-cycle reductions (Entry 1 & 2, Table 5). These two latter components are also a major component of Earth's core.[120] Though metallic iron is only occasionally found today in the Earth's crust, higher oxidation states of iron are widely abundant. Among the various reducing agents surveyed, Fe^0 was therefore selected for future experiments.

Regarding our initial interrogation, the selected condition (10 equiv Fe^0, in 1 M HCl) were tested on each step C, E and H separately, leading only to on-cycle corresponding products, with a minimum conversion of 60 % (Entry 1, 2 & 3, Table 9).

Table 5. Screen of reducing agents against a mixture of five rTCA intermediates.

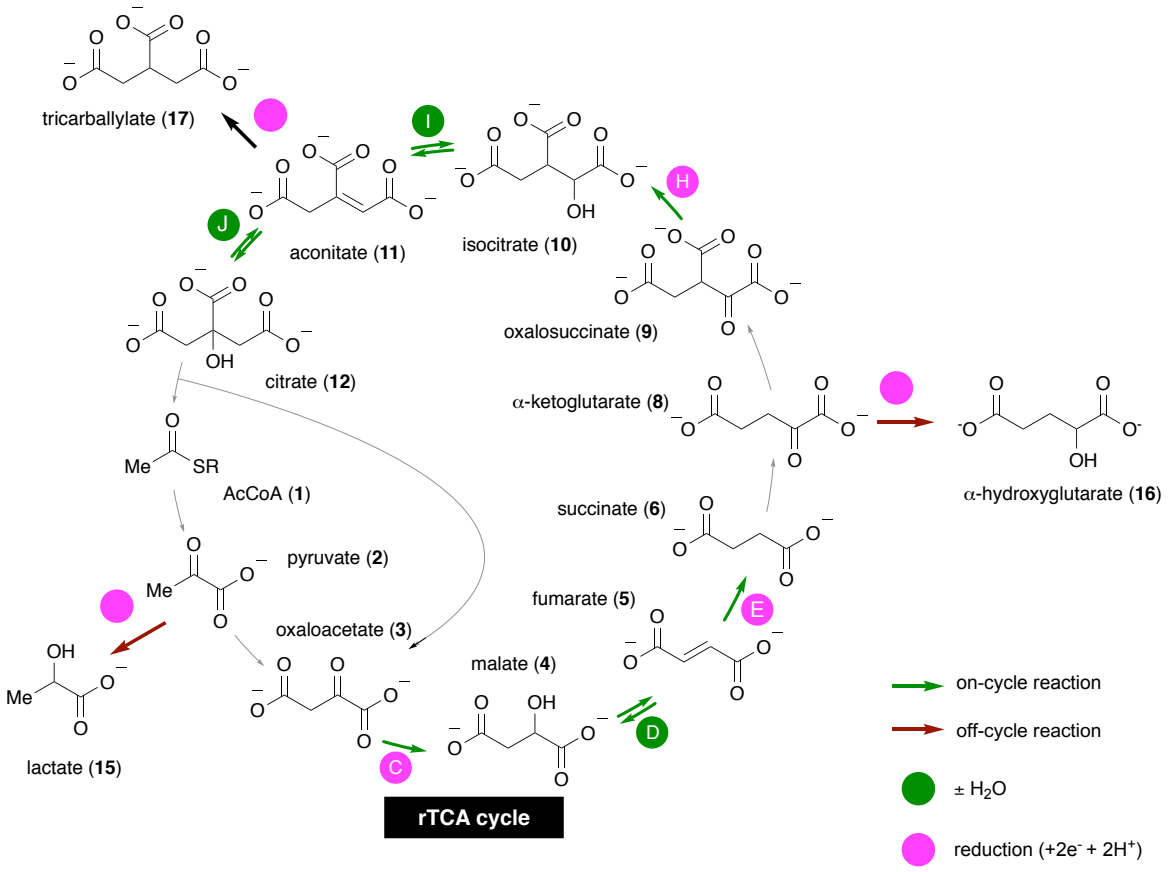

Entry	Substrates (0.1 mmol of each)	Reductant (1 mmol)	Species present in the mixture post-reaction (%)								
			On-cycle						Off-cycle		
			2	4[a]	5[a]	6	8	11	15	16	17
1		Fe	13	13	3	19	1	25	1	23	1
2		Ni	32	3	5	11	25	22	0	1	1
3		Zn	0	20	30	4	0	1	2	35	8
4	2+3+5+8+11	Mn	19	7	14	4	11	25	1	14	4
5		$Na_2S_2O_4$	35	0	14	3	14	33	0	0	1
6		Mo	No reaction (only starting materials present)								
7		MoO_2	No reaction (only starting materials present)								

Reaction conditions: 0.1 mmol of each: sodium pyruvate, oxaloacetic acid, fumaric acid, α-ketoglutaric acid, cis-aconitic acid; 10 equiv. of reductant, 3 mL 1M HCl in H_2O, 3 h, 40 °C. [a]Malate-fumarate equilibrium.

3.2. Dehydrations reactions

Next, our interest was focused on dehydration reactions (steps D & I), which are both slightly endergonic (+2.3 kJ.mol^{-1}) at neutral pH, and so unfavorable reactions compared to the hydration.[8] An initial screen of a variety of metals ions to promote the dehydration of malate **4** to fumarate **5** was unsuccessful, whatever temperature or pH tried. On the other hand, the reverse reaction, the hydration of fumarate **5** to malate **4**, was very easy to observe, even without the use of a metal catalyst (Entry 4, Table 9). To encourage the dehydrated product, we combined the dehydration reaction with the irreversible reduction step (steps D & E), to generate succinate directly from malate (Table 6).

Table 6. Screen for metals capable of promoting dehydration of malate to fumarate in tandem with reduction to succinate.

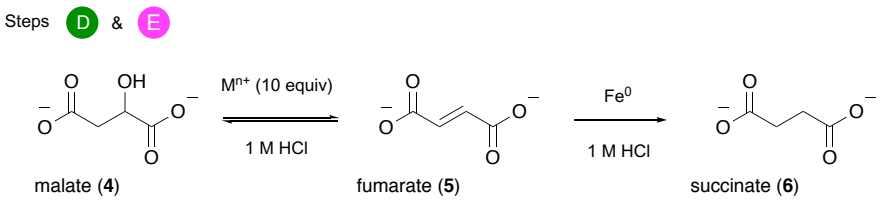

Entry	Metal salt (1 mmol)	Malate **4** (% of mixture)	Fumarate **5** (% of mixture)	Succinate **6** (% of mixture)
1	$Ni(acac)_2$	95	5	0
2	$NiCl_2$ $5H_2O$	88	12	<1
3	$FeSO_4$ $7H_2O$	94	6	0
4	$CuSO_4$ $5H_2O$	96	4	0
5	$MnSO_4$ H_2O	94	6	0
6[a]	$CoCl_2$ $6H_2O$	96	4	0
7	VCl_2	92	8	<1
8	$CrCl_2$	95	5	0
9	$Cr_2(SO_4)_3$ $12H_2O$	98	2	<1
10	$ZnCl_2$	94±1	4±1	2±1

Unless otherwise specified: 0.08 mmol malic acid, Fe^0 powder (10 equiv.), 3 mL 1 M HCl in H_2O, 16 h, 140 °C. Where applicable, errors correspond to ± mean absolute deviation.

A screen of metal ions in the presence of Fe^0 showed a little improvement, enabling low amounts of succinate formation through this two steps process with $ZnCl_2$ (Entry 10, Table 6). Some other metals offered better conversion of malate **4** to fumarate **5**, such as $NiCl_2$ (Entry 2, Table 6), but $ZnCl_2$ was selected for its ability, combined with Fe^0, to promote the best conversion to succinate **6**, also supported by some evidence on the importance of Zn^{2+} for the development of early life.[121,122]

A similar investigation has been done with the dehydration of isocitrate **10** to aconitate **11**, with a large screening of metal ions presented (Table 7). As the closer irreversible step to this step is the retro-aldol, still missing in our research expertise, the combination with another step to favorize the reversible reaction to the dehydrated product is impossible in this case. Fortunately, many metals promoted the conversion of isocitrate **10** to aconitate **11** with a good yield, and again the best one was achieved through ZnCl2 use (Entry 19, Table 7).

Table 7. Metal-promoted isocitrate dehydration screen.

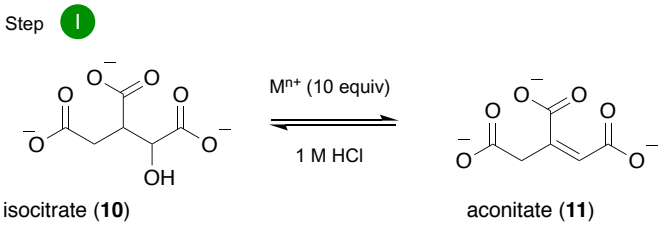

isocitrate (**10**) aconitate (**11**)

Entry	Metal salt (1 equiv.)	Isocitrate **10** (% of mixture)	Aconitate **11** (% of mixture)
1	$Ni(acac)_2$	91	9
2	$FeSO_4$ $7H_2O$	95	5
3	$CuSO_4$ $5H_2O$	94	6
4	$MnSO_4$ H_2O	94	6
5	$CoCl_2$ $6H_2O$	94	6
6	Cd(OAc) $2H_2O$	95	5
7	VCl_2	95	5
8	Fe_2O_3	95	5
9	Mn_2O_3	97	3
10	Cr_2O_3	95	5
11	As_2O_3	49	51
12	$RuCl_3$	58	42
13	$IrCl_3$	51	49
14	$RhCl_3$	54	46
15	$TiCl_3$	100	0
16[a]	$CrCl_3$	100	0
17	$Pd(acac)_2$	47	53
18[b]	$CrCl_2$	62	38
19	$ZnCl_2$	51±12	49±12
20[c]	$ZnCl_2$	93±1	7±1

Unless otherwise specified: 0.08 mmol isocitrate (as trisodium isocitrate hydrate), 3 mL 1 M HCl in H_2O, 48 h, 140 °C. [a]160 °C instead of 140 °C [b]$TiCl_3$ as 20% w/w solution in 2N HCl [c]0.5 M H_2SO_4 in H_2O, 48 h. Where applicable, errors correspond to ±mean absolute deviation.

3.3. Effect of compartmentalization

As our previous yield for malate dehydration was very low, we carried out this reaction in the presence of a 1 % w/w aqueous micellar solution of a-tocopherol methoxypolyethylene glycol succinate (TPGS), a popular non-ionic surfactant in biology. This micelle is known to promote metal-catalyzed cross-coupling reactions in water, which occurs within the spontaneously formed nanoparticles.[123] With the reaction conditions developed, the TPGS solution promoted the two-step sequence even at ambient temperature, enable the formation of succinate **6** up to 11 % (Entry 6, Table 9). Although this micelle has no direct prebiotic relevance, this experiment is a proof-of-concept that compartmentalization can improve the efficiency of prebiotic metabolic processes.[124] Unfortunately, other surfactants, such as anionic sodium dodecyl sulfate (SDC) and cationic cetrimonium bromide (CTAB), were tested without similar results.

3.4. Hydration reaction

There is only one hydration reaction in the rTCA cycle, the called step J, of aconitase **11** to citrate **12** (Table 8). First attempts were done using only acidic or basic conditions at different temperatures, but all have proved ineffective. So, an extensive screening of metal ions was performed, spanning a large pH and temperature range. That very few results are presented in Table 8, reporting only positive results among all tested conditions; a list of the different metals tested is reported in the legend. Only $Cr_2(SO_4)_3$ promote the hydration reaction with good yield, in acidic medium with 140 °C required temperature, without off-cycle reduction noted (Entry 2, Table 8). Only lower conversions were reported with other metals or lower temperature, and sometimes also promoting off-cycle product **17.**

Table 8. Metal-promoted aconitate hydration screen. ‡

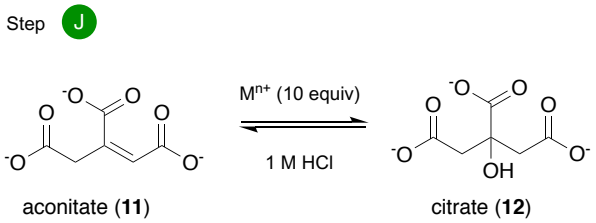

aconitate (**11**) citrate (**12**)

Entry	Metal salt (0.1 mmol)	Species present in the mixture post-reaction (%)			
		Isocitrate **10**	Aconitate **11**	Citrate **12**	Tricarballylate **17**
1	$FeCl_3$	-	99	1	-
2	$Cr_2(SO_4)_3$ $12H_2O$	-	67	33	-
3	$TiCl_3$[a]	-	82	10	9
4	$IrCl_3$	-	67	2	31
5	$RuCl_3$	-	97	3	-
6	$Co(OAc)_2$	-	98	2	-
7	$BiBr_3$	-	>99	<1	-
8	$TbCl_3$ $6H_2O$	8	92	<1	-
9	-	-	100	-	-

Unless otherwise specified: 0.08 mmol aconitate, 3 mL 1 M H_2SO_4 in H_2O, 1 h at 20 °C, then 16 h at 140 °C. [a]$TiCl_3$ as 20% w/w solution in 2N HCl

‡ In the aconitate hydration screen the following salts/oxides did not yield any citrate: CuI, $ZnSO_4$, $CuSO_4$ $5H_2O$, $NiSO_4$ $7H_2O$, $CoSO_4$ $7H_2O$, $FeSO_4$ $7H_2O$, $MnSO_4$ H_2O, $CrCl_2$, $Cd(OAc)_2$ $2H_2O$, $HgCl_2$, $Co(NH_3)_6Cl_3$, $Mn(OAc)_3$ $2H_2O$, MoO_2, MoO_3, WO_2, WO_3

Similar to the reaction enabled by the Fe-S cluster enzyme aconitase in biology, the reaction is reversible in this condition, but only using $Cr_2(SO_4)_3$ in 1 M HCl at 140 °C, starting from citrate **12** to aconitate **11** (Entry 10, Table 9). Here, the same observation with reversible step I can be made: it would be beneficial to couple the reversible hydration to a subsequent irreversible step (such as a retro-aldol reaction) in order to increase yield.

The conditions were working only in acidic conditions, with Zn^{2+} and Cr^{3+}. This phenomenon can be explained by the fact that metal cations have the tendency to become aquated at low pH, and so can coordinate with available carboxylic acids. On the contrary, under basic condition, this ability was no longer observed; metal hydroxides were formed and then precipitated. Moreover, the specific reactivity of $Cr_2(SO_4)_3$ was already observed by Olson in 1970, where he reported the hydration and isomerization of maleic acid when

coordinated to the metal.[114] By analogy, we propose mechanisms to explain the dehydration of isocitrate **10** to aconitate **11** (a, Fig 20) followed by the hydration of aconitate **11** to citrate **12** (b, Fig 20). The carboxylic acid of the intermediates can be linked to the metal center, by an exchange of one water molecule, then the hydration or dehydration can proceed with the aid of a water molecule in the second coordination sphere of the metal. This mechanism is similar to the aconitase mechanism, where Zn^{2+} acts as in its "*isocitrate mode*" and Cr^{3+} in its "citrate mode", described previously (section 3.2.4., Scheme 7).

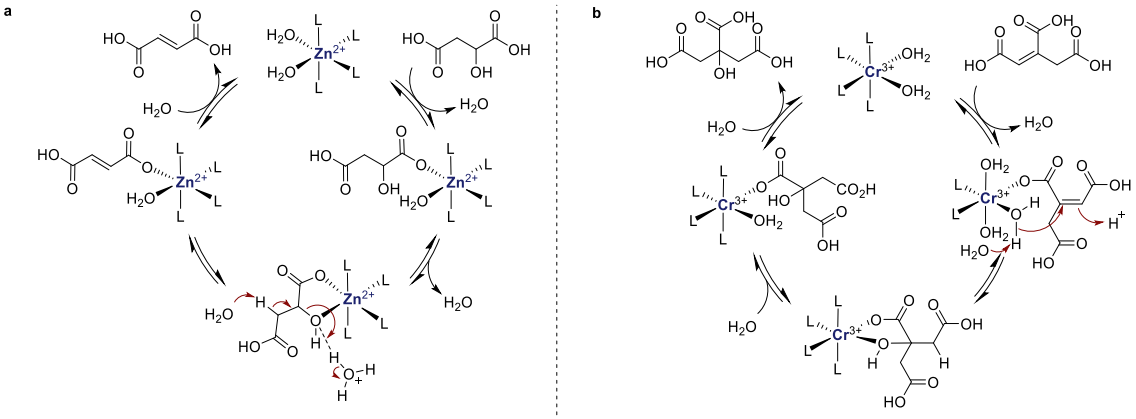

Fig 20. Mechanism of metal catalyzed dehydration and hydration reaction.

3.5. Combined reactions

As we discussed previously, a plausible prebiotic hypothesis requires the same set of conditions to enable the synthesis of multiple intermediates. In order to be the most relevant, we tried to combine the three metals (Fe^0, Zn^{2+} and Cr^{3+}) to promote three-step synthesis: Starting from oxaloacetate **3**, in micelle solution, the formation of succinate **6** was observed with 41 % yield after 24 hours at ambient temperature (Entry 11, Table 9). Only a small proportion of off-cycle product was observed, coming from the decarboxylation of oxaloacetate **3** to pyruvate **2**, which have been reduced to lactate **15**.

A similar experiment has been done, starting from oxalosuccinate **9** to citrate **12**, with and without micelle at 140 °C, required for the hydration step (Entry 12 & 13, Table 9). In both cases, the three-step sequences were working in a similar way, leading to very low yields to citrate **12**. In acidic medium, the formation of one product off-cycle was observed with

low yield, coming from the decarboxylation of oxalosuccinate **9** to α-ketoglutarate **8**, which have been reduced to α-hydroxyglutarate **16**. With micelle use, no off-cycle product was formed, the decarboxylation of oxalosuccinate **9** to α-ketoglutarate **8** went through a second decarboxylation to succinate **6**.

These results showed us the possibility to achieve two three-step sequences of the rTCA with a simple and single set of conditions, using only Fe^0 as reductant and two metal ions, Zn^{2+} and Cr^{3+} in an acidic medium. This represent more than half of the entire rTCA cycle, which can be promoted under prebiotic condition, without any enzyme.

3.6. Limitations

The main limitation of this work concerns the critical C-C bond forming reactions, the steps of reductive carboxylation and carboxylation, which are ATP-consuming. Efforts have been made in these reactions, which have so far been in vain. A substitute for ATP, or another energy supplier, seems absolutely necessary and cannot be replaced by simple metals.

The second limitation of study, which applies to all research aimed at imitating enzyme activity, concerns potential off-cycle reactions, all reducing steps, which have already been noticed previously (**Table 5**). These parasite reactions may discriminate against the plausibility of non-enzymatic metabolic cycles on the primitive Earth.[50] In fact, any simple autocatalytic cycle has to afford efficiency over > 50 % to be sustainable, and so selectively promote on-cycle reactions over off-cycle reactions. To respond to this criticism, the formation of lactate **15**, α-hydroxyglutarate **16** and tricarballylate **17** have been studied carefully: a mixture of the five intermediates of the rTCA, potential precursors to off-cycle products, were exposed to the conditions previously established (Fe^0, Zn^{2+} and Cr^{3+} in micelle solution at 40 °C for 3 hours). Less than 5 % of the compound in the mixture were off-cycle products, giving some hope concerning the sustainability of the cycle, which however requires a temperature gradient of approximately 20 °C – 140 °C (Entry 14, Table 9). Such a temperature range could be imagined to be achieved in a natural environment in regions proximal to hydrothermal vents, simply by varying the distance from the vent source. The

selectivity is more suitable to the hypothesis of a horseshoe rTCA cycle, since the three-step sequence from oxaloacetate **3** to succinate **6** is occurring even at ambient temperature.

Moreover, if a connection with another pathway to the rTCA cycle is possible, for example, by introduction of starting material for the cycle by a feeder pathway such as the AcCoA pathway, this could erase some of the remaining difficulties associated with the rTCA cycle as a potential prebiotic pathway. This "feeder" pathway of acetyl moieties would enable the cycle to be sufficient, even if the overall yield is less than 50 %. However, it is obvious that non-enzymatic conditions still need to be discovered to enable the C-C bond-forming steps of the rTCA cycle.

Table 9. Summary of reactions of rTCA cycle under unified set of conditions (Fe^0, Zn^{2+} and Cr^{3+} in 1 M HCl)

Entry	Substrate (0.1 mmol)	Conditions[a]				Species detected in the mixture post-reaction (%)[‡]										
						On-cycle								*Off-cycle*		
		Fe^0 (equiv.)	Zn^{2+} (equiv.)	Cr^{3+} (equiv.)	Micelles	**2**	**4**	**5**	**6**	**8**	**10**	**11**	**12**	**15**	**16**	**17**
Reduction																
1	**3**	10	-	-	-		90	10								
2[b]	**5**	10	-	-	-		15	20	65							
3[c]	**9**	10	-	-	-				2		98					
Hydration/Dehydration																
4[d]	**5**	-	-	-	-		77	23								
5[d]	**4**	10	10	-	-		94	4	2							
6[e]	**4**	10	10	-	yes		82	7	11							
7[d,f]	**10**	-	1	-	-						51	49				
8[d,f]	**11**	-	1	-	-						12	88				
9[g]	**11**	-	-	6	-							67	33			
10[g]	**12**	-	-	6	-							23	77			
Three-step sequences																
11[e]	**3**	10	15	4	yes		52	3	41					4		
12[h]	**9**	5	10	6	-						65	30	2		3	
13[h]	**9**	5	10	6	yes				5		72	21	2			
Competitive reduction																
14[c]	**2+3+5 8+11**	10	15	6	yes	20	6	18	4	20		28		2	2	<1

[‡] Reported values were determined by GC-MS after a derivatization procedure and represent the average of at least two runs. Compounds 3 and 8 were not detected by this method and are thus omitted. See the Supplementary Information for additional control experiments, mean absolute deviations, and crude ^{1}H NMR spectra of selected reactions. [a]Unless otherwise specified: 1 M HCl in H_2O, 16 h, 140 °C. [b]3 h, 140 °C. [c]3 h, 40 °C. [d]48 h, 140 °C. [e]20 °C, 24 h. [f]Reaction in 1 M H_2SO_4 in H_2O, 16 h, 140 °C. [g]1 h, 20 °C, 24 h, 140 °C. [h]Thermal cycling: 16 h, 140 °C; 10 h, 20 °C; 16 h, 140 °C.

4. Conclusion & perspectives

To conclude this chapter, I described herein a prebiotic way to drive in one pot two three-steps sequences of the rTCA cycle (reduction and hydration/dehydration), with only Fe^0 and two metal ions, Zn^{2+} and Cr^{3+}. These conditions, in an acidic medium with a temperature range of 20 °C to 140 °C, are compatible with acidic metal-rich environment such as those found in some hydrothermal vents.[45] Only a few proportions of parasite reactions have been observed, which support the hypothesis of a prebiotic and sustainable anabolic protometabolism which lead to the formation of five universal metabolic precursors for latter biosynthesis. Even if this study provides us some new insight on a possible prebiotic chemistry on the early Earth, the failure to replicate ATP-dependent reactions of the rTCA cycle makes us doubt its emergence at the very earliest stage of prebiotic chemistry.

Part II – The Wood-Ljungdahl pathway

1. Introduction

The Wood-Ljungdahl (W-L) pathway, as previously showed in the opening section, is considered the most ancient pathway of CO_2 fixation in nature. It connects two one-carbon molecules to make one two-carbon molecule,[7] and is hypothesized to have emerged as prebiotic chemistry.[14] Primitive organisms could have used CO or H_2 present on the early Earth as energy sources and CO_2 as an electron acceptor, a long time before O_2 appeared on the planet, to build their first intermediates.[125] The mechanism of the biological pathway is now well-understood, thanks to labelling experiments: one molecule of CO_2 undergoes reduction by six electrons to a methyl group, and another CO_2 molecule is reduced to CO by two electrons, followed by the condensation of both reduced molecules and CoA, yielding acetyl-CoA (in acetogens).[125] It is known that transition metals such as Fe, Ni, Co, Mo or W are present in the active sites of the enzymes or cofactors that catalyze the W-L pathway reactions.[75,77] However, when looking for a non-enzymatic protometabolism, we hypothesize that simple inorganic catalysts could have promoted these reactions at a prebiotic stage. In this chapter, I will first introduce different reports on replicating this biochemical process abiotically, including the findings of our laboratory. This will be followed by my attempts to reproduce this result electrochemically and to use different iron oxides in order to better understand the mechanism of this process and improve the reaction yield.

2. Previous studies on the W-L pathway

Several research teams in the origin of life field have attempted to discover a non-enzymatic way to produce acetate: many tried starting from CO_2 or HCO_3^- combined with an external reducing agent, such as reduced metals or a reducing electrode. Other more reduced C_1 building blocks have also been tested, such as CO or HCOOH, which can themselves act as the reducing agent. Wachtershäuser reported the formation of an acetyl thioester by mixing CO and CH_3SH in the presence of NiS-FeS. The thioester can then be hydrolyzed to acetic acid (Table 10, Entry 1).[126] Later, Cody proposed high CO pressure experiments (500-2000 bars) at 250 °C with alkyl thiols, exploring the catalytic role of FeS. In this experiment the formation of pyruvate from a C1 building block was observed for the first time (Table 10, Entry 2).[115] Some investigations have focused directly on CO_2 reduction. Bu used a combination of Fe powder and Ni powder at 300 °C, Takahashi and co-workers observed the formation of methane, formic acid and hydrogen, but no acetate during this process (Table 10, Entry 3).[127] Fend and co-workers used milder conditions, at 200 °C, in the presence of iron nanoparticles, which act as the reducing agent and also catalyze the reduction of CO_2 to formic acid and acetic acid (Table 10, Entry 4).[128] Some investigations also used electrochemical reduction. A study from chemists working outside a prebiotic context proposed N-doped nanodiamond to catalyze the CO_2 reduction with a high faradaic efficiency at a low reducing potential (Table 10, Entry 5).[129] Another study by de Leeuw and co-workers showed that CO_2 can be reduced into methanol, formic, acetic and pyruvic acid by using a greigite surface on application of a relatively small potential, at atmospheric pressure and room temperature (Table 10, Entry 6).[130]

These investigations are summarized in Table 10. Most of them are geologically unrealistic in a prebiotic context, since they involve high temperatures, high pressures and strong reducing potentials.

Table 10. Non-enzymatic W-L pathway analogues

Entry	Carbon source	Reducing agent/catalyst	Reaction Conditions	Product Yields				Ref.
				Formate	Methanol	Acetate	Pyruvate	
1	CO (1 bar), CH_3SH	FeS-NiS (1:1)	pH 8, 100 °C, 7 days	-	-	3.28 mM	-	126
2	CO, RSH	FeS	500-2000 bar, 250 °C, 6h	-	-	5.5×10^{-5} mmol	7.7×10^{-5} mmol	115
3	CO_2 (22.5 mmol)	FeNi	300 °C, 6h	1.4 mM	-	-	-	127
4	CO_2 (14 bar), H_2O	Fe^0 (5 mmol)	200 °C, 72 h	8.5 mM	-	3.5 mM	-	128
5	$NaHCO_3$ (aq)	N-doped diamond electrode	rt, 1 h, - 0.8V *vs.* RHE	1.2 mM	-	16.1 mM	-	129
6	sat. CO_2	Greigite electrode	pH 6.5, 120 h, rt, cycle between 0.2 and - 0.8V *vs.* NHE	1.3 µmol	0.35 µmol	0.57 µmol	0.48 µmol	130

In order to find a suitable way to form acetate and pyruvate, the first two intermediates of the rTCA cycle, our laboratory studied the reduction and fixation of CO_2 into higher-carbon products under prebiotically plausible conditions. An introduction of this discovery, which led to my project, will be now briefly presented.

3. Fe^0 as a catalyst for CO_2 fixation

Anticipating a link between the role of metallic cofactors found in the biochemistry of living organisms and natural catalysts required for prebiotic chemistry, we postulated that the native forms of the metals involved in the reductive W-L pathway might promote C-C bond formation from CO_2 in water. Therefore, an extensive screening of metal iron powders was performed in 1 M KCl aqueous solution at different temperatures, reaction times and CO_2 pressures. The main results will be presented below.

Parts of this section have been published as: Varma, S., J., Muchowska, K., B., Chatelain, P., Moran, J. Native iron reduces CO_2 to intermediates and end-products of the acetyl-CoA pathway, *Nat. Eco. & Evo.* **2**, 1019-1024 (2018).

3.1. Effect of physical parameters

In the initial experiments, Fe, Co, Ni, Mn, Mo and W powders in 1 M KCl aqueous solution were screened. Upon heating to 100 °C under 35 bar CO_2 pressure for 16 hours, all of these metals promoted the formation of acetate with a concentration of up to 0.28 mM in the case of Mo, and some traces of pyruvate were observed with Fe, Ni and Co. Substantial quantities of formate and methanol (up to 2.3 mM and 0.4 mM respectively) were also found in almost all cases. Due to being the most Earth-abundant metal,[131] iron was selected for further experiments to test the influence of temperature, pressure, time, pH, salt identity and salt concentration on the reaction outcome (for the complete study, see Supporting information of Native iron reduces CO_2 to intermediates and end-products of the acetyl-CoA pathway).

Experiments evaluating the effect of temperature over the 30-150 °C range (Fig 21, **a**) showed that acetate is formed across the whole temperature range tested, and its concentration increases with the temperature. At 100 °C, the appearance of methanol and other products is observed. Pyruvate is no longer observed at 150 °, probably due to its thermal oxidative decarboxylation to acetate.

Then, the influence of CO_2 pressure over a range of 1-40 bar was investigated and revealed that the reaction is robust (acetate is observed over the entire pressure range). Acetate and pyruvate are the two major products at lower pressures (Fig 21, **b**).

Finally, the reaction was followed over time: at 30 °C and 1 bar CO_2 (Fig 21, **c**), and at 100 °C and 35 bar CO_2 (Fig 21, **d**). In the first case, acetate and pyruvate are the major products, with a maximum concentration of 0.7 mM and 0.04 mM obtained after 40 hours and 20 hours respectively. In the second case, the formation of formate is initially rapid and starts to decrease after 6 hours, whereby acetate and pyruvate are formed. After 60 hours, acetate and pyruvate reach maximum concentrations of 1.09 and 0.11 mM respectively.

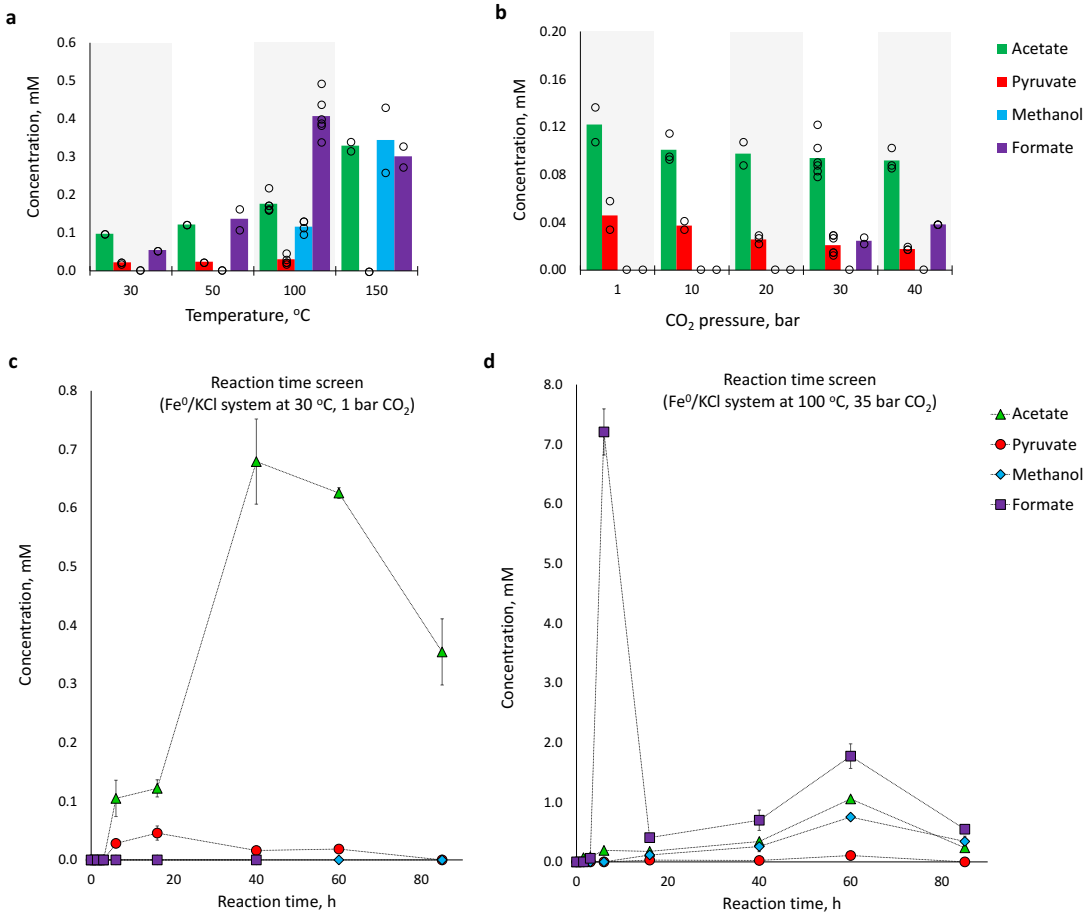

Fig 21. Effect of temperature, pressure and reaction time on iron-promoted CO_2 fixation in aqueous solution. **a** Effect of temperature (35 bar CO_2; 16 h). **b** Effect of CO_2 pressure (30 ˚C; 16 h). **c** Reaction progress over time (30 ˚C; 1 bar CO_2). **d** Reaction progress over time (100 ˚C; 35 bar CO_2). All reactions are 1 M Fe in 1 mL of a 1 M KCl solution. In **a** and **b** bar charts show mean values of at least two independent runs. In **c** and **d** error bars correspond to the mean average deviation from at least two independent runs. Lines connecting the data points do not represent a model fit.

To conclude, our laboratory found that several transition metals in their elemental forms are capable of reducing CO_2 to acetate and pyruvate under different sets of conditions. The reaction is robust to differences in temperature, pH, pressure and salts tested. The Fe-promoted CO_2 fixation is potentially relevant for prebiotic chemistry, since it was possible in the early Earth's environment.

3.2. Mechanistic considerations

Several experimental observations helped us to propose a plausible mechanism for this CO_2 reduction reaction (Fig 22). The main one was the absence of product unless a basic workup with KOH is performed before the NMR analysis (for complete study, see [16]). We concluded that CO_2 reduction occurs on the surface of the metal, combined with migratory insertion of CO or reductive carboxylation with CO_2, where its intermediates and end-products remain bound to the surface during the reaction. The basic workup at the end of the reaction is required to liberate the different observed intermediates in solution, such as formate, methanol, acetate and pyruvate. Lactate is not observed despite the fact that pyruvate is readily reduced in solution in the presence of Fe^0, which can be rationalized by a diminished reactivity of pyruvate bound to the surface.

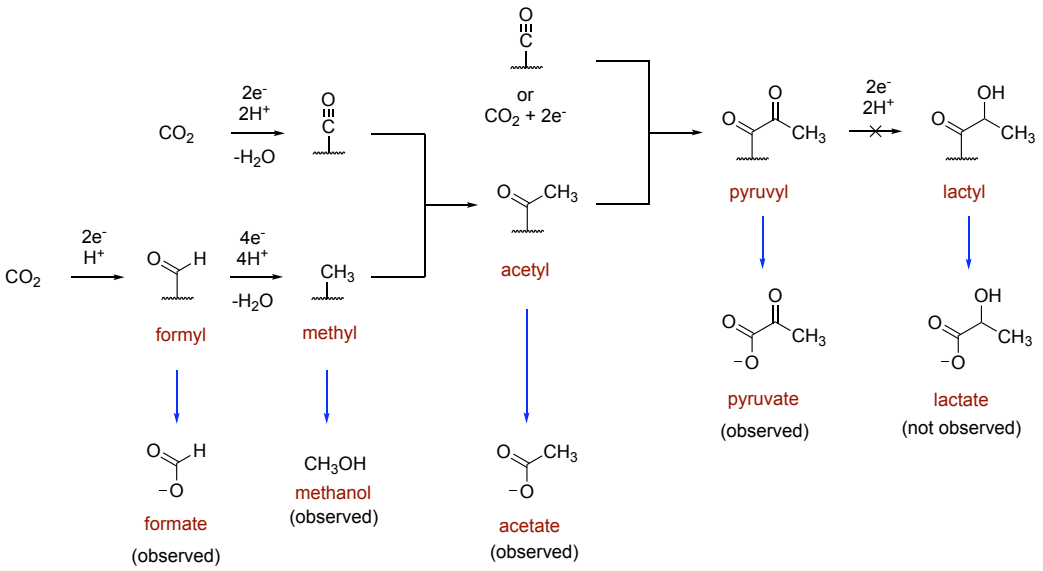

Fig 22. Plausible mechanism for carbon fixation on the surface of Fe^0 accounting for the detection of formate, methanol, acetate and pyruvate in aqueous solution upon hydrolysis with KOH. The depicted surface bound acyl structures are deliberately ambiguous and may represent a surface-bound carboxylate or an acyl metal species.

The observed product distribution demonstrates an important parallel between prebiotic chemistry and the ancient W-L pathway used by primitive autotrophic organism, supporting the hypothesis that geochemistry could have played an important role in the origin of life, as first proposed by Wachtershäuser with his surface metabolism theory.[132]

In order to investigate the reaction mechanism, I have conducted metal analysis, attempted to develop an electrochemical version of the reaction on iron wire, and screened various iron oxides as catalysts. I will introduce the results from these studies in the following sections.

4. Physical studies on iron powder for CO_2 fixation

To better understand the reaction mechanism proposed in the previous section on CO_2 fixation on the metal surface, an investigation on the metal itself was first conducted. The iron powder was characterized by a collaborator, Dr. Harun Tueysuez from the Max Planck Institut für Kolenforschung. The analyses were performed on a sample of commercial iron powder (Sigma Aldrich), and four different samples of the iron powder left after the reaction (35 bar of CO_2, heated at 100 °C for 16 hours).

Different methods were used to characterize the five samples: first, Scanning Electron Microscopy (SEM) was used to investigate the morphology and structure of the materials (Fig 23). From this, it can be noticed that the initial sample is mainly composed of bulk particles with a diameter of 100 µm (Fig 23, Initial sample), with small particles of a few micrometers found on the surface of bulk particles. After the reaction under CO_2 pressure (Fig 23, Batch 1), the samples collected showed much smaller particles with a much smaller size, in a range of several micrometers.

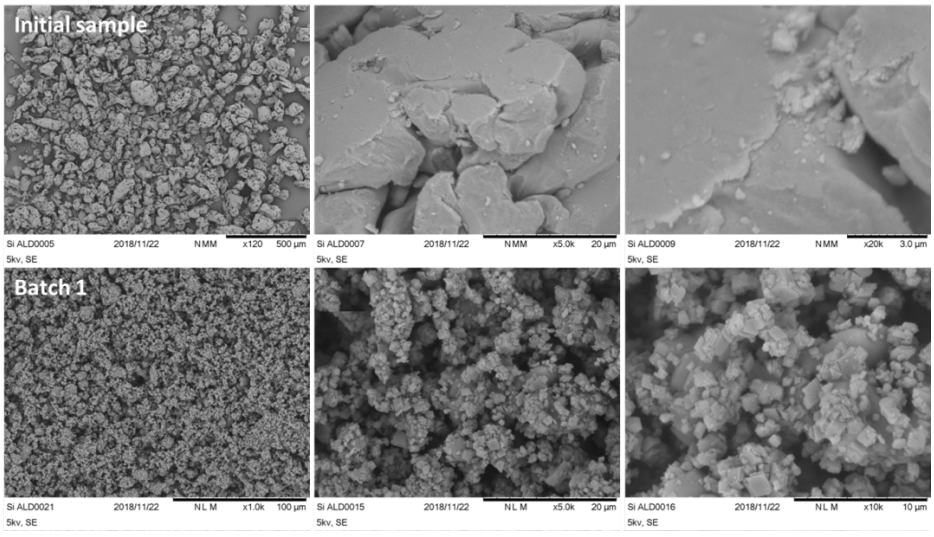

Fig 23. SEM images of the Fe^0 powder before (initial sample) and after the reaction (35bar of CO_2, 100 °C, 16 hours – Batch 1)

The crystal structure of the samples was then examined by using wide-angle X-ray diffraction (XRD) analysis (Fig 24). The XRD pattern of the initial sample shows distinct reflection that matched with the crystal structure of metallic Fe^0 (Fig 24, Initial sample). After reaction, the collected samples exhibit a characteristic crystal phase of $FeCO_3$ (Fig 24, batch 1–4). From this, it is evident that the iron surface morphology and its crystal structure change throughout the CO_2 fixation reaction. There might still be some amount of Fe^0 remaining after the reaction (which cannot be detected by XRD due to the detection limit), since the samples (batch 1–4) respond to a strong magnet, just like Fe^0 (see Part V - Experimental part, Fig 78 for data).

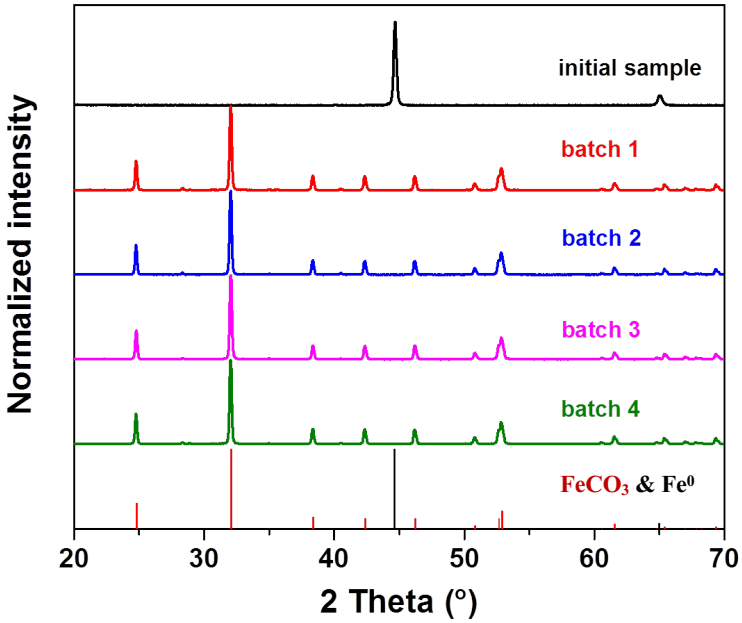

Fig 24. XRD patterns of the Fe^0 powder before (initial sample) and after the reaction (35 bar of CO_2, 100 °C, 16 hours – Batch 1-4) Last plot is the simulation of pure samples (red: $FeCO_3$, black: Fe^0)

In addition, Fourier-Transform InfraRed (FT-IR) spectra of each sample were collected to verify the formation of $FeCO_3$, thanks to the characteristic vibrational modes of carbonate anion (CO_3^{2-}) (Fig 25). As expected, the three specific vibrational absorptions of CO_3^{2-} at 1387, 858 and 738 cm^{-1} were visible on the samples after the reaction ((Fig 25, batch 1–4). These are the fingerprint peaks of carbonate vibrations of the asymmetric stretch (ν_3 mode), the

out-of-plane bend (ν_2 mode), and the in-plane bend (ν_4 mode), respectively. These results validated the formation of iron carbonate from Fe^0, in line with the XRD results.

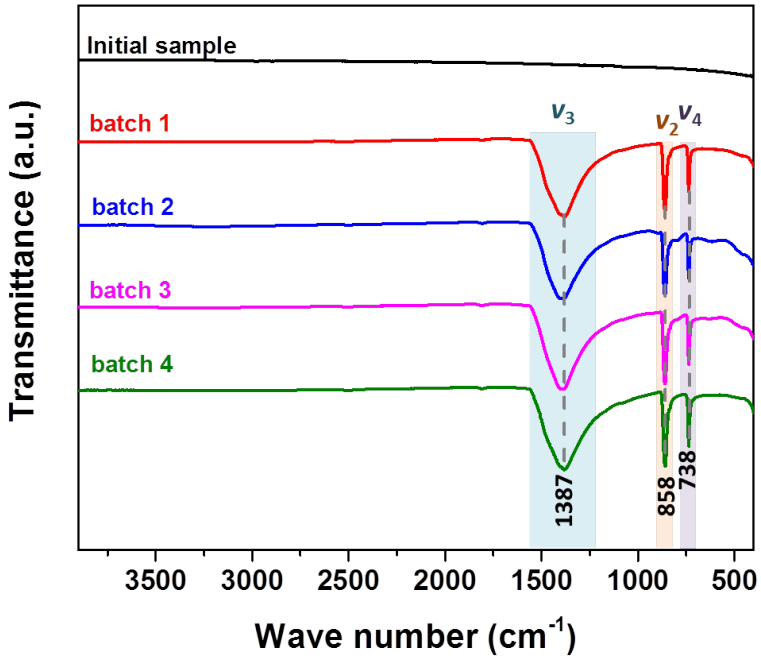

CO3 bonding:

- V2 (858 cm^{-1}): out of plane bend
- V3 (1387 cm^{-1}): asymmetric stretch
- V4 (738 cm^{-1}): in plane bend

Fig 25. FT-IR spectra of the Fe^0 powder before (initial sample) and after the reaction (35 bar of CO_2, 100 °C, 16 hours – Batch 1-4)

To conclude this section, the initial bulk metallic sample is converted to iron carbonate under CO_2 pressure and heat, with changes observed in its crystal structure and its morphology. Neither the SEM nor the XRD measurements support the hypothesized mechanism where different intermediates bound to the surface were expected to be observed. However, iron oxides formed from the reaction could have reacted with CO_2 present in the atmosphere, during the transport or the time between the experiment and the analysis, which could explain these results. Nevertheless, it is certain that the structure of the metal changes as a result of the reaction, meaning that iron takes part in the reaction, as expected, and is oxidized during the process. To explore the mechanism further, electrochemical investigations were carried out.

(more detailed data of this study can be found in the Part V - Experimental part)

5. Electrochemistry on iron wire

Electrochemical reduction of CO_2 to acetate using metal catalysts has been reported in the literature.[129,130] The objective here was to verify if it is possible to use Fe^0 as electrode to fix CO_2 into C_2 and C3 products under milder condition, at ambient temperature and under atmospheric CO_2 pressure. For this reason, the study of the activity of an iron wire under applied electrochemical potentials was chosen to help better understand the mechanism and support the hypothetical surface mechanism of CO_2 reduction.

5.1. Previous electrochemical studies on CO_2 reduction to acetate and pyruvate

A major need exists to develop renewable sources to meet the growing global energy demand. This is why many laboratories focused their efforts on developing catalysts capable of reducing CO_2 to value-added products. As already mentioned earlier, an efficient nonmetallic electrocatalyst for CO_2 reduction was proposed by Yu and coworkers, who used an N-doped nanodiamond with a high faradaic efficiency of 90 % achieved at -1.0 V.[129] This material preferentially and rapidly converted CO_2 to acetate over formate.

Metallic copper was also largely explored, with an incomparable efficiency in forming hydrocarbons compared to other metals, but showing a poor stability, selectivity, and high overpotentials.[133–135] Indeed, Jaramillo and co-workers reported the formation of up to 16 CO_2 reduction products on a Cu electrode surface.[136] Then, Baker and co-workers reported the use of a mixed Fe-Cu oxide catalyst which under a visible light illumination converted CO_2 to acetate with 80 % faradaic efficiency.[137] They demonstrated that CuO itself is not selective to CO_2, Fe_2O_3 alone is not active as a photocatalyst for H_2 evolution or CO_2 reduction, but a good mix of both offers a selectivity for CO_2 over H^+ reduction.

The study of de Leeuw and co-workers showed that an iron sulfide mineral, greigite, is also able to promote the formation of acetate from CO_2 in aqueous solution, with relatively small potential and under mild conditions.[130] They found an optimum pH of 6.5 for the

reaction on the greigite surface. At lower pH values, H_2 generation competes with HCO^{3-} reduction, and at higher pH values the active sites are deactivated due to OH accumulation. More recently, Arrigo and co-workers reported a nanostructured iron (III) oxyhydroxide on nitrogen-doped carbon could be used for CO_2 reduction at an up to 97% faradaic efficiency and selectivity for acetic acid at very low potential.[138] They demonstrated that carbon surface chemistry influences significantly the redox chemistry of Fe, with a strong impact on the catalytic performance.

Finally, the surface mechanism of CO_2 reduction has been studied in detail for copper catalysts or other more complex materials, but no investigations have been done for Earth-abundant metals like Fe^0 which may offer similar reactivity. In the following sections, I will describe my attempts to reproduce our previous results (section 3) under milder conditions, with an iron wire as catalyst and electrode for CO_2 reduction.

5.2. Fe^0 wire as the catalyst

In order to test the hypothesis that an iron wire could act as a catalyst for CO_2 reduction under applied electrochemical potentials, collaborations were established with two electrochemistry laboratories from the Université de Strasbourg, directed by Pr. Ruhlmann and Pr. Hellwig.

A pure iron wire (99,99+ %) was used for all the experiments, instead of metallic iron powder used for the previous study. In each of the collaborations, different reaction conditions were tested. I will first describe the experiments performed with Pr. Ruhlmann. The experimental setup was composed of an iron wire (working electrode), a saturated calomel electrode (SCE – reference electrode) and glassy carbon (counter electrode), which were all assembled within a cell, with or without a separation for the cathode (Fig 26). CO_2 was added as gas, with a slow and constant flow into the electrolyte (0.5 M K_2SO_4/0.05 M $KHCO_3$). The experiments were analyzed by ^1H NMR with water suppression, as previously described (full description is available in the Part V - Experimental Part).

a

b

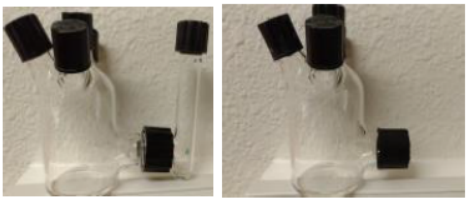

Fig 26. Electrochemical cell setup used for CO_2 reduction. **a.** Entire assembly of the cell with all connections and the three electrodes (SCE, glassy carbon and iron wire). **b.** Cell with and without sintered glass.

The experiments were conducted over a potential range of - 0.75 to – 1.25 V, with the intention to stay in the immunity area of iron (pH = 6.8, $E^0(Fe^{2+}/Fe)$ = - 0.68 V vs SCE), as Fe^0 was believed to be the active catalyst for CO_2 reduction (Fig 27).

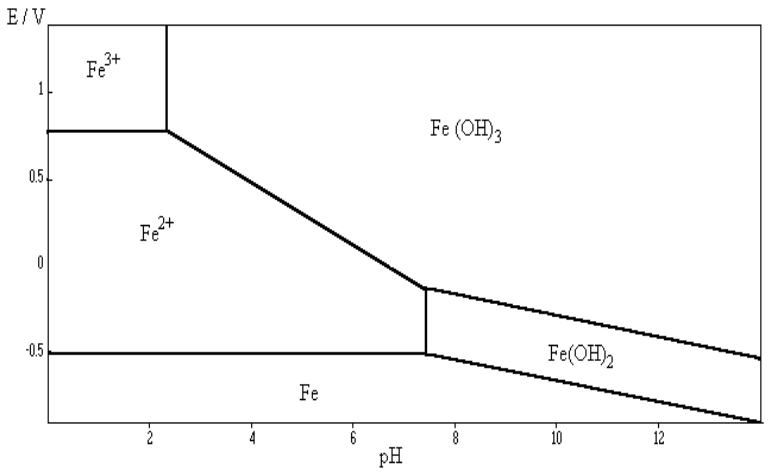

Fig 27. Potential/pH diagram of iron.

The initial results were promising (Fig 28), with high concentrations of acetate obtained after only 20 min (5 mM at – 0.75 V and 6 mM at – 1 V), but the observed values fluctuated strongly over time. Moreover, some acetate was observed from the beginning, coming directly from the cell (this value was lower than the maximum obtained). In one run, lactate, which results from pyruvate reduction, was observed in large quantities. This result was really exciting, because lactate is the result of a three steps sequence: first acetate formation from CO_2, followed by reductive carboxylation leading to pyruvate, which can then be reduced to lactate. However, subsequent attempts to reproduce this result were unsuccessful. Control experiments with water or KOH alone did not reveal any contamination. In order to remove potential impurities which could have come from the sintered glass, the same experiments were done in the cell without separation (Fig 26, b).

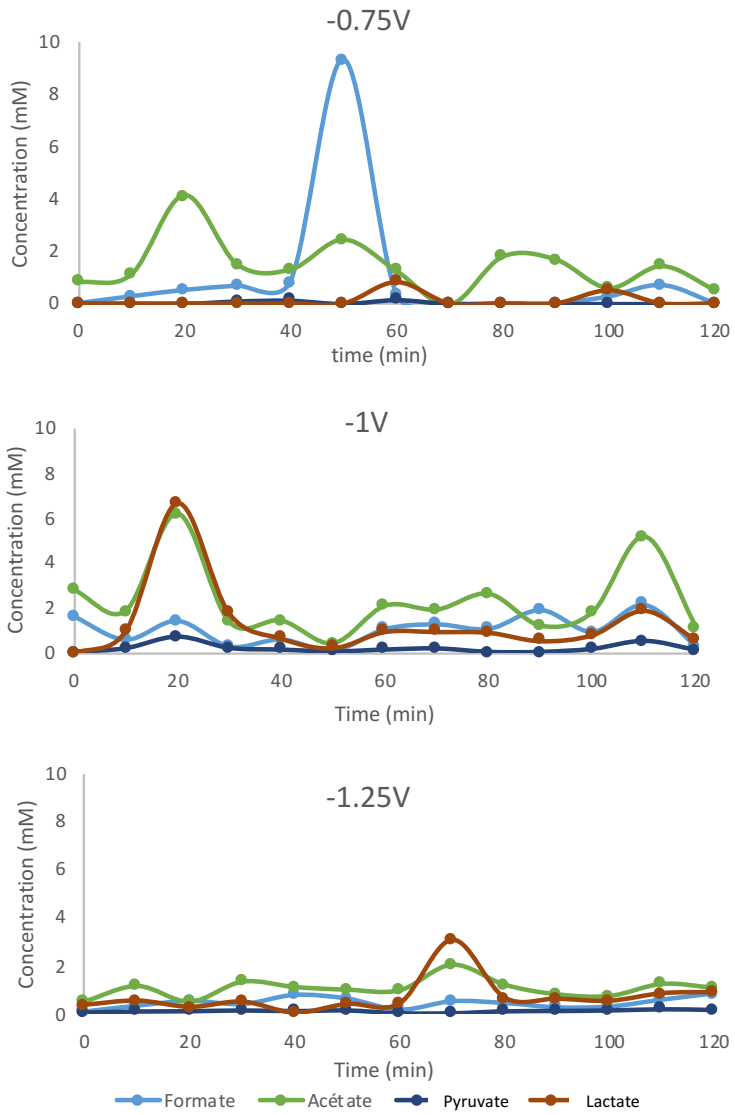

Fig 28. Concentrations of formate, acetate, pyruvate and lactate over time, with different applied potentials in a cell with sintered glass separation of the cathode (- 0.75 V, - 1 V, - 1.25 V).

The same experiments without the cathode separation (meaning that the counter electrode is in the same compartment as the two other electrodes) also returned inconclusive results (Fig 29). Lactate was still detected at -0.75 V and -1.0 V, but the observed concentrations were lower than those shown in Fig 28. Moreover, these results were not reproducible and lactate concentrations in subsequent experiments dropped to zero, even when the iron wire was replaced with a fresh one.

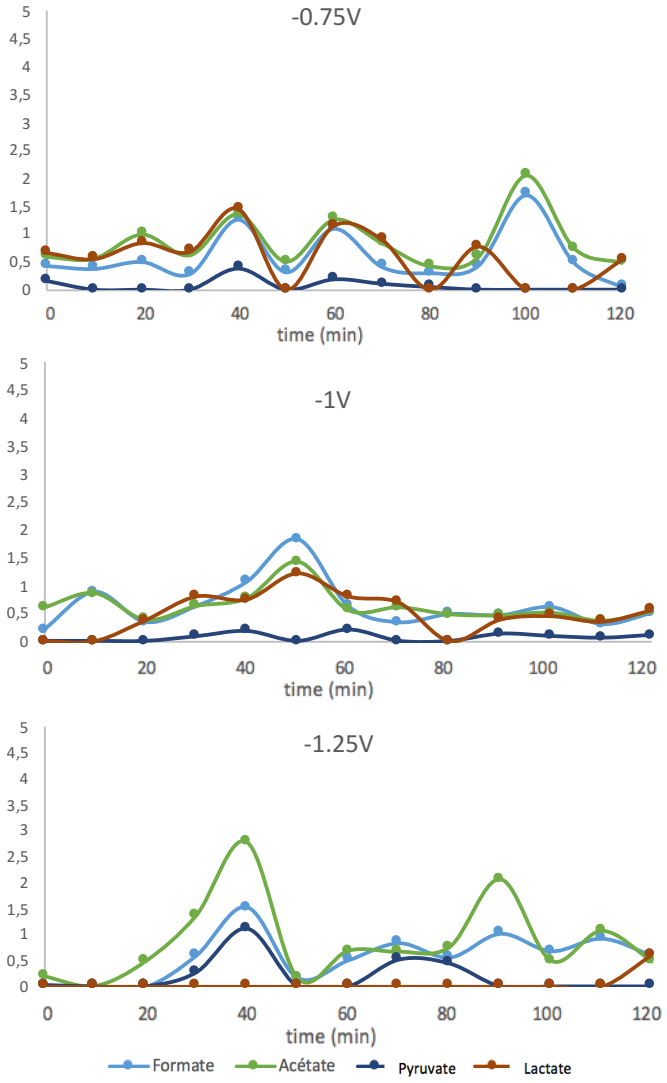

Fig 29. Concentrations of formate, acetate, pyruvate and lactate measured over time, with different applied potentials in a cell without sintered glass separation of the cathode (- 0.75 V, - 1 V, - 1.25 V).

Due to the impossibility to reproduce the results above, we considered a different experimental setup in collaboration with Pr. Hellwig. Oxygen is known to interfere with electrochemical experiments, reacting with the metal electrode to form a layer of metal oxide on its surface, making the electrode surface inactive.[139] To prevent this, the experimental setup was assembled in a glove bag. The assembly was composed of an iron wire (working electrode), a silver chloride electrode (AgCl/Ag - reference electrode) and a graphite one (counter electrode), which were all combined within a beaker. CO_2 was added as gas, with a slow and constant flow into the electrolyte (0.1 M K_2HPO_4 or 0.1 M KCl). The experiments were conducted in a potential range of - 0.72 to – 1.25 V, with the intention to stay in the immunity area of iron (pH = 7, $E^0(Fe^{2+}/Fe)$ = - 0.65 V vs AgCl/Ag). No W-L pathway intermediates were found in solution, except for occasional low quantities of acetate (> 0.01 mM). Overall, the exclusion of oxygen did not influence the reactivity, and did not bring us closer to understanding the results.

5.3. Fe oxide as the catalyst

Another hypothesis could be that iron oxide, and not metallic iron, is the true CO_2 fixation catalyst. Our first promising results could have been obtained after a partial oxidation of the iron wire, which was then able to catalyze the reduction of CO_2. After some time, the iron oxides were not any more present at the surface, oxidized into some inactive species or released from the surface. That may explain why interesting results were obtained at first, but then concentrations started to decrease in the subsequent experiments.

In order to confirm this hypothesis, we swapped around the cathode and the anode, meaning the iron wire became the counter electrode, and the graphite one was the working electrode. By applying a negative potential to the graphite electrode (- 1 V), we oxidized the iron wire. After 3 hours of experiment, no intermediates were detected, but the iron wire was found to be oxidized on the surface. Subsequently, a negative potential was applied to the oxidized iron wire (- 1.25 V) for 5 hours, in order to reduce CO_2 at the surface of this electrode. Unfortunately, no WL pathway products were detected in this experiment. Possible reasons might be that the time of the experiment was too short to enable the formation of products above the detection limits, or the oxides at the surface of the electrode were too rapidly reduced to Fe^0 (which does not take part in surface chemistry here).

The non-enzymatic CO_2 fixation seems to proceed through a complex mechanism, which we could not reproduce with electrochemistry. The failure to reproduce the results from section 3 could not be explained so far, and no information about the mechanism could be extracted from these experiments. Nevertheless, the role of iron oxides in the formation of the W-L pathway intermediates was investigated further, in experiments under pressure, analogously to those described in section 3. These experiments described below could help us understand the active species required for the reaction and provide insight into its surface-mediated mechanism.

6. Iron oxides as the true catalysts for CO_2 fixation

Results from physical studies and electrochemistry indicate the possibility that iron oxides promote the reaction of CO_2 fixation, and not Fe^0. In order to verify this hypothesis, different iron oxides will be tested under CO_2 fixation conditions and the results - presented in this section.

6.1. Recent updates

Recently, a paper from a collaboration between our group, and the groups of William F. Martin and Harun Tüysüz described a new abiotic analogue of the acetyl-CoA pathway from H_2 and CO_2, with three minerals found in hydrothermal vents – awaruite (Ni_2Fe), magnetite (Fe_3O_4) and greigite (Fe_3S_4).[140] Using these minerals as catalysts enables the synthesis of formate and acetate (major products) as well as methanol and pyruvate (minor products) from CO_2 and H_2 under hydrothermal conditions. The idea to employ iron minerals was inspired by the fact that under physiological conditions the reducing power of H_2 is insufficient to reduce CO_2. For this reason, living organisms using the W-L pathway employ flavin-based electron bifurcation to synthetize reduced iron sulfur clusters in ferredoxin, a protein used in CO_2 fixation. This study shows that sufficient H_2 combined with suitable inorganic catalysts also allows for the synthesis of W-L intermediates, which are essential at the origin of metabolism, with no additional energy source. These findings suggest that H_2 could have played a role in the reduction of CO_2 on the early Earth, and minerals could act as catalysts.

In the Fe^0-mediated CO_2 fixation experiments[16], one possible mechanistic scenario is that Fe^0 could have been the reagent for H^+ reduction, generating H_2 in-situ which would then act for CO_2 reduction. However, in the scenario involving H_2 and iron minerals, the iron oxide could then act as catalyst for CO_2 reduction by H_2. In order to evaluate this hypothesis, we tested different iron oxides under different conditions, e.g. pressurized with only CO_2 or CO_2 mixed with H_2, to understand the role of each reagents in this reaction. A new plausible mechanism will be presented in a subsequent section.

6.2. Effect of different iron oxides

In order to test the reactivity of different iron oxides that could be formed from Fe^0 oxidation, the same conditions as those used by Martin and co-workers were tried: acidic (pH 4-5) and neutral (pH 7-8, adjusted by adding KOH).[140] First, the oxides were mixed with water and pressurized under 10 bar of H_2 and 15 bar of CO_2 (25 bar total gas pressure), and heated for 16 hours at 100 °C. The stoichiometry of the oxides was scaled to correspond to either 1 mmol of metal atoms ("M low") or 3 mmol of metal atoms ("M high"). The results are presented below for both conditions (Fig 30-Fig 31). All concentrations shown were calculated based on the ^{1}H NMR data. All experimental and analytical details are described in Part V-Experimental Part.

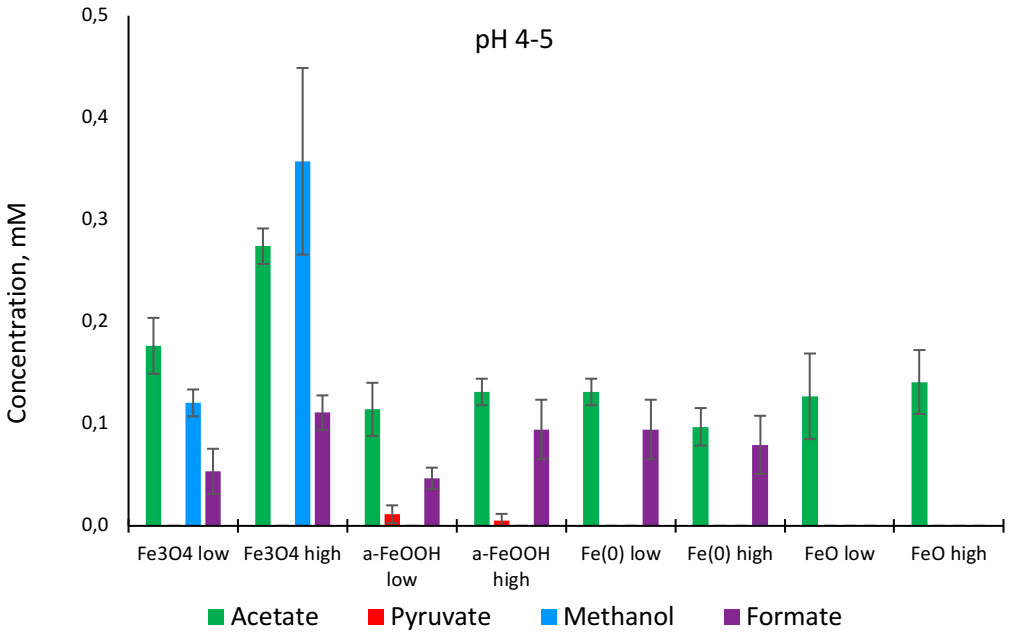

Fig 30. Concentrations of detected CO_2 reduction products obtained under CO_2/H_2 atmosphere (total pressure 25 bars) with iron oxide or metallic iron powder (low meaning 1 mmol of metal atoms, high meaning 3 mmol of metal atoms) in 1 mL H_2O each, at pH 4-5 at 100 °C for 16 hours.

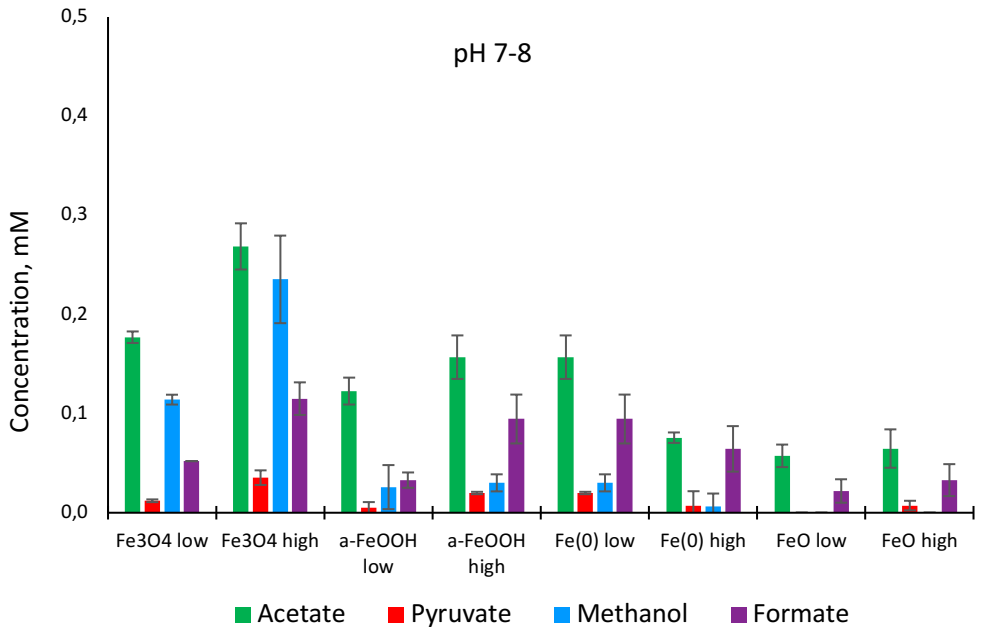

Fig 31. Concentrations of detected CO_2 reduction products obtained under CO_2/H_2 atmosphere (total pressure 25 bars) with iron oxide or metallic iron powder (low meaning 1 mmol of metal atoms, high meaning 3 mmol of metal atoms) in 1 mL H_2O + 45 mg KOH each, at pH 7-8 at 100 °C for 16 hours.

From these results, one iron oxide seems to stand out from the others: magnetite (Fe_3O_4). Compared to the results obtained with Fe^0 in the previous publication from our laboratory[16], the concentrations of acetate are 2 times higher with magnetite, up to 0.3 mM with 1 mmol Fe_3O_4 per 1 mL H_2O (3 mmol metal atoms, "Fe_3O_4 high" in Fig. 10 and 11). Slightly basic conditions enable the formation of pyruvate for almost every mineral, up to 0.035 mM with high Fe_3O_4. The pH seems important for promoting a further insertion of a C_1 unit. Moreover, Fe_3O_4 yields the highest concentration of formate (0.11 mM) and methanol (0.35 mM), compared to 0.03 mM and 0.09 mM respectively, with Fe^0. As the mechanism is still unknown, it is not known if formate and methanol are side products, which could be detrimental, or if they are intermediates that could eventually lead to acetate or pyruvate but are cleaved off from the surface during the analysis. Analysis of this catalyst in collaboration with the Tüysüz group revealed the surface of the mineral catalyst to be unchanged after the reaction[140], which means it is a robust catalyst for CO_2 reduction with H_2, giving C3 products. Moreover, Fe_3O_4 was probably abundant on the early Earth, and might have occurred in hydrothermal vents[141], which suggests that this simple route is a good candidate for the origin of protometabolism, as proposed by Martin and coworkers[140].

Results obtained with goethite (α-FeOOH) are also interesting, since it catalyzes the synthesis of pyruvate (up to 0.02 mM) under both slightly acidic and slightly basic conditions. The production of methanol is observed only under basic conditions, while acetate and formate are obtained in both pH ranges. It is known that α-FeOOH can be transformed to Fe_3O_4 upon immersion in deoxygenated water, by a dissolution-precipitation mechanism as a cathodic reaction in the corrosion cell.[142] This could explain the results obtained with goethite, with a similar mechanism proposed in a recent joint pre-print from the Martin, Moran and Tüysüz groups for magnetite, which explain the Fe^{3+} reactivity for CO_2 reduction to formate (Fig 32).[140] This mechanism proposes that H_2 reduces Fe^{3+} species to Fe^{2+}, leading to a proton (H^+) and a hydrogen atom, which picks up an electron from Fe^{2+} to become hydride (H^-). Then, one molecule of CO_2 physiosorbs on Fe^{2+} or Fe^{3+} can react with the hydride to yield formate. Further reduction on the metal surface could explain the formation of other intermediates.

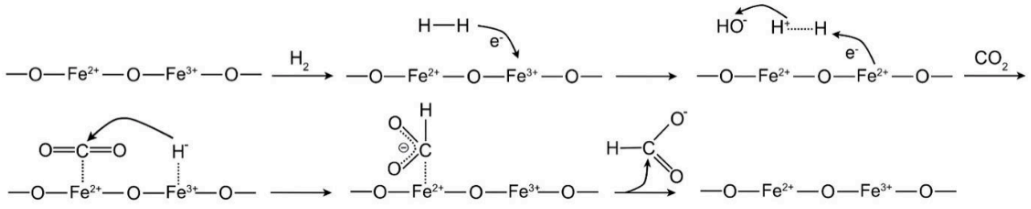

Fig 32. Proposed mechanism for CO2 reduction with H2 catalyzed by Fe_3O_4. Taken with permission from reference [140].

FeO was also tested as a catalyst for CO_2 reduction with H_2: a high selectivity for acetate production is observed under mildly acidic conditions, with similar yield to that observed with Fe^0. Under slightly basic condition, formate and a low concentration of pyruvate are also observed, 0.06 mM and 0.03 mM respectively, but no methanol. In light of these results, the mechanism could be different to the one proposed with magnetite, where both Fe^{2+} and Fe^{3+} species seem to be required to produce more intermediates.

In parallel control experiments, metal-free samples pressurized in the same way as the others, were performed to determine background levels of carbon compounds without catalysts. A trace amount of formate and acetate can be observed (below 0.01 mM), coming either form the steel walls of the reactor or from contaminants in KOH, but these concentrations are negligible compared to the ones observed with catalysts. These results underline that H_2 alone does not reduce CO_2, and that this reaction requires a suitable inorganic catalyst to yield intermediates and products of the Acetyl-CoA pathway.

As the next step of these investigations, we performed the same experiments as those described above but this time without H_2, with 25 bar of CO_2 only (Fig 33 - Fig 34).

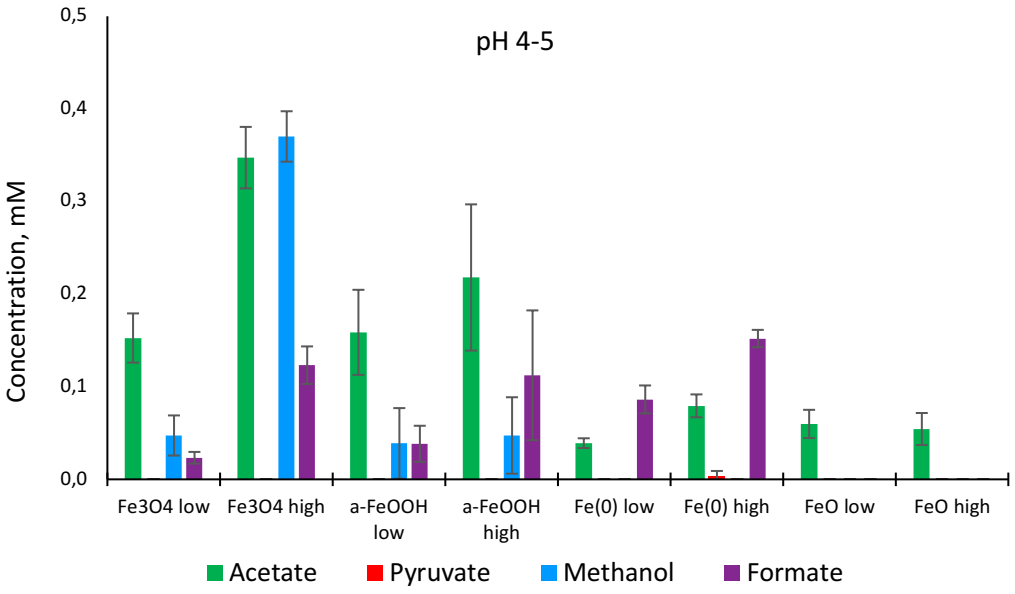

Fig 33. Concentrations of detected CO_2 reduction products obtained under CO_2 atmosphere (25 bars) with iron oxide or metallic iron powder (low meaning 1 mmol of metal atoms, high meaning 3 mmol of metal atoms) in 1 mL H_2O each, at pH 4-5 at 100 °C for 16 hours.

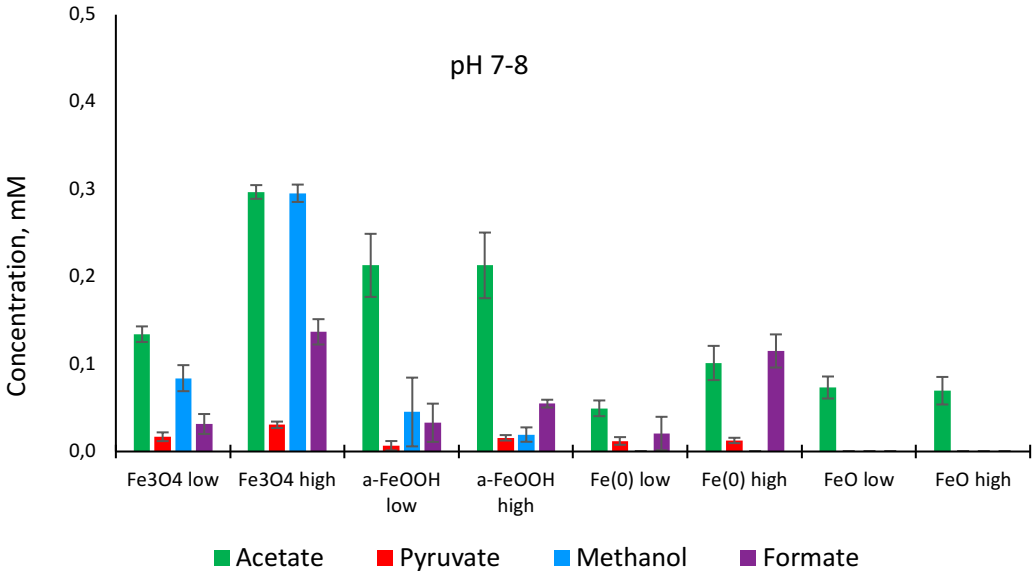

Fig 34. Concentrations of detected CO_2 reduction products obtained under CO_2 atmosphere (total pressure 25 bars) with iron oxide or metallic iron powder (low meaning 1 mmol of metal atoms, high meaning 3 mmol of metal atoms) in 1 mL H_2O + 45 mg KOH each, at pH 7-8 at 100 °C for 16 hours.

Interestingly, CO_2-only experiments show that intermediates such as acetate, pyruvate, methanol and formate, can be formed over iron oxides also without H_2 gas. The results were quite similar to the ones with H_2/CO_2 mixtures, following the same trend, with slightly higher acetate concentration (0.35 mM for "high" Fe_3O_4). Different hypotheses can be proposed to explain these results. For example, the Fe^{2+} species can reduce water, in order to produce H_2 in situ; or Fe^{2+} can directly reduce CO_2, physiosorbed on Fe^{2+} or Fe^{3+}. In both cases, these reactions are not thermodynamically favorable under standard conditions (Fe^{3+}/Fe^{2+}: E_0= +0.77 V, H^+/H_2: E_0 = -0.41 V at pH 7), hypothetically the high pressure and temperature could help to make the reaction possible.

The reactivity of goethite (α-FeOOH) in CO_2 reduction was particularly surprising, as Fe^{3+} cannot be further oxidized, and so cannot reduce water or CO_2 as proposed before. Therefore, the mechanism is not clear.

Results obtained with FeO are again selective for acetate, which was observed in both pH ranges. With Fe^0, no methanol is observed under the same conditions. If a mixture of Fe^{2+}/Fe^{3+} is the actual catalyst, it could mean that not enough Fe^{2+}/Fe^{3+} is produced to make methanol. It could also indicate that this reaction happens through different mechanisms depending of the iron oxidation state.

To conclude this part, different iron species are able to promote the formation of acetate and pyruvate, end products of the W-L pathway, crucial intermediates of carbon and energy metabolism. It can happen with or without the presence of H_2, over a pH range 4-8, with product distribution changing depending on the catalyst used. This reinforces the geological plausibility and suggests these reactions could have occurred in the environment of the early Earth, e.g. in hydrothermal vents.

7. Conclusion & perspectives

In summary, these results are complementary to the ones obtained from the collaboration of our group with the groups of William F. Martin and Harun Tüysüz[140], showing that several iron oxides can promote CO_2 reduction leading to organic compounds, up to C3, with or without H_2. These results are definitely an advance over our previous Fe^0-mediated CO_2 fixation[16], because iron oxides are very abundant on earth up to this day, which support the plausibility of this early reaction for life's emergence. However, there are still major open questions concerning the reaction mechanism, especially the production of acetate using iron oxides without H_2. There might be more than one mechanism, depending on the catalyst type and gases involved. More studies will be required to deconvolute the mechanism.

The electrochemical study supports the hypothesis that iron oxides are necessary for CO_2 fixation instead of native iron. The potential required for CO_2 reduction is too low to maintain iron oxides on the surface of the iron wire, and so the Fe^0 reduction takes place first in the cell. This could explain why we cannot reproduce the results by electrochemistry.

Finally, this study delivers insights concerning iron oxides required for this reaction, a mix of Fe^{2+} and Fe^{3+} seems to be the right combination to produce a maximum of acetate and pyruvate, two intermediates interesting for the rest of our research.

Part IV - Thioesters

1. Introduction

A "thioester world", a term coined by De Duve in 1998, has been hypothesized to be at the heart of a protometabolism before the incorporation of phosphate, driven by the energy of thioester hydrolysis.[11] It was peripherally supported by a few experimental investigations on sulfur chemistry (Scheme 21): Weber showed that thioesters could be synthesized from glyceraldehyde and *N*-acetylcysteine under prebiotic anaerobic conditions, requiring phosphate buffer.[143] He also showed the capacity of thioesters to act as condensing agents for the formation of pyrophosphate.[144] Miller and co-workers published a synthesis of the pantetheine moiety of CoA by heating pantoyl lactone, β-alanine and cysteamine, extrapolating from this simple synthesis that CoA is important in the earliest metabolic systems.[145] Later, Orgel showed the oxidative acylation of thioacids to form amide bonds in aqueous solution.[146]

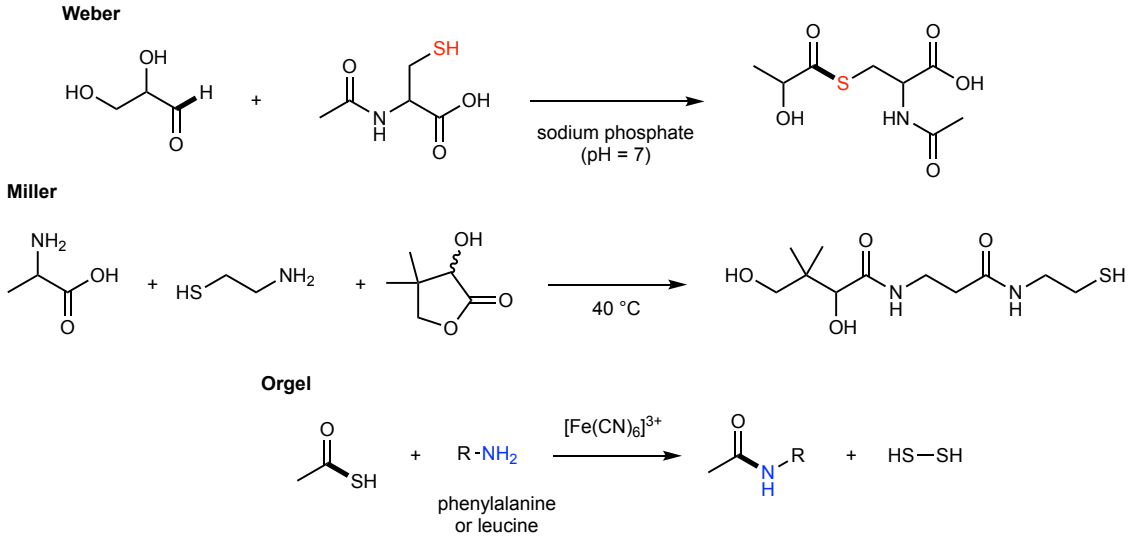

Scheme 21. Experiments supporting the plausibility of a prebiotic "Thioester World"

These aforementioned reactions illustrate prebiotic variants of some biomolecules or biochemical mechanisms using highly specific starting materials. These reactions alone are insufficient to support the plausibility of a pre-phosphate metabolic network, which might allow the emergence of a rich and complex organized biochemistry. To this end, Segrè and co-workers used computational systems biology approaches to study the size, architecture

and physicochemical properties of phosphate-independent biochemical networks, as could be extracted from all documented biochemical reactions in the biosphere, rather than from a single organism.[17] From this, a fully connected network of 315 reactions and 260 metabolites, including several precursors for DNA/RNA, could have been generated from prebiotic environments only. On the basis of the thermodynamics of reactions within the network, the same team showed that environmental sources of fixed nitrogen and low-potential electron donors may not have been necessary to generate a complex primitive network.[104] A hypothetical core network (Fig 35) was extracted, that starts only from prebiotically plausible material ("seed molecules", Fig 35), without nitrogen or phosphate. From the WL pathway combined with the rTCA cycle, ketoacids precursors for 8 common amino acids are synthetized, leading to some routes for fatty acid and polyketides synthesis. In this context, a core organo-sulfur proto-metabolism is accessible from really simple materials, as a plausible prebiotic roadmap to the biochemistry of early life.

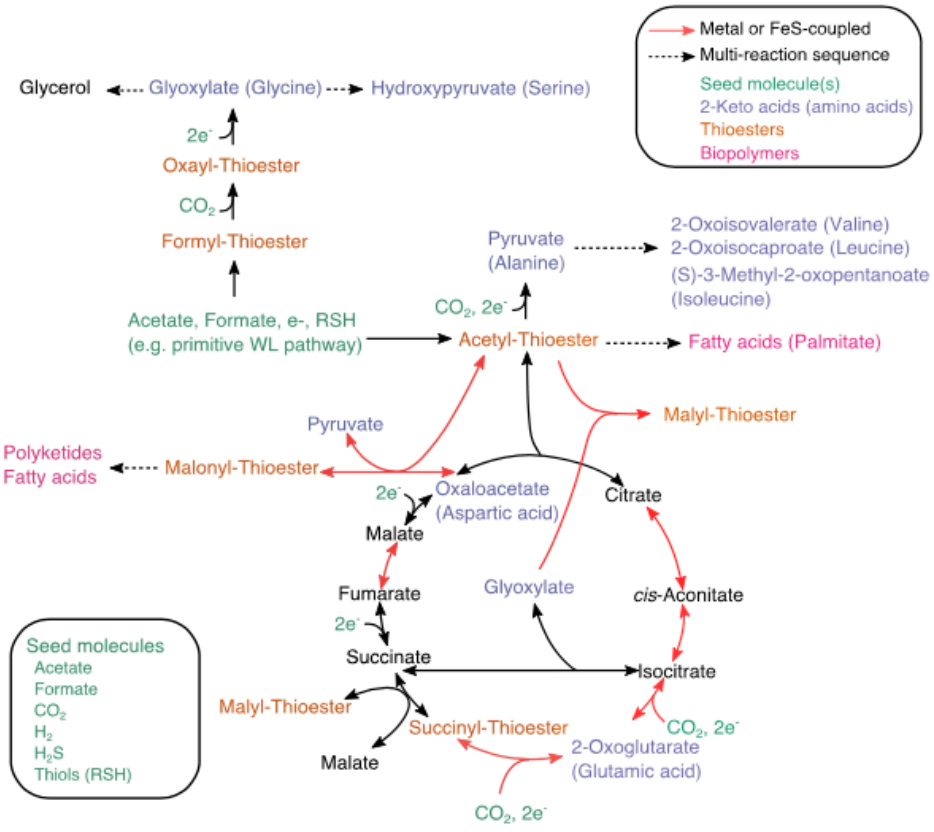

Fig 35. A representation of the thermodynamically plausible paths within the core phosphate-free network calculated by Sègre and co-workers. Taken with permission from reference [104].

In light of these new insights, I explore within this chapter different chemical ways of making thioesters from keto-acids or aldehydes under plausible early life conditions. Then, I introduce a complex reaction network that forms most of the TCA intermediates from only two organic reagents, recently published by others in our laboratory.[9] Finally, I demonstrate that this network can be combined with our new conditions, and thus allows the formation of thioesters from the keto-acids generated by the network, in a way similar to that proposed by Segrè and co-workers.[104]

2. Formation of thioesters from keto-acids

To start, the synthetic organic chemistry literature on decarboxylative coupling of α-ketoacids with thiols is overviewed. Several groups have demonstrated decarboxylation of α-ketoacids to thioesters using various oxidants, such as O_2, $Na_2S_2O_8$, $(NH_4)_2S_2O_8$ or $K_2S_2O_8$ with or without catalyst in various organic solvents, using thiols or disulfides (Fig 36).[18,147,148]

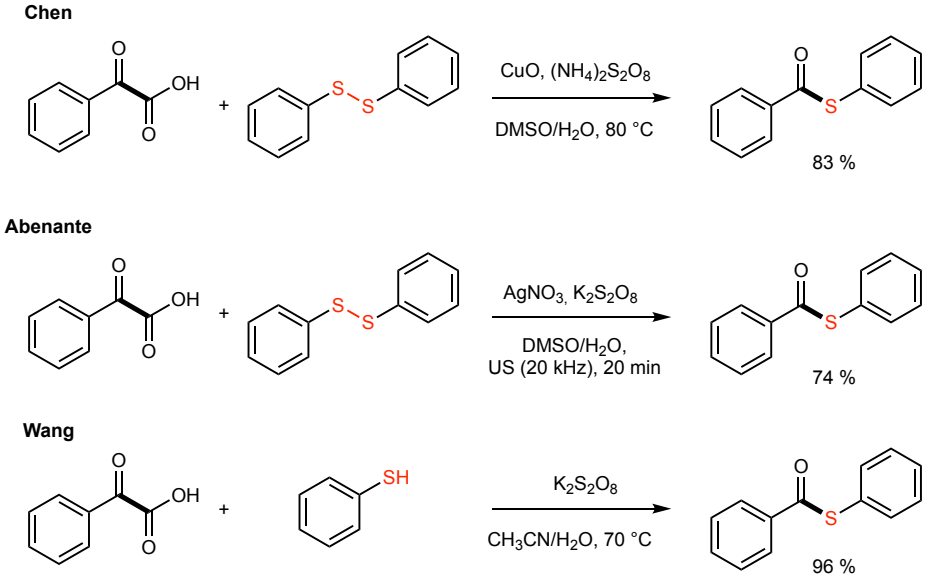

Fig 36. Oxidative decarboxylation of α-ketoacids in the presence of thiols or disulfides to form thioesters

A possible mechanism for the oxidative decarboxylation has been proposed[18] (Scheme 22): $K_2S_2O_8$ first generates the active radical anion $SO_4^{-\cdot}$, which can abstract a hydrogen atom, leading to either α-keto carboxyl radical or a sulfur radical. The decarboxylation of α-keto carboxyl radical affords the corresponding acyl radical, which allows the coupling with the sulfur radical, forming the thioester. According to the proposed mechanisms, $K_2S_2O_8$ is used to generate the active redox state of the catalyst from the various pre-catalysts (to generate Ag(II) from Ag(I)) or to regenerate (Cu(II) from Cu(I)). However, we have no certainty that the catalyst plays a redox role or simply serves as a Lewis acid catalyst for the homolytic cleavage of $K_2S_2O_8$, since any mechanistic studies into the role of the catalyst have not been performed.

In any case, the general mechanism, through the formation of the acyl radical after decarboxylation, is the same.[147,148]

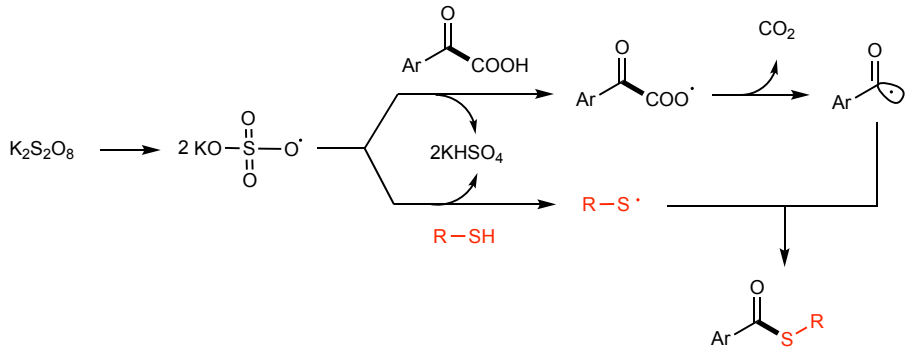

Scheme 22. A possible mechanism for thioesters formation from α-ketoacids[18]

In aqueous solution, the use of oxidants on α-ketoacids can also lead to the formation of carboxylic acids, which are then not available for the described thioester formation: the teams of Springsteen and Krishnamurthy studied the oxidation of TCA intermediates to malonate using H_2O_2, promoting decarboxylation and alcohol oxidation in aqueous solution.[149] The rapid decarboxylation of pyruvic acid in the presence of H_2O_2 to acetic acid has also been observed, over the pH range 2 – 9 at 25 °C.[150]

Similar research has been done on aldehydes instead of α-ketoacids, combining an oxidant, such as $K_2S_2O_8$, di-*tert*-butyl peroxide (DTBP), tert-butyl hydroperoxide (TBHP) or tetraethylammonium bromide (TEAB), with catalysts, such as CuCl or $FeBr_2$, in water or organic solvents (Fig 37).[151–154] The mechanism should be similar, through the formation of an acyl radical which can react with the thiol or disulfide (Scheme 23).

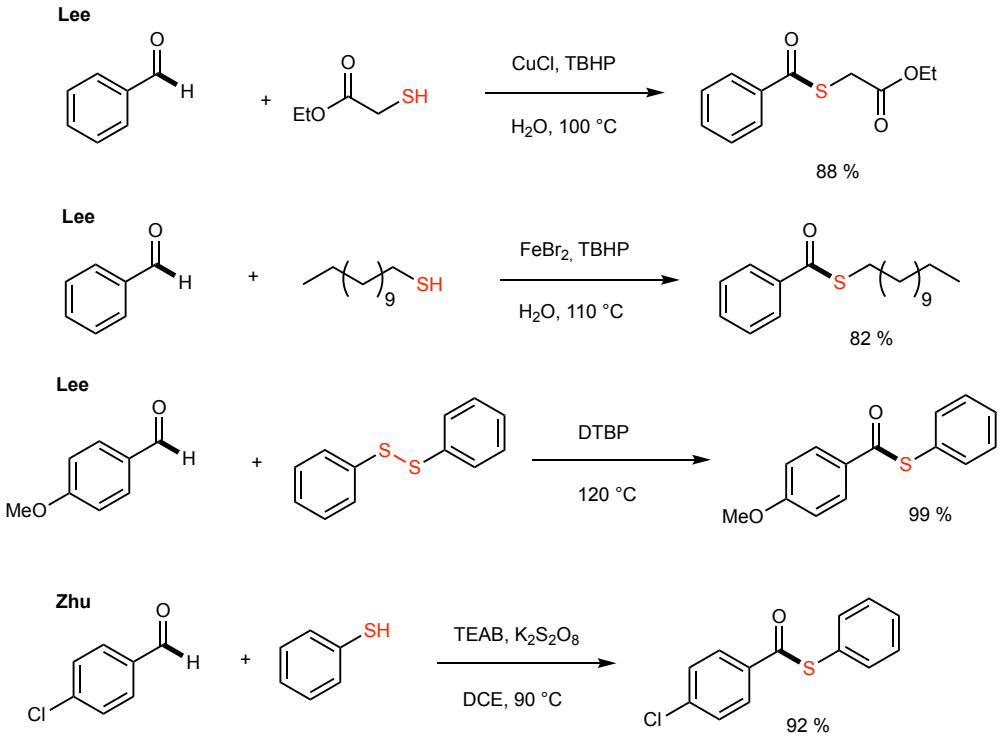

Fig 37. Oxidation of aldehydes to form thioesters

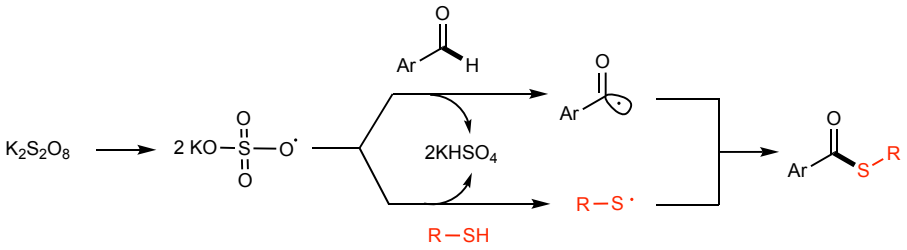

Scheme 23. A possible mechanism for thioesters formation from aldehydes

From this literature, I have explored different thermal conditions to obtain thioesters by coupling α-ketoacids and thiols in the presence of oxidants. Then, I have investigated some photochemical conditions, using different UV-lamps, to reproduce the solar spectrum on the early Earth. I also investigated the influence of different additives on thioester-generating reactions. I then applied these conditions to a variety of biologically relevant α-ketoacids and aldehydes. Finally, I developed a one-pot procedure in which thioesters are generated from α-ketoacids directly within a C-C bond-forming reaction network.

2.1. Thioester formation under thermal conditions

The initial investigations were focused on the reaction between pyruvate **2**, an intermediate of the TCA cycle generated through the W-L pathway, and *N*-acetylcysteamine **18a**, a simpler analogue of CoA (Scheme 24-Scheme 25).

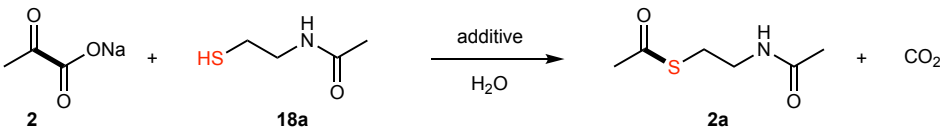

Scheme 24. Formation of the acetyl thioester **2a**.

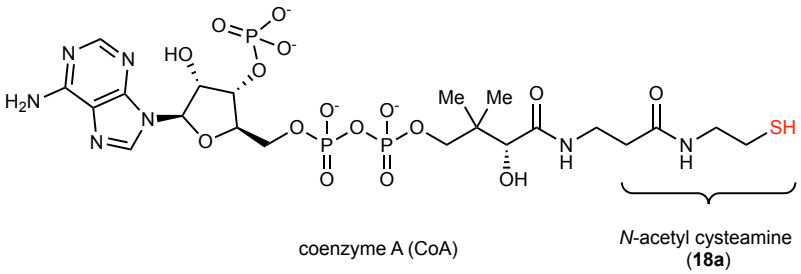

Scheme 25. Structure of CoA.

Based on the publications presented above, $K_2S_2O_8$ seems to be the best choice of oxidant.[155] Although the reactive radicals themselves have not been preserved over billions of years, there remain indirect traces of an sulfur redox chemistry on the early Earth, supported by geologic investigation on early Archaean rocks suggesting the presence of microbes with metabolisms based on sulphur.[156]

To our delight, this reaction was found to work under more prebiotic conditions, using water as the solvent, over a large temperature range (Fig 38). The maximum yield of thioester was obtained at 70 °C, as the optimal temperature for the activation of $K_2S_2O_8$ to produce sulfate radicals. This temperature was kept constant in future experiments, in order to optimize the other reaction parameters.

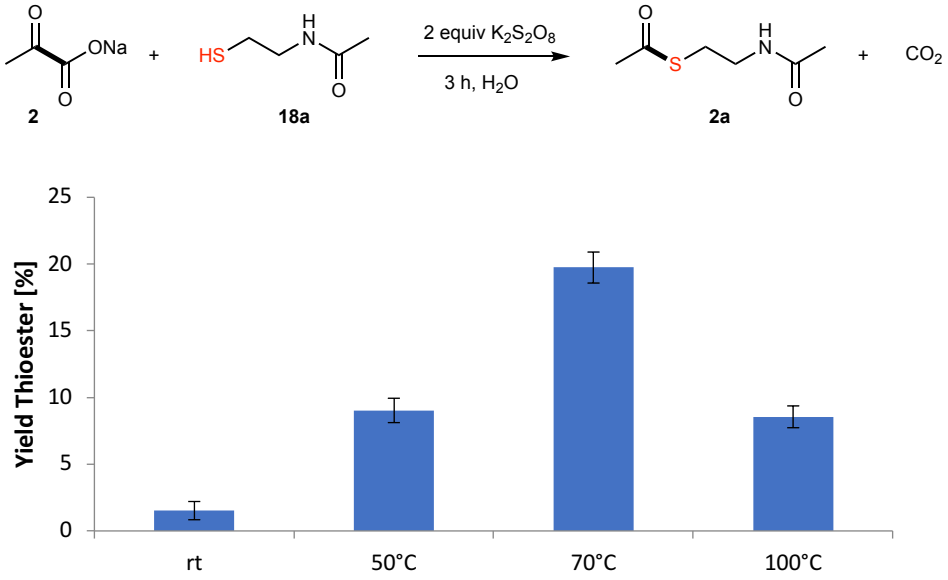

Fig 38. Temperature screening
Reaction conditions: sodium pyruvate (0.5 mmol), *N*-acetylcysteamine (0.1 mmol), $K_2S_2O_8$ (0.2 mmol) in H_2O, 3 h.

Then, the yield of the reaction as a function of time was investigated, to observe if the production of thioesters can be improved by changing the reaction time (Fig 39). Unfortunately, since CO_2 is released in solution from the decarboxylation, the slight acidity produced favors the hydrolysis of the formed thioesters, which explain the decrease in the overall concentration of thioester over time. From a prebiotic point of view, the thioester formed will be integrated and consumed in a large chemical network, the hydrolysis after some time does not have consequences on the robustness of this reaction, or its plausibility as a prebiotic concept. As the difference in yield between 3 hours and 6 hours was small, 3 hours has been chosen for the following experiments.

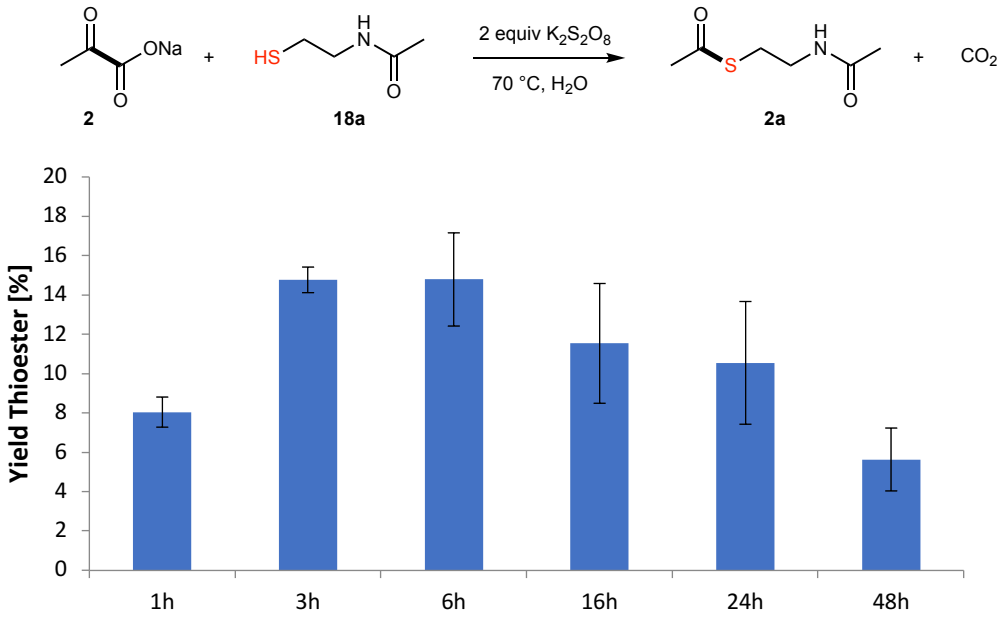

Fig 39. Time screen
Reaction conditions: sodium pyruvate (0.5 mmol), N-acetylcysteamine (0.1 mmol), $K_2S_2O_8$ (0.2 mmol) in H_2O, 70 °C.

As might be expected, a screen of different equivalents of $K_2S_2O_8$ showed higher yields for thioester formation by increasing the amount of oxidant (Fig 40). Despite this, since the amount of oxidant might be limited in a prebiotic environment, a quantity of 2 equivalents of $K_2S_2O_8$ was selected for further optimization.

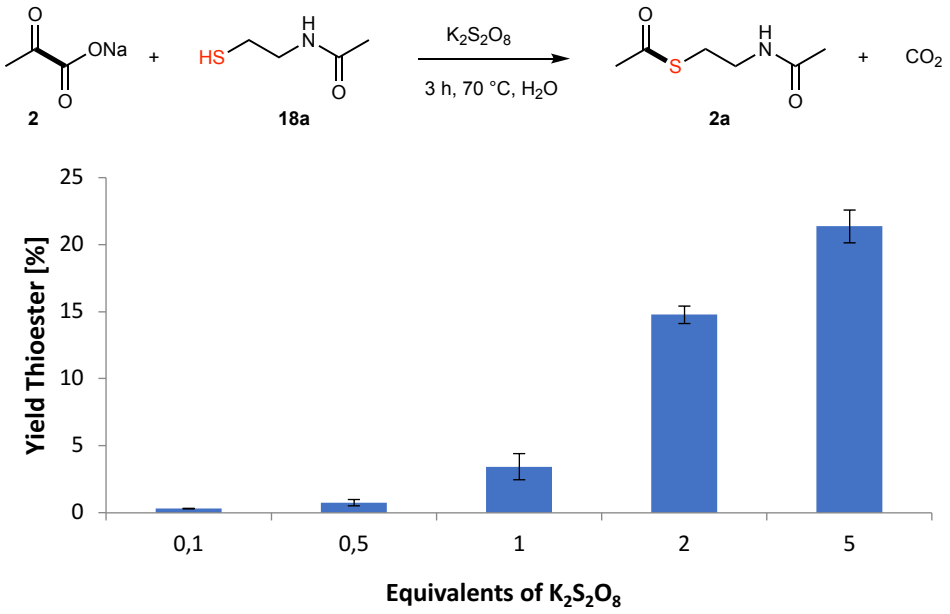

Fig 40. Thioester synthesis as a function of the equivalents of $K_2S_2O_8$
Reaction conditions: sodium pyruvate (0.5 mmol), *N*-acetylcysteamine (0.1 mmol) in H_2O, 70 °C, 3 h.

The influence of different additives has been investigated (Fig 41), to find the optimal thermal conditions. Interestingly, the addition of 0.5 equivalents of FeS improved the yield by about 10%.

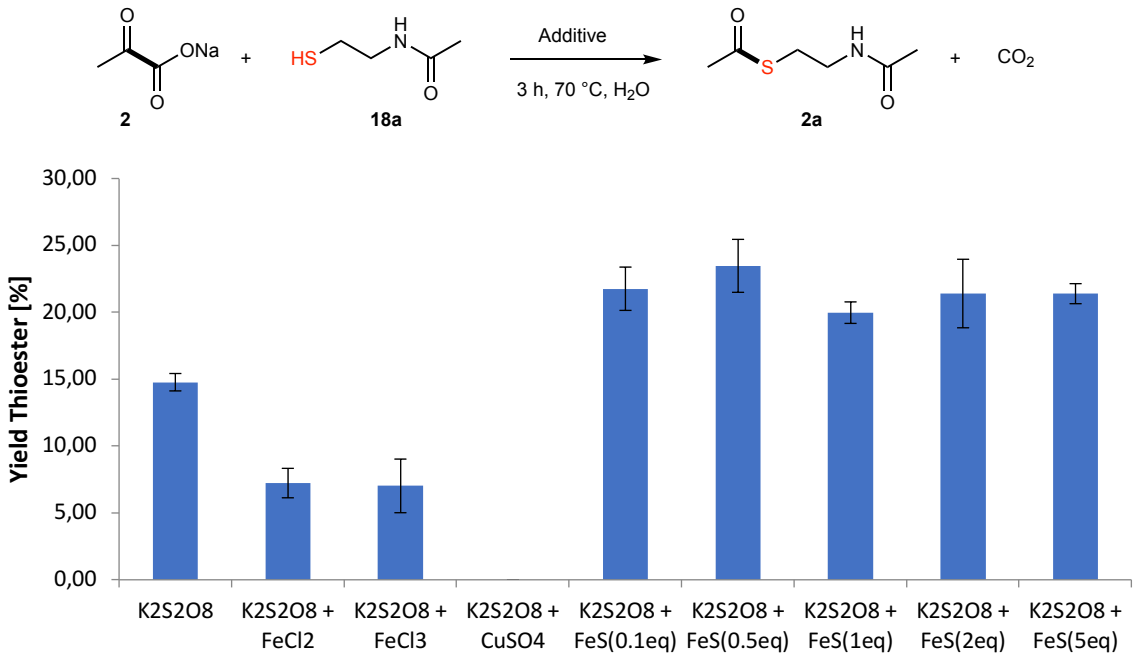

Fig 41. Thioester synthesis as a function of the presence of additives.
Reaction conditions: sodium pyruvate (0.5 mmol), N-acetylcysteamine (0.1 mmol), oxidant (0.2 mmol), unless otherwise noted: additive (0.2 mmol) in H_2O, 70 °C, 3 h.

Finally, the optimization of oxidizing agent ($K_2S_2O_8$), additive (FeS) and temperature (70 °C) to enable thioester formation converged on conditions identical to those reported by Ralser and his team to drive Krebs cycle-like breakdown of core metabolites.[19] They have reported a chemical network, promoted by sulfate radicals, which interconverts TCA cycle intermediates with more than 90% carbon efficiency. While it is not clear whether $K_2S_2O_8$ is compatible with an origin of life scenario on the prebiotic Earth, photochemical conditions which promote sulfate radical formation, could also fit to a prebiotic scenario.

2.2. Thioester formation under photochemical conditions

After this first investigation on thermal conditions, I was looking for another method to facilitate thioester formation, with softer conditions. It is known that UV-light can promote the formation of sulfate radicals from $K_2S_2O_8$, in the absence of external heating.[157] Moreover, to support our hypothesis, the sea-level UV exposure on the early Earth was more than 400 times as intense as today.[158] After the formation of Earth's ozone layer 2 billion years ago, the sea-level UV decreased since that time, becoming more hospitable to life as we know it, along increased levels of oxygen. Using this property of high sea-level UV, many photochemical early life scenarios have been proposed, including that "life is energy and the energy is sunlight".[159,160]

Combined with UV-light, other additives could be used to promote the formation of radicals, such as iron species. Iron(III) chloride and iron(III) perchlorate are known to generate OH radicals in aqueous solution.[161,162] They showed a maximum in quantum yield at a wavelength of 300 nm, where the primary photoprocess observed is the homolytic cleavage of the Fe(III)-OH bond.

Considering all of this, the reaction between pyruvate **2** and *N*-acetylcysteamine **18a** (Fig 42) was investigated under photochemical conditions. Different additives were tested, with UV-A (400-315 nm), UV-B (315-280 nm), UV-C (280-100 nm) and visible light (380-740 nm) combined, in aqueous solution.

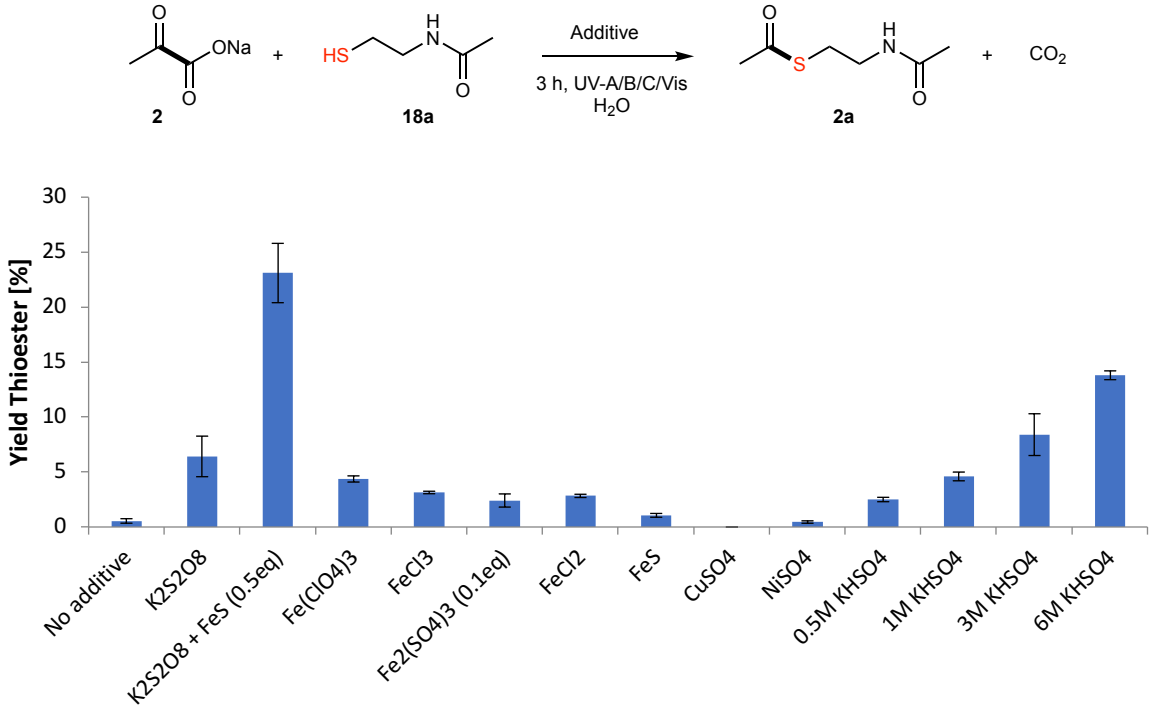

Fig 42. Thioester formation under photochemical conditions as a function of additives. **Reaction conditions:** sodium pyruvate (0.5 mmol), N-acetylcysteamine (0.1 mmol) and catalyst (0.2 mmol) unless otherwise specified, in H_2O, UV-A/B/C/Visible, 3 h.

The conversion with only UV-light is small (<1%), but additives can improve the yield of the acetyl thioester **2a**, up to 23% with $K_2S_2O_8$ and FeS (similar to optimal thermal conditions). Interestingly, iron(III) perchlorate ($Fe(ClO_4)_3$) and potassium bisulfate ($KHSO_4$) also gave good yields, and are plausible materials in a prebiotic scenario. $KHSO_4$ was selected for its potential to generate the same sulfate radical as $K_2S_2O_8$. In addition, it has a lower oxidative potential that could avoid any side-oxidation, and it is supposed to be more prebiotic, still present on Earth in mineral form (named Mercallite). To obtain higher conversion, different parameters were investigated, such as wavelengths (Fig 43) and reaction time (Fig 44).

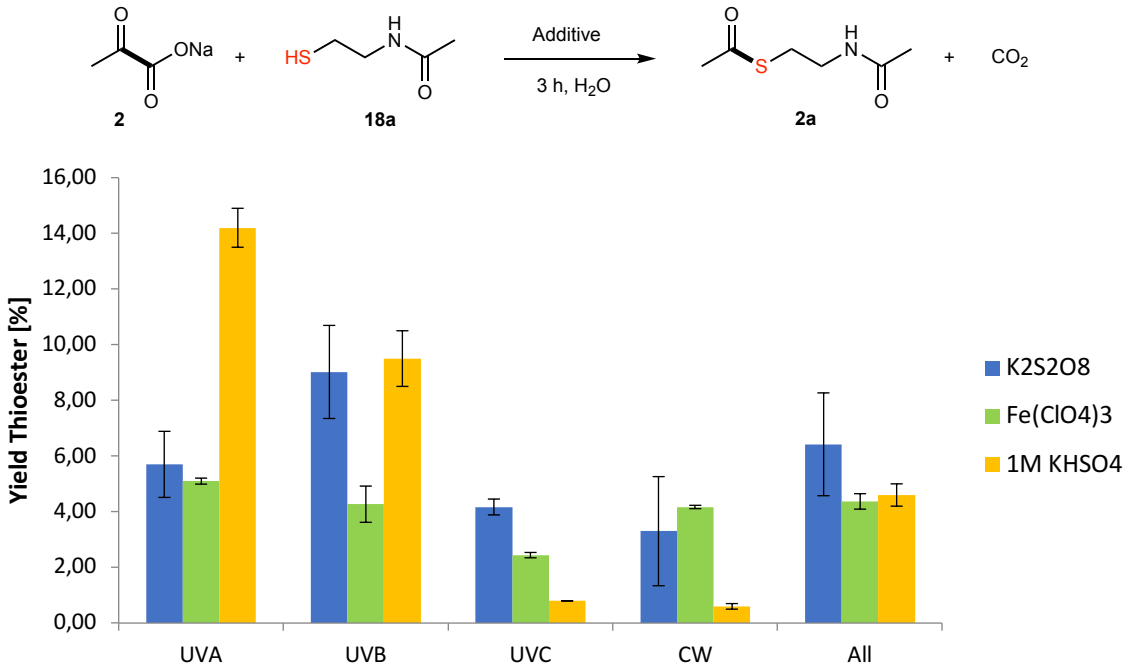

Fig 43. Wavelength screening

Reaction conditions: sodium pyruvate (0.5 mmol), N-acetylcysteamine (0.1 mmol) and catalyst (0.2 mmol) in H_2O, 3 h

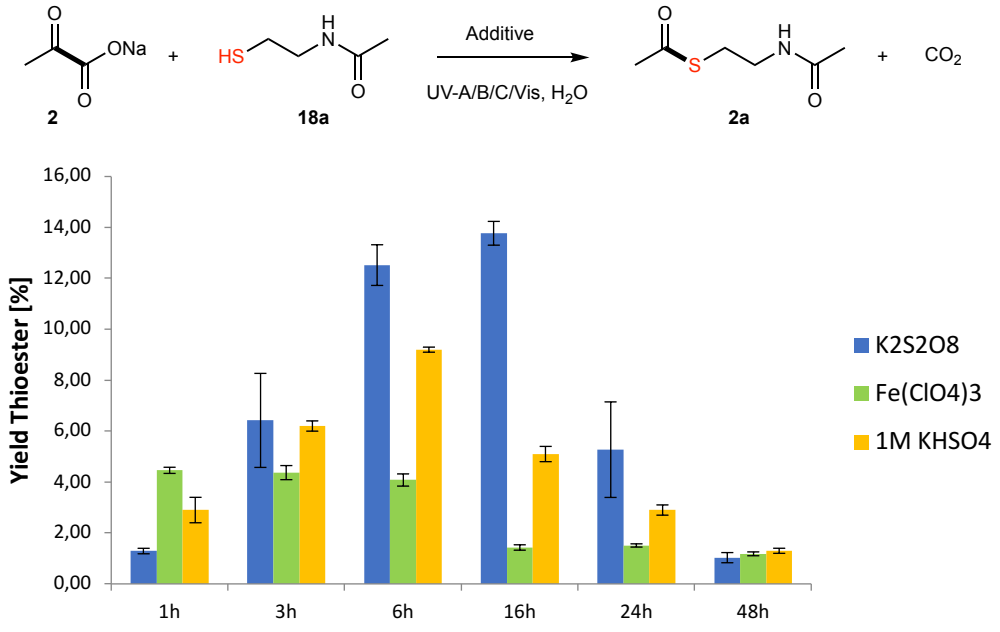

Fig 44. Times screening

Reaction conditions: sodium pyruvate (0.5 mmol), N-acetylcysteamine (0.1 mmol) and catalyst (0.2 mmol) in H_2O, UV-A/B/C/Visible

From these experiments, UV-A alone seems optimal to form thioesters using $Fe(ClO_4)_3$ or $KHSO_4$ as additives, and the maximum conversion was obtained after 1 hour or 6 hours respectively. Similar results were obtained using $K_2S_2O_8$ with UV-A or B, and the conversion reached a maximum after 16 hours. To facilitate experimental set up, UV-A for 6 hours, either with $K_2S_2O_8$ and FeS, $Fe(ClO_4)_3$ or $KHSO_4$ (3 M) have been selected as the conditions for further experiments.

An interesting observation has been done from the comparison of two similar experiments: by exchanging sodium pyruvate with pyruvic acid, the conversion increased from 0.6 % to 1.8%, without any use of additive. We therefore wondered whether the pH of the reaction solution could be critical to reactivity. An investigation on different acids at different concentrations (Fig 45) and a pH screening using sulfates (Fig 46) was performed, to better understand thioester formation under photochemical conditions.

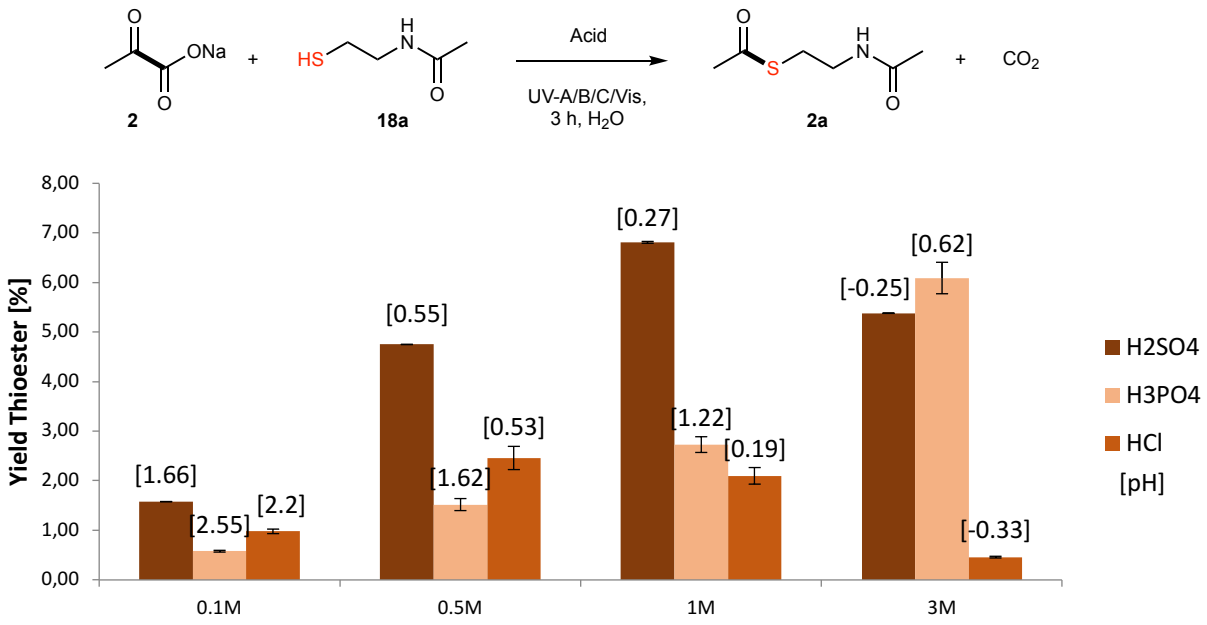

Fig 45. pH and acids screening

Reaction conditions: sodium pyruvate (0.5 mmol), N-acetylcysteamine (0.1 mmol) in H_2O, UV-A/B/C/Visible, 3 h.

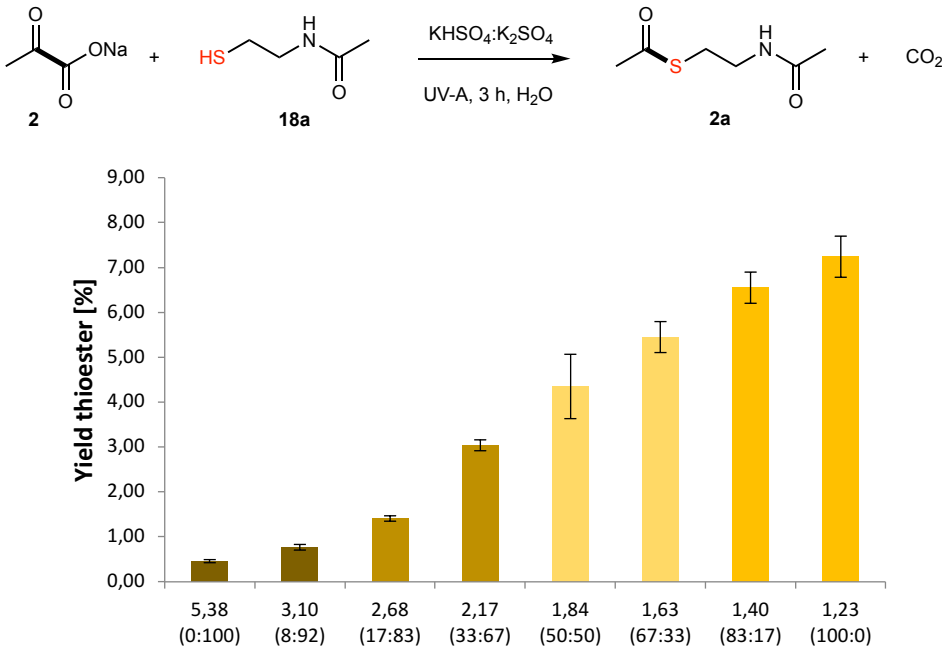

Fig 46. pH screening ($KHSO_4$:K_2SO_4)
Reaction conditions: sodium pyruvate (0.5 mmol), N-acetylcysteamine (0.1 mmol), additive (0.5M) in H_2O, UV-A, 3 h.

The direct photochemical reaction was found to be pH dependent, and independent of the chemical nature of the acid. An acidic medium, close to pH 1, under UV-A is able to trigger thioester formation, ruling out the involvement of photogenerated sulfate radicals. A pH that is too acidic (< 0) favors the hydrolysis of the formed thioester, resulting in a decrease in the yield.

2.3. Different keto-acids and thiols

From the previous section, four different methods to generate the acetyl thioester **2a** from pyruvate **2** have been selected: one thermal condition with $K_2S_2O_8$ and FeS at 70 °C for 3 hours (Method A), and three photochemical conditions with $K_2S_2O_8$ and FeS, $KHSO_4$ (3 M) or $Fe(ClO_4)_3$ using UV-A for 6 hours (Method B, C or D respectively). These four methods have been tested on different substrates with different thiols to determine whether this concept can be applied to a wide range of molecules (Table 11). For some substrates, Method D has not been investigated, because of its low yield compared to the other methods.

Four α-ketoacids were tested, three of them are key intermediates of the TCA cycle (pyruvate **2**, oxaloacetate **3,** α-ketoglutarate **8**), and the hydroxyketoglutarate **19** is produced from the enzymatic and non-enzymatic aldol reaction between pyruvate and glyoxylate, a dominant reaction in the non-enzymatic iron(II) promoted reaction network that will be presented later. There is one representative aldehyde, acetaldehyde **20**, another plausible prebiotic source of acetyl groups. Aldehyde oxidation is another common oxidative by which thioesters are formed. Acetaldehyde oxidation to acetyl CoA is a common way in which ethanol is degraded in the body. Aldehyde oxidation is also a key reaction in the glycolysis pathway. Finally, we also examined one off-cycle product of the rTCA cycle, lactate **15**, which arises from the reduction of pyruvate. The disulfide **18c**, formed from the oxidation of *N*-acetylcysteamine, and another synthetized water-soluble thiol **18b** have also been tested. The results are summarized in Table 11.

Table 11. Thioester formation under various conditions

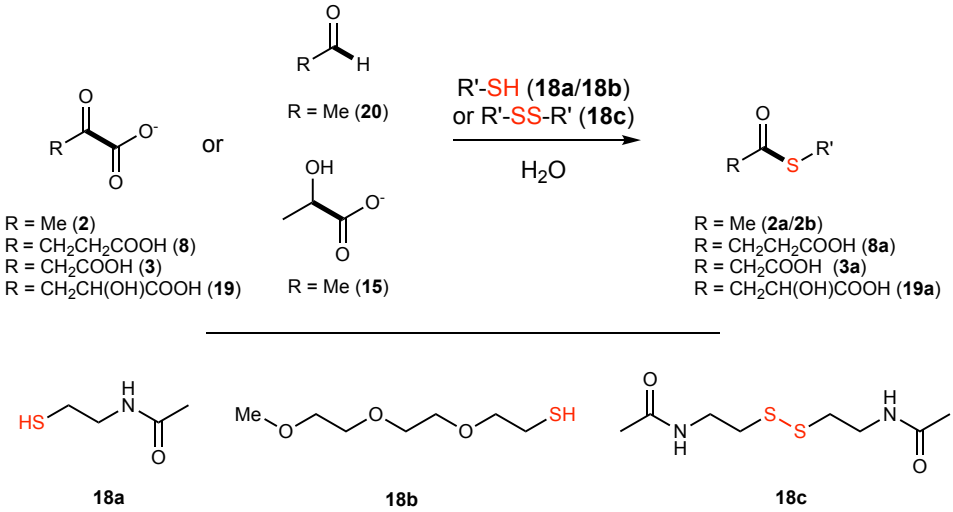

18a **18b** **18c**

Entry	Substrate *(0.5 mmol)*	Thio-compd. *(0.1 mmol)*	Product	Product Yield (%) ± SD			
				Method A[a]	Method B[b]	Method C[c]	Method D[d]
1	Pyruvate **2**	**18a**	**2a**	26.6 ± 0.7	31.2 ± 0.4	22.1 ± 0.4	5.1 ± 0.1
2	Pyruvate **2**	**18b**	**2b**	14.6 ± 0.1	24.1 ± 0.6	17.6 ± 1.0	5.6 ± 0.2
3	Pyruvate **2**	**18c**[e]	**2a**	32.9 ± 0.8	31.9 ± 1.7	4.9 ± 0.2	0.5 ± 0.1
4	α-ketoglutarate **8**	**18a**	**8a**	9.5 ± 1.9	24.5 ± 1.8	13.1 ± 0.9	/
4'			**19a**	11.4 ± 0.5	3.8 ± 0.2	< 0.5	/
5	Oxaloacetate **3**	**18a**	**3a**	6.7 ± 0.4	23.6 ± 1.6	7.9 ± 1.6	/
5'			**2a**	2.6 ± 0.3	2.4 ± 0.3	< 0.5	/
6	Hydroxyketoglutarate **19**	**18a**	**19a**	2.0 ± 0.1	9.9 ± 0.8	3.5 ± 0.2	/
7	Acetaldehyde[f] **20**	**18a**	**2a**	14.7 ± 1.4	12.9 ± 2.1	19.6 ± 1.6	1.7 ± 0.2
8	Lactate **15**	**18a**	**2a**	3.6 ± 0.1	3.5 ± 0.2	0 ± 0.0	0.8 ± 0.1

[a]$K_2S_2O_8$ (2.0 equiv), FeS (0.5 equiv) in H_2O, 3 h, 70 °C. [b]$K_2S_2O_8$ (2.0 equiv), FeS (0.5 equiv) in H_2O, 6 h, UV-A. [c]$KHSO_4$ (3 M) in H_2O, 6 h, UV-A. [d]$Fe(ClO_4)_3$ (2.0 equiv) in H_2O, 6 h, UV-A. [e]0.05 mmol of the disulfide were used, the yield was still calculated based on 0.1 mmol of the thiol [f]1.0 mmol of the substrate were used.

Thioester synthesis could equally be carried out with another water-soluble thiol **18b**, or with disulfide **18c** (Entry 2-3). However, the reduced reactivity with disulfide **18c** using direct photochemistry suggests the mechanism is distinct from the sulfate-radical-forming reactions (Entry 2, Method C). Two other ketoacids, α-ketoglutarate **8** and oxaloacetate **3**, also underwent decarboxylative thioesterification to give the corresponding succinyl thioester **8a**, an analogue of succinyl-CoA, a precursor to many co-factors (described in the introduction section), and malonyl thioester **3a**, an analogue of malonyl-CoA, a precursor to biological fatty acid synthesis (Entry 4-5). Malonyl-CoA is formed by carboxylation acetyl-CoA using the enzyme *acetyl-CoA carboxylase*, requiring ATP. From these reactions, additional thioesters can be formed: the malyl thioester **19a** can be observed, possibly from direct oxidation of the starting material, α-ketoglutarate **8**, to hydroxyketoglutarate **19** which can react with the thiol to produce the thioesters (Entry 4'). No intermediates have been isolated to support this hypothesis, but a control experiment demonstrated the absence of reactivity of succinyl thioester **8a** to give malyl thioester **19a** under similar oxidative condition. The decarboxylation of malonyl thioester **3a** can also give access to acetyl thioester **2a** as a second product (Entry 5'). The yields with thermal conditions are slightly lower (Entry 4-5, Method A) due to the favored decarboxylation of these unstable α-ketoacids under high temperatures.

Acetaldehyde **20**, a simple representative aldehyde, was also found to furnish acetyl thioester **2a** under thermal and photochemical conditions (Entry 7). Good conversion was observed either with sulfate radical-forming conditions or with direct photochemical conditions (Entry 7, Method A, B and C). The direct photochemical conversion of aldehydes to thioesters (equivalent to Method C) has already been reported by Weber, using glyceraldehyde and *N*-acetylcysteine in aqueous solution of phosphate under neutral condition, but the conversion was much slower and lower than that reported here (0.3 %/day).[143]

The reactivity of lactate **15** has also been studied (Entry 8), which requires first its oxidation to pyruvate, before it can react with the thiol. This reaction is of interest because it enables side products of the TCA cycle to be reintegrated into the cycle. Unfortunately, the conversion of lactate **15** to acetyl thioester **2a** is really low in the presence of oxidant (Entry

8, Method A-B), and was, as expected given the lack of oxidants, not observed under photochemical conditions (Entry 8, Method C-D).

To conclude this part, three conditions (Method A, B and C) are able to generate thioesters in yields up to 33% from both α-ketoacids and aldehydes. The remaining material was found largely to be unreacted pyruvate and a small amount of acetate (for entry 1, 2 and 3), according to NMR analysis (for data analysis, see Part V- Experimental part).

2.4. Multiple ketoacids in one pot

Next, we wished to evaluate whether the three intermediates of the TCA cycle, pyruvate **2**, α-ketoglutarate **8** and oxaloacetate **3**, could still undergo the three previously described methods for thioester formation as a mixture, rather than one compound at a time (Scheme 26).

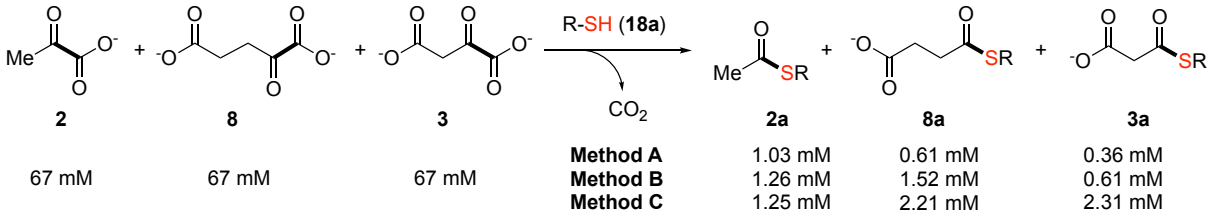

Scheme 26. Thioester formation from complex mixtures of α-ketoacids

The total amount of α-ketoacids is 0.6 mmol (0.2 mmol for each) instead of 0.5 mmol for previous experiments, but we have decided to keep the same conditions, since the change in the total concentration is small. As the chemical pathway of formation for each thioester is difficult to know at this stage (e.g. **2a** can also be formed from **3a** by decarboxylation), the concentration of each intermediates will be specified instead of the yield. The concentrations observed are low, but all three methods deliver all three of the corresponding thioesters in the mixture. This gave me confidence to attempt to integrate these conditions into a larger, more complex reaction network.

3. Thioester formation from a complex ketoacid-generating reaction network

A chemical reaction network (CRN) consists of a set of chemical reactions and a set of chemical compounds. Each chemical compound is a node of the network. Each chemical reaction is a directed vertex of the network, connecting the chemical compounds involved in the reaction, from the reactants towards the products.[163] Nowadays, thanks to applied mathematics, it is possible to model the behavior of real-world chemical reaction networks. This science has attracted a growing research community, mainly due to its applications in biochemistry and theoretical chemistry, and so can be used to predict how life could have evolved from the very beginning.

3.1. Introduction of the network

In this section, I will briefly introduce a recent important discovery from our laboratory, which provides a way to bypass the reliance of C-C bond formation on ATP-dependent reactions in our previous research on the rTCA cycle.[9,13] Based on the computational work of Segrè and co-workers, pyruvate and glyoxylate are described as the most well-connected compounds made up of only C, H and O atoms at the root of the protometabolism previously described.[17] A screen of glyoxylate and pyruvate with various transition metal salts revealed that Fe^{2+} salts at 70 °C in water can promote the formation of a complex reaction network, starting from only pyruvate and glyoxylate (Fig 47).

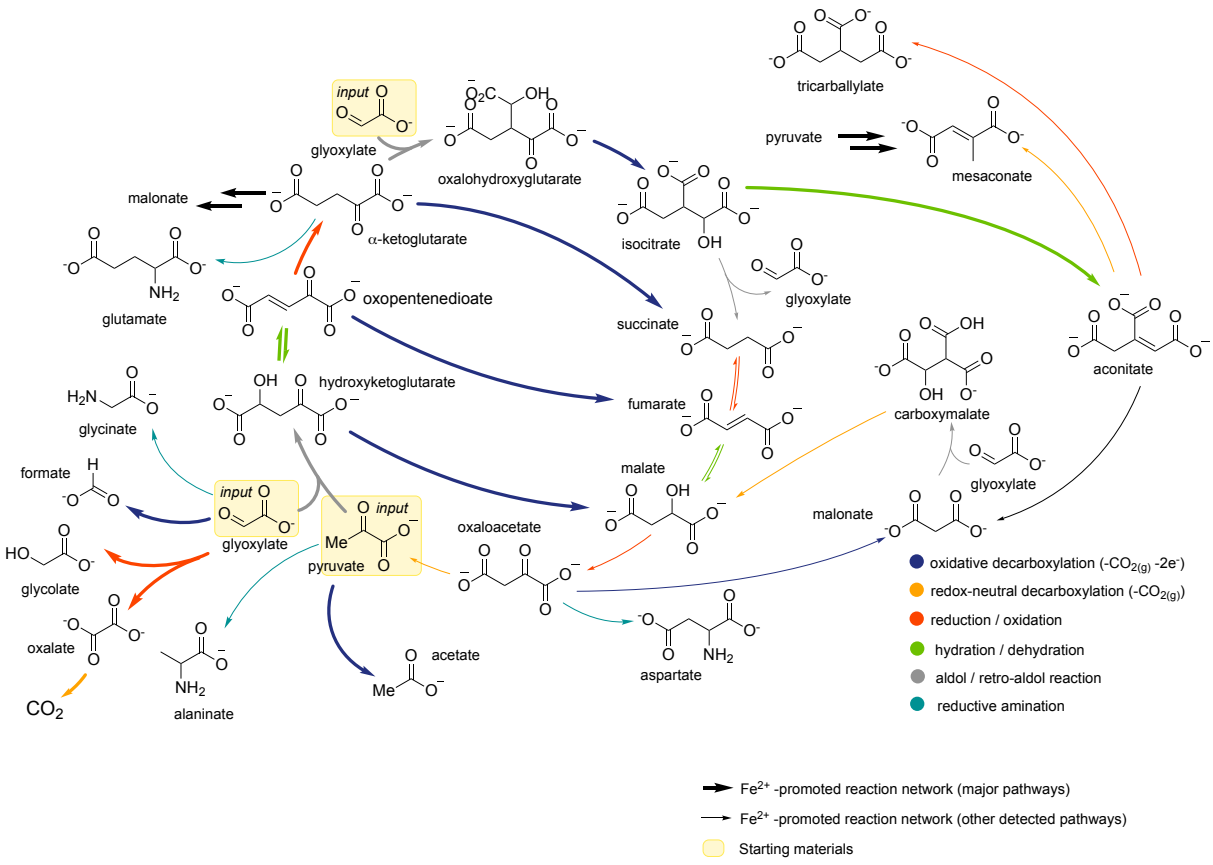

Fig 47. Fe^{2+} promoted synthesis and breakdown of the precursors of biological metabolism.[9]

18 compounds, nearly all of which are biological metabolites, and many of which are intermediates of the TCA and glyoxylate cycles, are observed through this reaction network, including all five universal metabolic precursors. The chemical composition of the reaction network was followed over time, showing that a maximum amount of complexity was obtained after 24 h. C-C bonds were formed via aldol reactions and broken through oxidative decarboxylation, decarboxylation and retro-aldol reactions. The reaction sequence within the network (Fig 47) was established by studying the reactivity over time of most of the observed intermediates under typical reaction conditions, in the presence and absence of glyoxylate. One important aspect of that work is that it provides an extraordinarily simple set of conditions under which the core metabolites of biochemistry as we know them could have been built in the absence of complex enzymatic machinery. Moreover, unlike Ralser's non-enzymatic network,[19] this network does not require a strong oxidant, thanks to the spontaneous Fe-catalyzed oxidative decarboxylation of ketoacids. Finally, given that this complex chemical reaction network promoted by Fe^{2+}, overlaps with the TCA and the

glyoxylate cycles, it is possible that it could represent a prebiotic precursor to these core metabolism pathways.

However, the TCA and glyoxylate cycles as we know them today rely heavily on the chemistry of thioesters, and the reaction network described above does not involve them. The introduction of thioesters to this network would therefore make it more like the biological pathway and give more insight into the hypothesis that similar metabolic chemistry could have had prebiotic precursors. Thioesters are also the starting point for many other biological pathways, which could ultimately lead to the formation of more complex biomolecules. To this end, I will describe in the following section our attempts to combine both conditions, the network and thioester formation, in order to achieve the formation of thioesters from in-situ generated ketoacids.

3.2. Formation of thioesters from the network

To mimic the biological integration of α-ketoacid synthesis, α-ketoacid breakdown and thioester formation in a non-enzymatic reaction network, different non-equilibrium environments were simulated. The first step has to generate different intermediates from pyruvate **2** and glyoxylate **14,** including α-keto acids, which could then enable the formation of thioesters, through the second step, by integration of the previously described methods (Table 12). Within this scenario, intermediates could cycle between neutral and oxidized regions, or between dark and light regions depending of the chosen method for thioester formation, leading to a complex biochemical-like network.

Some selected results are presented in Table 12. Different equivalents of pyruvate **2** have been tested, combined with either one or two separate additions of reagents and using different experimental conditions. First, the separation of the two set of conditions has been investigated, to first reproduce the iron-promoted network at 70 °C and then change the condition to UV-A (Entry 1), leading to the formation of small concentration of thioesters.

In the next experiments, all starting materials except the oxidant were mixed directly at the beginning and the reaction mixture was kept at 70 °C for the whole experiment (Entry 2-3). The acetyl thioester **2a** yields are higher, due to the use of a strong oxidant, the reaction

with the remaining pyruvate **2** is faster in these cases compared to the use of photochemical condition (Entry 1). Under this set of conditions, the acetyl **2a** and the malyl thioester **19a** were formed in concentrations of 1.1 to 3.6 mM and the succinyl thioester **8a** was observed at concentrations around 0.1 mM.

Unfortunately, the production of α-ketoacids from the network required high temperature, our attempts to combine the network with thioesters formations under only UV-light were not successful, only the acetyl thioester **2a** was observed from the unreactive pyruvate **2** (Entry 4-7). The efforts to separate the addition of $KHSO_4$ did not help to overcome this problem (Entry 8).

Our last experiments were focused on the first condition (Entry 1), but with the addition of the thiol from the beginning (Entry 9-10), in order to minimize the human intervention needed to perform the combination of the network with the thioester formation. Unfortunately, also here only the acetyl thioester **2a** was observed. It is possible that the reaction worked as expected but the concentrations of the thioesters were not high enough to be visible with the used analytical technique.

Table 12. Thioester formation from a non-enzymatic reaction network

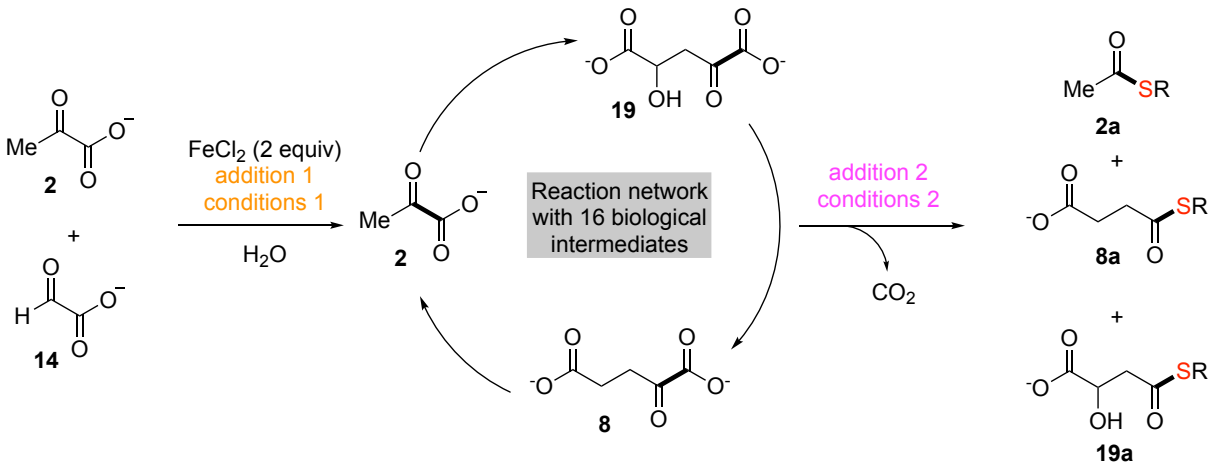

Entry	Pyruvate **2** equiv	addition 1 (equiv)	conditions 1	addition 2 (equiv)	conditions 2	Concentration (mM) Acetyl thioester **2a**[a]	Succinyl thioester **8a**[b]	Malyl thioester **19a**[b]
1	2		70 °C, 1 h	Thiol **18a** (1) $KHSO_4$ (3 M)	UVA, 3 h	0.11 ± 0.01	0.19 ± 0.04	0.06 ± 0.00
2	2	Thiol **18a** (1)	70 °C, 1 h	$K_2S_2O_8$ (2)	70 °C, 3 h	1.41 ± 0.11	0.11 ± 0.01	3.60 ± 0.30
3	2	Thiol **18a** (1)	70 °C, 3 h	$K_2S_2O_8$ (2)	70 °C, 3 h	1.11 ± 0.14	0.11 ± 0.02	3.63 ± 0.28
4	1	Thiol **18a** (1) $KHSO_4$ (3 M)	UVA, 3 h	-	-	0.06 ± 0.05	-	-
5	1	Thiol **18a** (1) $KHSO_4$ (3 M)	UVA, 6 h	-	-	0.16 ± 0.02	-	-
6	2	Thiol **18a** (1) $KHSO_4$ (3 M)	UVA, 3 h	-	-	0.11 ± 0.05	-	-
7	2	Thiol **18a** (1) $KHSO_4$ (3 M)	UVA, 6 h	-	-	0.31 ± 0.05	-	-
8	2	Thiol **18a** (1)	UVA, 1 h	$KHSO_4$ (3M)	UVA, 3 h	0.22 ± 0.02		
9	2	Thiol **18a** (1)	70 °C, 1 h	$KHSO_4$ (3M)	UVA, 3 h	0.12 ± 0.01	-	-
10	2	Thiol **18a** (1)	70 °C, 1 h	$KHSO_4$ (3M)	UVA, 6 h	0.15 ± 0.01	-	-

[a]Determined by GC-FID analysis after extraction with ethyl acetate. [b]Determined by LCMS-analysis. For the network experiments 0.5 µL instead of 0.1 µL were injected, the resulting value calculated using the calibration curves was divided by 5 afterwards.

By combining the previous iron-promoted network with our previous results to make thioesters, we were able to draw a global view of the network, including the formation and hydrolysis of the observed thioesters (Scheme 27). In this scheme, molecules in black represent those observed after thioester formation. Molecules in grey represent those observed in the previous reported iron-promoted network or expected intermediates that have not been detected.[9]

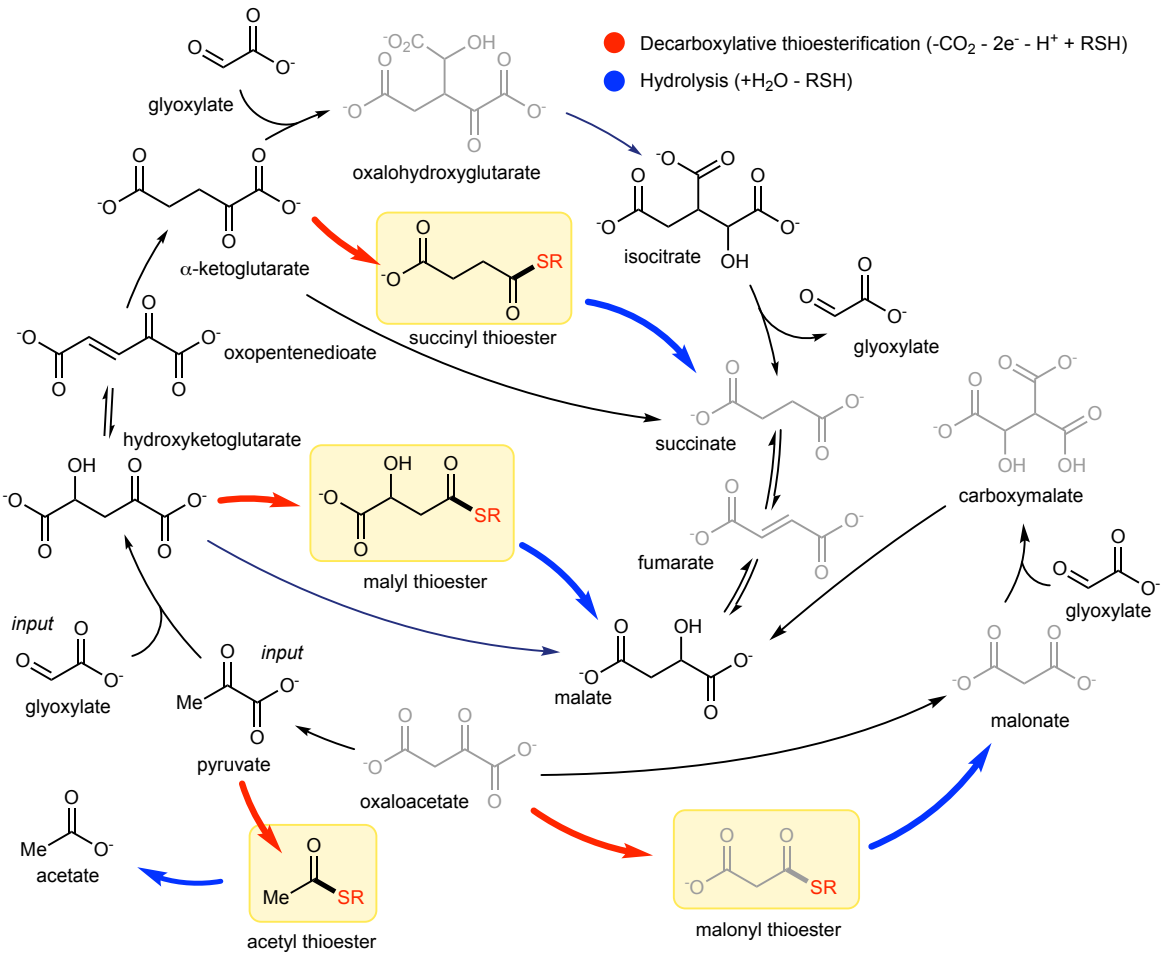

Scheme 27. Overview of the non-enzymatic chemical reaction network

In conclusion, the thioester formation from an iron-catalyzed reaction network generated from pyruvate, glyoxylate and *N*-acetylcysteamine was achieved through redox or light cycling (Scheme 27). Higher complexity of the network could be achieved after increased reaction time (24 h), but also concentrations of the formed keto acids will be lower, making it more difficult to analyze the resulting thioesters. From this overview, the sequence of reactions is already huge: starting from only three molecules, nine can be formed, including three thioesters. These thioesters can possibly be used for further reactions like Claisen condensations, giving also access to fatty acids and similar structures.

4. Conclusion & perspectives

In summary, both simple inorganic oxidants and light enable non-enzymatic thioester synthesis from α-ketoacids or aldehydes, in a way that closely mimics energy conservation within biological catabolism. The simplicity of the conditions is in line with the Thioester World hypothesis, requiring only light, α-ketoacids or aldehydes and thiols.[11] These conditions can also be integrated within non-enzymatic metabolite-generating networks, which reproduce synthesis and breakdown of metabolites, including thioesters. These results support the Segrè computational models of metabolism rising from initially only carbon, hydrogen and oxygen from the environment, to incorporate sulfur for thioesters, nitrogen for amino acids and later phosphorous leading to genetic apparition.[17] Finally, the synthesis of metabolites in an iron-rich environment could occur near oxidants or light, such as near-surface hydrothermal vents, and thus allow the emergence of a first non-enzymatic protometabolic network.[164]

Part V – Experimental part

1. The reverse Tricarboxylic Acid Cycle

1.1. General information

All reactions were carried out in 10 mL Pyrex glass culture tubes under inert atmosphere unless otherwise noted.

GCMS analysis was performed on a GC System 7820A (G4320) connected to a MSD block 5977E (G7036A), using Agilent High Resolution Gas Chromatography Column: PN 19091S – 433UI, HP – 5MS UI, 28 m×0.250 mm, 0.25 Micron, SN USD 489634H. All samples were prepared in ethyl acetate (200 µL sample volume). The analysis was carried out on a splitless 1 µL injection volume with an injection port temperature 250 °C. Column oven temperature program was as follows: 60 °C for 1 min, ramped at 30 °C min^{-1} to 310 °C with 3 min hold, with a total running time of 12.33 min. The mass spectrometer was turned on after 2 min and was operated at the electron ionization mode with quadrupole temperature of 150 °C. Data acquisition was performed in the full-scan mode (50-500). Hydrogen (99.999 % purity) was used as carrier gas at a constant flow rate of 1.5 mL min^{-1}.

1.2. Materials

Unless otherwise noted, all reagents and solvents were purchased from commercial suppliers and used without further purification. Fe^0 used was a ≥99% reduced fine powder. $ZnCl_2$ was used as an anhydrous powder (reagent grade). $Cr_2(SO_4)_3$ was used as a dodecahydrate (reagent grade). Cis-aconitic acid and triethyl oxalosuccinate were prepared using literature procedures, as described in the paper Muchowska, K., B., Varma, S., J., Chevallot-Beroux, E., Lethuillier-Karl, L., Li, G., Moran, J. Metals promote sequences of the reverse Krebs cycle, *Nat. Eco. & Evo.* **1**, 1716-1721 (2017).

1.3. Analytical method for GC-MS analysis

Derivatisation procedure

Derivatization of carboxylic acids to esters was performed using a modified literature procedure.[165] For optimal gas chromatography resolution, the carboxylic acids were converted to ethyl esters using a mixture of ethanol/ethyl chloroformate (EtOH/ECF) or to methyl esters using a mixture of methanol/methyl chloroformate (MeOH/MCF).

A ca. 0.5-0.7 mL aliquot of the reaction mixture was basified using solid KOH (in order to minimize volume change due to the usage of aqueous solution) and centrifuged (6000 rpm, 3 min). To 100 µL of the supernatant was added 1 M NaOH solution (150 µL), EtOH or MeOH (240 µL) and pyridine (30 µL), followed by ethyl chloroformate (ECF, 35 µL) or methyl chloroformate (MCF, 35 µL). This was vortexed for 30 s. A second 35 µL portion of ECF (or MCF) was added and the mixture was vortexed again for 30 s. Next, $CHCl_3$ (200 µL) was added, followed by vortexing (10 s). Finally, $NaHCO_3$ (400 µL) was added and the mixture was vortexed again for 10 s. The $CHCl_3$ layer was separated and dried over anhydrous Na_2SO_4. 50 µL of the dry $CHCl_3$ layer was used with 150 µL of ethyl acetate for the GC-MS analysis.

Product identification

Reaction products derivatized to methyl or ethyl esters of carboxylic acids were identified by comparing the mass spectra and retention times against analogously derivatized authentic samples (Appendix I, Fig. S1 – S15). ECF derivatization was preferred for small molecule substrates (pyruvate, lactate, malate, fumarate, succinate, **α**-ketoglutarate and **α**-hydroxyglutarate, alanine), while MCF derivatization gave clearer results (less elimination by-products and better resolution) for cis-aconitate, tricarballylate, isocitrate and citrate.

Yield determination and error analysis

3 mL standard aqueous solutions of rTCA carboxylic acids at different concentrations (0.006 M, 0.013 M, 0.020 M, 0.027 M, 0.033 M and 0.040 M) were prepared by diluting 0.1 – 0.5 M stock solutions of these acids. 100 µL of each standard solution was derivatized using the derivatization procedure described herein (see: Analytical procedures). For each acid, a six-point graph was plotted, correlating the sum of characteristic GC peaks (as integrated automatically by the Agilent MassHunter Workstation v.B.06.00 software) with substrate concentration (Figure S 94 – S 105). Each data point was obtained from three independent measurements (carried out by three different researchers) and the correlation line was obtained from the least-squares fitting (intercept = 0). Error bars on graphs are shown as ± standard deviation for each data point. Overall percentage error of the response factor corresponds to ± standard deviation for each slope value.

The yields of products were calculated by comparing the product peak area with the calibration line. For the purpose of this study, reported are not the absolute percentage yields based on the number of moles of the starting materials, but rather percentage contributions to the total composition of the final reaction mixture. This allows to account for potential concentration changes due to solvent loss (since many reactions were carried out in sealed tubes at temperatures above the boiling point of water), as well as potentially incomplete extraction during the derivatization procedure. Each reaction was performed at least twice to ensure reproducibility, and reported percentage compositions are an average of these two runs, with an error corresponding to ± mean absolute deviation.

Derivatization with ethyl chloroformate (ECF)

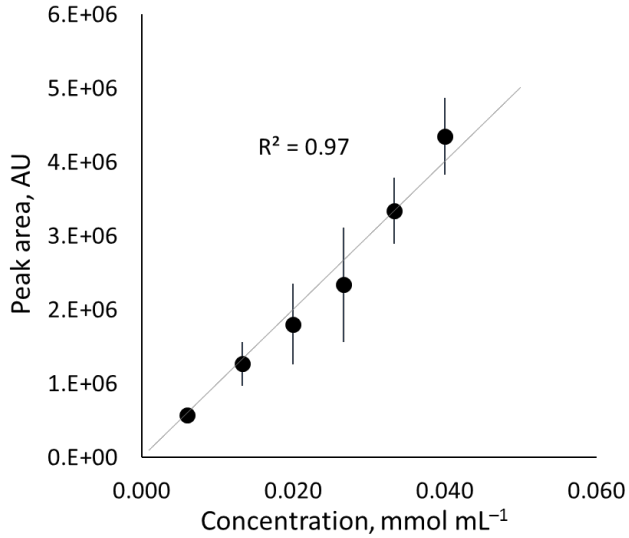

Fig 48. Correlation between the concentration of an aqueous solution of pyruvate and the measured gas chromatography area.

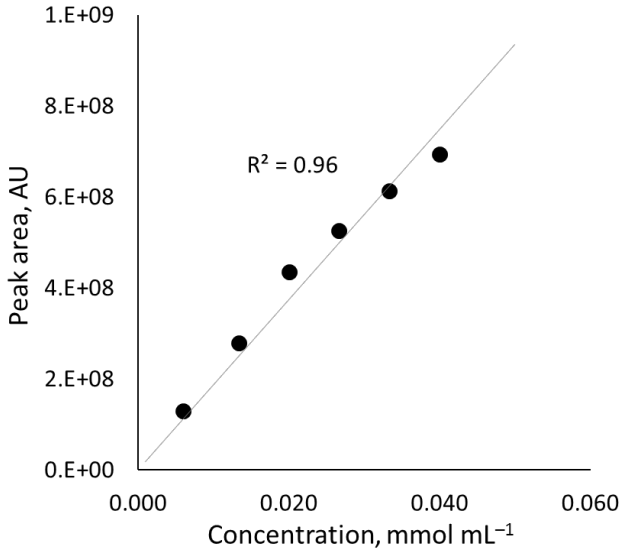

Fig 49. Correlation between the concentration of an aqueous solution of lactate and the measured gas chromatography area. Lactate was obtained by a complete reduction of an aqueous solution of sodium pyruvate with $NaBH_4$. The correlation line shown here correspond to a single run.

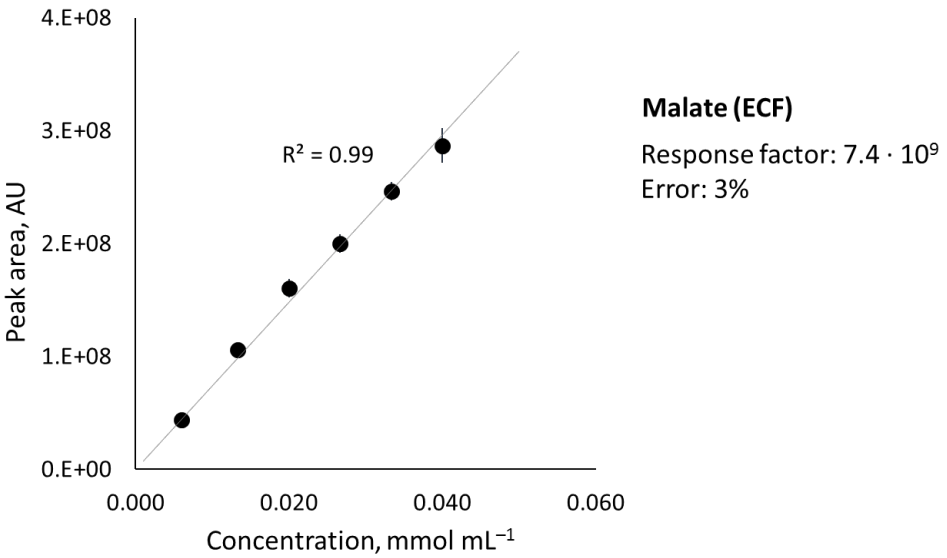

Fig 50. Correlation between the concentration of an aqueous solution of malate and the measured gas chromatography area.

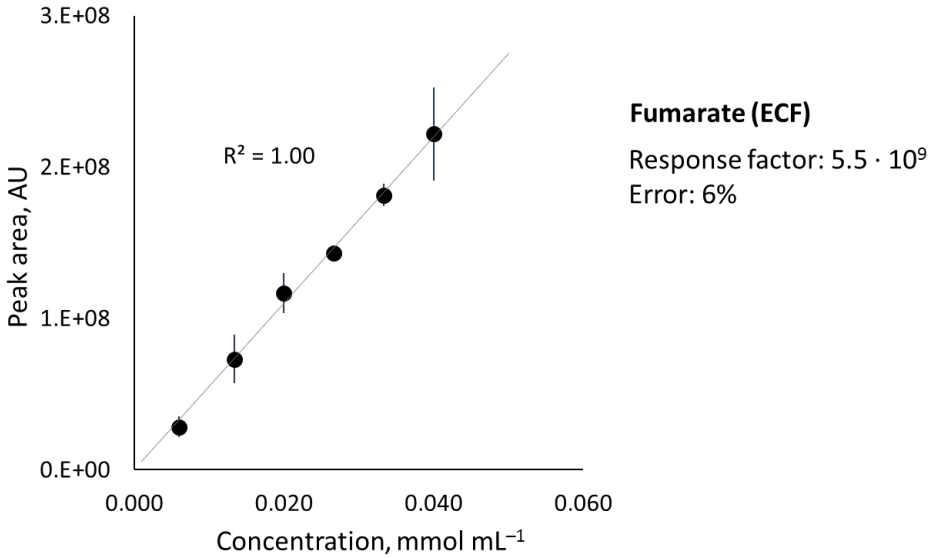

Fig 51. Correlation between the concentration of an aqueous solution of fumarate and the measured gas chromatography area.

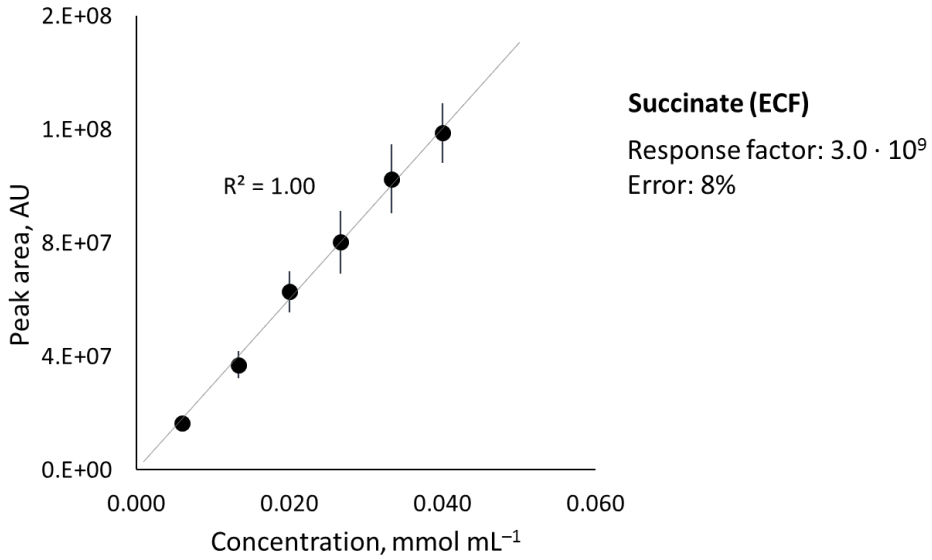

Fig 52. Correlation between the concentration of an aqueous solution of succinate and the measured gas chromatography area.

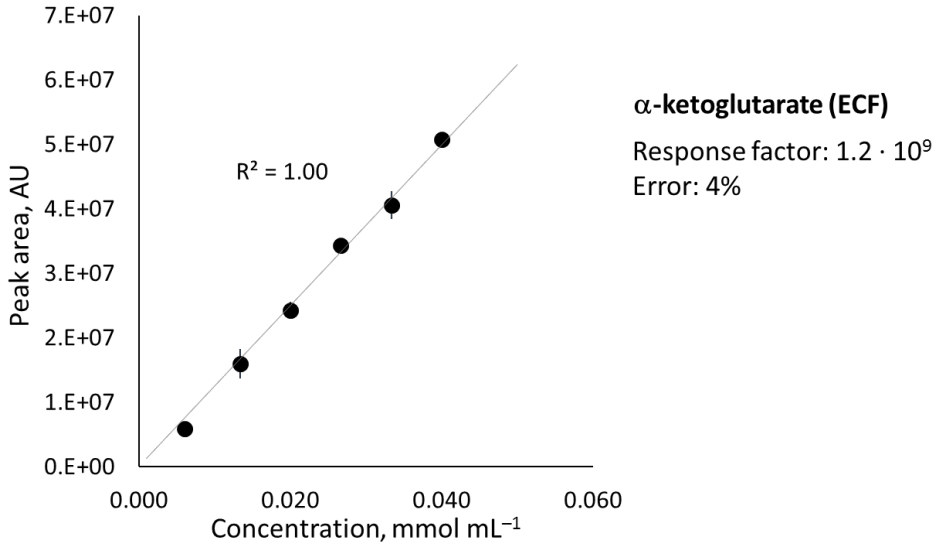

Fig 53. Correlation between the concentration of an aqueous solution of α-ketoglutarate and the measured gas chromatography area.

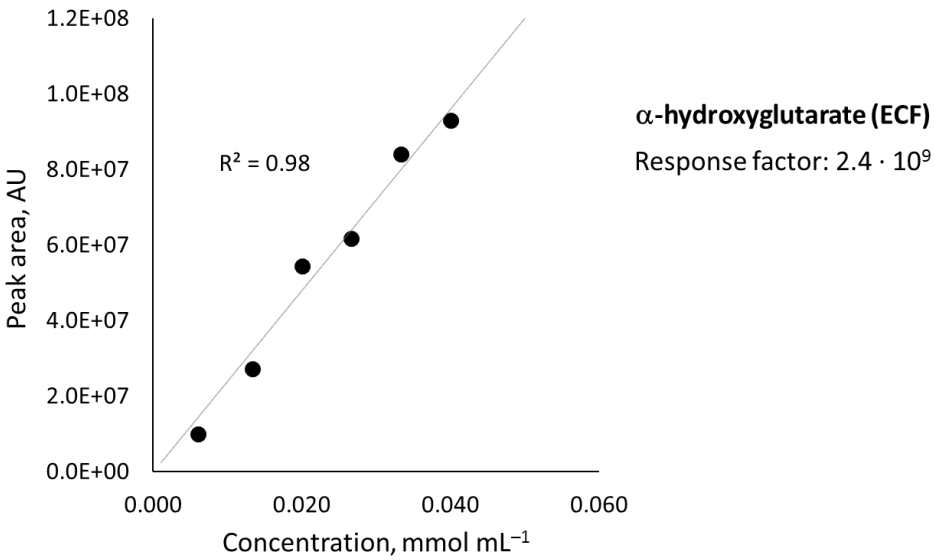

Fig 54. Correlation between the concentration of an aqueous solution of α -hydroxyglutarate and the measured gas chromatography peak area. α-Hydroxyglutarate was obtained by a complete reduction of an aqueous solution of α -ketoglutarate with $NaBH_4$. The correlation line shown here corresponds to a single run.

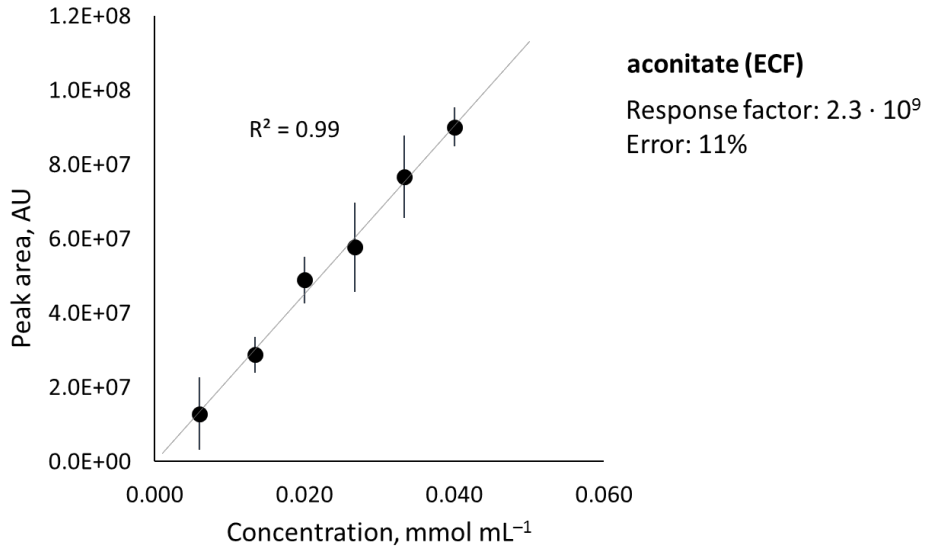

Fig 55. Correlation between the concentration of an aqueous solution of cis-aconitate and the measured gas chromatography peak area.

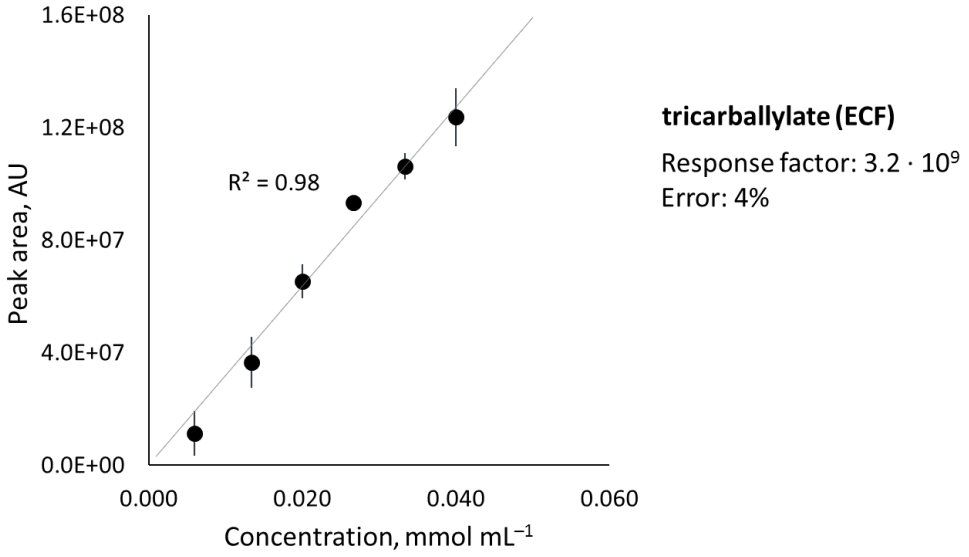

Fig 56. Correlation between the concentration of an aqueous solution of tricarballylate and the measured gas chromatography peak area.

Derivatization with methyl chloroformate (MCF)

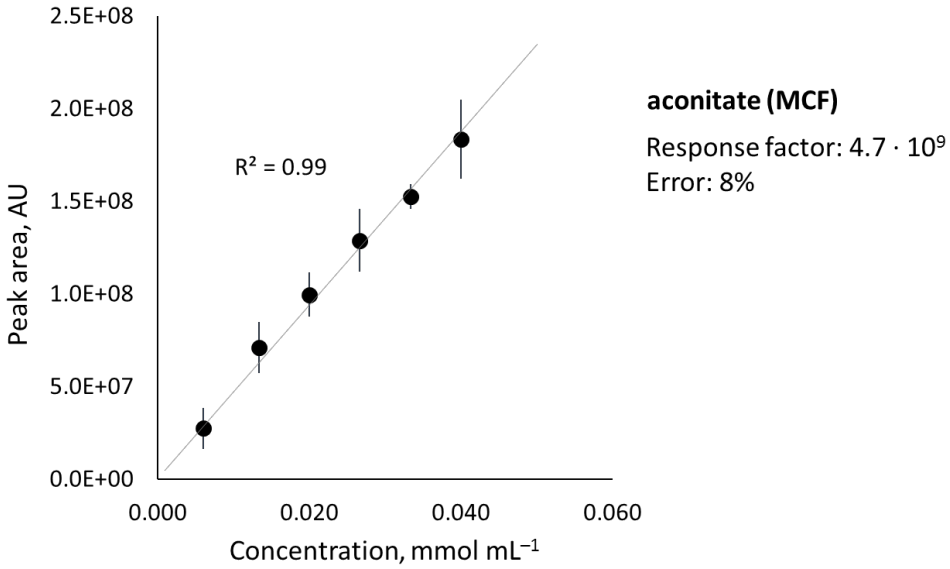

Fig 57. Correlation between the concentration of an aqueous solution of cis-aconitate and the measured gas chromatography peak area.

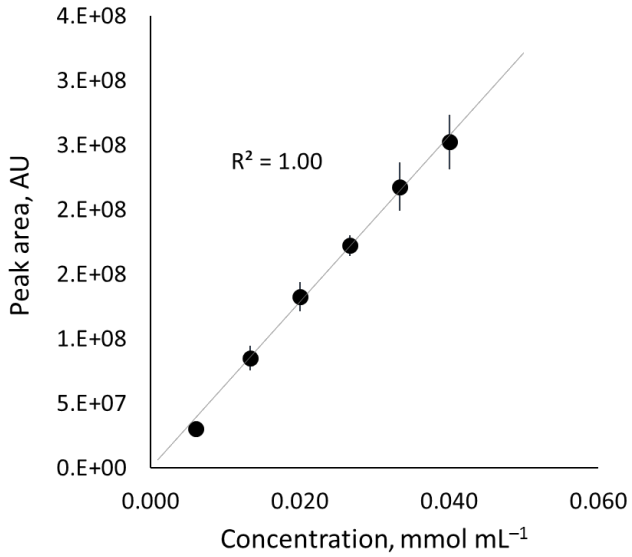

Fig 58. Correlation between the concentration of an aqueous solution of isocitrate and the measured gas chromatography peak area.

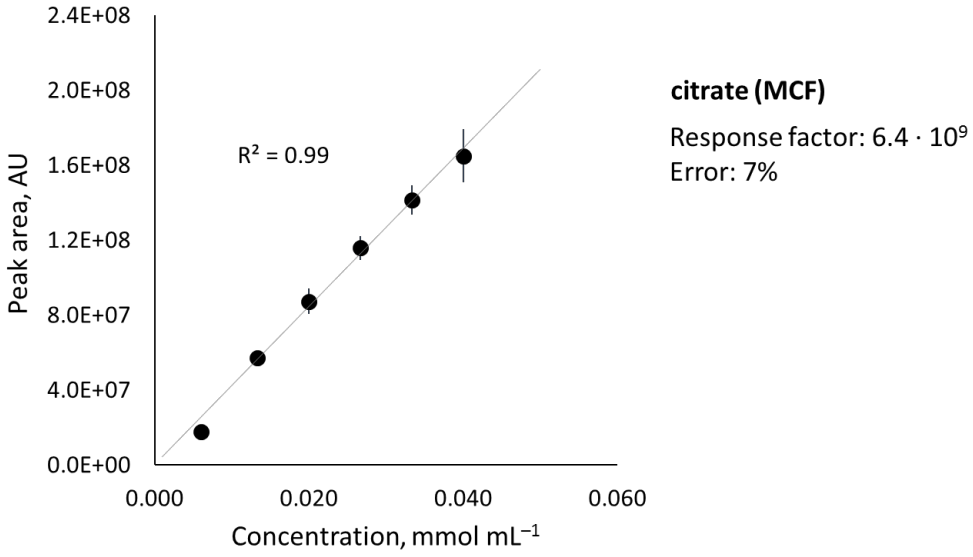

Fig 59. Correlation between the concentration of an aqueous solution of citrate and the measured gas chromatography peak area.

1.4. Formation of rTCA intermediates

1.4.1. General procedure: Fe^0 / Zn^{2+}/ Cr^{3+}reactions

For Table 17.

To a 10 mL Pyrex pressure tube containing a Teflon-coated magnetic stir bar was added (unless otherwise specified) carboxylic acid substrate(s) (1 equiv, 0.100 mmol of each acid), Fe^0 powder (10 equiv, 1.0 mmol, 56 mg Fe^0 or 59 mg Ni^0), and/or $ZnCl_2$ (15 equiv, 1.50 mmol, 204 mg), and/or $Cr_2(SO_4)_3 \cdot 12H_2O$ (3 equiv, 0.300 mmol, 183 mg). This was followed by the addition of 3 mL of solvent (unless otherwise specified: 1 M HCl in H_2O). The contents of the tube were flushed for ≈ 30 s with Ar. The tube was then quickly sealed, and the reaction mixture magnetically agitated for 16 h in a 12-tube metal heating block that was maintained at an internal temperature of 140 °C using an electronic thermocouple. The reaction tube was subsequently removed from the heating block and allowed to cool to room temperature before derivatization and GC-MS analysis.

1.4.2. Metal screens

Malate dehydration – inorganic salts of the following metals were used in the malate dehydration reaction screen: Zn^{2+}, Cu^{2+}, Ni^{2+}, Co^{2+}, Fe^{2+}, Mn^{2+}, Cr^{2+}, V^{2+}. Zn^{2+} gave the best yields when used together with Fe^0 (2-step reaction) (Table 13).

Isocitrate dehydration – inorganic salts of the following metals were used in the isocitrate dehydration reaction screen: Zn^{2+}, Cu^{2+}, Ni^{2+}, Co^{2+}, Fe^{2+}, Mn^{2+}, Cr^{2+}, V^{2+}, Pd^{2+}, Cd^{2+}, Fe^{3+}, Mn^{3+}, Cr^{3+}, As^{3+}, Ru^{3+}, Ir^{3+}, Rh^{3+}, Ti^{3+}. Zn^{2+} was chosen for further experiments due to high yields and geochemical accessibility, although considerable reactivity was also seen for Cr^{2+}, Pd^{2+}, Fe^{3+}, Mn^{3+}, As^{3+}, Ru^{3+}, Ir^{3+} and Rh^{3+} (Table 14).

Aconitate hydration – inorganic salts of the following metals were used in the aconitate hydration reaction screen: Cu^{+}, Zn^{2+}, Cu^{2+}, Ni^{2+}, Co^{2+}, Fe^{2+}, Mn^{2+}, Cr^{2+}, Cd^{2+}, Hg^{2+}, Fe^{3+}, Co^{3+}, Mn^{3+}, Cr^{3+}, Ti^{3+}, Ru^{3+}, Mo^{4+}, W^{4+}, Mo^{6+}, W^{6+}. Only Cr^{3+} yielded a significant positive result (Table 15).

Reductions – Metals Zn, Fe, Ni, Mo were used in powder form. These results were compared against MoO_2 and sodium dithionite. Through a control experiment, the reducing properties of TPGS-750-M were excluded (Table 16).

1.4.3. Reactions in micellar solutions

For reactions carried out in micelles, 3 mL of a TPGS-750-M solution (DL-α-tocopherol methoxypolyethylene glycol succinate, 1% w/w) in 1 M HCl was used as the solvent. Stirring was maintained at 1000 rpm. In order to control for the contribution of the surfactant molecule towards succinate detected in the chromatograms, a control reaction was carried out (Reaction 26 in Table S1). A mixture of Fe^0 powder (10 equiv., 1.0 mmol, 56 mg), $ZnCl_2$ (15 equiv. 1.5 mmol, 204 mg), $Cr_2(SO_4)_3 \cdot 12H_2O$ (3 equiv., 0.3 mmol, 183 mg) in TPGS-750-M (3 mL, 1% w/w in 1 M HCl in H_2O) was heated at 140 ˚C for 16 h. After cooling, a 0.1 mmol portion of malic acid was dissolved in the mixture, a 100 µL aliquot of which was immediately derivatized. It was found (two runs) that succinate originating from TPGS-750-M (DL- α-tocopherol methoxypolyethylene glycol succinate) contributes to not more than 1% of the control reaction composition (Entry 25 - Table 17). Micelles may play various roles in the oxaloacetate-malate-fumarate-succinate sequence, e.g. bias the malate-fumarate equilibrium towards fumarate by increasing solubilities of fumarate and succinate or increase the stability of carboxylic acids and thus minimize the mass loss as carbon dioxide.

1.4.4. Portion-wise reagent addition

For Table 17: Entries 1 and 15:

The first half of reagents was added at the beginning of the reaction; the second portion was added after 24 h to a cooled reaction mixture, after which the reaction vessel was re-sealed and heating resumed.

1.4.5. Reaction with oxalosuccinic acid

For* Table 17*: entries 3 and 19 – 23:

Due to its high instability, rapid decarboxylation and storage difficulties, oxalosuccinic acid was prepared on demand by in situ hydrolysis of triethyl oxalosuccinate ester under typical acidic reaction conditions (1 M HCl).

1.5. Experimental data

1.5.1. GC-MS chromatograms of authentic samples

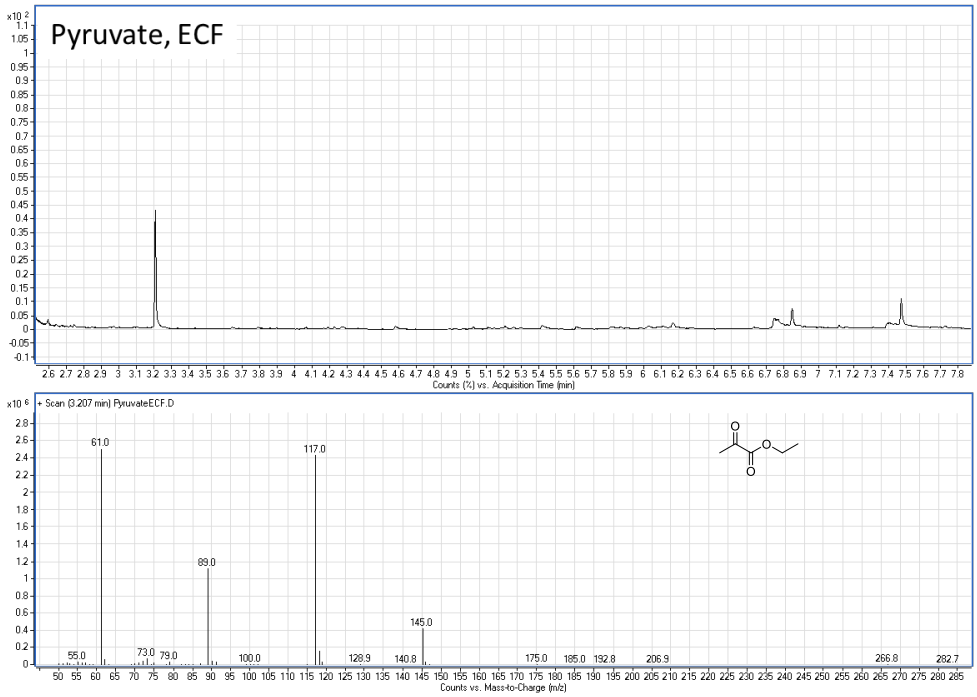

Fig 60. GC trace and mass spectrum of pyruvate characteristic peak (ECF derivatization).

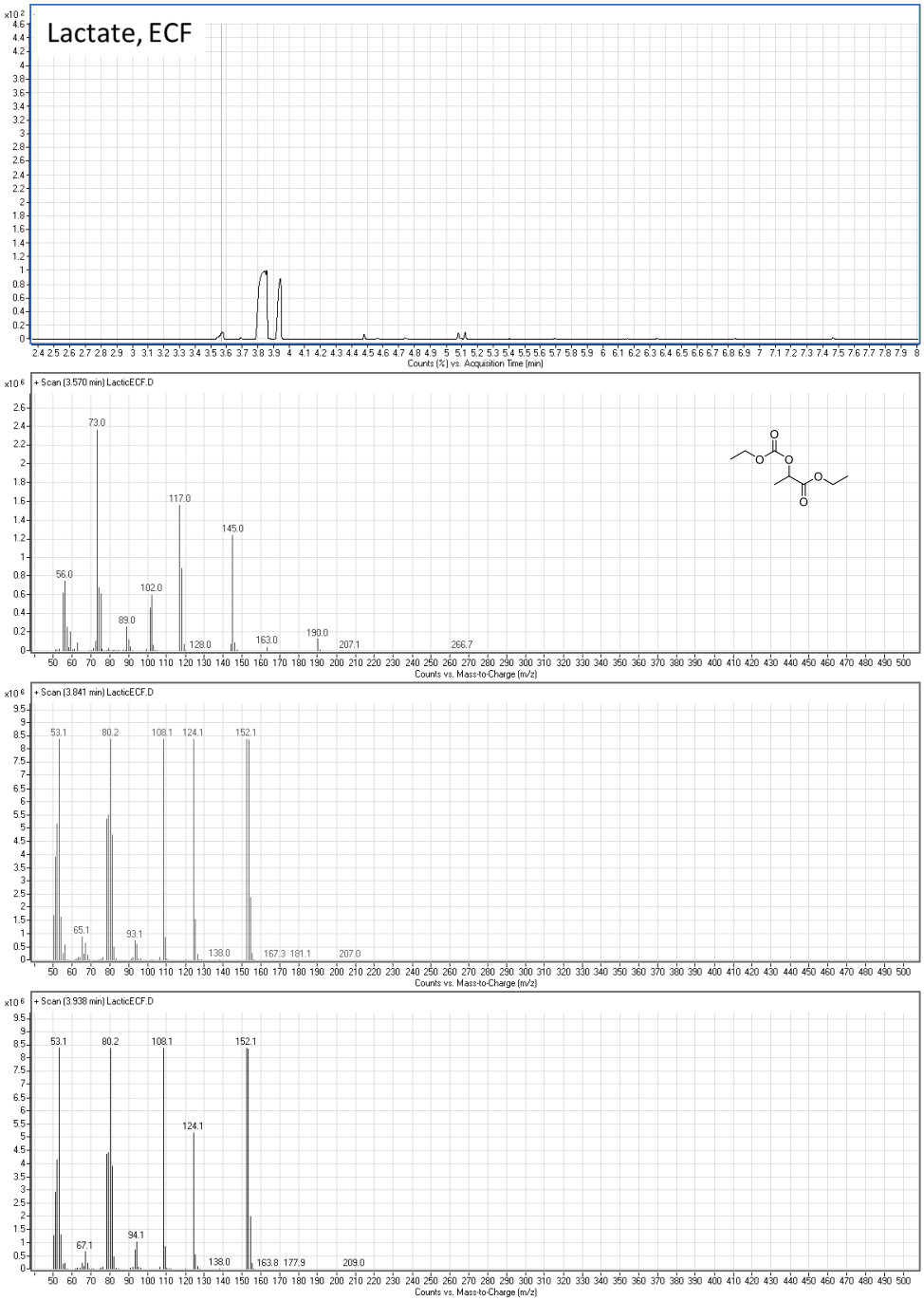

Fig 61. GC trace and mass spectra of lactate characteristic peaks (ECF derivatization).

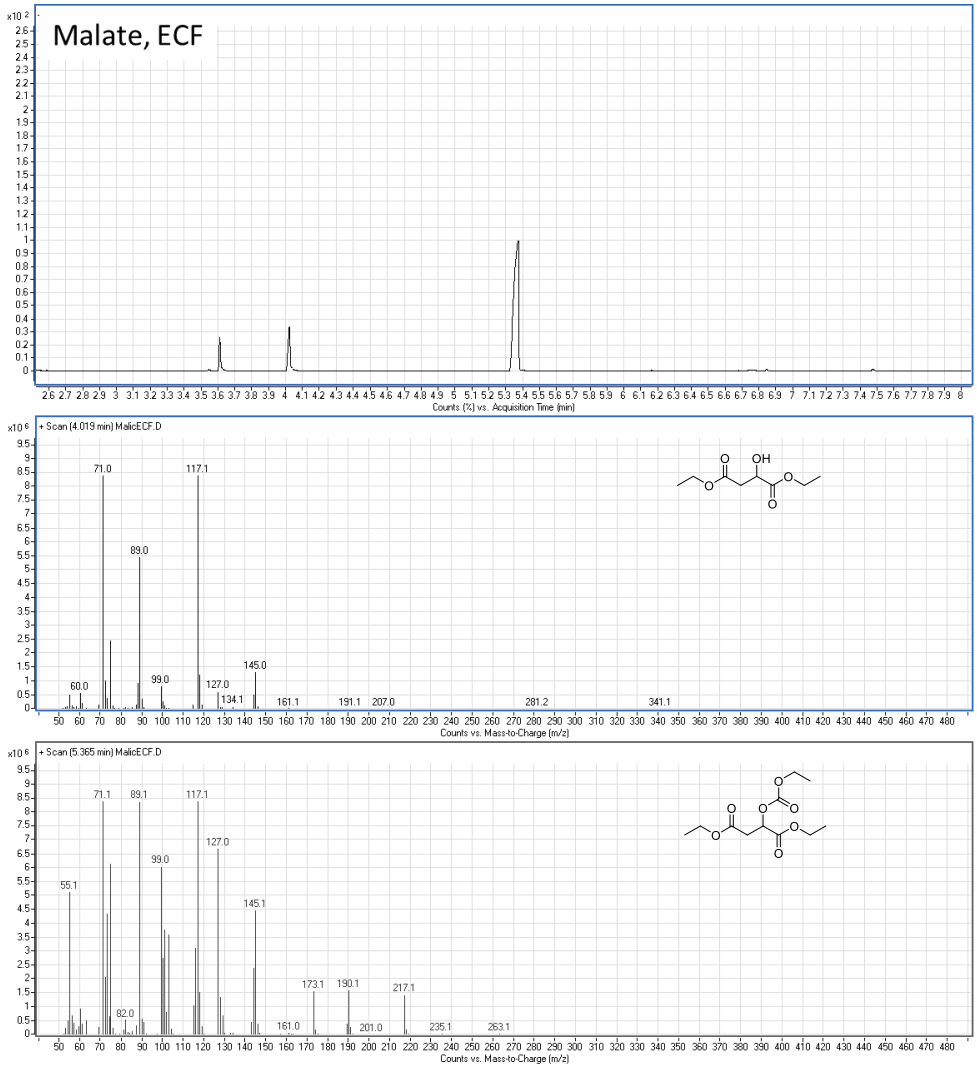

Fig 62. GC trace and mass spectra of malate characteristic peaks (ECF derivatization). The additional peak at ~3.6 min corresponds to trace fumarate (result of O-acylation of the hydroxyl group during derivatization and subsequent elimination, well below 5 % at malate concentrations ≤ 0.04 M).

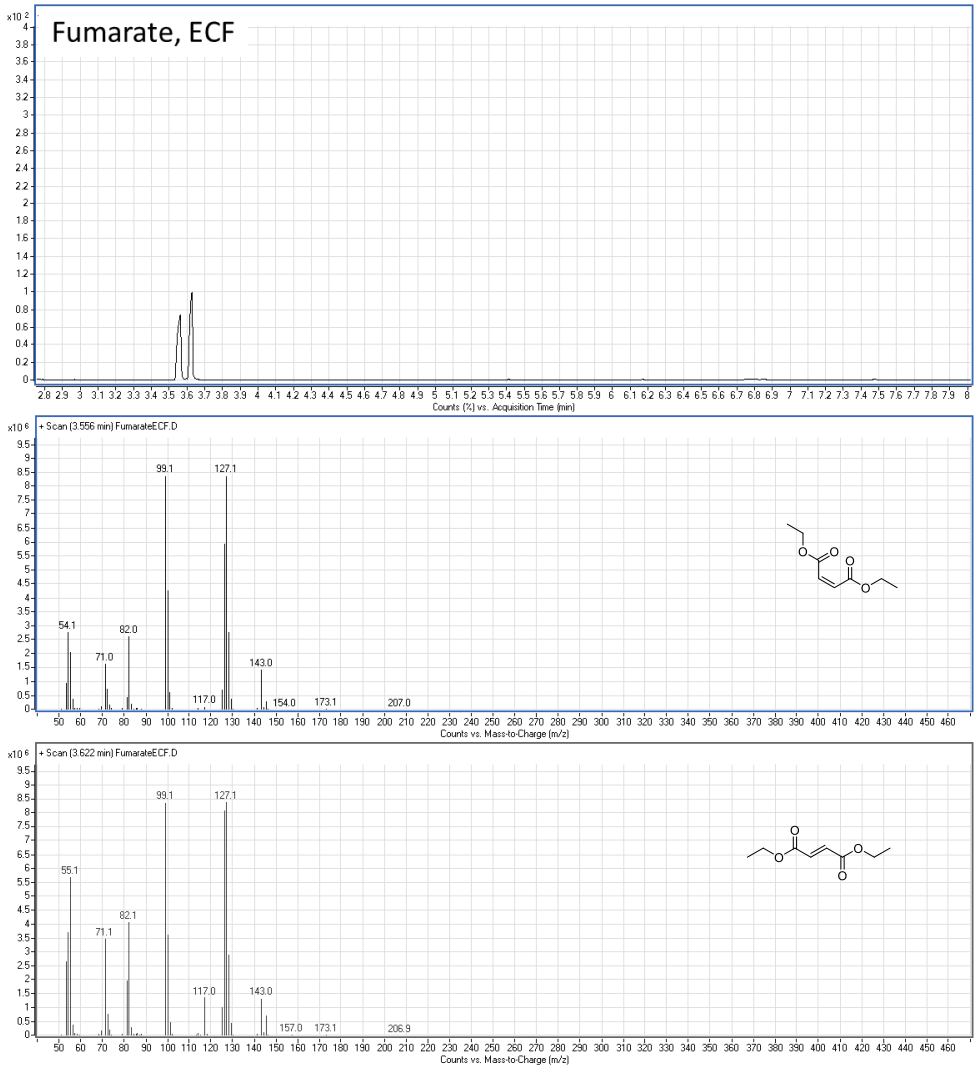

Fig 63. GC trace and mass spectra of fumarate characteristic peaks (ECF derivatization).

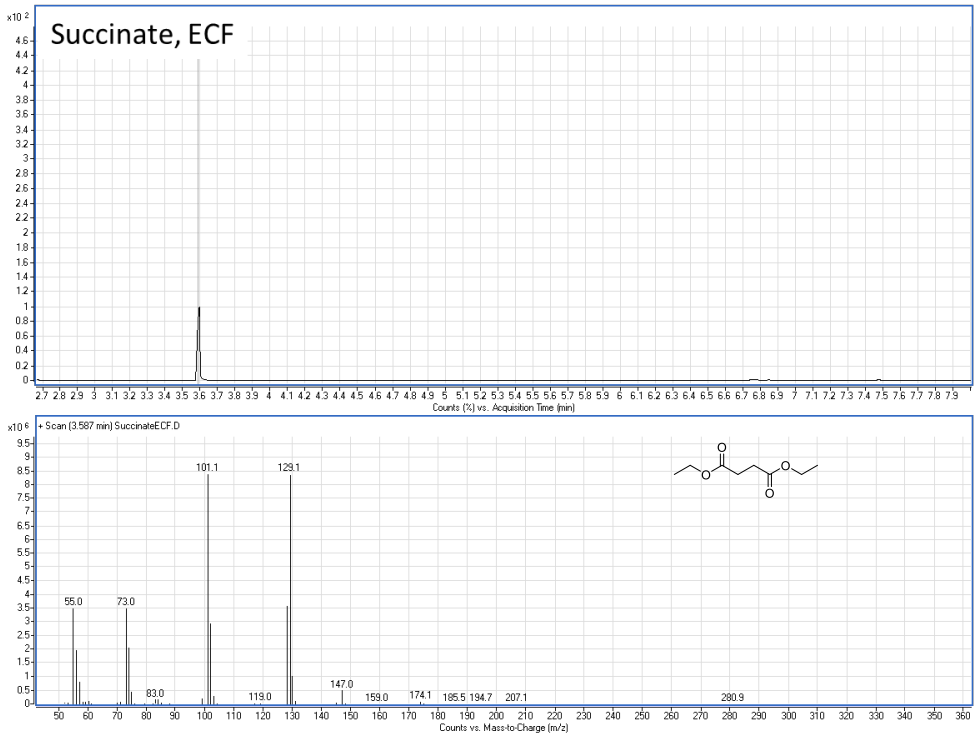

Fig 64. GC trace and mass spectrum of succinate characteristic peak (ECF derivatization).

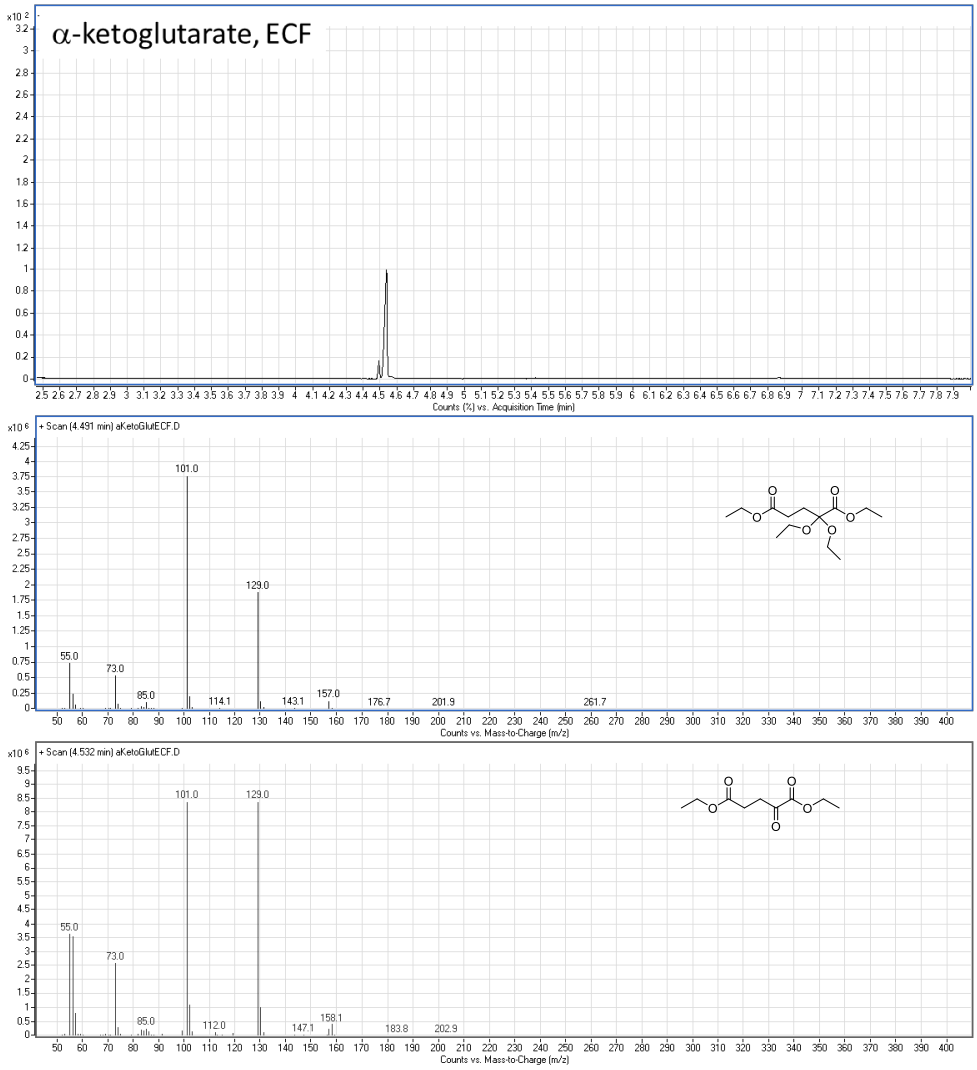

Fig 65. GC trace and mass spectra of α-ketoglutarate characteristic peaks (ECF derivatization).

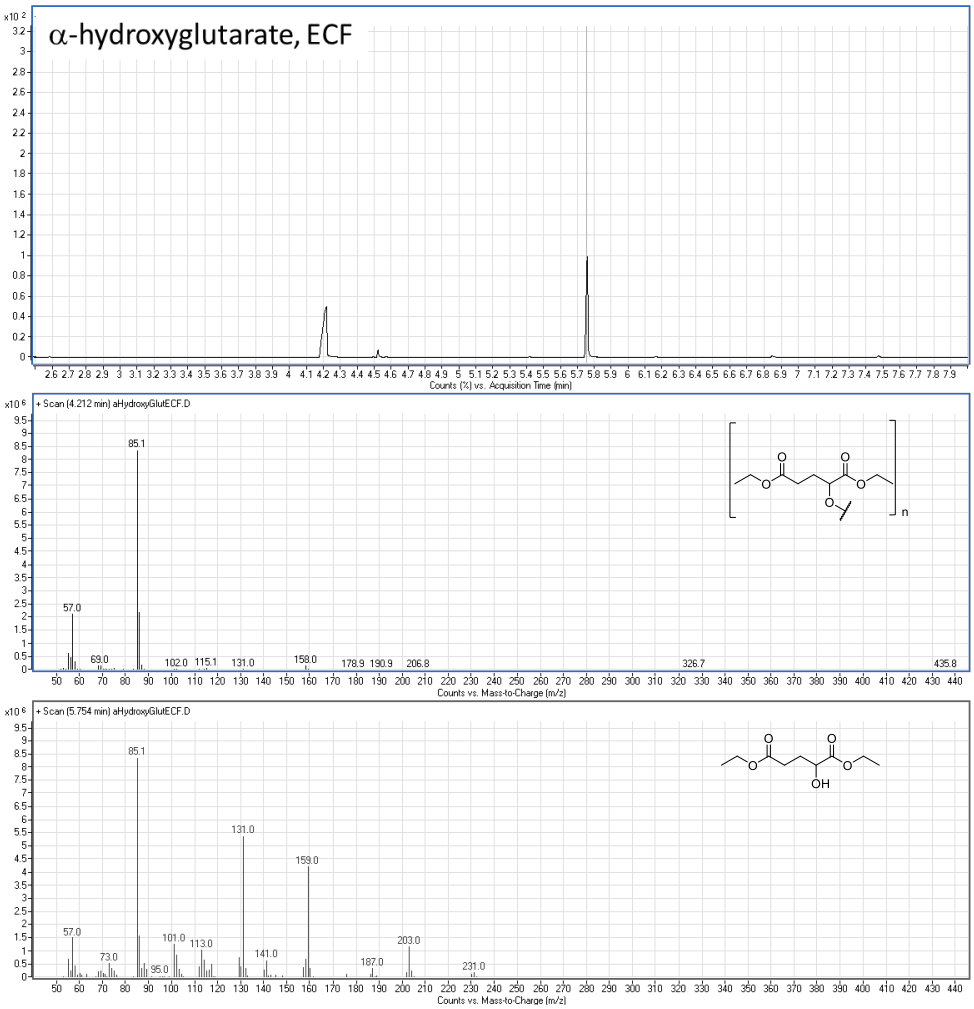

Fig 66. GC trace and mass spectra of α-hydroxyglutarate characteristic peaks (ECF derivatization).

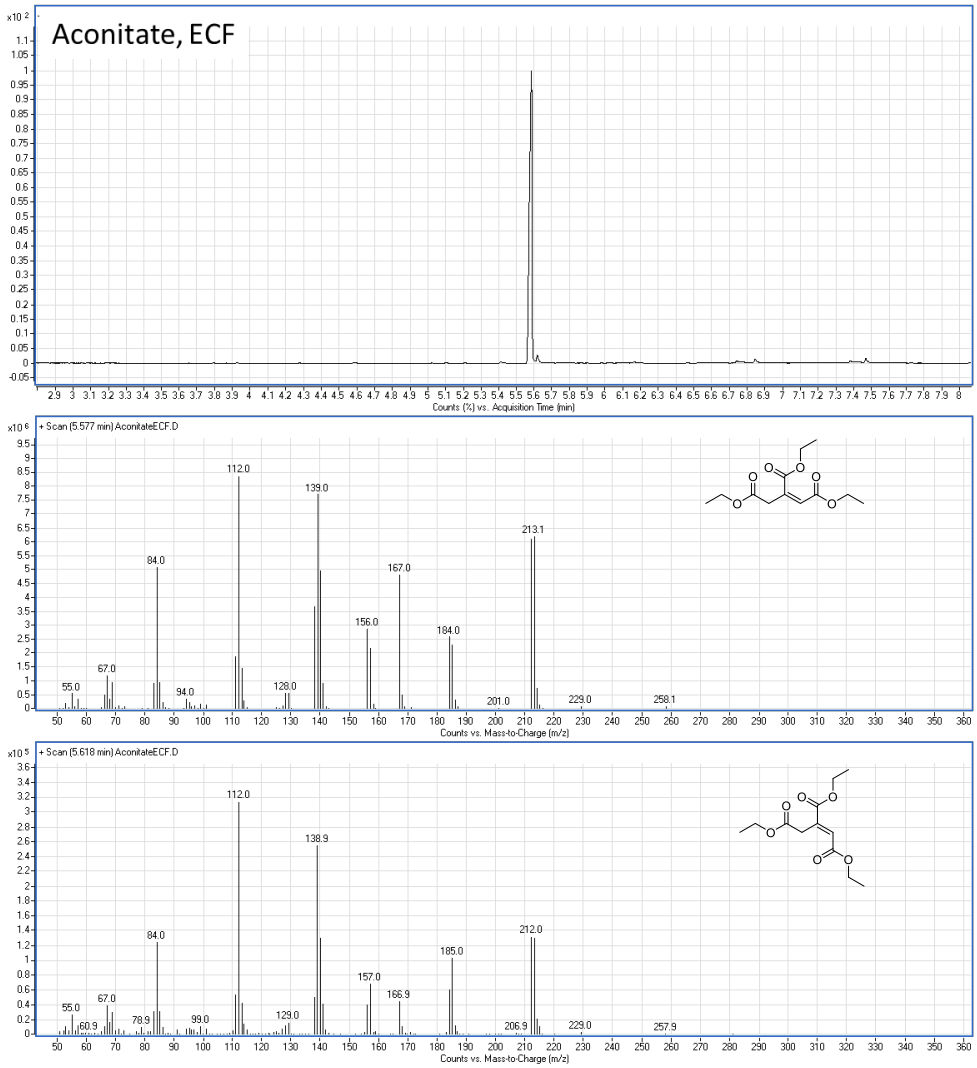

Fig 67. GC trace and mass spectra of cis-aconitate characteristic peaks (ECF derivatization).

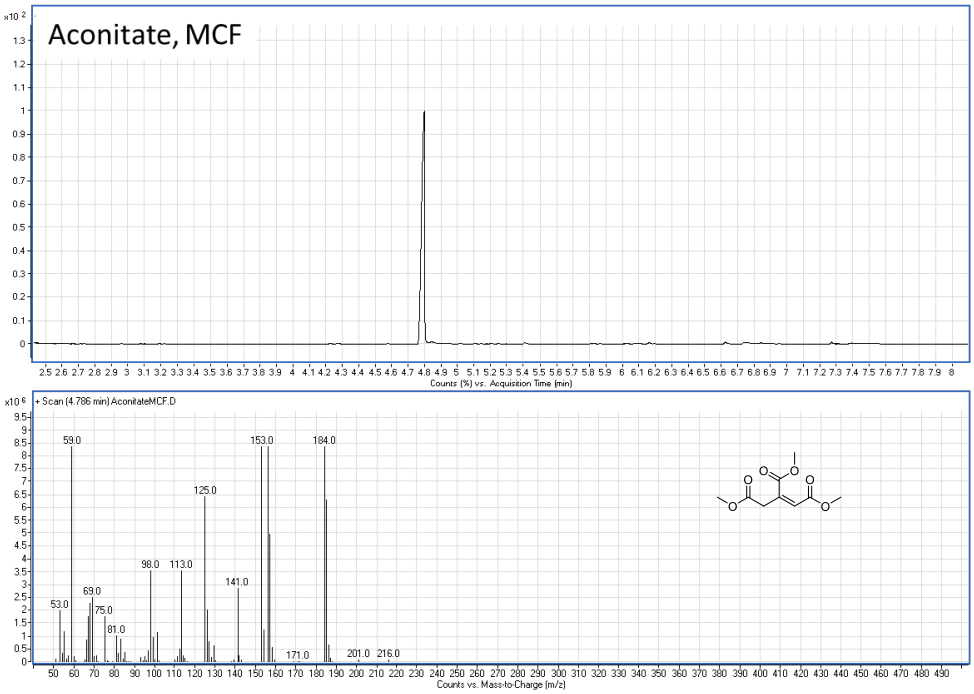

Fig 68. GC trace and mass spectrum of cis-aconitate characteristic peak (MCF derivatization).

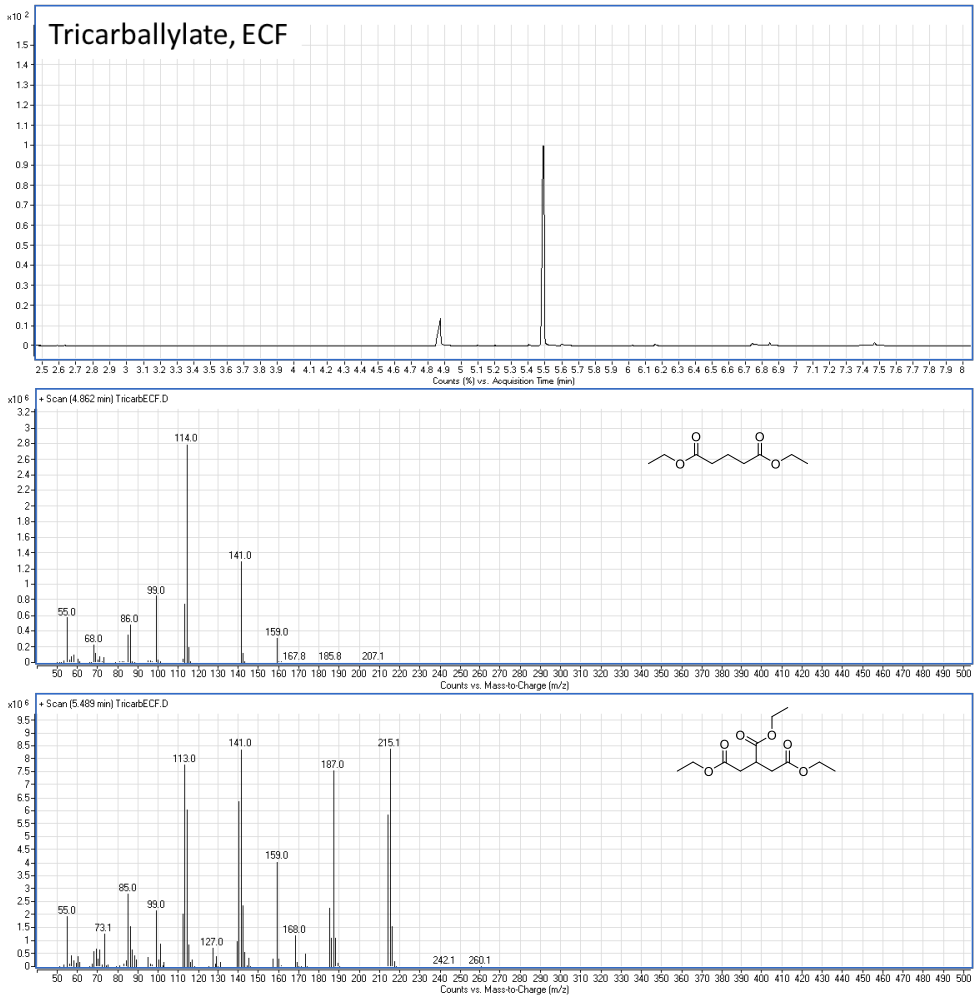

Fig 69. GC trace and mass spectra of tricarballylate characteristic peaks (ECF derivatization).

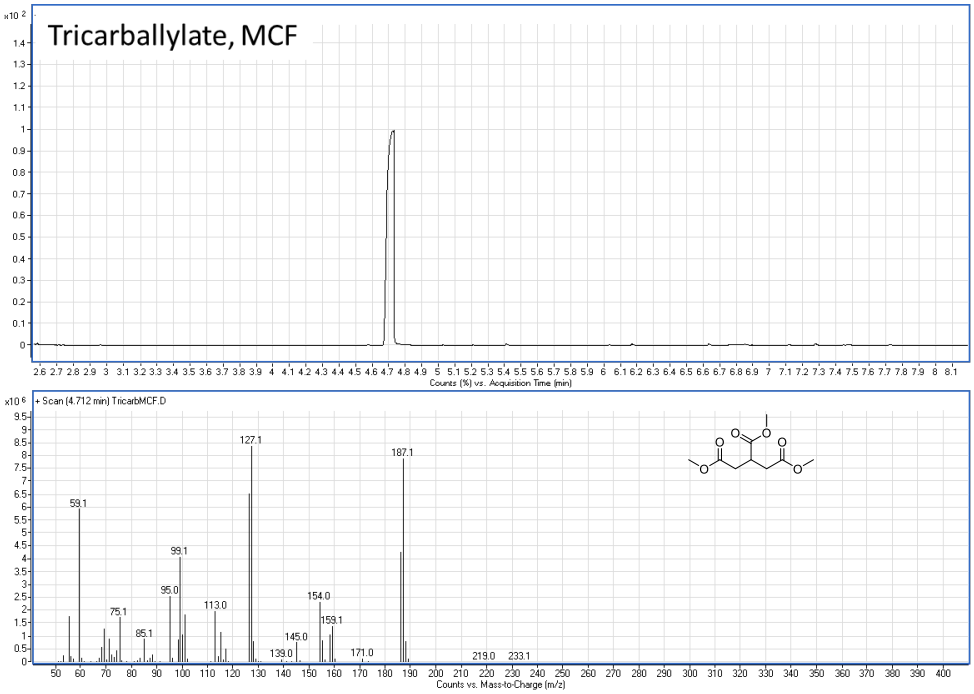

Fig 70. GC trace and mass spectrum of tricarballylate characteristic peak (MCF derivatization).

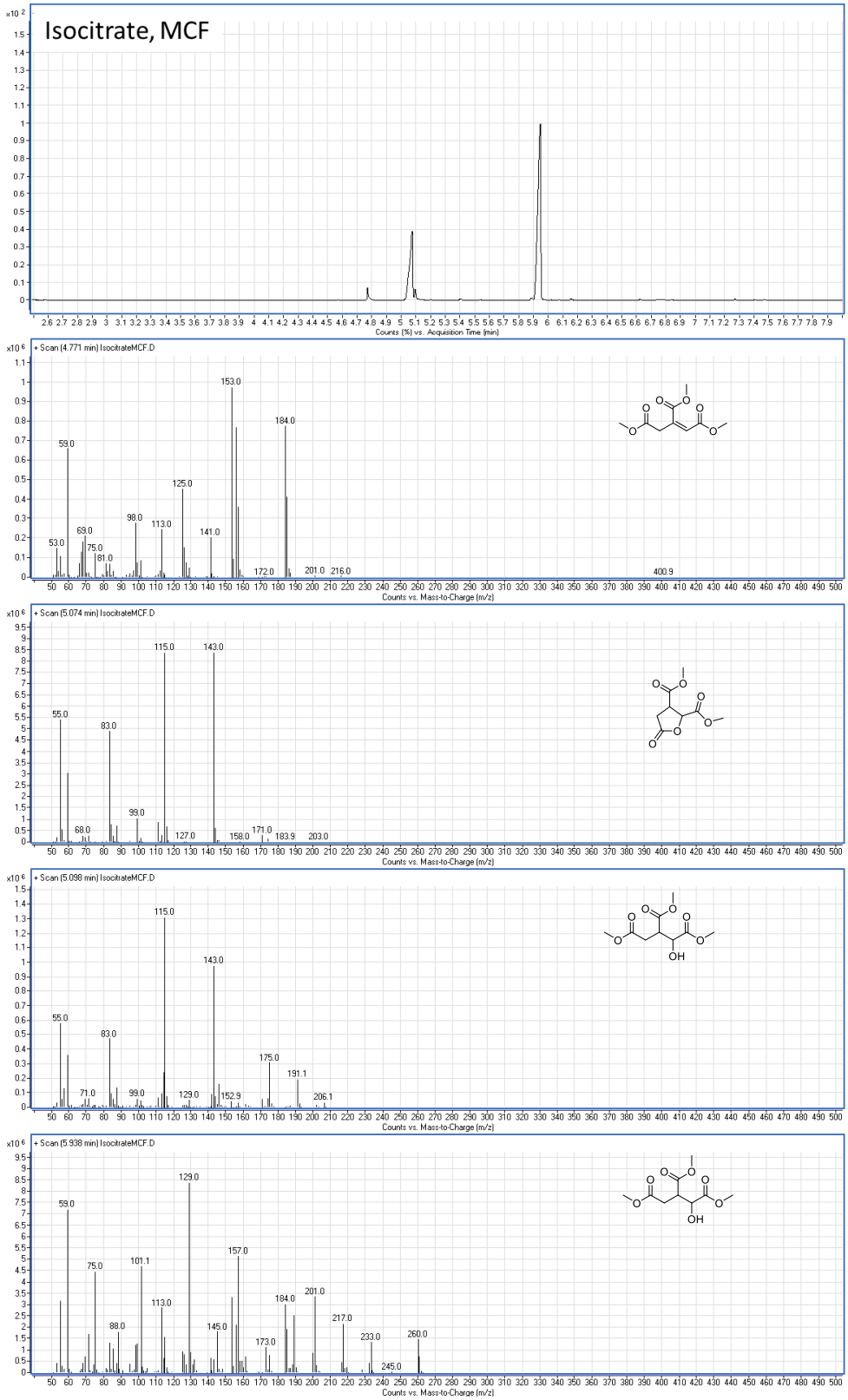

Fig 71. GC trace and mass spectra of isocitrate characteristic peaks (MCF derivatization). The additional peak at ~4.8 min corresponds to trace aconitate (result of O-acylation of the hydroxyl group during derivatization and subsequent elimination, < 5 % at isocitrate concentrations ≤ 0.04 M).

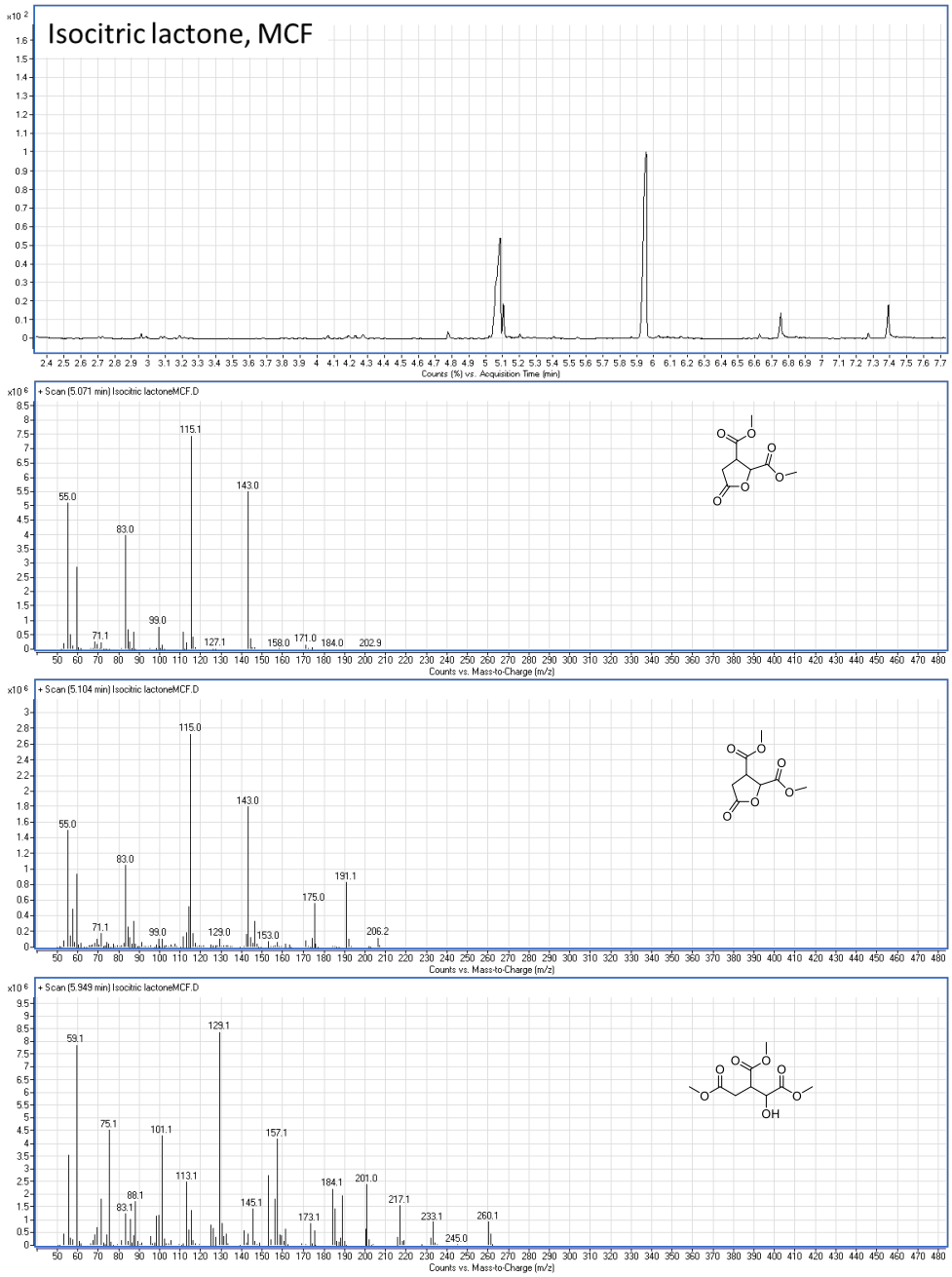

Fig 72. GC trace and mass spectra of isocitric lactone characteristic peaks (MCF derivatization).

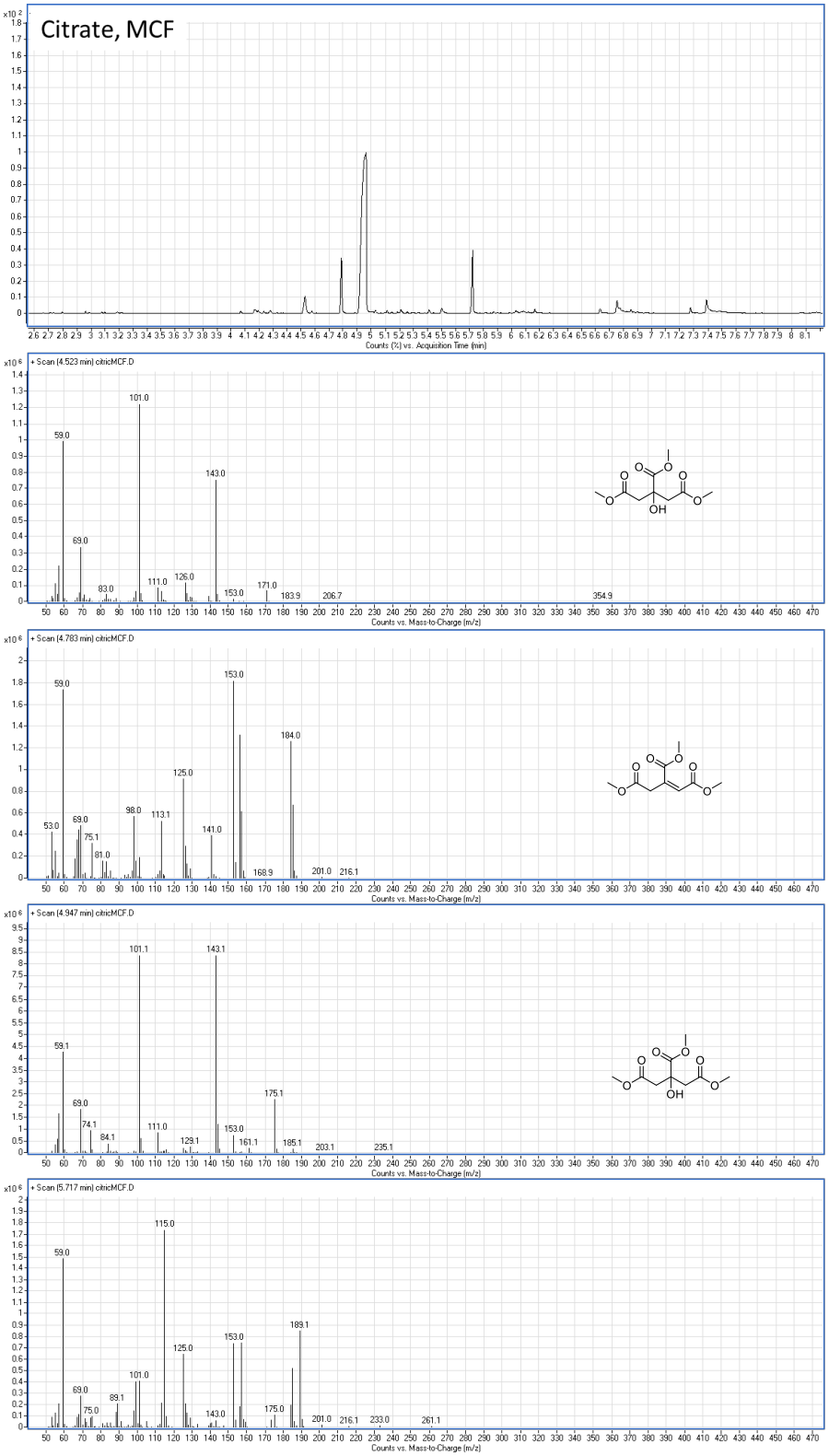

Fig 73. GC trace and mass spectra of citrate characteristic peaks (MCF derivatization). The additional peak at ~4.8 min corresponds to trace aconitate (result of O-acylation of the hydroxyl group during derivatization and subsequent elimination, < 5 % at citrate concentrations ≤ 0.04M).

1.5.2. Metal-promoted malate dehydration screen.

Table 13. Metal-promoted malate **4** dehydration screen.[a]

Entry	Metal salt (10 equiv.)	Malate (**4**) (% of mixture)	Fumarate (**5**) (% of mixture)	Succinate (**6**) (% of mixture)
1	$Ni(acac)_2$	95	5	0
2	$NiCl_2\ 5H_2O$	88	12	<1
3	$FeSO_4\ 7H_2O$	94	6	0
4	$CuSO_4\ 5H_2O$	96	4	0
5	$MnSO_4\ H_2O$	94	6	0
6	$CoCl_2\ 6H_2O$	96	4	0
7	VCl_2	92	8	<1
8	$CrCl_2$	95	5	0
9	$Cr_2(SO_4)_3\ 12H_2O$	98	2	<1
10	$ZnCl_2$	94±1	4±1	2±1

[a] Unless otherwise specified: 0.08 mmol malic acid, Fe^0 powder (10 equiv.), 3 mL 1 M HCl in H_2O, 16 h, 140 ˚C. Where applicable, errors correspond to ±mean absolute deviation.

1.5.3. Metal-promoted isocitrate dehydration screen.

Table 14. Metal-promoted isocitrate **10** dehydration screen.[a]

Entry	Metal salt (1 equiv.)	Temp. (°C)	Micelles	Isocitrate (**9**) (% of mixture)	Aconitate (**10**) (% of mixture)
1	$Ni(acac)_2$	140 °C	-	91	9
2	$FeSO_4$ $7H_2O$	140 °C	-	95	5
3	$CuSO_4$ $5H_2O$	140 °C	-	94	6
4	$MnSO_4$ H_2O	140 °C	-	94	6
5	$CoCl_2$ $6H_2O$	140 °C	-	94	6
6	Cd(OAc) $2H_2O$	140 °C	-	95	5
7	VCl_2	140 °C	-	95	5
8	Fe_2O_3	140 °C	-	95	5
9	Mn_2O_3	140 °C	-	97	3
10	Cr_2O_3	140 °C	-	95	5
11	As_2O_3	140 °C	-	49	51
12	$RuCl_3$	140 °C	-	58	42
13	$IrCl_3$	140 °C	-	51	49
14	$RhCl_3$	140 °C	-	54	46
15	$TiCl_3$	140 °C	-	100	0
16	$CrCl_3$	160 °C	-	100	0
17	$Pd(acac)_2$	140 °C	-	47	53
18 [b]	$CrCl_2$	140 °C	-	62	38
19	$ZnCl_2$	140 °C	-	51±12	49±12
20[c]	$ZnCl_2$	140 °C	-	93±1	7±1
21[c]	$ZnCl_2$	140 °C	1% w/w	88±2	12±2
22[c]	$ZnCl_2$	25 °C	-	97	3
23[c]	$ZnCl_2$	25 °C	1% w/w	97	3
24[c]	-	140 °C	-	97	3
25[c]	-	140 °C	1% w/w	98	2
26[c]	-	25 °C	-	97	3

[a] Unless otherwise specified: 0.08 mmol isocitrate (as trisodium isocitrate hydrate),3 mL 1 M H_2SO_4 in H_2O, 48 h, 140 °C. [b] $TiCl_3$ as 20% w/w solution in 2N HCl [c] 1 M HCl in H_2O, 48 h. Where applicable, errors correspond to ±mean absolute deviation.

1.5.4. Metal-promoted aconitate hydration screen.

Table 15. Metal-promoted aconitate **11** hydration screen.[a]

Entry	Metal salt (1 equiv.)	Species present in the mixture post-reaction (%)			
		Isocitrate (**10**)	Aconitate (**11**)	Citrate (**12**)	Tricarballylate (**17**)
1	$FeCl_3$	-	99	1	-
2	$Cr_2(SO_4)_3$ $12H_2O$	-	67	33	-
3	$TiCl_3$[b]	-	82	10	9
4	$IrCl_3$	-	67	2	31
5	$RuCl_3$	-	97	3	-
6	$Co(OAc)_2$	-	98	2	-
7	$BiBr_3$	-	>99	<1	-
8	$TbCl_3$ $6H_2O$	8	92	<1	-
9	-	-	100	-	-

[a] Unless otherwise specified: 0.08 mmol aconitate, 3 mL 1 M H_2SO_4 in H_2O, 1 h at 20 °C, then 16 h at 140 °C. [b] $TiCl_3$ as 20% w/w solution in 2N HCl

‡ In the aconitate hydration screen the following salts/oxides did not yield any citrate: CuI, $ZnSO_4$, $CuSO_4$ $5H_2O$, $NiSO_4$ $7H_2O$, $CoSO_4$ $7H_2O$, $FeSO_4$ $7H_2O$, $MnSO_4$ H_2O, $CrCl_2$, $Cd(OAc)_2$ $2H_2O$, $HgCl_2$, $Co(NH_3)_6Cl_3$, $Mn(OAc)_3$ $2H_2O$, MoO_2, MoO_3, WO_2, WO_3

1.5.5. Reduction selectivity screen.

Table 16. Reduction selectivity screen on five rTCA intermediates.[a]

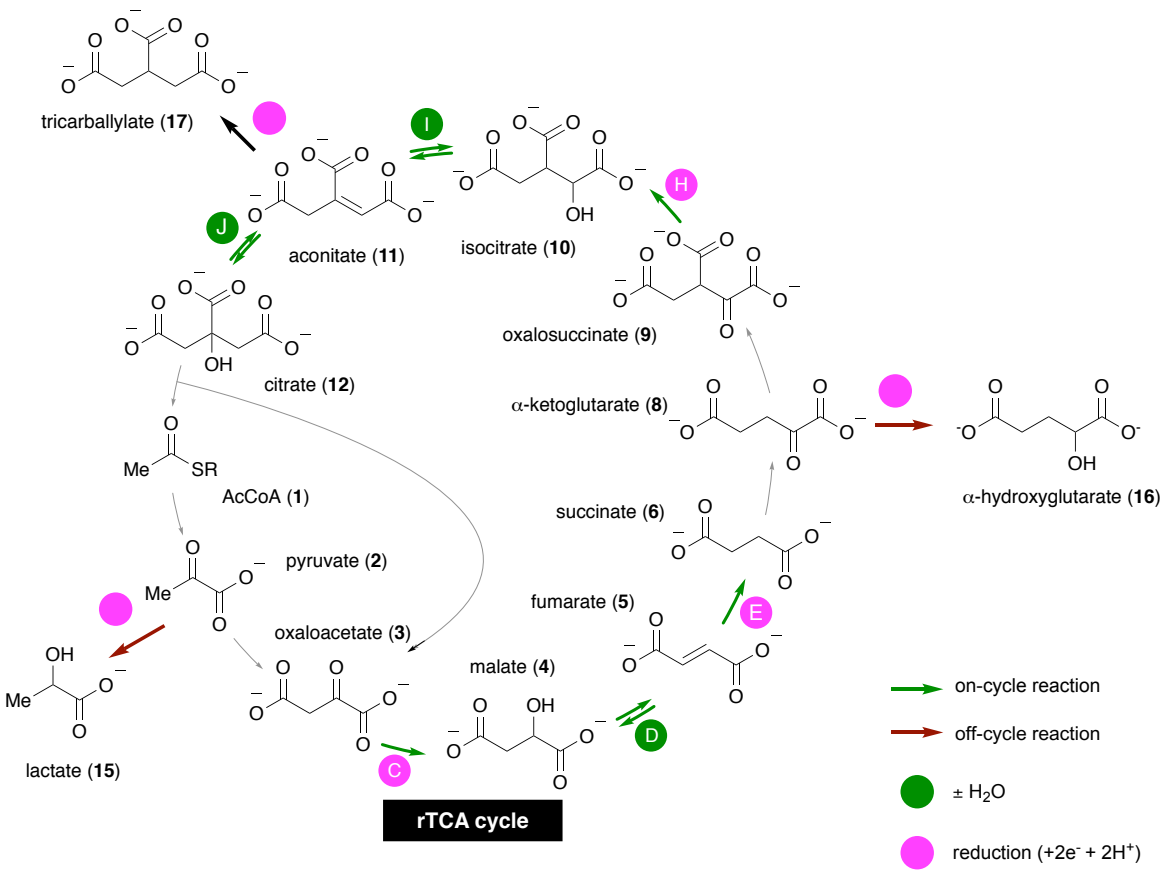

Entry	Substrates	Reductant	Species present in the mixture post-reaction (%)								
			On-cycle						*Off-cycle*		
			2	**4**[b]	**5**[b]	**6**	**8**	**11**	**15**	**16**	**17**
1	**2+3+5+8+11**	Fe	13	13	3	19	1	25	1	23	1
2		Ni	32	3	5	11	25	22	0	1	1
3		Zn	0	20	30	4	0	1	2	35	8
4		Mn	19	7	14	4	11	25	1	14	4
5		$Na_2S_2O_4$	35	0	14	3	14	33	0	0	1
6		Mo	*No reaction (only starting materials present)*								
7		MoO2	*No reaction (only starting materials present)*								
8		TPGS-750-M[c]	*No reaction (only starting materials present)*								

[a] Reaction conditions: 0.1 mmol of each: sodium pyruvate, oxaloacetic acid, fumaric acid, **α**-ketoglutaric acid, cis-aconitic acid; 10 equiv. of reductant, 3 mL 1M HCl in H_2O, 3 h, 40°C. [b] Malate-fumarate equilibrium. [c] Control experiment to exclude reducing properties of micelles (1% w/w TPGS-750-M in 1M HCl in H_2O).

1.5.6. Non-enzymatic reaction of the rTCA cycle.

Table 17. Non-enzymatic reactions of the rTCA cycle. **Table 17** continues the following page.

Entry	Substrate (0.1 mmol each)	Conditions[a]				Species present in the mixture post-reaction (%)										
						On-cycle								*Off-cycle*		
		Fe^0 (equiv.)	Zn^{2+} (equiv.)	Cr^{3+} (equiv.)	Micelles	**2**	**4**	**5**	**6**	**8**	**10**	**11**	**12**	**15**	**16**	**17**
Reduction																
1	**3**	10	-	-	-		90±2	10±2								
2[b]	**5**	10	-	-	-		15±5	20±2	65±7							
3[b]	**9**	10	-	-	-				12±5		83±4	5±1				
Hydration/Dehydration																
4[c]	**4**	-	10	-	-		86±1	14±1								
5[c]	**4**	10	10	-	-		94±1	4±1	2±1							
6[c]	**4**	10	10	-	yes		84±1	6±1	10±2							
7[d]	**4**	10	10	-	yes		82±1	7±2	11±3							
8[c,e]	**10**	-	1	-	-						51±12	49±12				
9[e]	**10**	-	1	-	-						93±1	7±1				
10[c,e]	**11**	-	1	-	-						12±9	88±9				
11[c]	**11**	-	1	-	-						8±0	92±0				
12[f]	**11**	-		6	-							67±0	33±0			
13[f]	**12**	-		6	-							23±5	77±5			
Three-step sequences																
14[c,g]	**3**	20	-	-	-		90±2	8±1	2±1							
15[c,h]	**3**	10	15	4	-		83±1	6±3	4±1					7±3		
16	**3**	10	15	4	yes		55±7	4±0	23±6					19±5		
17[d]	**3**	10	15	4	-		98±0	2±0								
18[d]	**3**	10	15	4	yes		52±2	3±3	41±3					4±2		
19[c,g,i]	**9**	10	-	1	-				13±7		64±11	20±4	3±1			
20[j]	**9**	5	10	-	-				16±2	4±2	76±3	4±1				
21[j]	**9**	-	10	6	-	*Mixture of oxalosuccinate decomposition products, incl. succinate*										
22[j]	**9**	5	10	6	-						65±7	30±4	2±1		3±4	
23[j]	**9**	5	10	6	yes				5±4		72±5	21±0	2±1			

Continued from the previous page

Table 17. Non-enzymatic reactions of the rTCA cycle.

Entry	Substrate (0.1 mmol each)	Conditions[a]				Species present in the mixture post-reaction (%)										
						On-cycle								*Off-cycle*		
		Fe^0 (equiv.)	Zn^{2+} (equiv.)	Cr^{3+} (equiv.)	Micelles	**2**	**4**	**5**	**6**	**8**	**10**	**11**	**12**	**15**	**16**	**17**
Competitive reduction																
24[k]	**2+3+5+8+11**	10	15	6	yes	20±0	6[l]±2	18[l]±2	4±2	20±3		28±4		2±0	2±1	<1±0
Micelle control experiment																
25[m]	**-**	10	15	6	yes		99±0	1±0								

[a] Unless otherwise specified: 1 M HCl in H_2O, 16 h, 140 °C. [b] 3 h, 140 °C. [c] 48 h, 140 °C. [d] 20 °C, 24 h. [e] 1 M H_2SO_4 in H_2O, 16 h, 140 °C. [f] 1 h at 20 °C, 24 h at 140 °C. [g] pH adjusted with conc. HCl to <1 after 24 h. [h] Fe^0 and/or Zn^{2+} added in two portions. [i] Cr^{3+} added after 24 h. [j] Thermal cycling: 16 h at 140 °C, 10 h at 20 °C, 16 h 140 °C. [k] 3 h, 40 °C. [l] Malate-fumarate equilibrium. [m] 0.1 mmol malic acid (4) added post-reaction and immediately derivatized (see Synthetic procedures for details). Reported yields are average values of at least two runs. Errors correspond to ±mean absolute deviation.

Table 17. Entry 1

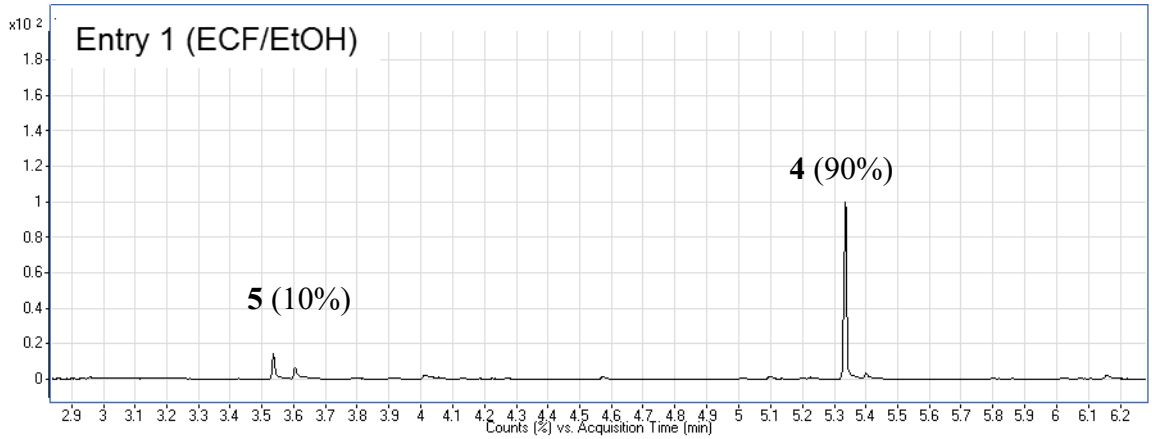

Table 17. Entry 2

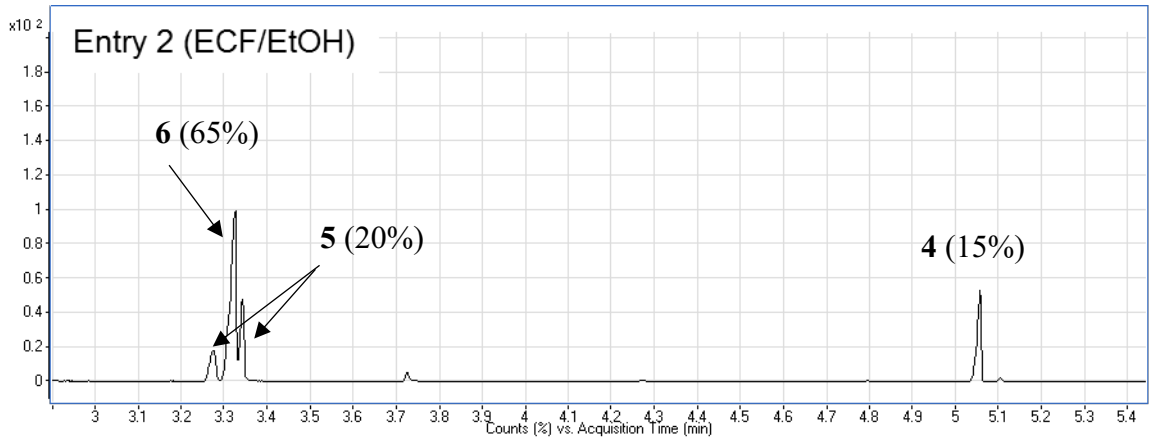

Table 17. Entry 3

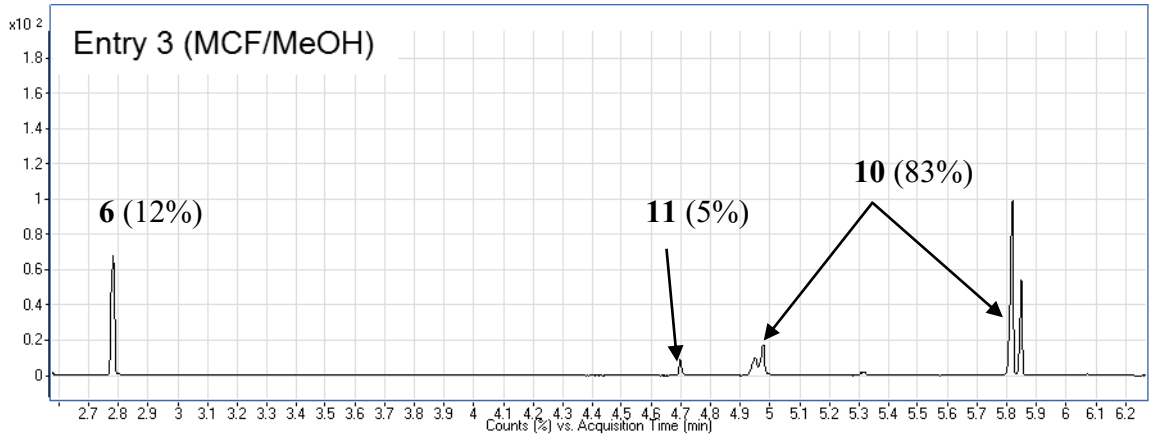

Table 17. Entry 4

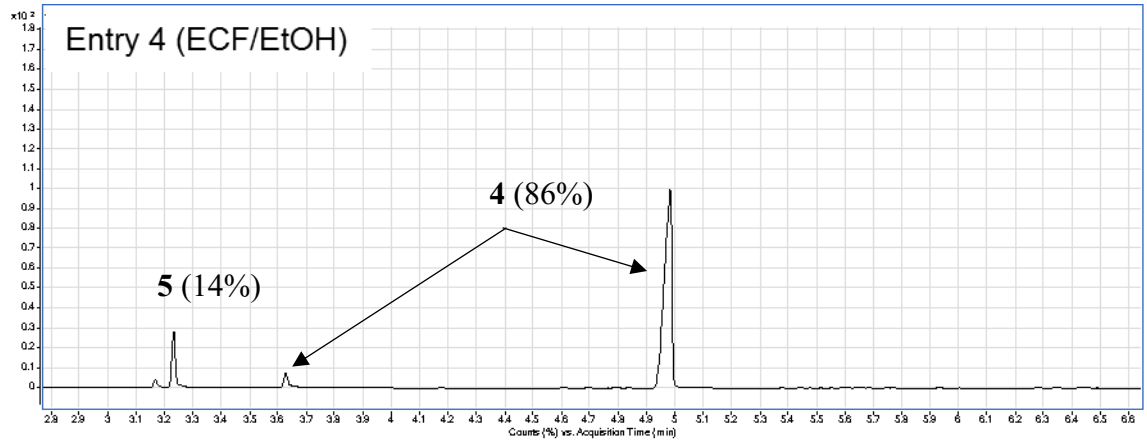

Table 17. Entry 5

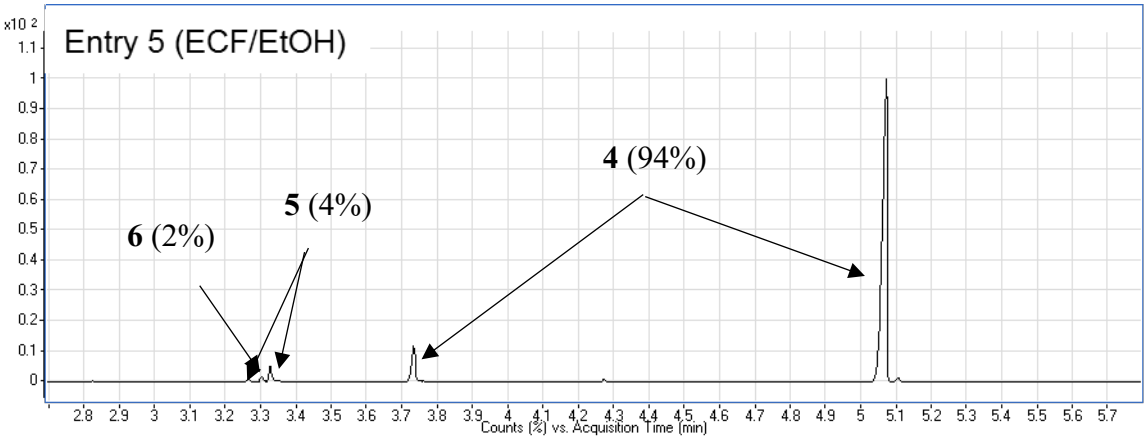

Table 17. Entry 6

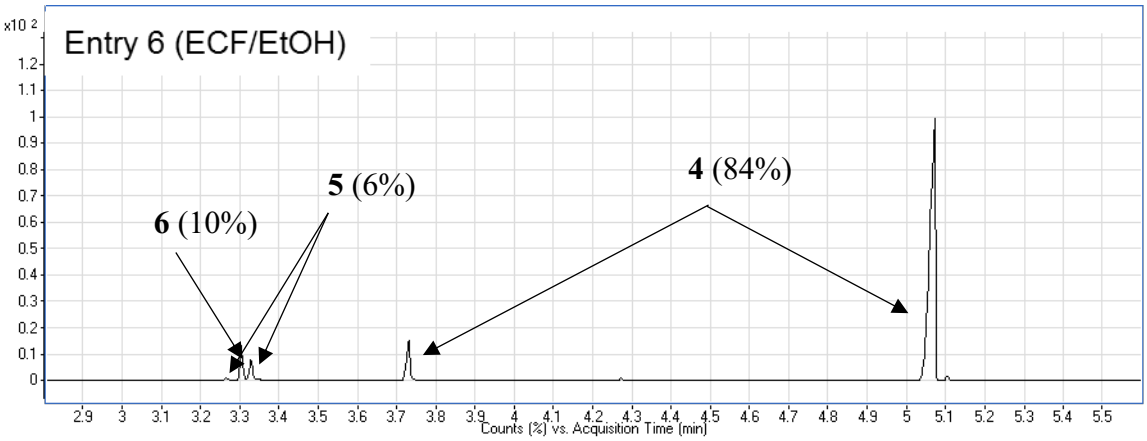

Table 17. Entry 7

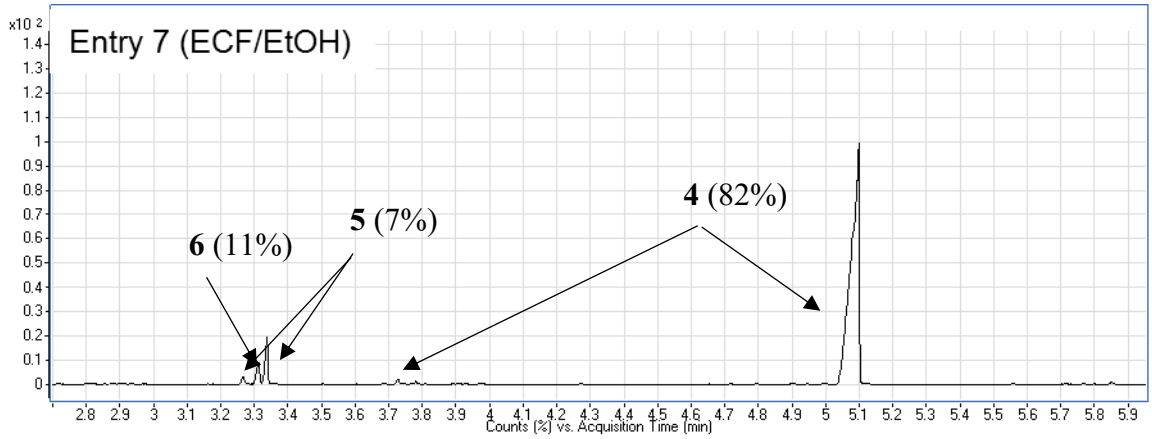

Table 17. Entry 8

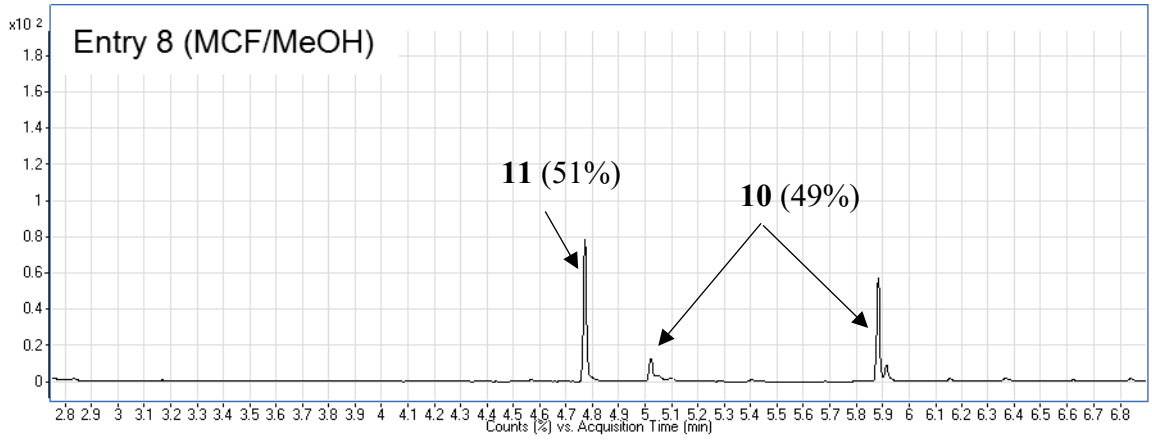

Table 17. Entry 9

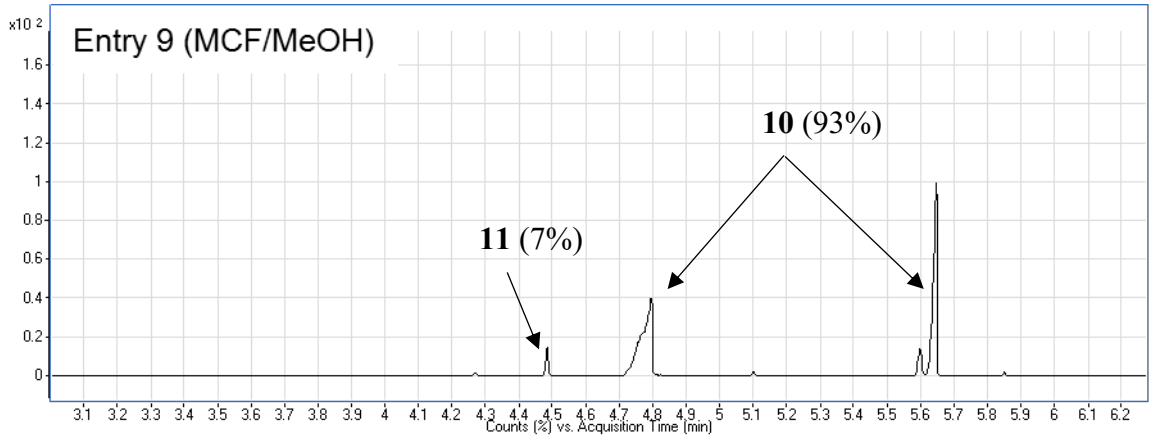

Table 17. Entry 10

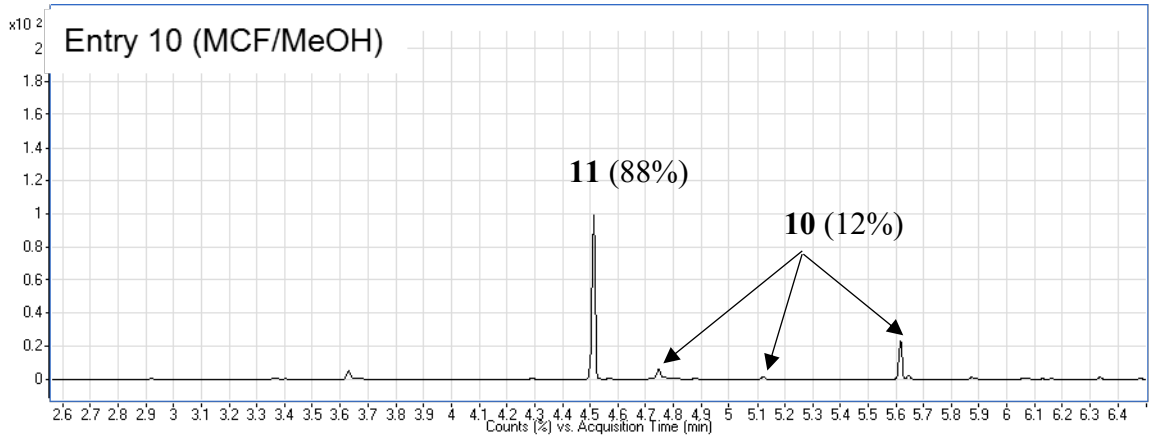

Table 17. Entry 11

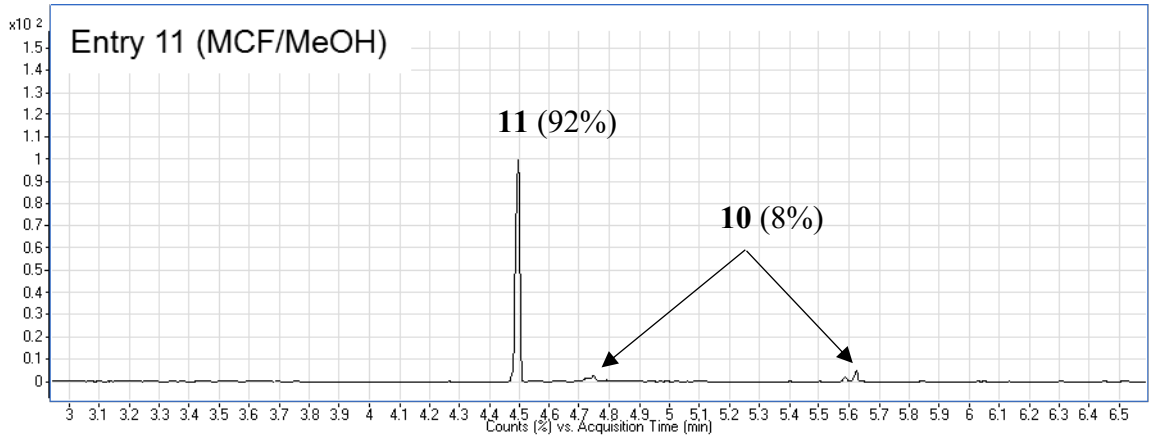

Table 17. Entry 12

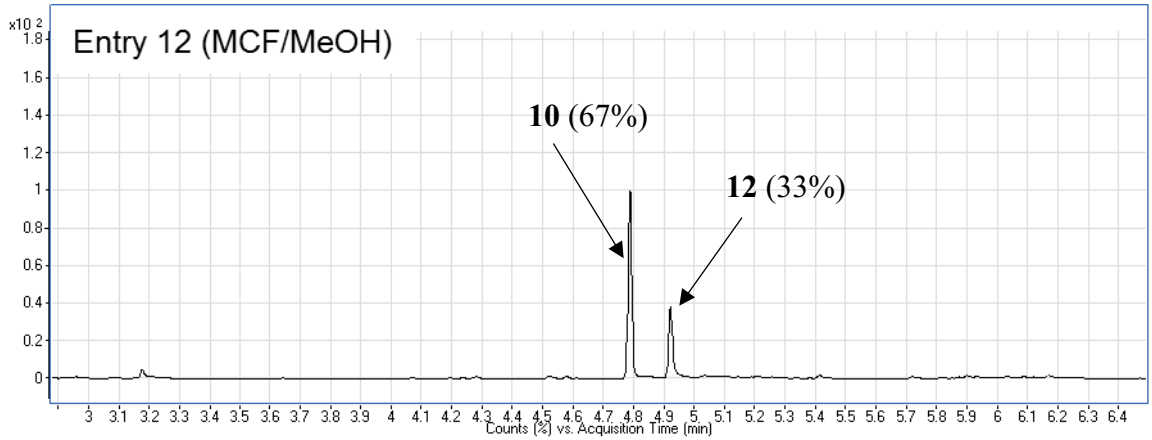

Table 17. Entry 13

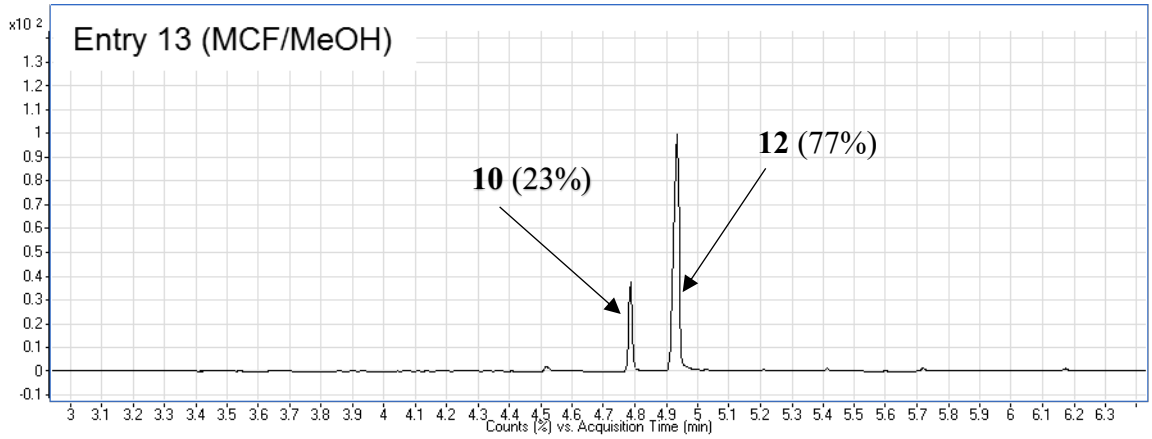

Table 17. Entry 14

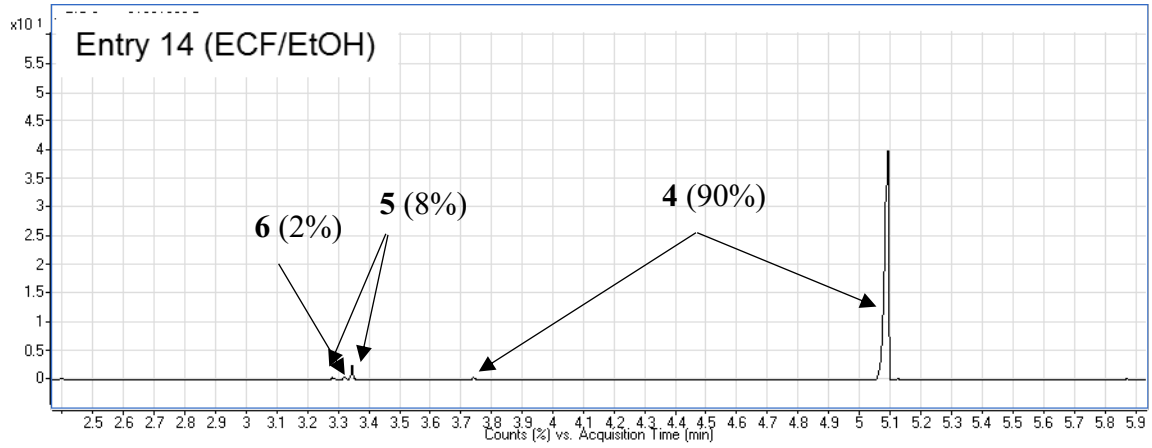

Table 17. Entry 15

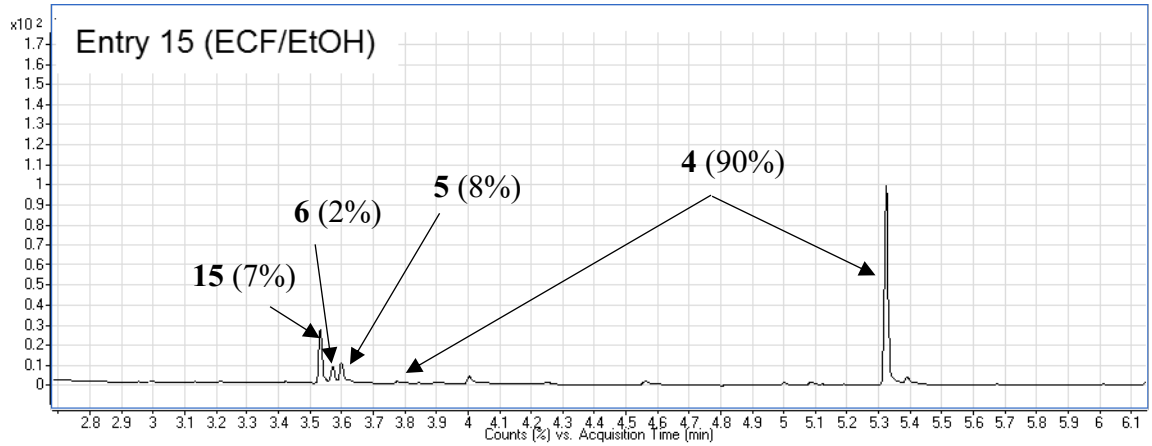

Table 17. Entry 16

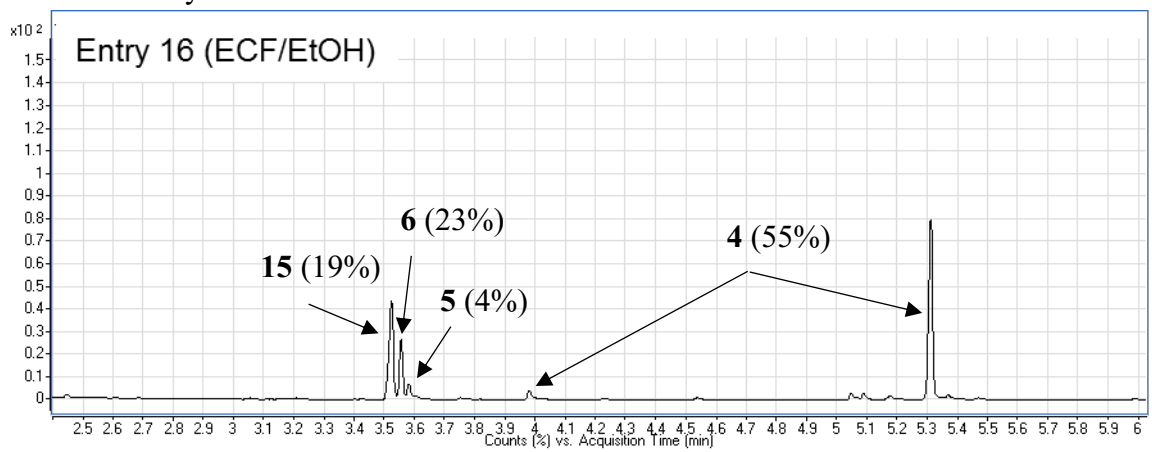

Table 17. Entry 17

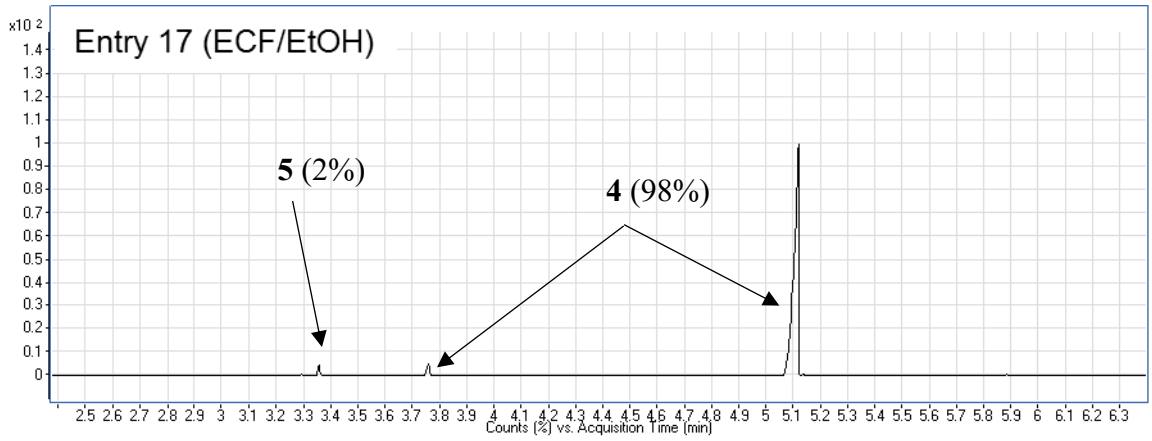

Table 17. Entry 18

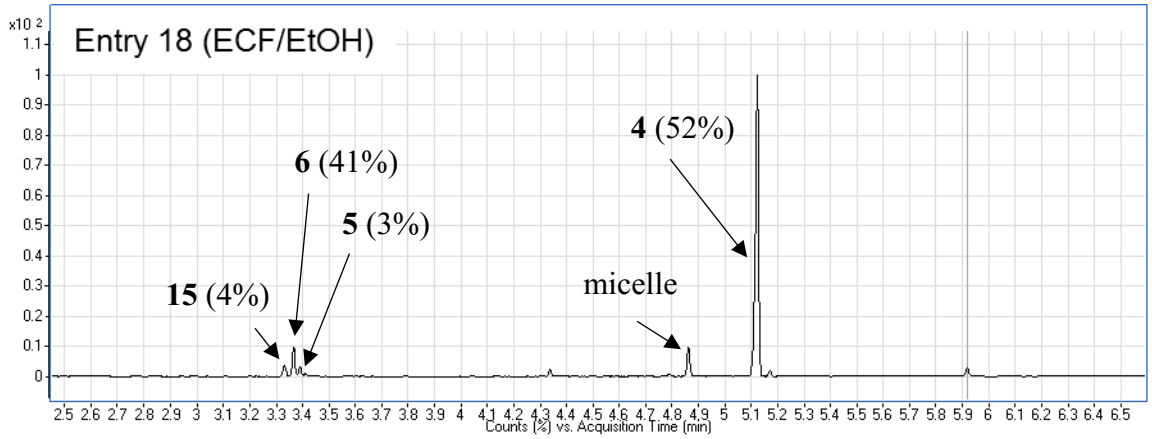

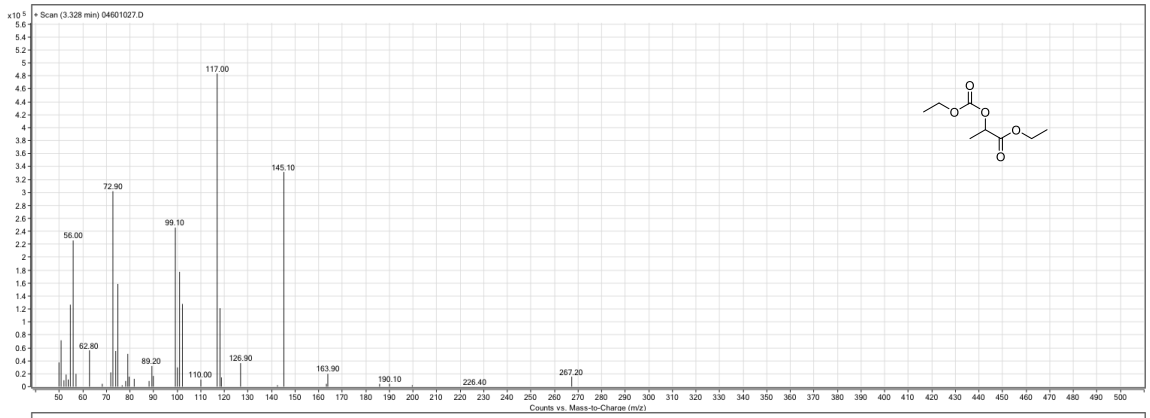
+ Scan (3.328 min) 04601027.D
117.00
145.10
72.90
99.10
56.00
62.80
89.20
110.00
126.90
163.90
190.10
226.40
267.20
Counts vs. Mass-to-Charge (m/z)

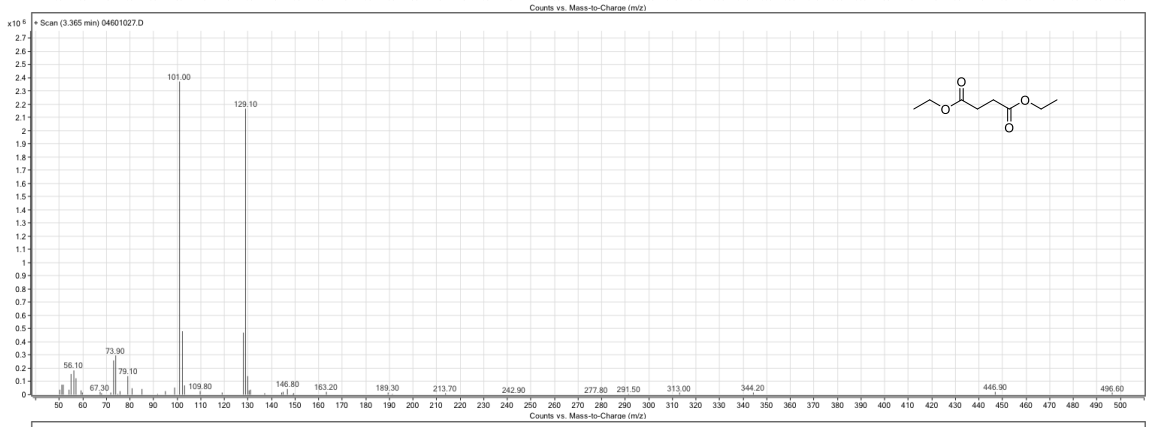
+ Scan (3.365 min) 04601027.D
101.00
129.10
73.90
56.10
79.10
67.30
109.80
146.80
163.20
189.30
213.70
242.90
277.80
291.50
313.00
344.20
446.90
496.60
Counts vs. Mass-to-Charge (m/z)

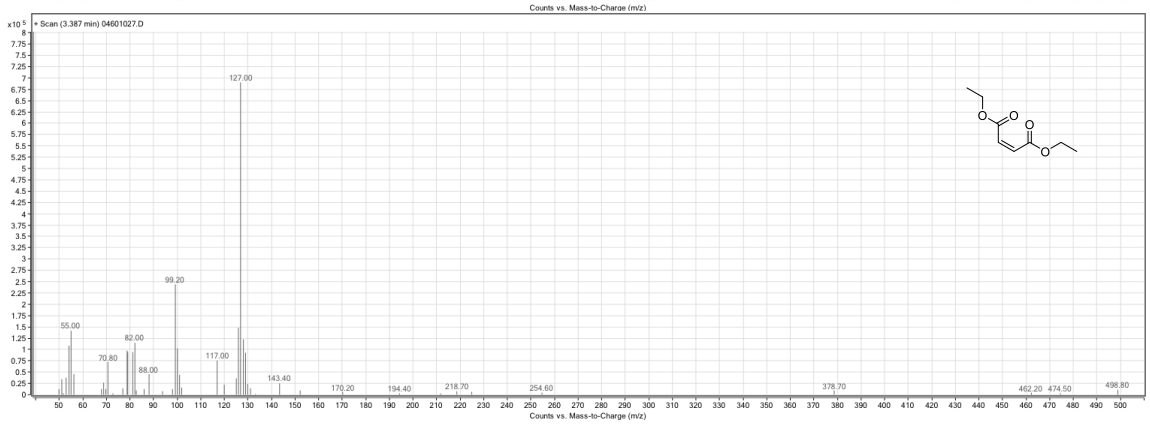
+ Scan (3.387 min) 04601027.D
127.00
99.20
55.00
82.00
70.80
88.00
117.00
143.40
170.20
194.40
218.70
254.60
378.70
462.20
474.50
498.80
Counts vs. Mass-to-Charge (m/z)

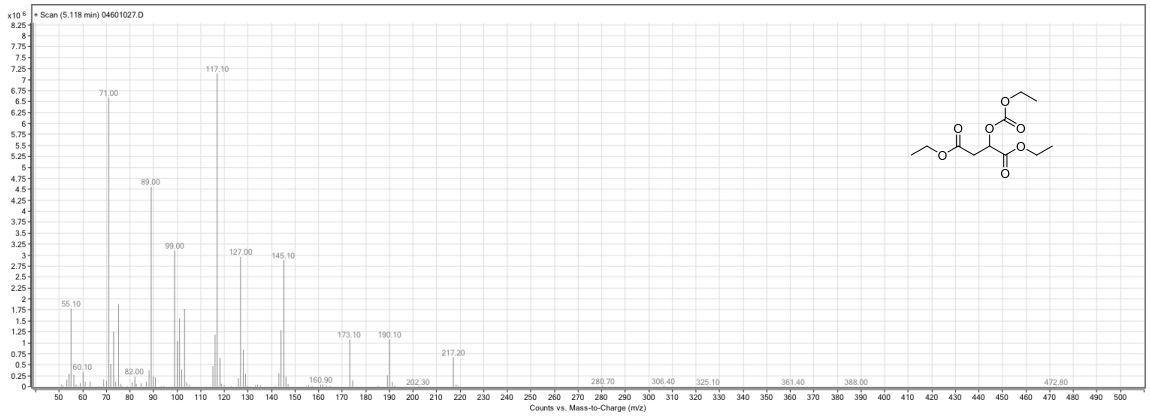
+ Scan (5.118 min) 04601027.D
117.10
71.00
89.00
99.00
127.00
145.10
55.10
173.10
190.10
217.20
60.10
82.00
160.90
202.30
280.70
306.40
325.10
361.40
388.00
472.80
Counts vs. Mass-to-Charge (m/z)

Table 17. Entry 19

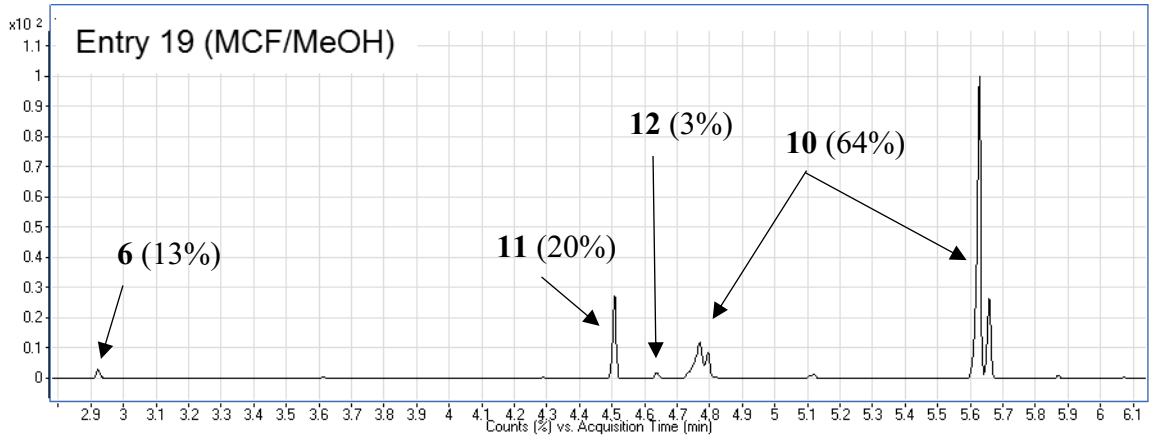

Table 17. Entry 20

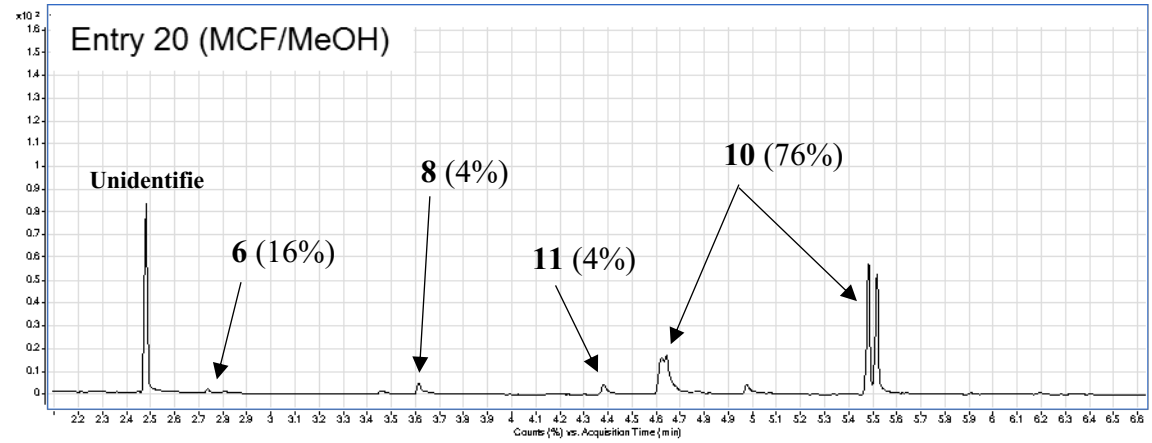

Table 17. Entry 21

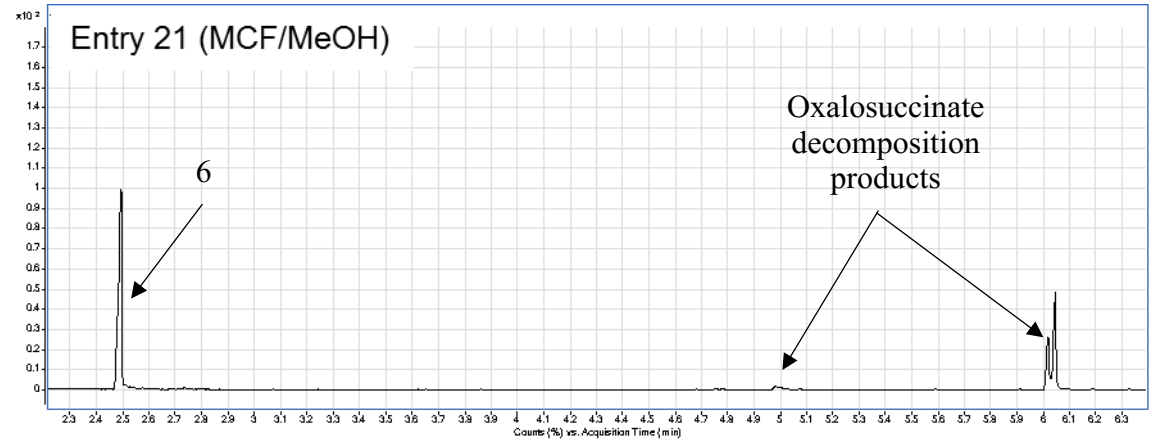

Table 17. Entry 22

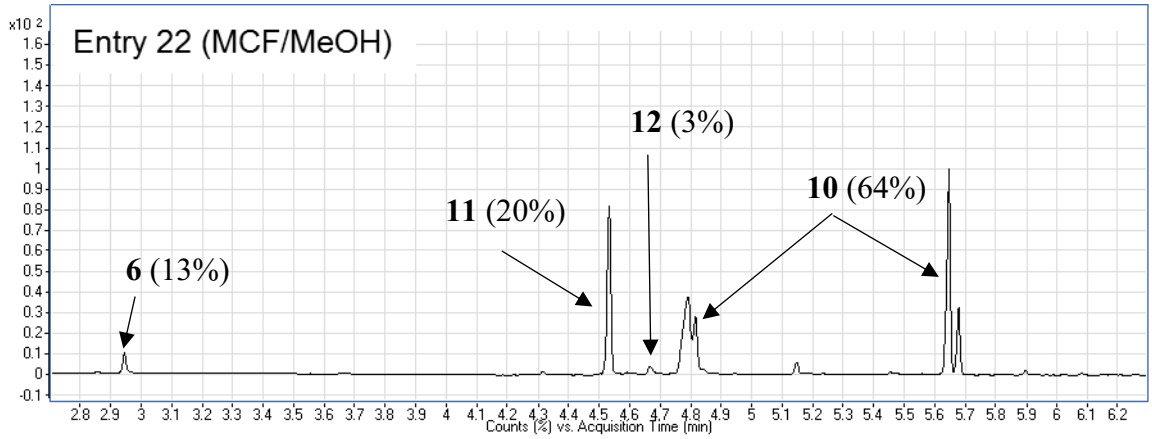

Table 17. Entry 23

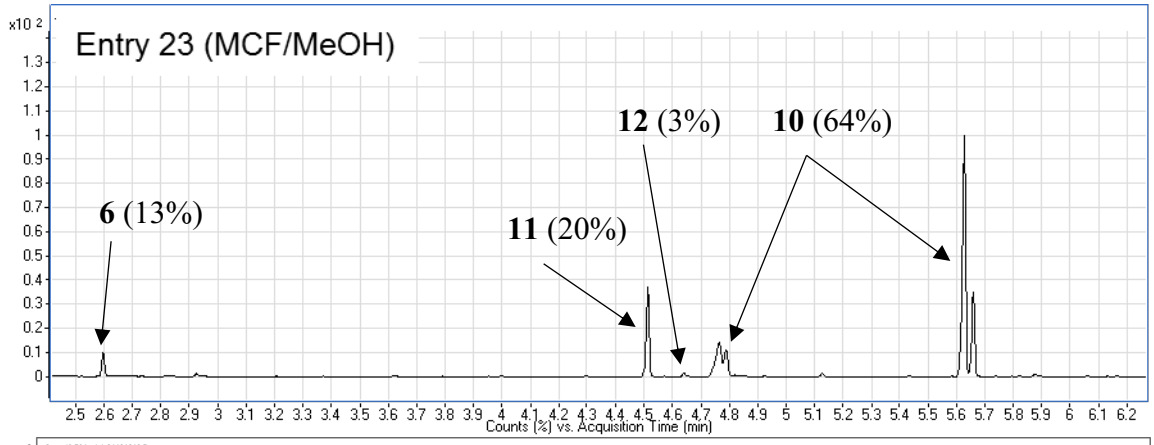

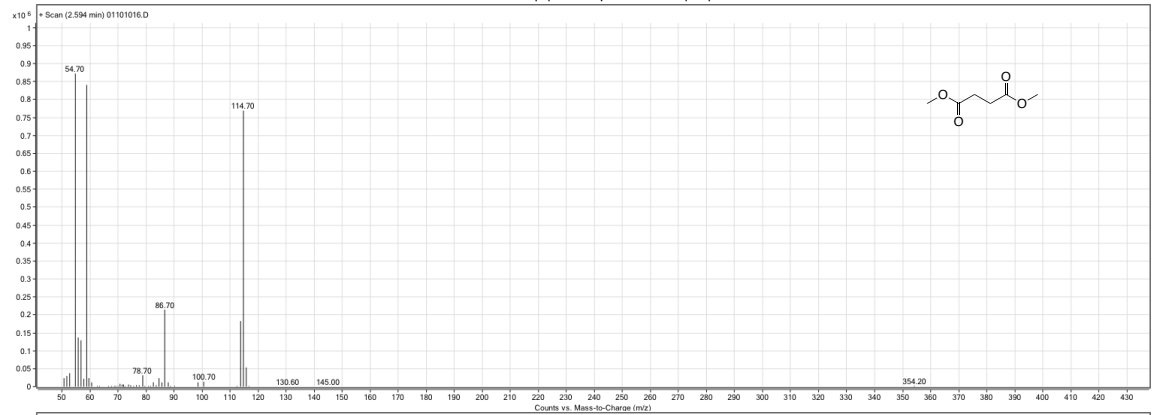

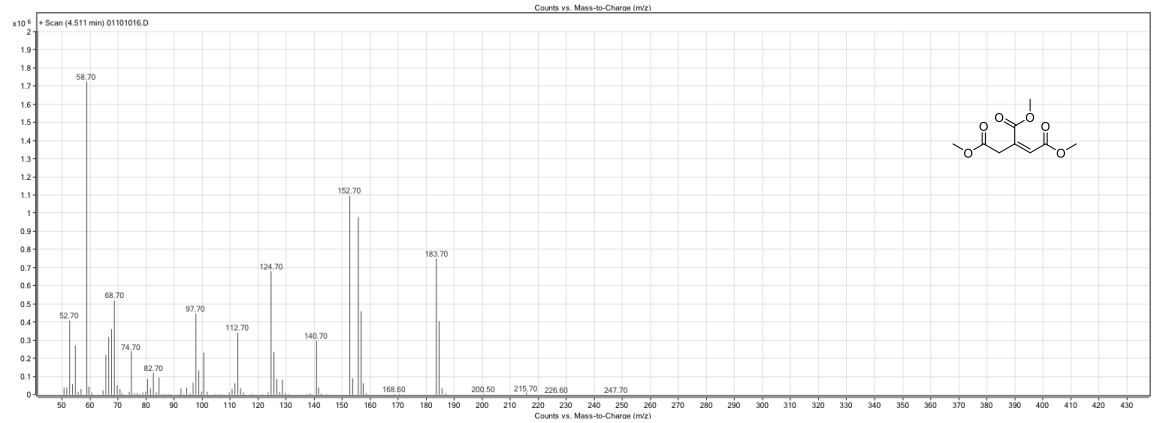

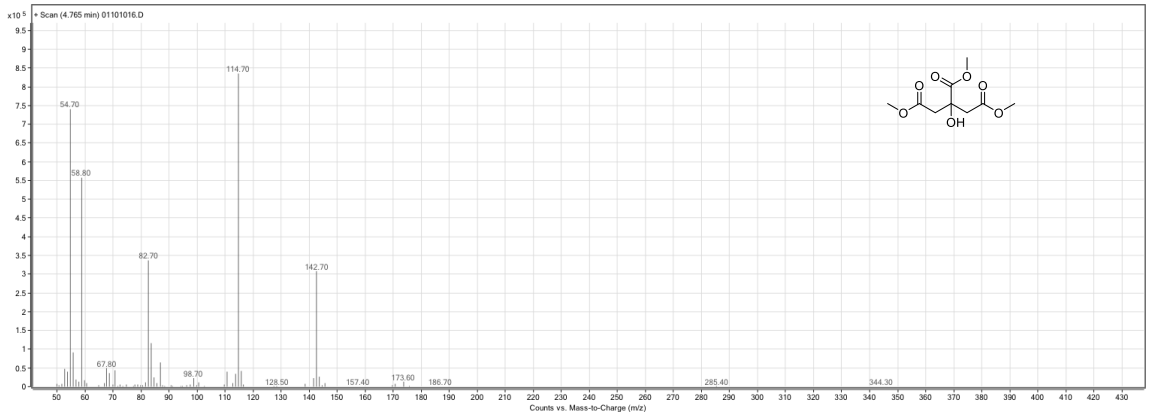

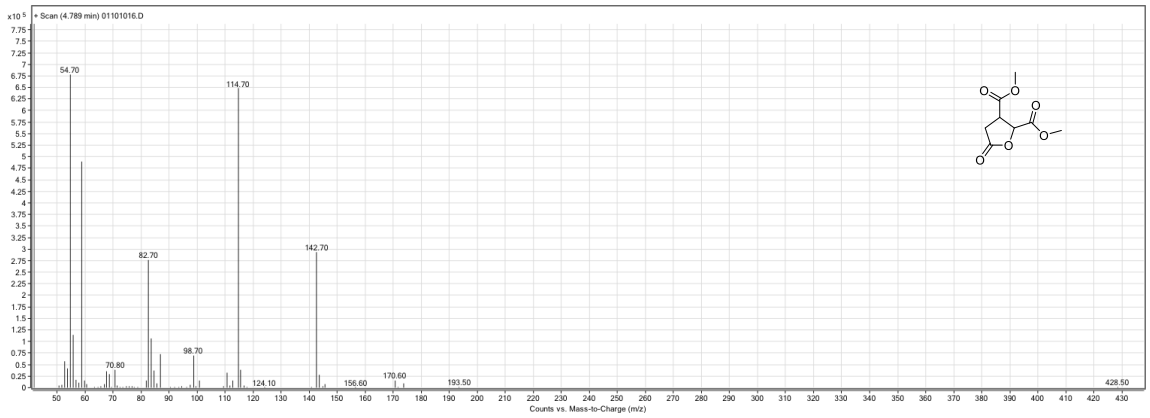

Table 17. Entry 24

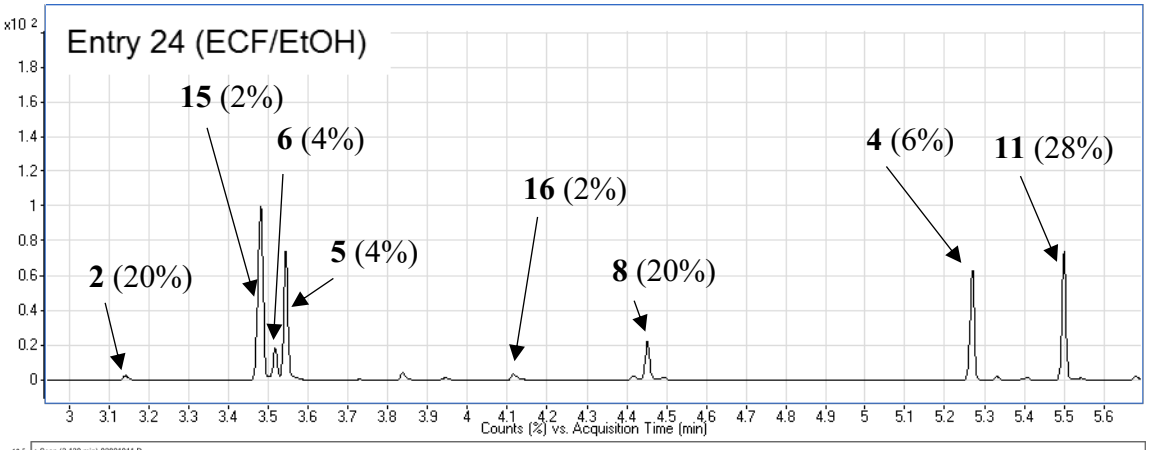

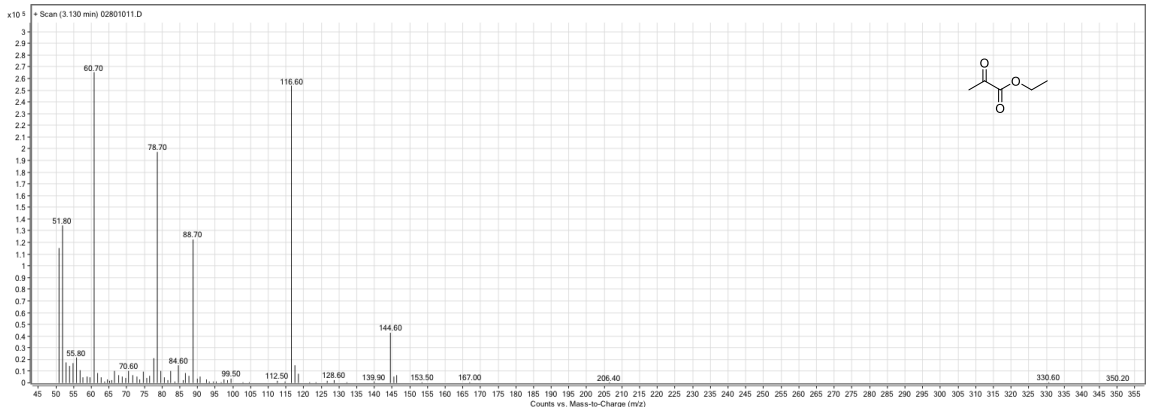

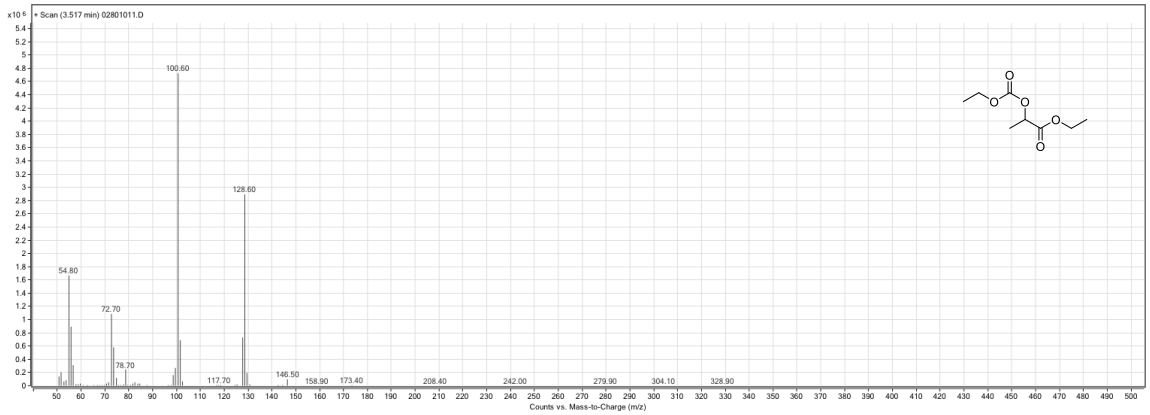
x10 6
+ Scan (3.517 min) 0280101l.D
100.60
128.60
54.80
72.70
78.70
117.70
146.50
158.90
173.40
208.40
242.00
279.90
304.10
328.90
Counts vs. Mass-to-Charge (m/z)

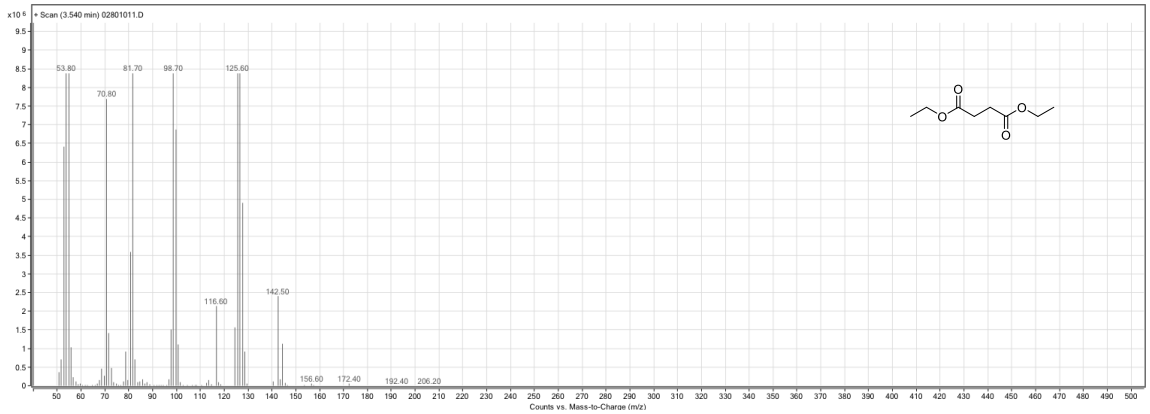
x10 6
+ Scan (3.540 min) 0280101l.D
53.80
81.70
98.70
125.60
70.80
116.60
142.50
156.60
172.40
192.40
206.20
Counts vs. Mass-to-Charge (m/z)

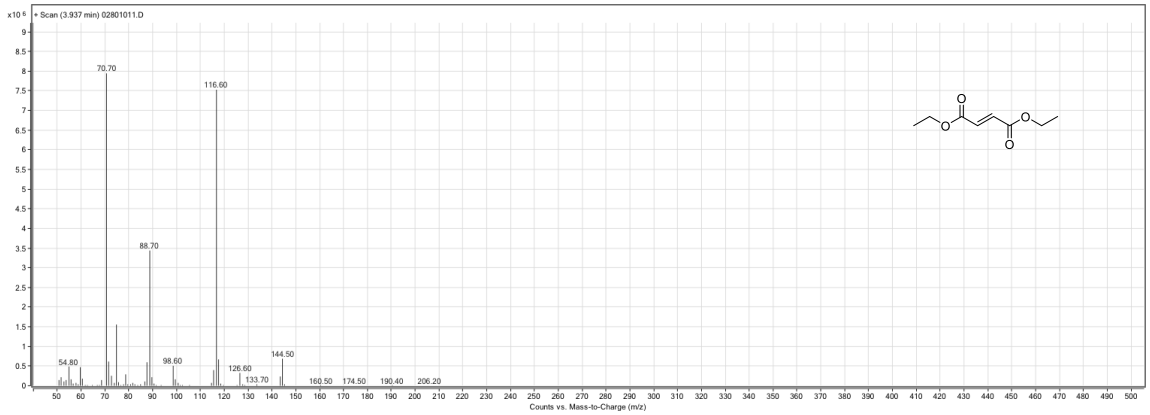
x10 6
+ Scan (3.937 min) 0280101l.D
70.70
116.60
88.70
54.80
98.60
126.60
133.70
144.50
160.50
174.50
190.40
206.20
Counts vs. Mass-to-Charge (m/z)

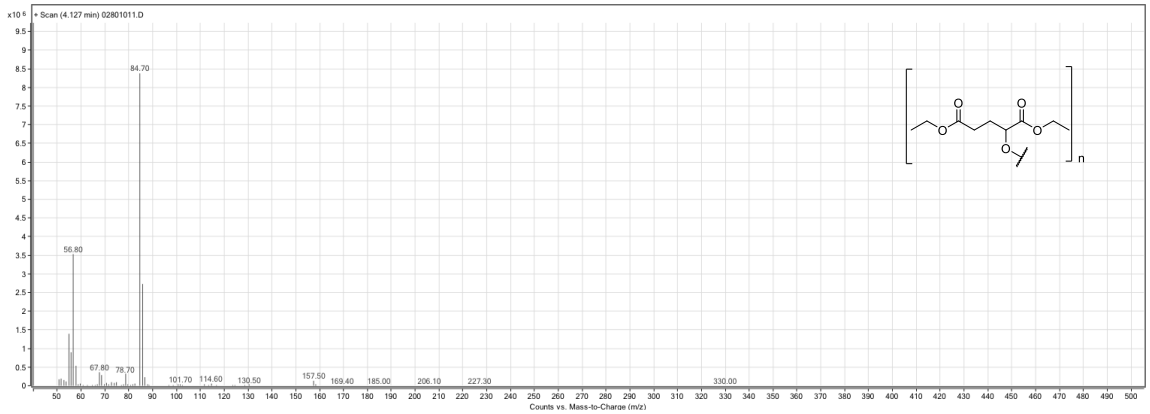
x10 6
+ Scan (4.127 min) 0280101l.D
84.70
56.80
67.80
78.70
101.70
114.60
130.50
157.50
169.40
185.00
206.10
227.30
330.00
Counts vs. Mass-to-Charge (m/z)

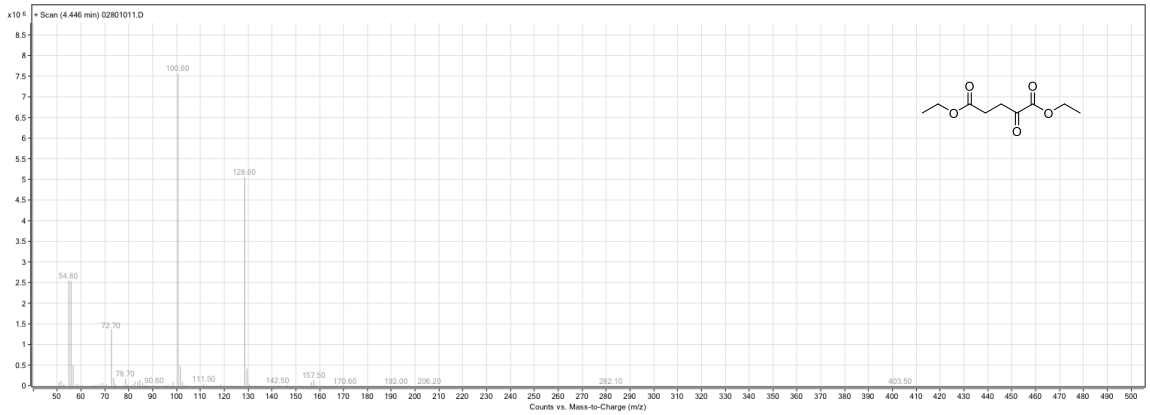
x10 6
+ Scan (4.446 min) 0280101.D
100.60
128.60
54.80
72.70
78.70
90.60
111.50
142.50
157.50
170.60
192.00
206.20
282.10
403.50
Counts vs. Mass-to-Charge (m/z)

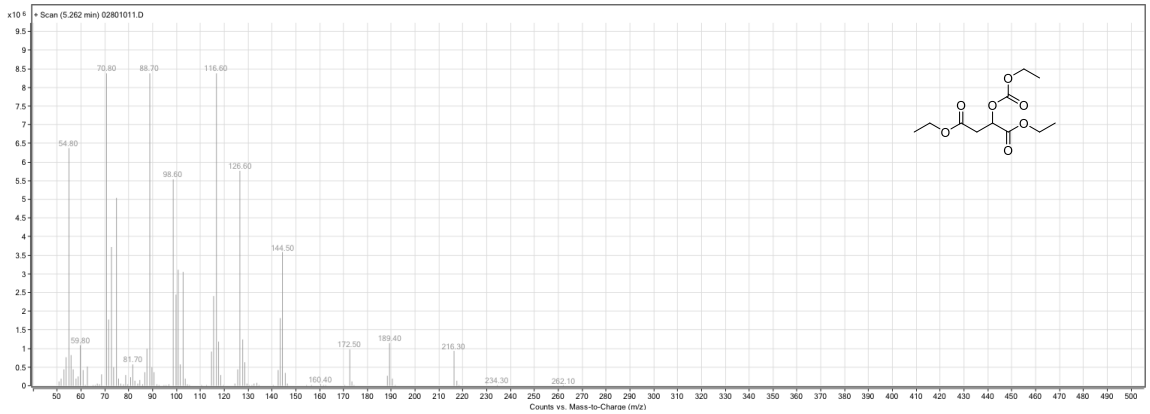
x10 6
+ Scan (5.262 min) 0280101.D
70.80
88.70
116.60
54.80
126.60
98.60
144.50
59.80
81.70
172.50
189.40
216.30
160.40
234.30
262.10
Counts vs. Mass-to-Charge (m/z)

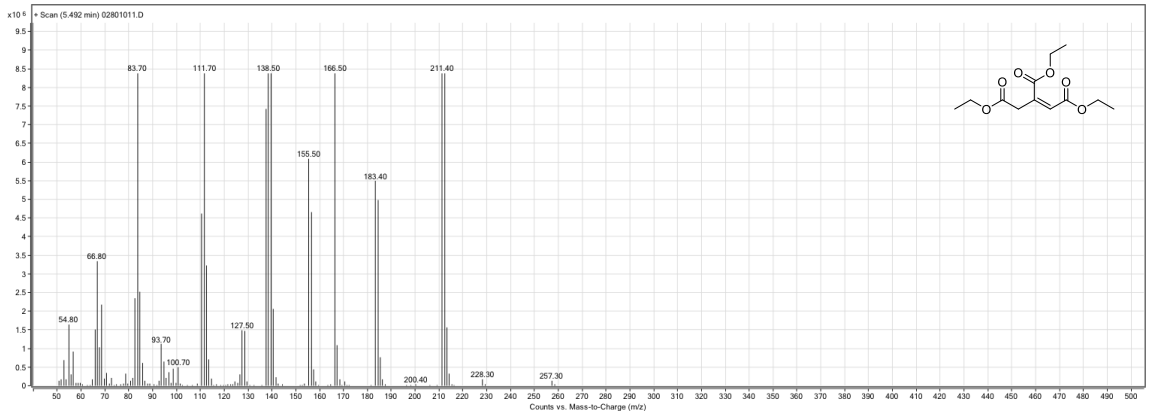
x10 6
+ Scan (5.492 min) 0280101.D
83.70
111.70
138.50
166.50
211.40
155.50
183.40
66.80
54.80
127.50
93.70
100.70
200.40
228.30
257.30
Counts vs. Mass-to-Charge (m/z)

Table 17. Entry 25

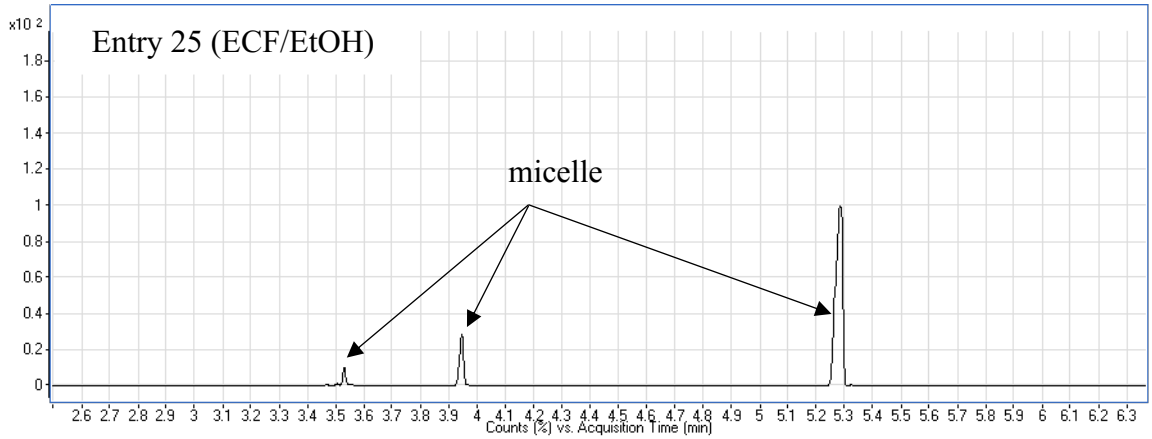

2. The W-L pathway

2.1. General information

For pressurized reactions: All reactions were carried out in stainless-steel Parr pressure reactors in 1.5 mL vials with pierced PTFA-lined caps either under CO_2 or H_2/CO_2 atmosphere, unless otherwise noted.

^1H NMR spectra were recorded on a Bruker Avance300 (300 MHz) spectrometer at ambient temperature in a H_2O:D_2O mixture (6:1) as solvent, with sodium 3-(trimethylsilyl)-1-propanesulfonate (DSS-Na) as the internal standard (CH_3 peak at 0 ppm). Solvent suppression was achieved through excitation sculpting, using the Bruker ZGESGP pulse program adjusted for the water resonance. 32 scans were acquired for each sample. Relaxation delay D1 was set to 87 s, with time domain size TD = 32768 and sweep width SWH = 4789.27 Hz (11.963 ppm), to allow for quantitative measurements. Integration was performed using MestReNova v6.0.2 software.

Standard potentials vs SHE (pH = 6.8)[166,167]***:***

Reaction	E (V) vs. SHE
$2H^+ + 2e^- \rightarrow H_2$	-0.41
$CO_2 + 2H^+ + 2e^- \rightarrow HCOOH$	-0.61
$CO_2 + 2H^+ + 2e^- \rightarrow CO + H_2O$	-0.53
$CO_2 + 6H^+ + 6e^- \rightarrow CH_3OH + H_2O$	-0.38
$CO_2 + 8H^+ + 8e^- \rightarrow CH_4 + 2H_2O$	-0.24
$CH_3COOH + CO_2 + 2H^+ + 2e^- \rightarrow CH_3COCOOH + H_2O$	-1.11
$CH_3COCOOH + 2H^+ + 2e^- \rightarrow CH_3CHOHCOOH$	-0.60
$Fe^{2+} + 2e^- \rightarrow Fe^0$	-0.44
$Cu^{2+} + 2e^- \rightarrow Cu^0$	+0.34

$E_{ECS} = E_{SHE} - 0.241V$

$E_{AgCl/Ag} = E_{SHE} - 0.208V$

2.2. Materials

2.2.1. Chemistry

All reagents were purchased from commercial suppliers and were of a grade presented below in Table 18.

Table 18. Specifications of materials used

No.	Reagent	CAS	Supplier
1	Fe powder (fine), ≥ 99 %, reduced	7439-89-6	Sigma Aldrich
2	Iron(III) oxide powder, Fe_2O_3, <5 μm, ≥ 96 %	1309-37-1	Sigma Aldrich
3	Goethite, α-FeO(OH), 30-65 % Fe	20344-94-4	Sigma Aldrich
4	Iron(II) oxide, FeO, -10 mesh, 99.7% trace metal basis	1345-25-1	Sigma Aldrich

All reagents were tested for the presence of trace acetate and/or formate impurities prior to use. Water was obtained from a Milli-Q purification system (18 MΩcm).

2.2.2. Electrochemistry

The iron wire used for all experiments was purchased from Goodfellow (99.99+ % Fe, 1.0 mm diameter, 0.5 m length).

With Pr. Ruhlmann: Electrochemical measurements were performed in a standard electrochemical cell composed of three electrodes (SCE, iron wire and glassy carbon) at room temperature and in a nitrogen or CO2 atmosphere. The potentials were applied using a PARSTAT 2273 potentiostat (Princeton). The chronoamperometry curves were acquired with the Powersuite software. The electrolyte was a solution of 0.5 M of K_2SO_4 and 0.05 M of $KHCO_3$. The cell was washed with acid and the wire was hand stripped between each experiment.

With Pr. Hellwig: Electrochemical measurements were performed in a beaker composed of three electrodes (AgCl/Ag, iron wire and graphite), in a glove bag at room temperature and in a nitrogen or CO2 atmosphere. The potentials were applied using a VersaSTAT 4 potentiostat (Princeton applied research). The chronoamperometry curves were acquired with the VersaSTAT software. The electrolyte was a solution of 0.1 M K_2HPO_4 or 0.1 M KCl. The cell and the wire were washed with water between experiments.

2.3. Analytical methods

2.3.1. Product identification

All compounds detected in this study were analyzed using the Bruker ZGESGP 1D pulse sequence with water suppression, as described in section 1.1 above. Sodium 3-(trimethylsilyl)-1-propanesulfonate (DSS-Na) was used as the internal standard (Fig 74). Acetate, pyruvate, methanol, formate and lactate were identified based on their chemical shifts which were compared to those of authentic samples (Fig 75).

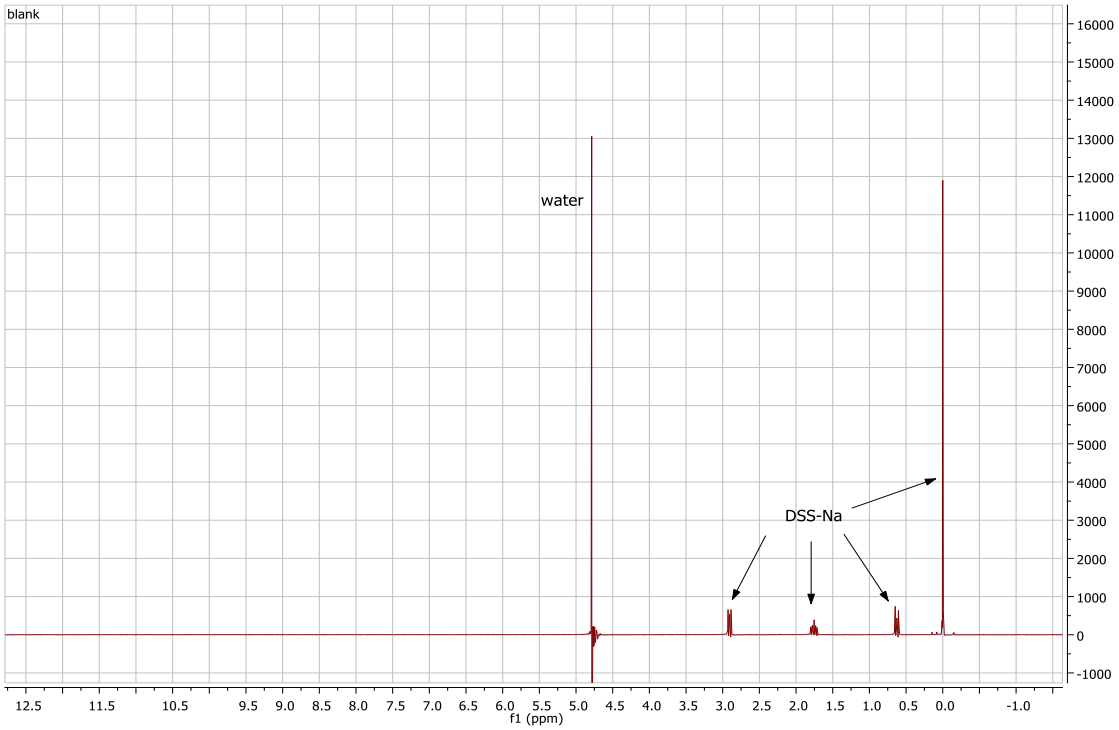

Fig 74. ^{1}H NMR spectrum of sodium 3-(trimethylsilyl)-1-propanesulfonate (DSS-Na) in H_2O : D_2O (6 : 1).[16]

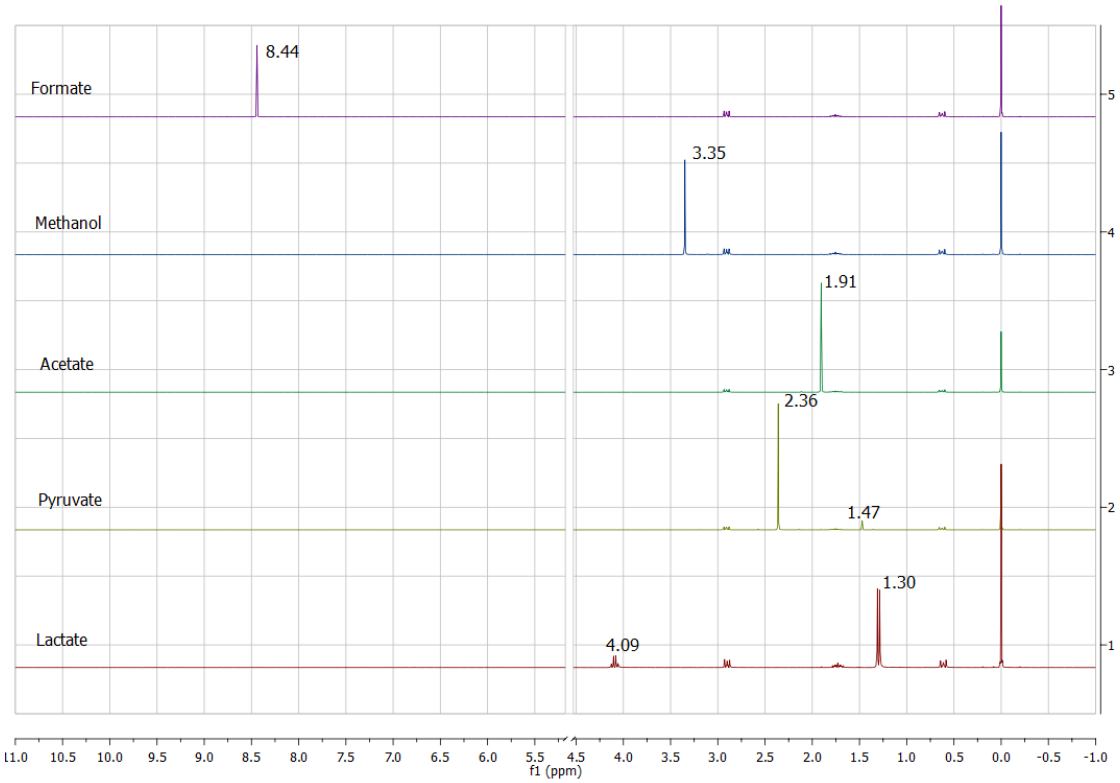

Fig 75. ^{1}H NMR spectra of products detected in this study – formate, methanol, acetate, pyruvate and lactate – with DSS-Na standard in H_2O:D_2O (6:1). The residual suppressed water peak was omitted for clarity.[16]

2.3.2. NMR sample preparation

To the reaction mixture or sample (reactions under acidic conditions, i.e. without KOH) was added ~100 mg of solid KOH in order to precipitate out any metal ions as their hydroxides. The mixture was stirred thoroughly. The resulting suspension was transferred to a 1.5 mL plastic microtube and centrifuged at 10 000 rpm for 2 minutes. To 600 µL of the supernatant was added 100 µL of 0.05 M solution of internal standard (DSS-Na in D_2O). The resulting solution was analyzed by NMR using the Bruker ZGESGP pulse program, as described in the General Information section.

The yield determination and error analysis for CO_2 fixation reactions are based on an average of 3 (or 4) independent runs for each value, and each analyte was calibrated with a 6-points calibration line. It is described in detail in the supporting information of "Native iron reduces CO_2 to intermediates and end- products of the acetyl-CoA pathway".[16]

2.4. Synthetic procedures

2.4.1. For metal-promoted CO_2 fixation reactions

To a 1.5 mL glass vial was added 1 mmol/3 mmol metal atoms for each candidate (56/168 mg Fe, or 80/240 mg Fe_2O_3, or 77/232 mg Fe_3O_4, or 72/216 mg FeO, or 89/267 mg α-FeO(OH)) and 1 mL of Milli-Q water. In reactions run under basic conditions, the initial pH was adjusted with 45 mg of KOH. To prevent cross-contamination, the vials were closed with caps with punctured PTFE septa. After placing the vials in a stainless-steel Parr pressure reactor, it was flushed with ca. 5 bar CO_2, pressurized with either 25 bar CO_2 or 10 bar H_2 mixed with 15 bar CO_2, and heated at 100 °C (an external heating mantle was used where needed) for 16 h.

2.4.2. Electrochemistry

With Pr. Ruhlmann: Tests were performed on a range of potentials from -0.5V to -1.25V, in a cell that contained 30 mL of electrolyte, with or without sintered glass (Fig 26). The cell was first degassed with N_2 for 20 min, then with CO_2 for additional 20 min, followed by the application of the chosen potential under a constant CO_2 flux. Samples (~1.5 mL) were taken from the cell every 10 minutes, for 2 hours.

a

b

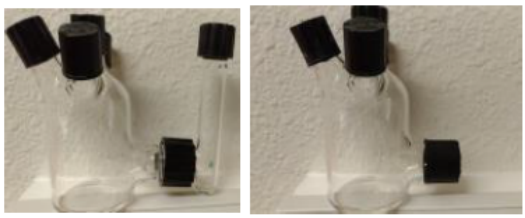

Fig 26. Electrochemical cell setup used for CO_2 reduction. **a.** Entire assembly of the cell with all connections and the three electrodes (SCE, glassy carbon and iron wire). **b.** Cell with and without sintered glass..

With Pr. Hellwig: Tests were performed on a range of potentials from -0.72V to -1.25V, in a beaker that contained 25mL of electrolyte, inside a glove bag (**Fig** 76). The solution was first degassed with Ar for 30 min, followed by 3 cycles of "vacuum"-Ar of the glove bag, and finally the solution was degassed with CO_2 for 30 min additional. The chosen potential was applied under a constant CO_2 flux. Samples (~1.5 mL) were taken from the beaker every 30 minutes, for 3 hours.

Fig 76. Picture of a glove bag from Cole-Parmer®

2.5. Experimental data

2.5.1. Iron oxides screens in CO_2 fixation reactions

Table 19. Values for **Erreur ! Source du renvoi introuvable.**.

		pH 4-5								pH 7-8							
		Fe_3O_4		FeO		Fe^0		α-FeO(OH)		Fe_3O_4		FeO		Fe^0		α-FeO(OH)	
		high	low	high	low	high	low	high	low	high	low	high	low	high	low	high	low
Products, mM	Acetate	0.27 ± 0.02	0.18 ± 0.03	0.14 ± 0.03	0.13 ± 0.04	0.10 ± 0.02	0.13 ± 0.01	0.13 ± 0.01	0.11 ± 0.03	0.27 ± 0.02	0.18 ± 0.01	0.06 ± 0.02	0.06 ± 0.01	0.08 ± 0.01	0.16 ± 0.02	0.16 ± 0.02	0.12 ± 0.01
	Pyruvate	0.0 ± 0.0	0.0 ± 0.0	0.0 ± 0.0	0.0 ± 0.0	0.0 ± 0.0	0.0 ± 0.0	0.01 ± 0.01	0.01 ± 0.01	0.03 ± 0.01	0.01 ± 0.0	0.01 ± 0.0	0.0 ± 0.0	0.01 ± 0.01	0.02 ± 0.0	0.02 ± 0.0	0.0 ± 0.01
	Methanol	0.36 ± 0.09	0.12 ± 0.01	0.0 ± 0.0	0.0 ± 0.0	0.0 ± 0.0	0.0 ± 0.0	0.0 ± 0.0	0.0 ± 0.0	0.23 ± 0.04	0.11 ± 0.0	0.0 ± 0.0	0.0 ± 0.0	0.01 ± 0.01	0.03 ± 0.01	0.03 ± 0.01	0.03 ± 0.02
	Formate	0.11 ± 0.02	0.05 ± 0.02	0.0 ± 0.0	0.0 ± 0.0	0.08 ± 0.03	0.09 ± 0.03	0.09 ± 0.03	0.05 ± 0.01	0.11 ± 0.02	0.05 ± 0.0	0.03 ± 0.02	0.02 ± 0.01	0.06 ± 0.02	0.09 ± 0.02	0.09 ± 0.02	0.03 ± 0.01

Table 20. Values for **Erreur ! Source du renvoi introuvable.**.

		pH 4-5								pH 7-8							
		Fe_3O_4		FeO		Fe^0		α-FeO(OH)		Fe_3O_4		FeO		Fe^0		α-FeO(OH)	
		high	low	high	low	high	low	high	low	high	low	high	low	high	low	high	low
Products, mM	Acetate	0.35 ± 0.03	0.15 ± 0.03	0.05 ± 0.02	0.15 ± 0.03	0.08 ± 0.01	0.04 ± 0.01	0.22 ± 0.08	0.16 ± 0.05	0.30 ± 0.01	0.13 ± 0.01	0.07 ± 0.02	0.07 ± 0.01	0.10 ± 0.02	0.05 ± 0.02	0.21 ± 0.04	0.21 ± 0.04
	Pyruvate	0.0 ± 0.0	0.0 ± 0.0	0.0 ± 0.0	0.15 ± 0.03	0.0 ± 0.0	0.0 ± 0.0	0.0 ± 0.0	0.0 ± 0.0	0.03 ± 0.0	0.02 ± 0.0	0.0 ± 0.0	0.0 ± 0.0	0.01 ± 0.0	0.01 ± 0.0	0.02 ± 0.0	0.01 ± 0.0
	Methanol	0.37 ± 0.03	0.05 ± 0.02	0.0 ± 0.0	0.15 ± 0.03	0.0 ± 0.0	0.0 ± 0.0	0.05 ± 0.04	0.04 ± 0.04	0.29 ± 0.01	0.08 ± 0.01	0.0 ± 0.0	0.0 ± 0.0	0.0 ± 0.0	0.0 ± 0.0	0.02 ± 0.01	0.04 ± 0.04
	Formate	0.12 ± 0.02	0.02 ± 0.01	0.0 ± 0.0	0.15 ± 0.03	0.15 ± 0.01	0.15 ± 0.01	0.11 ± 0.07	0.04 ± 0.02	0.14 ± 0.01	0.03 ± 0.01	0.0 ± 0.0	0.0 ± 0.0	0.11 ± 0.02	0.11 ± 0.02	0.05 ± 0.0	0.03 ± 0.02

2.5.2. Electrochemistry data

Table 21. Values from **Erreur ! Source du renvoi introuvable.**.

	Concentration (mM)											
	- 0.75V				- 1V				- 1.25V			
Time	Formate	Acetate	Pyruvate	Lactate	Formate	Acetate	Pyruvate	Lactate	Formate	Acetate	Pyruvate	Lactate
0'	0,00	0,84	0,00	0,00	1,62	2,77	0,00	0,00	0,13	0,50	0,03	0,33
10'	0,26	1,14	0,00	0,00	0,55	1,82	0,17	0,97	0,35	1,15	0,08	0,51
20'	0,51	4,12	0,00	0,00	1,41	6,19	0,71	6,65	0,53	0,48	0,09	0,24
30'	0,67	1,52	0,12	0,00	0,23	1,33	0,18	1,76	0,41	1,33	0,13	0,46
40'	0,83	1,32	0,15	0,00	0,55	1,39	0,11	0,65	0,76	1,10	0,10	0,00
50'	9,35	2,45	0,00	0,00	0,04	0,37	0,02	0,23	0,62	0,99	0,13	0,36
1h	0,36	1,27	0,18	0,87	1,03	2,05	0,11	0,95	0,20	0,97	0,00	0,40
1h10	/	/	/	/	1,25	1,88	0,16	0,94	0,52	2,05	0,00	3,07
1h20	0,00	1,81	0,00	0,00	1,04	2,58	0,00	0,91	0,45	1,20	0,09	0,63
1h30	0,00	1,71	0,00	0,00	1,90	1,15	0,00	0,54	0,28	0,79	0,11	0,59
1h40	0,26	0,62	0,00	0,53	0,91	1,77	0,14	0,81	0,32	0,72	0,13	0,50
1h50	0,70	1,45	0,00	0,00	2,14	5,16	0,51	1,88	0,58	1,24	0,19	0,82
2h	0,00	0,56	0,00	0,00	0,22	1,07	0,08	0,57	0,82	1,07	0,15	0,87

Table 22. Values from **Erreur ! Source du renvoi introuvable.**

	Concentration (mM)											
	- 0.75V				- 1V				- 1.25V			
Time	Formate	Acetate	Pyruvate	Lactate	Formate	Acetate	Pyruvate	Lactate	Formate	Acetate	Pyruvate	Lactate
0'	0,44	0,60	0,16	0,67	0,21	0,60	0,00	0,00	0,01	0,19	0,03	0,00
10'	0,38	0,56	0,00	0,55	0,89	0,86	0,00	0,00	/	/	/	/
20'	0,51	1,00	0,00	0,84	0,35	0,39	0,00	0,38	0,00	0,47	0,00	0,00
30'	0,29	0,63	0,00	0,69	0,63	0,63	0,08	0,81	0,60	1,36	0,27	0,00
40'	1,27	1,36	0,38	1,46	1,07	0,77	0,18	0,76	1,53	2,78	1,12	0,00
50'	0,32	0,51	0,00	0,00	1,83	1,42	0,00	1,23	0,18	0,15	0,00	0,00
1h	1,11	1,26	0,19	1,16	0,63	0,56	0,21	0,81	0,51	0,68	0,00	0,00
1h10	0,42	0,84	0,11	0,90	0,34	0,61	0,00	0,70	0,84	0,66	0,52	0,00
1h20	0,31	0,43	0,05	0,00	0,49	0,48	0,00	0,00	0,56	0,75	0,44	0,00
1h30	0,44	0,59	0,00	0,78	0,47	0,47	0,13	0,39	1,02	2,06	0,00	0,00
1h40	1,71	2,05	0,00	0,00	0,61	0,51	0,09	0,45	0,68	0,49	0,00	0,00
1h50	0,49	0,75	0,00	0,00	0,31	0,37	0,06	0,35	0,93	1,06	0,00	0,00
2h	0,05	0,49	0,00	0,55	0,51	0,54	0,11	0,56	0,60	0,47	0,00	0,60

2.5.3. Data obtained from a collaboration with Harun Tueysuez

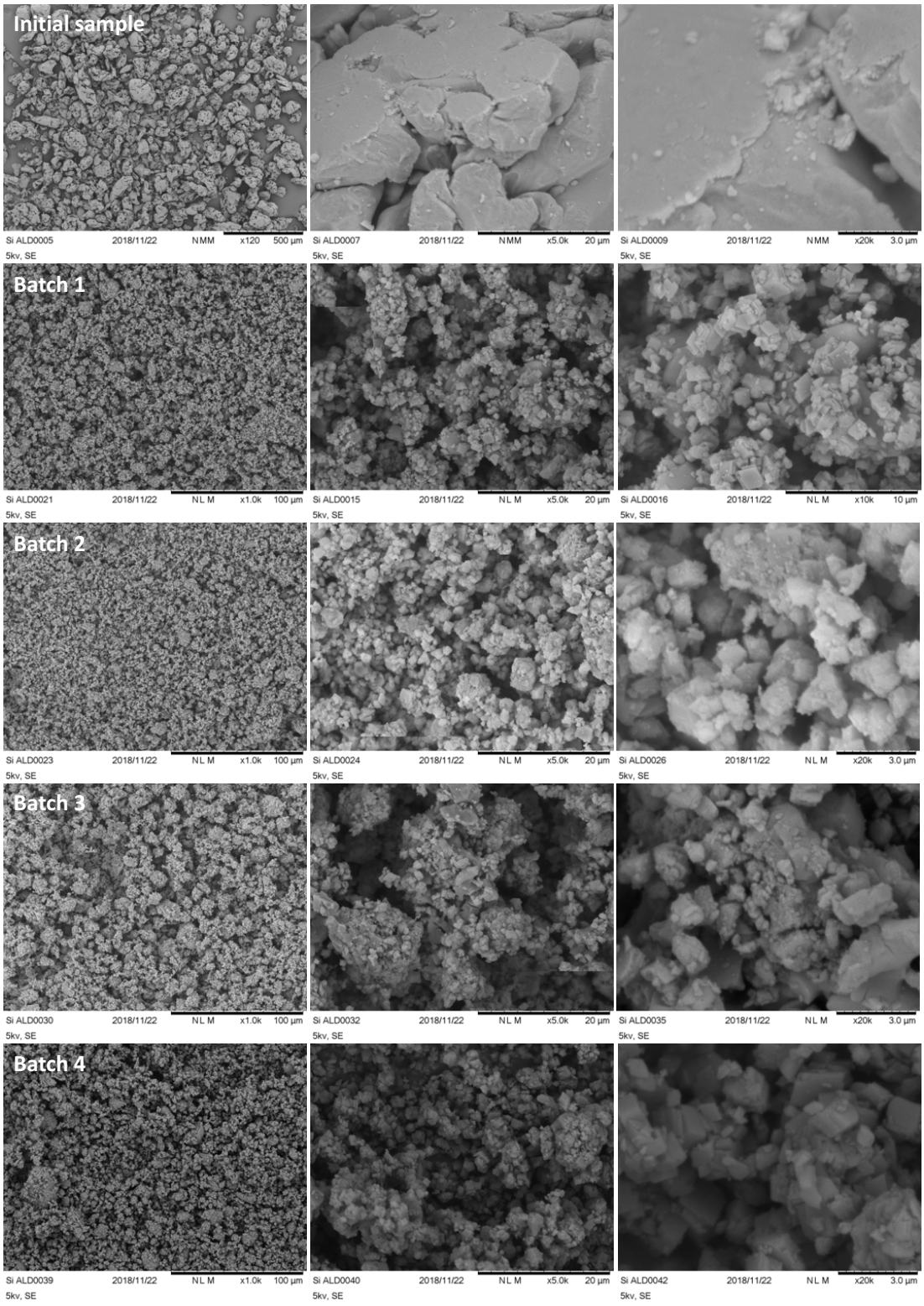

Fig 77. SEM images of Fe^0 powder before (initial sample) and after the reaction (35 bar of CO_2, 100 °C, 16 hours – 4 samples, Batch 1-4).

Fig 78. Magnet test of an iron powder sample before the reaction (01), and after the reaction: batch 1 (02), batch 2 (03), batch 3 (04) and batch 4 (05).

3. Thioesters

3.1. General information

All reactions were carried out in oven dried glassware under an atmosphere of argon. All glassware and stir bars were pre-washed with acid, followed by distilled water and acetone, and oven dried to prevent any cross-contamination by metal salts. Water was obtained from a Milli-Q purification system (18 MΩcm) and was purged with argon before use.

LC-MS analysis was performed on a ThermoFisher Scientific UltiMate 3000 UHPLC-system equipped with an C_{18} ThermoFisher Hypersil Gold 10 mm column using an Exactive Plus EMR Orbitrap detector. Acetonitrile (+ 0.1 % formic acid) and water (+ 0.1 % formic acid) were used for the mobile phase. The column was maintained at 25 °C and the solvent gradient was used as following: 2% MeCN for 1 min, linear gradient to 15% MeCN over 3.5 min, linear gradient to 100% MeCN over 1 min, 100% MeCN for 2.5 min, linear gradient to 2% MeCN over 0.5 min, 2% MeCN for 1.5 min. The analytes were quantified using a calibration of authentic samples by integration of the peak area of a specified m/z range. Unless otherwise noted 0.1 µL of the sample solutions were injected.

GC-MS analysis was performed on a GC System 7820A (G4320) using an Agilent High Resolution Gas Chromatography Column (PN 19091S – 433UI, HP – 5MS UI, 28 m×0.250 mm, 0.25 Micron, SN USD 489634H). The system was connected to an MSD block 5977E (G7036A). Hydrogen (99.999 % purity) was used as carrier gas at a constant flow rate of 1.5 mL/min. The analysis was carried out in a splitless mode with 1 µL injection volume, at the injection port temperature of 250 °C. The column was maintained at 60 °C for 1 min, then ramped at 30 °C/min to 310 °C with 3 min hold, and the total running time was 12.33 min. The mass spectrometer was turned on after a 2-min solvent delay and was operated at the electron ionization (EI) mode with quadrupole temperature of 150 °C. Data was acquired in the full-scan mode (50-500 amu).

GC-FID analysis was performed on a GC System GC7890B with an FID-detector using an Agilent High Resolution Gas Chromatography Column (PN 19091S – 433UI, HP – 5MS UI, 28 m×0.250 mm, 0.25 Micron, SN USD 489634H). Hydrogen (99.999 % purity) was used as carrier gas at a constant flow rate of 5.0 mL/min. The analysis was carried out in a splitless

mode with 1 µL injection volume, at the injection port temperature of 250 °C. The column was maintained at 60 °C for 1 min, then ramped at 30 °C/min to 300 °C with 3 min hold, and the total running time was 12 min. The FID detector was used with an airflow of 400 mL/min, a H_2 fuel flow of 25 mL/min and a N_2 makeup flow of 10 mL/min. The software used was Agilent OpenLAB CDS ChemStation Edition Rev. C.01.09[144].

For water suppression ^{1}H-NMR spectra were recorded on a Bruker Avance300 (300 MHz) spectrometer at ambient temperature in a H_2O:D_2O mixture (6:1) as solvent, with sodium 3-(trimethylsilyl)-1-propanesulfonate (DSS) as the internal standard (TMS peak at 0 ppm). Solvent suppression was achieved through excitation sculpting, using the Bruker ZGESGP pulse program adjusted for the water resonance. Integration was performed using ACD/NMR Processor Academic Version 12.00 software.

3.2. Materials

Unless otherwise noted, all reagents and solvents were purchased from commercial suppliers and used without further purification. Few starting materials (**18b**, **18c** and **19**) and all reference compounds (**2a**, **2b**, **8a**, **3a** and **19a**) were prepared using literature procedures, described in the paper "Energy conservation via thioesters in a non-enzymatic metabolism-like reaction network". The products were characterized by ^{1}H NMR, ^{13}C NMR, HRMS and melting point.

3.3. Analytical method

3.3.1. GC-FID analysis

Extraction procedure for GC-FID analysis

A 0.5 mL aliquot of the reaction mixture was added to 0.5 mL of EA, followed by vortexing for 30 s. The EA layer was separated and dried over anhydrous Na_2SO_4. 40 µL of the dry EA layer was diluted with 960 µL of EA and subjected to GC-FID analysis.

Yield determination and error analysis for GC-FID analysis

1 mL standard aqueous solutions of thioesters at different concentrations (1 mM, 2 mM, 5 mM, 10 mM, 20 mM, 40 mM) were prepared by dilution 100 mM stock solutions of these thioesters. 500 µL of each standard solution were extracted using the extraction procedure as described herein (see: Extraction procedures). For each thioester, a six-point graph was plotted, correlating the characteristic GC peak (as integrated automatically by the Agilent OpenLAB CDS ChemStation Edition Rev. C.01.09[144] software) with substrate concentration (**Fig 79**, **Fig 80**). Each data point was obtained from three independent measurements and the correlation line was obtained from the least-squares fitting (intercept = 0). Error bars on graphs are shown as ± standard deviation for each data point. Overall percentage error of the response factor corresponds to ± standard deviation for each slope value.

The concentrations of the compounds were calculated by comparing the product peak area with the calibration curve. The yields of the products were calculated by multiplication of the determined concentration with the reaction volume, divided by the amount of limiting starting material (in most cases 0.1 mmol of the thio compound). Each reaction was performed at least three times to ensure reproducibility and reported percentage yields are an average of these three runs, with an error corresponding to ± standard deviation.

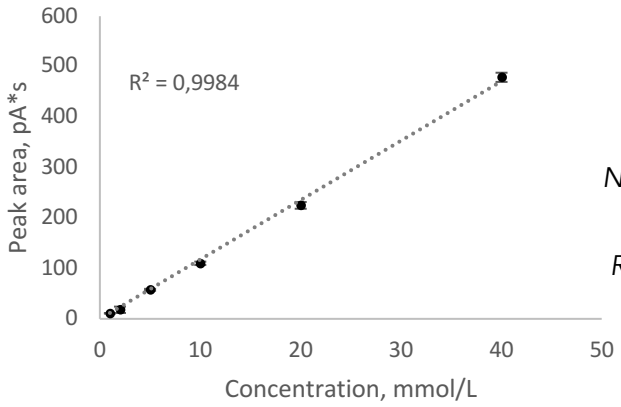

N,S-diacetyl cysteamine (**2a**)

Response factor: 11.773

Fig 79. Correlation between the concentration of an aqueous solutions of **2a** and the measured GC-Fid peak area

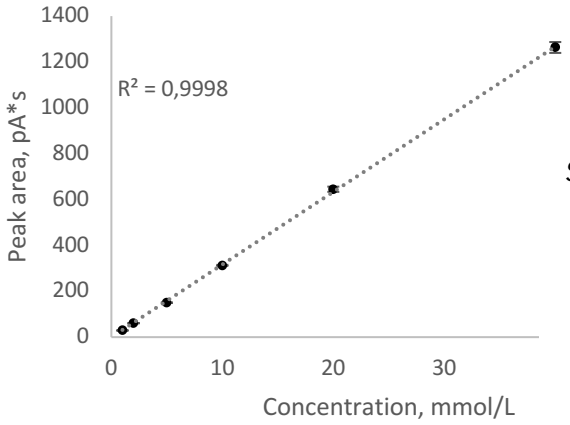

S-(2-(2-(2-methoxyethoxy)ethoxy)ethyl) ethanethioate (**2b**)

Response factor: 31.655

Fig 80. Correlation between the concentration of an aqueous solution of **2b** and the measured GC-Fid peak area

3.3.2. LCMS analysis

Sample preparation of LCMS analysis

After treatment of 1 mL of the reaction mixture with Chelex® 100 resin followed by centrifugation 20 µL of the supernatant were diluted with 180 µL of MilliQ-water and subjected to LCMS analysis (injection volume = 0.1 µL unless otherwise noted).

Yield determination and error analysis for LCMS analysis

1 mL standard aqueous solutions of authentic samples at different concentrations (selection of 0.5 mM, 1 mM, 2 mM, 4 mM, 5 mM, 10 mM, 20 mM, 40 mM, 80 mM) were prepared by dilution of 100 mM stock solutions of these compounds. For each of these solutions 20 µL were diluted with 180 µL MilliQ-water and subjected to LCMS-analysis. For each compound, a six-point graph was plotted, correlating the characteristic LCMS-peak (as integrated by the Thermo Xcalibur 4.2.28.14 Qual Browser software) with substrate concentration (Fig 81-Fig 86). Each data point was obtained from three independent measurements and the correlation line was obtained from the least-squares fitting (intercept = 0). Error bars on graphs are shown as ± standard deviation for each data point. Overall percentage error of the response factor corresponds to ± standard deviation for each slope value.

The concentrations of the compounds were calculated by comparing the product peak area with the calibration curve. The yields of the products were calculated by multiplication of the determined concentration with the reaction volume, divided by the amount of limiting starting material (in most cases 0.1 mmol of the thio compound). Each reaction was performed at least three times to ensure reproducibility, and reported percentage yields are an average of these three runs, with an error corresponding to ± standard deviation.

4-[[2-(Acetylamino)ethyl]thio]-4-oxobutanoic acid (8a)

Response factor: 3.95597×10^7

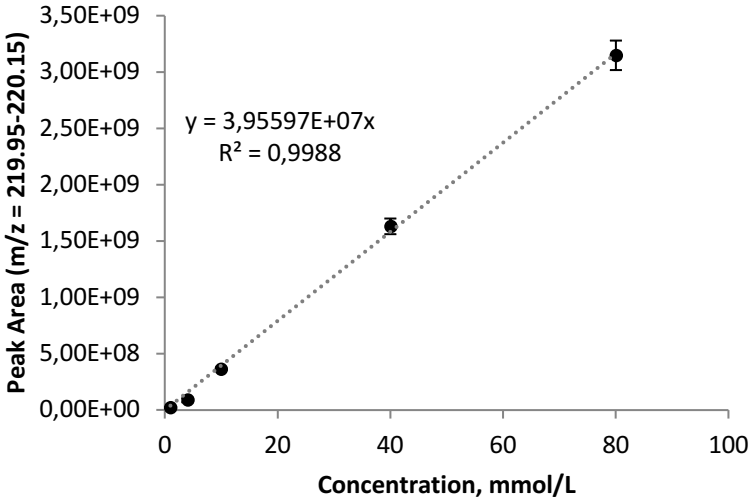

Fig 81. Correlation between the concentration of an aqueous solution of **8a** and the measured LCMS peak area (m/z = 219.95-220.15)

3-((2-acetamidoethyl)thio)-3-oxopropanoic acid (3a)

Response factor: 3.64713×10^7

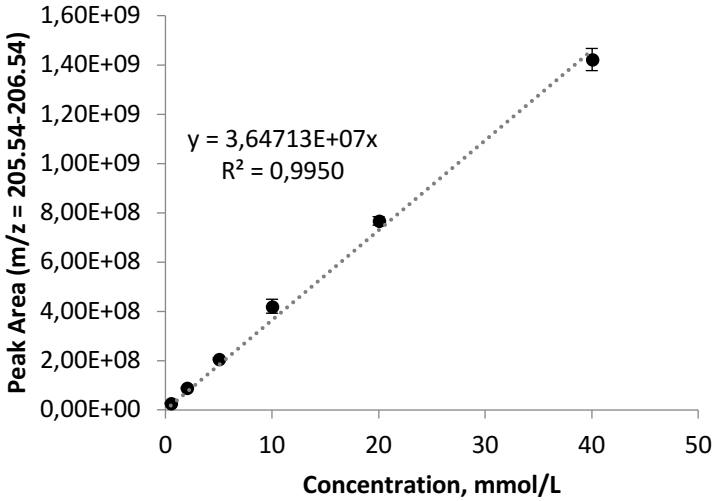

Fig 82. Correlation between the concentration of an aqueous solution of **3a** and the measured LCMS peak area (m/z = 205.54-206.54)

4-((2-acetamidoethyl)thio)-2-hydroxy-4-oxobutanoic acid (19a)

Response factor: 1.08917×10^7

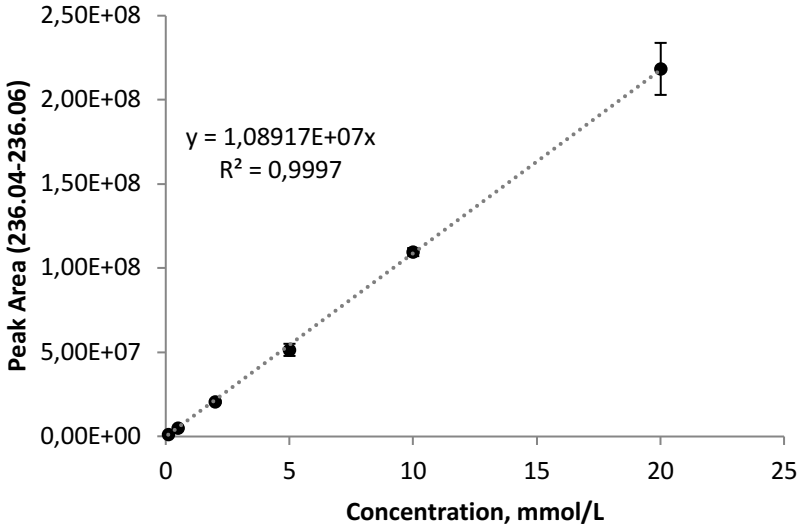

Fig 83. Correlation between the concentration of an aqueous solution of **19a** and the measured LCMS peak area (m/z = 236.04-236.06)

N -acetylcysteamine (18a)

Response factor: 2.55663×10^7

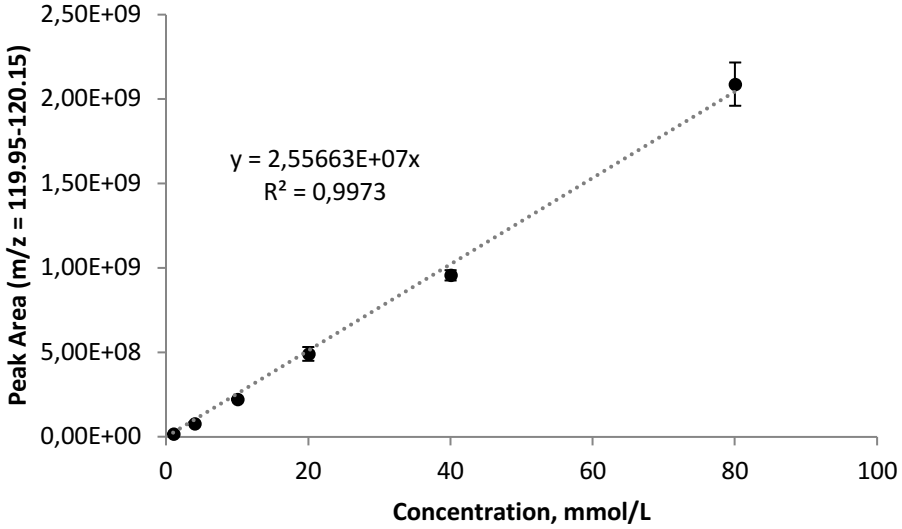

Fig 84. Correlation between the concentration of an aqueous solution of **18a** and the measured LCMS peak area (m/z = 119.95-120.15)

N,N'-(disulfanediylbis(ethane-2,1-diyl))diacetamide (18c)

Response factor: 8.26212×10^7

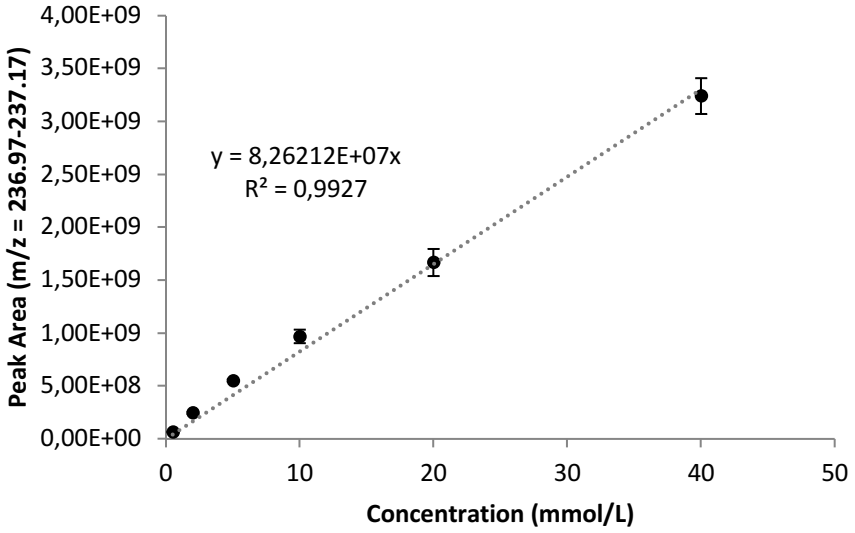

Fig 85. Correlation between the concentration of an aqueous solution of **18c** and the measured LCMS peak area (m/z = 236.97-237.17)

N,S-diacetylcysteamine (2a)

Response factor: 5.72370×10^7

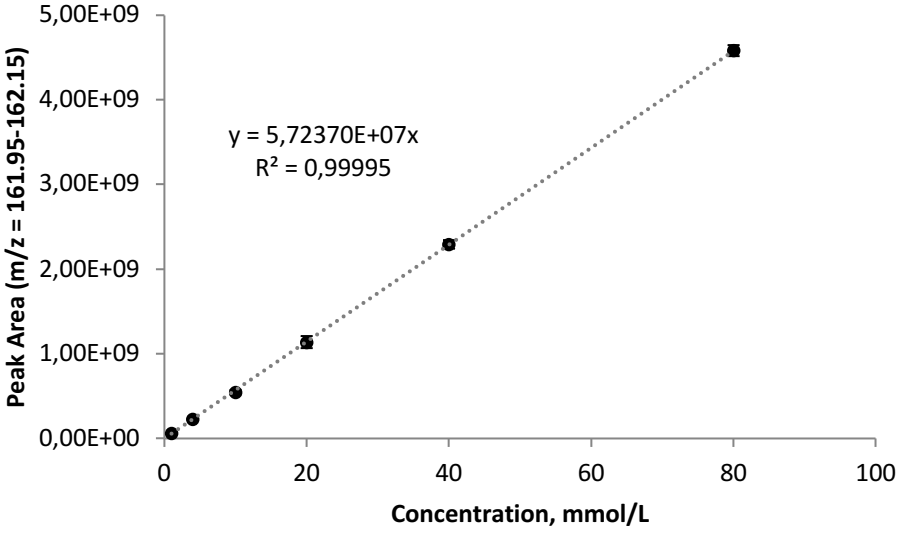

Fig 86. Correlation between the concentration of an aqueous solution of **2a** and the measured LCMS peak area (m/z = 161.95-161.15)

3.3.3. GC-MS analysis

Derivatisation procedure for GC-MS analysis

To facilitate GC-MS analysis, a literature ECF-derivatization procedure[13,16] was applied to the sample to convert carboxy groups to ethyl esters, hydroxy groups to ethyl carbonates, ketones to diethyl ketals, and aldehydes to diethyl acetals, using a mixture of ethanol/ethyl chloroformate (EtOH/ECF). For optimal gas chromatography resolution, heavy metal atoms were first removed using a resin (Chelex® 100 sodium form).

A ca. 1 mL aliquot of the reaction mixture was added to 50 mg of Chelex®, briefly shaken and then centrifuged (6000 rpm, 3 min). To 600 µL of the supernatant was added EtOH (300 µL) and pyridine (40 µL), followed by ethyl chloroformate (ECF, 40 µL). The mixture vortexed for 30 s. A second 40 µL portion of ECF was added and the mixture was vortexed again for 30 s. Next, $CHCl_3$ (200 µL) was added, followed by vortexing (10 s). Finally, $NaHCO_3$ (600 µL) was added and the mixture was vortexed again for 10 s. The $CHCl_3$ layer was separated and dried over anhydrous Na_2SO_4. 50 µL of the dry $CHCl_3$ layer were diluted with 150 µL of ethyl acetate prior to GC-MS analysis.

Product identification

Reaction products derivatized were identified by comparing the mass spectra and retention times with analogously derivatized authentic samples, as described in a previous paper.[9]

3.4. Formation of thioesters under prebiotic conditions

3.4.1. General procedures for thioester formation

Method A ($K_2S_2O_8$, FeS, 70 °C):

To a solution of the thiol (0.1 mmol) in 3 mL of MilliQ water in a Pyrex pressure tube with a stirring bar was added the corresponding **α**-keto acid (0.50 mmol; 0.42 mmol for hydroxyketoglutarate) or acetaldehyde (1.0 mmol) under a constant argon flow. Iron(II) sulfide (0.05 mmol) and potassium persulfate (0.2 mmol) were added. The reaction vessel was closed and heated to 70 °C for 3 hours. After cooling to room temperature, the amount of thioester formed was determined by GC-FID analysis or LCMS analysis (see section 3.3.1 and 3.3.2).

Method B ($K_2S_2O_8$, FeS, UV-A):

To a solution of the thiol (0.1 mmol) in 3 mL of MilliQ water in a quartz tube with a stirring bar was added the corresponding α-keto acid (0.50 mmol; 0.42 mmol for hydroxyketoglutarate) or acetaldehyde (1.0 mmol) under a constant argon flow. Iron(II) sulfide (0.05 mmol) and potassium persulfate (0.2 mmol) were added. The tube was closed with a septum and irradiated in a Luzchem LZC-ORG photoreactor equipped with 10 LZC-UVA lamps for 6 hours. The amount of thioester formed was determined by GC-FID analysis or LCMS analysis (see section 3.3.1 and 3.3.2).

Method C ($KHSO_4$, UV-A):

To a solution of the thiol (0.1 mmol) in 3 mL of a $KHSO_4$-solution (3 M in MilliQ water) in a quartz tube with a stirring bar was added the corresponding α-keto acid (0.50 mmol; 0.42 mmol for hydroxyketoglutarate) or acetaldehyde (1.0 mmol) under a constant argon flow. The tube was closed with a septum and irradiated in a Luzchem LZC-ORG photoreactor equipped with 10 LZC-UVA lamps for 6 hours. The amount of thioester formed was determined by GC-FID analysis or LCMS analysis (see section 3.3.1 and 3.3.2).

3.4.2. Thioester formation from a non-enzymatic reaction network

A solution of sodium pyruvate **2** (110 mg, 1.0 mmol, 2.0 equiv), glyoxylic acid monohydrate (46 mg, 0.5 mmol, 1.0 equiv) and $FeCl_2 \cdot 4H_2O$ (200 mg, 1.0 mmol, 2.0 equiv) in 3 mL of MilliQ water was prepared in a Pyrex pressure tube equipped with a stirring bar under a constant argon flow. For oxidation procedure A *N*-acetylcysteamine **18a** (59 mg, 0.5 mmol, 1.0 equiv) was added. The reaction vessel was closed and heated to 70 °C for 1 h or 3 h, followed by an oxidation procedure.

Oxidation procedure A:

To the solution prepared as described above, potassium persulfate (270 mg, 1.0 mmol, 1.0 equiv) was added under a constant argon flow. The reaction vessel was closed and heated to 70 °C for 3 hours. After cooling to room temperature, the amount of thioesters formed was determined by GC-FID analysis or LCMS analysis (see section 3.3.1 and 3.3.2), the different intermediates of the network were determined by GC-MS analysis (see section 3.3.3).

Oxidation procedure B:

To the solution prepared as described above, $KHSO_4$ (1.2 g, 9.0 mmol, to form a ~3 M solution) and *N*-acetylcysteamine **18a** (59 mg, 0.50 mmol 1.0 equiv) were added, the mixture was transferred in a quartz tube under a constant argon flow. The tube was closed with a septum and irradiated in a Luzchem LZC-ORG photoreactor equipped with 10 LZC-UVA lamps for 3 hours. The amount of thioesters formed was determined by GC-FID analysis or LCMS analysis (see section 3.3.1 and 3.3.2), the different intermediates of the network were determined by GC-MS analysis (see section 3.3.3).

3.5. Experimental data

3.5.1. GC-Fid chromatograms of authentic samples

***N*-acetylcysteamine (18a)**

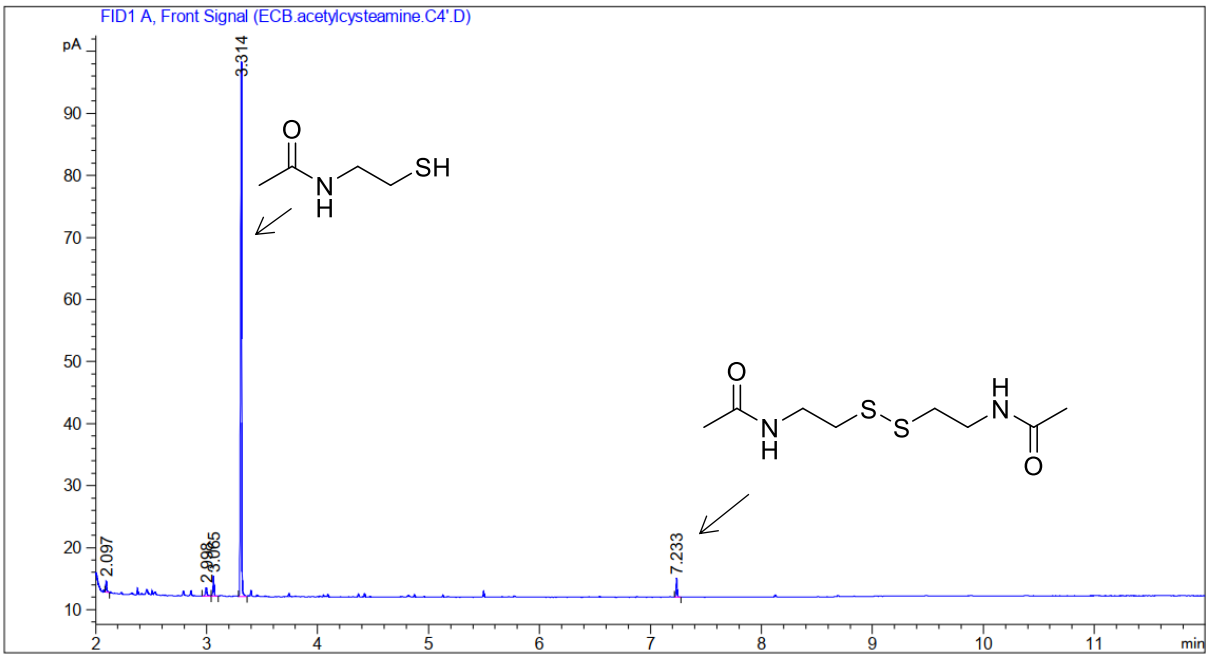

2-(2-(2-methoxyethoxy)ethoxy)ethane-1-thiol (18b)

N,N'-(disulfanediylbis(ethane-2,1-diyl))diacetamide (18c)

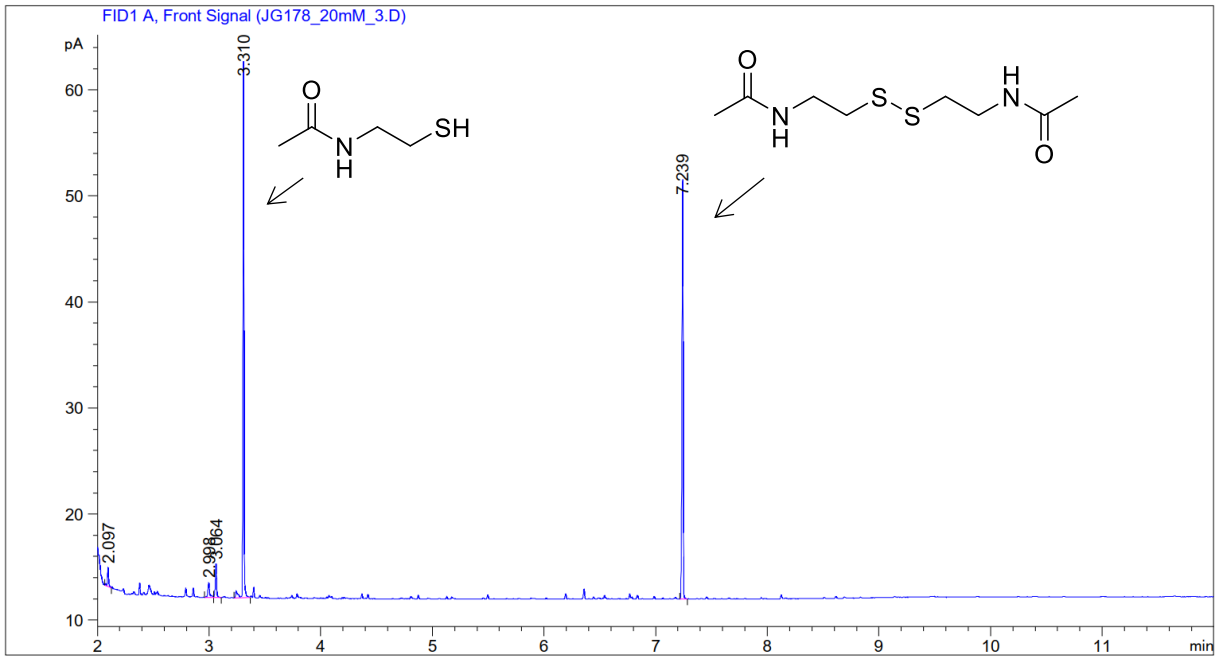

N,S-diacetyl cysteamine (2a)

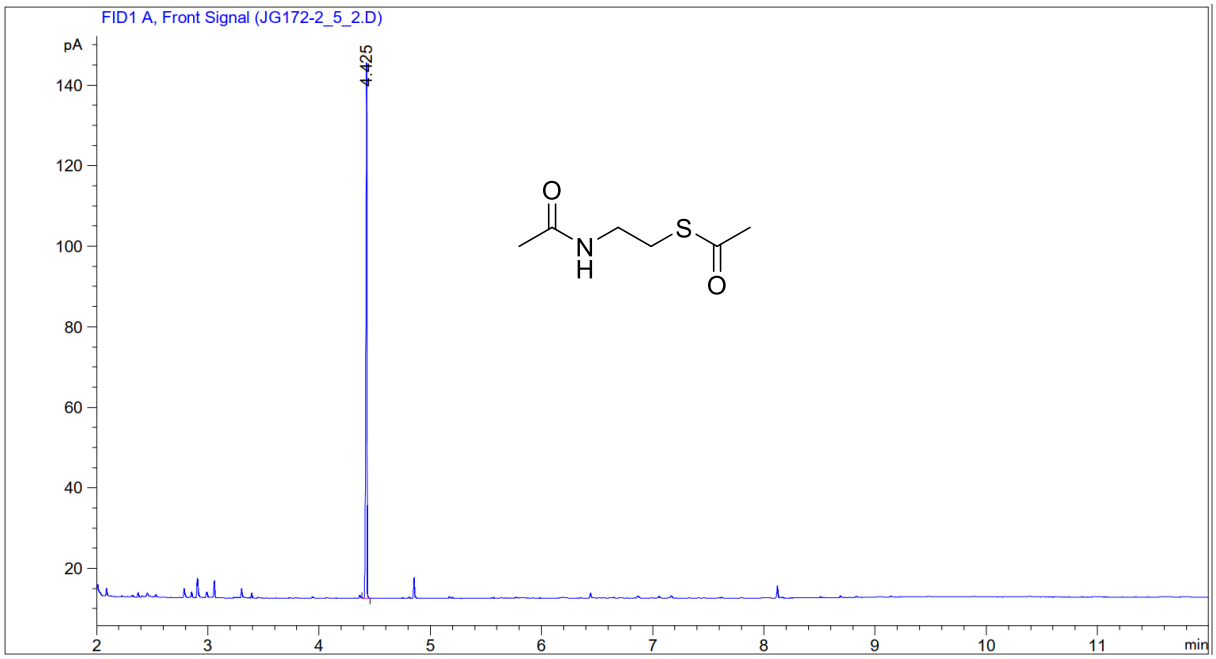

S-(2-(2-(2-methoxyethoxy)ethoxy)ethyl) ethanethioate (2b)

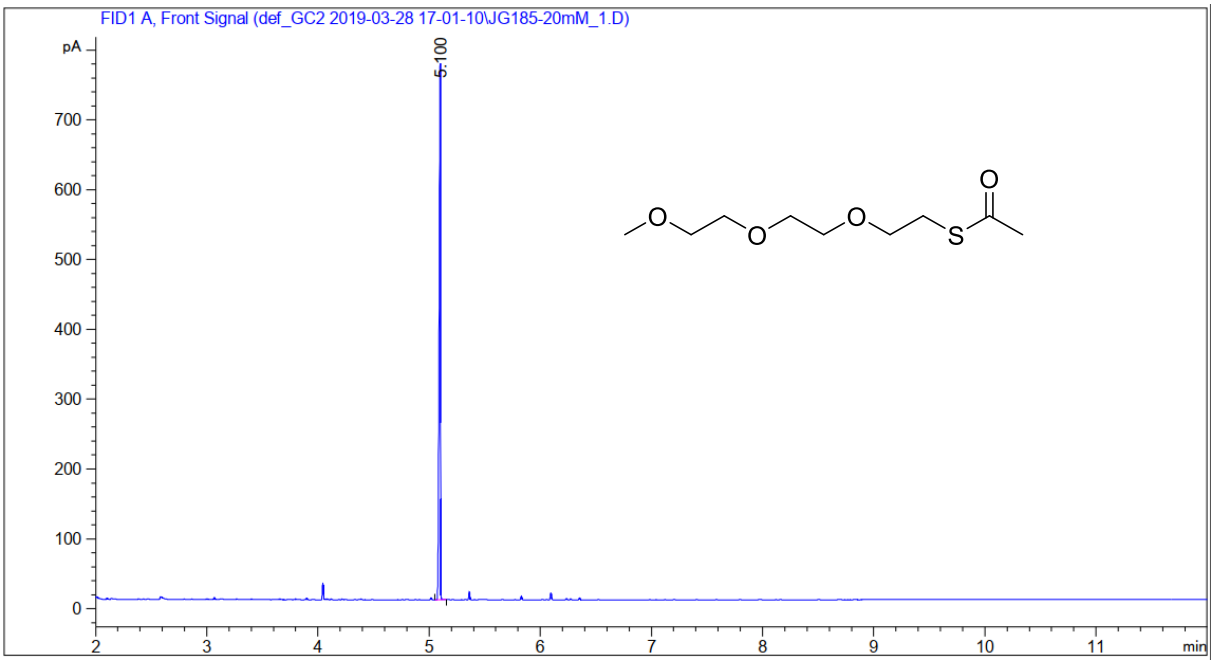

2,5,8,15,18,21-hexaoxa-11,12-dithiadocosane

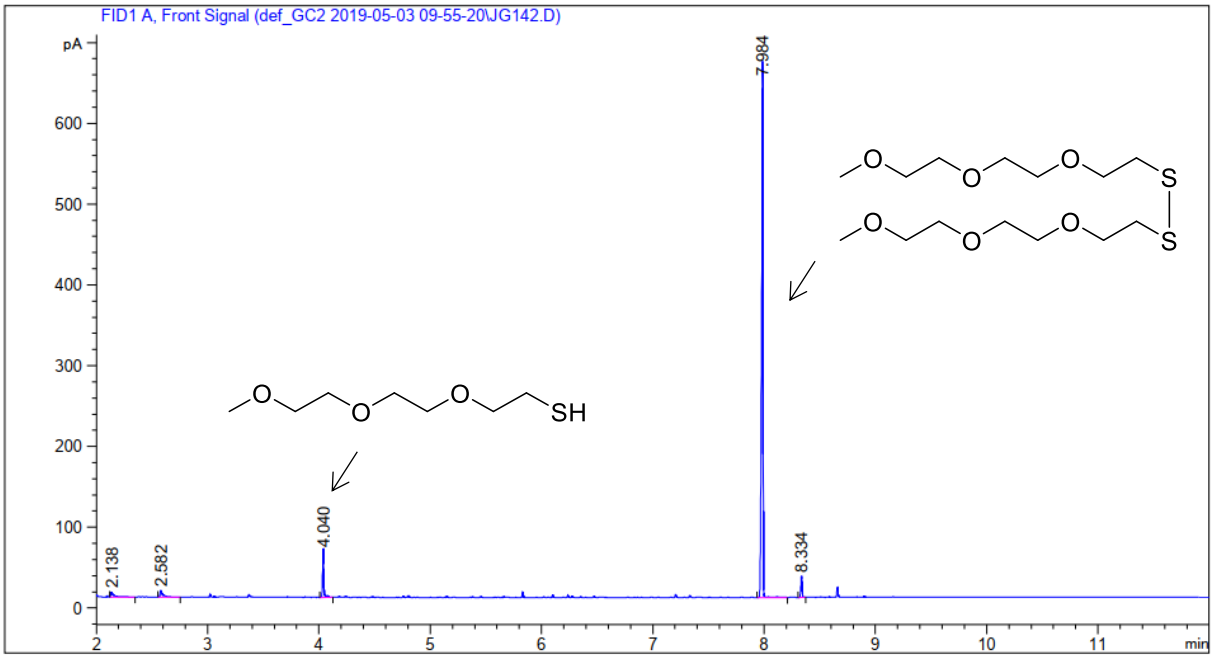

3.5.2. LC-MS of authentic samples

***N*-acetyl cysteamine (18a)**

m/z = 119.95–120.15

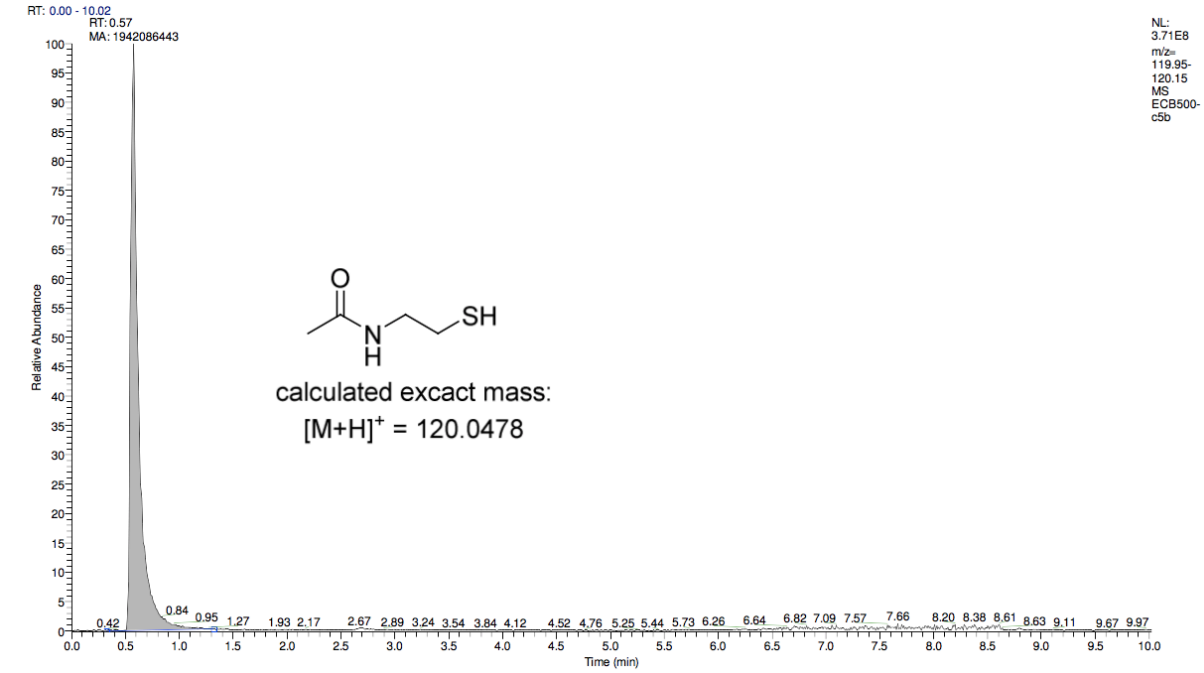

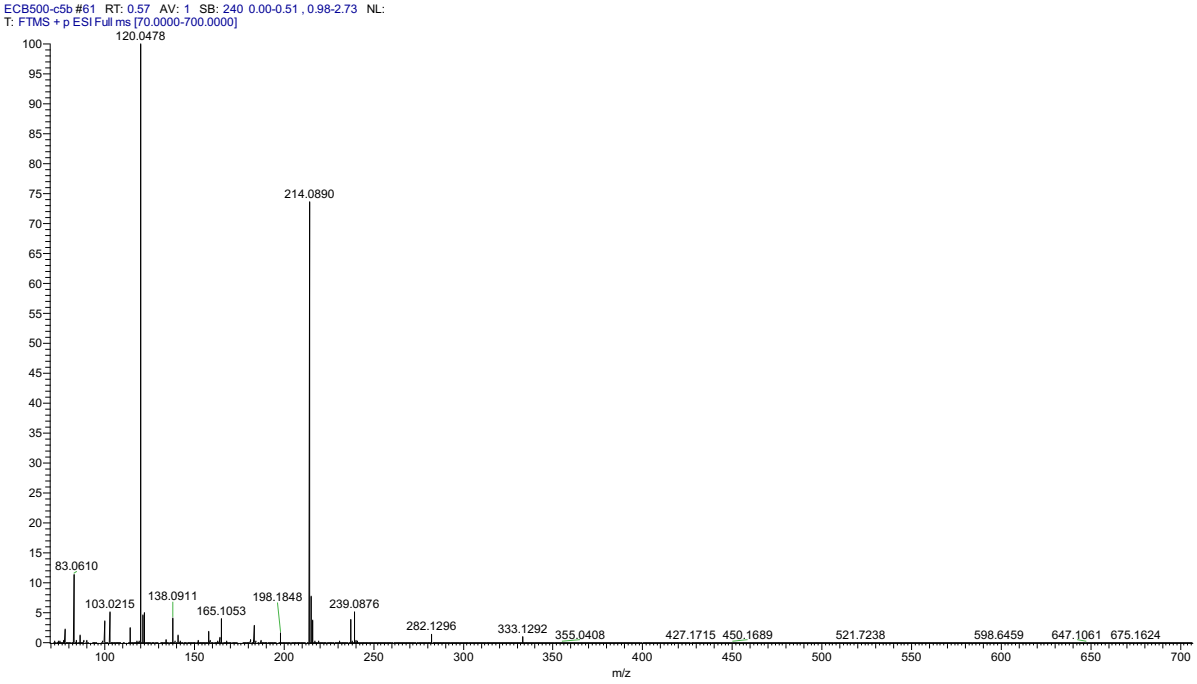

N,N'-(disulfanediylbis(ethane-2,1-diyl))diacetamide (18c)

m/z = 236.97–237.17

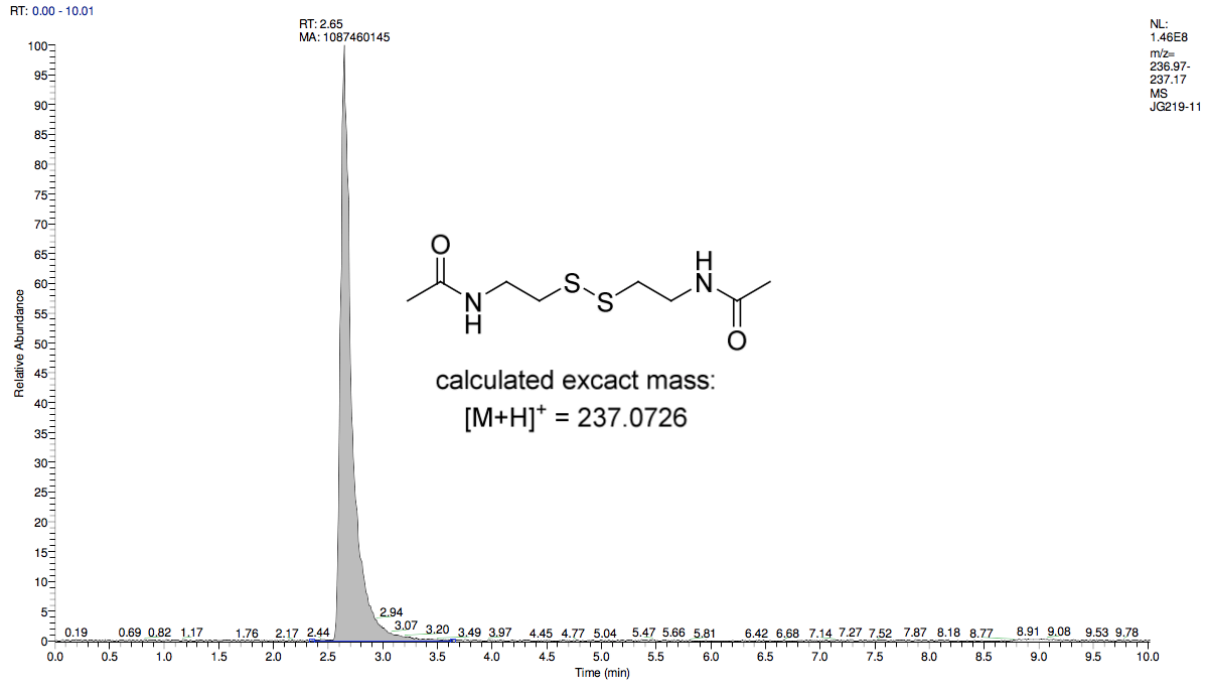

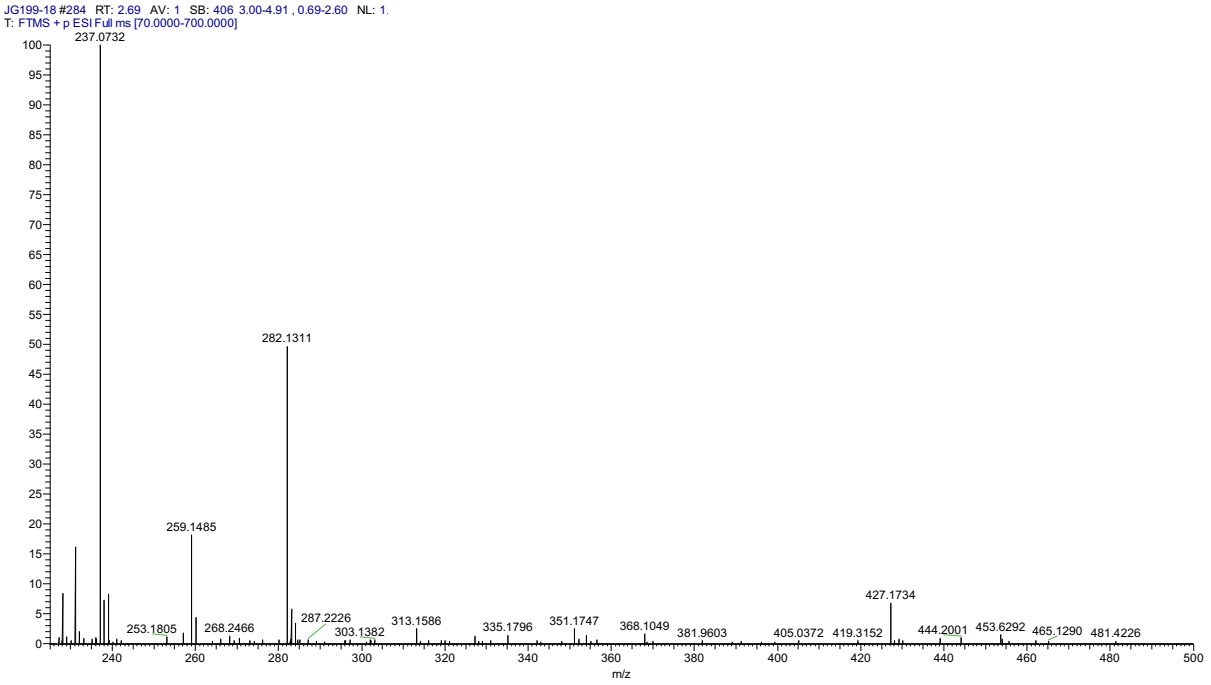

N,S-diacetyl cysteamine (2a)

m/z = 161.95–162.15

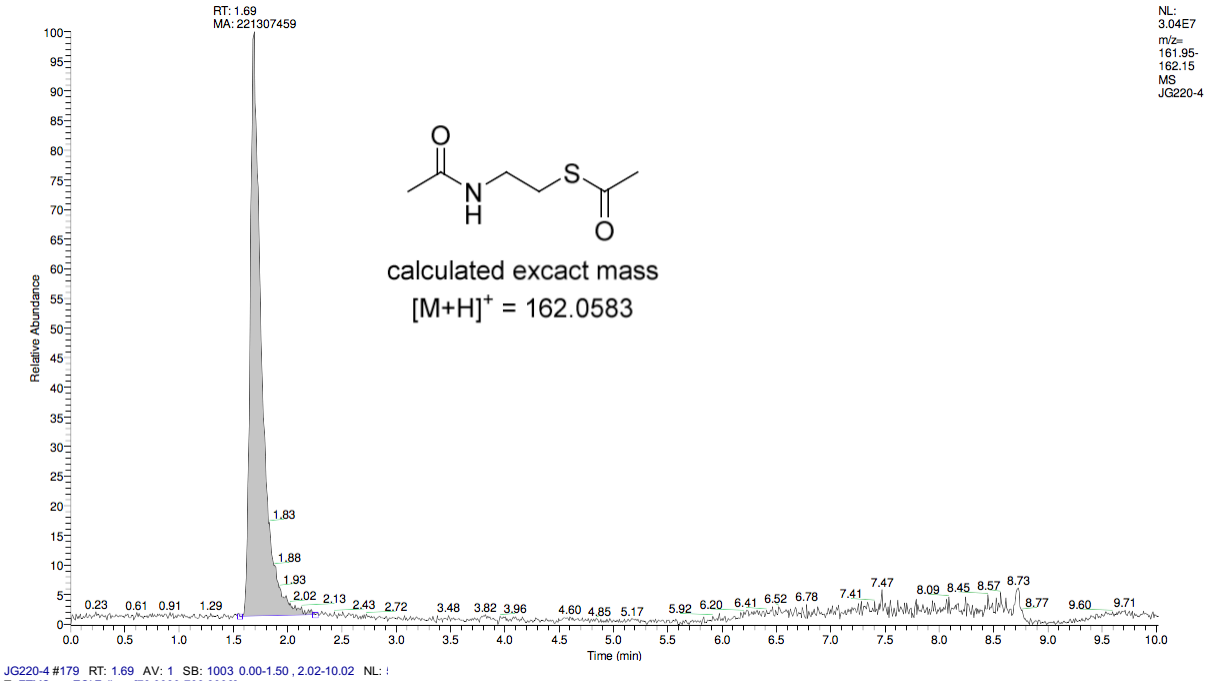

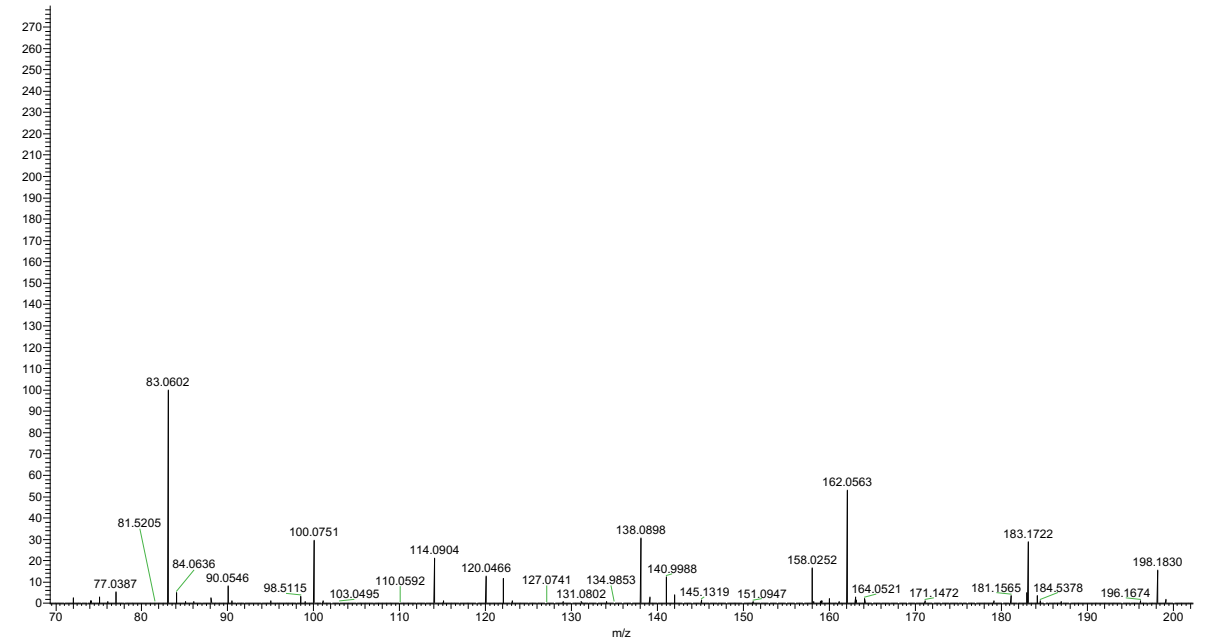

4-[[2-(Acetylamino)ethyl]thio]-4-oxobutanoic acid (8a)

m/z = 219.95–220.15

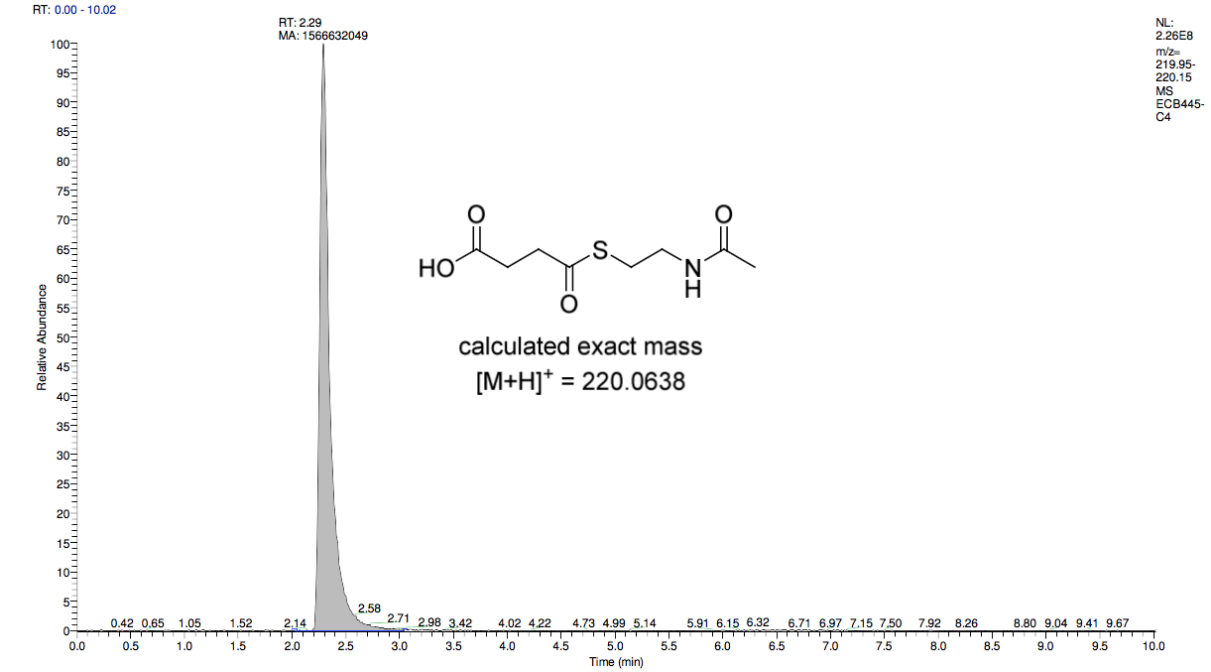

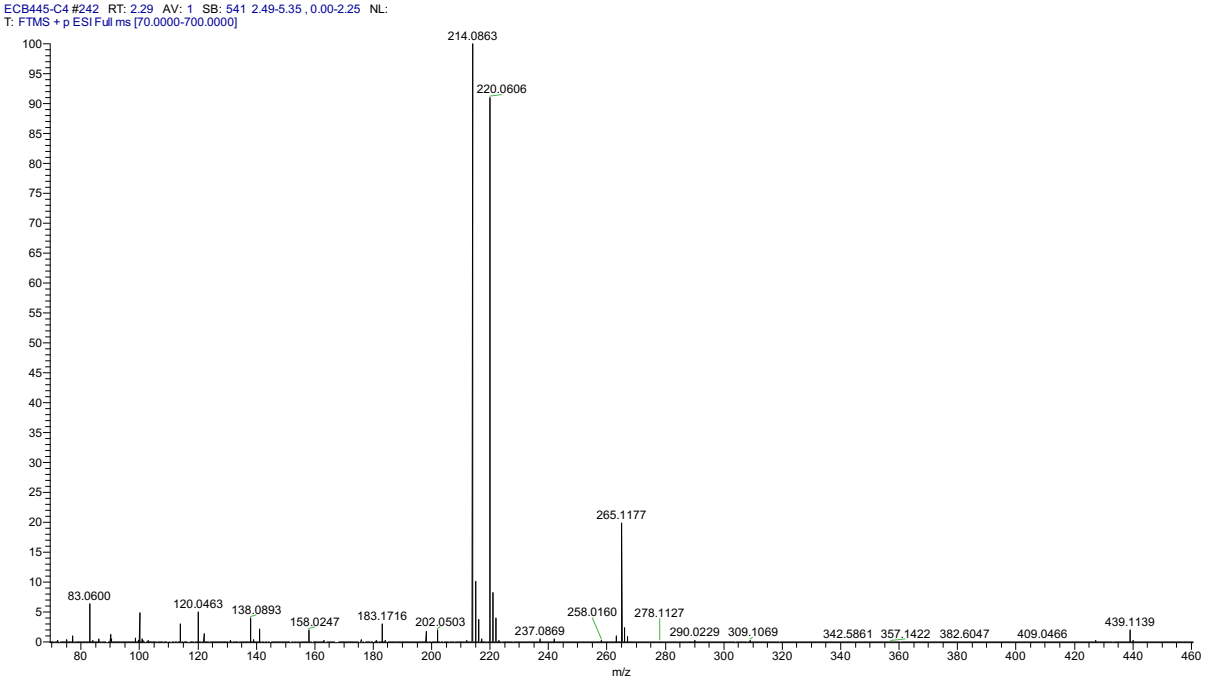

3-((2-acetamidoethyl)thio)-3-oxopropanoic acid (3a)

m/z = 205.54–206.54

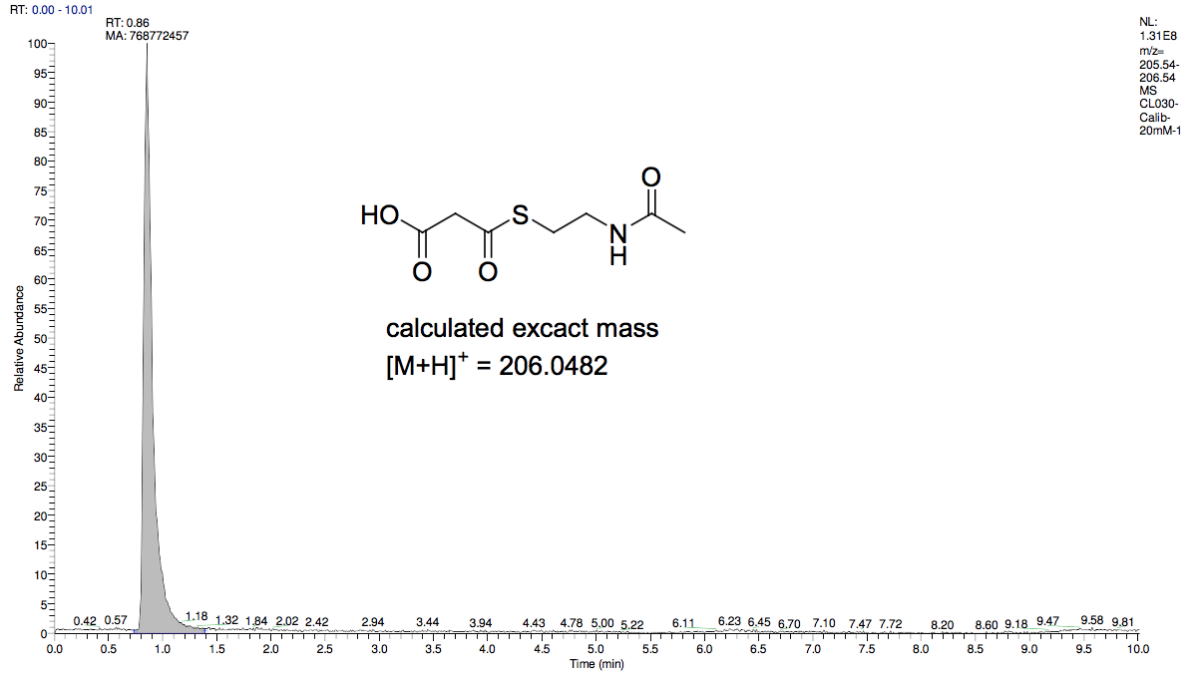

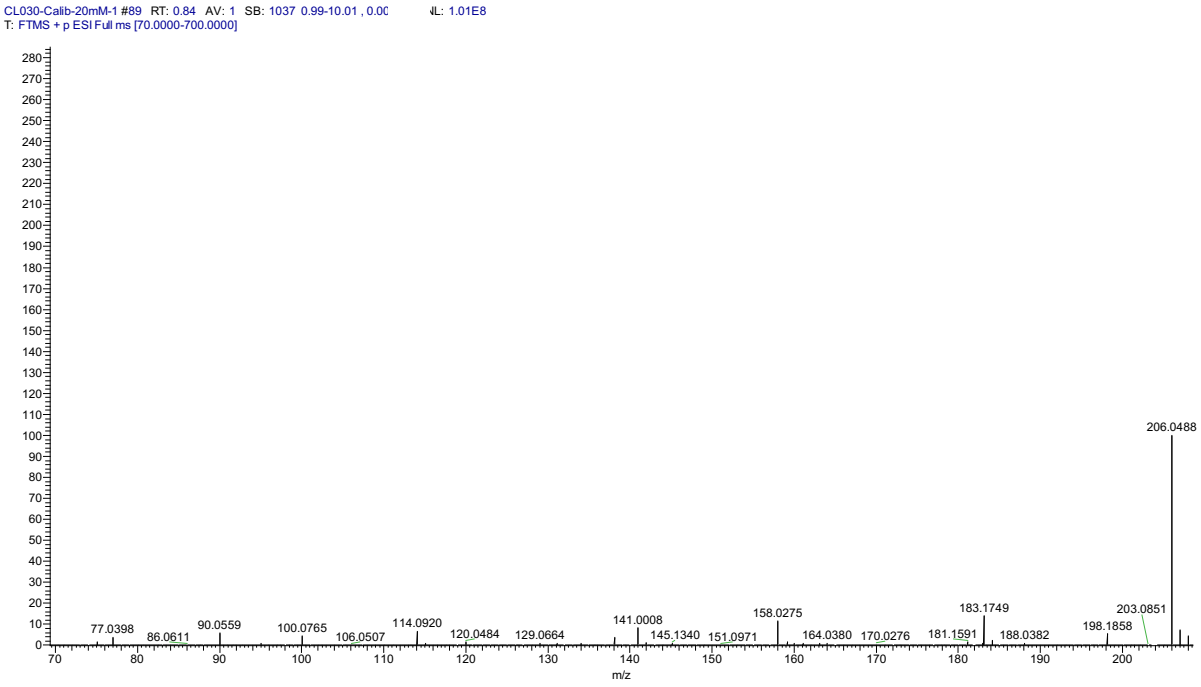

4-((2-acetamidoethyl)thio)-2-hydroxy-4-oxobutanoic acid (19a)

m/z = 236.04-236.06

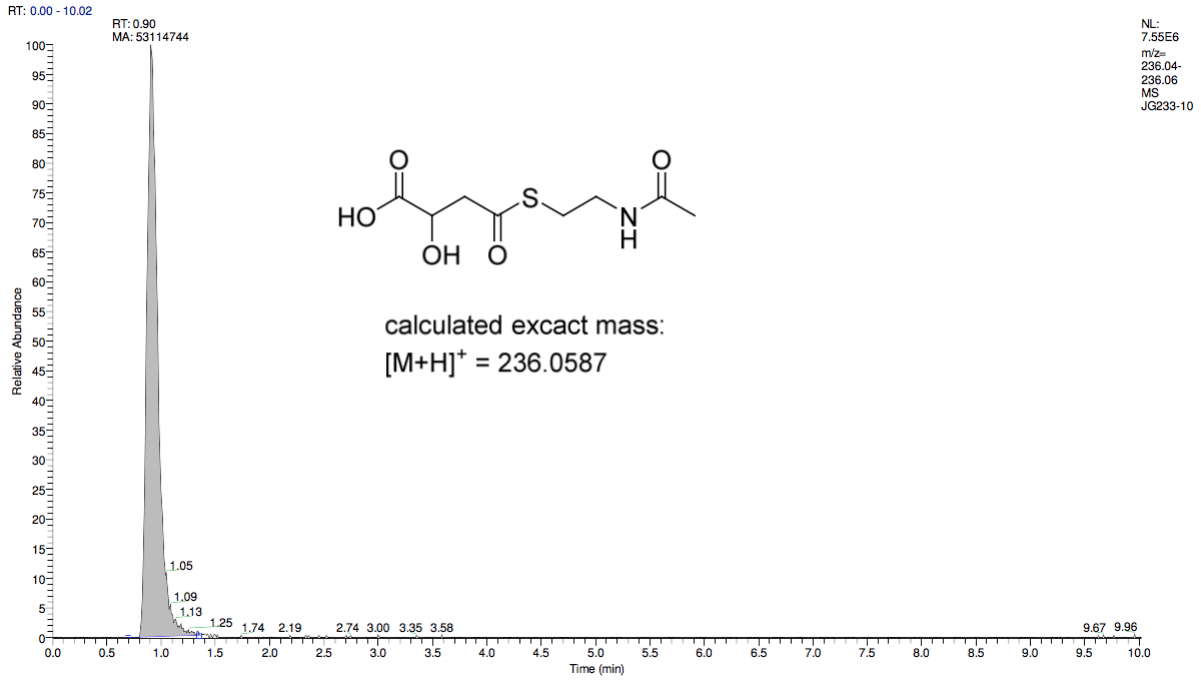

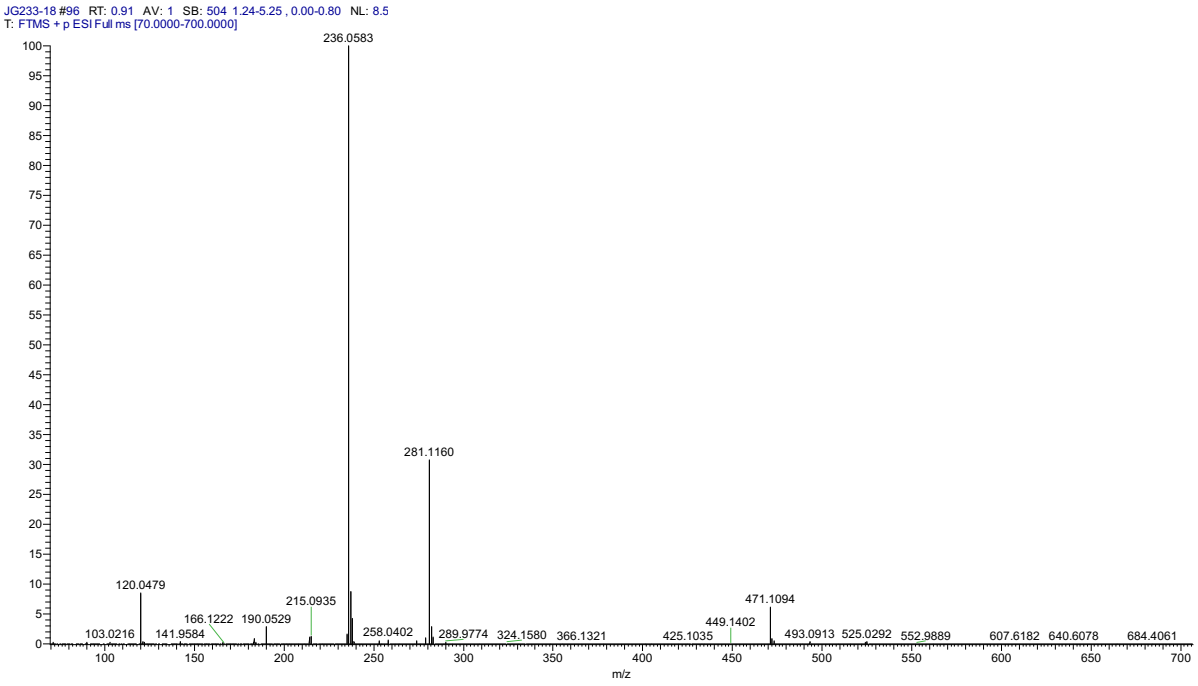

3.5.3. Thioesters formation under various conditions

Table 11. Thioester formation under various conditions

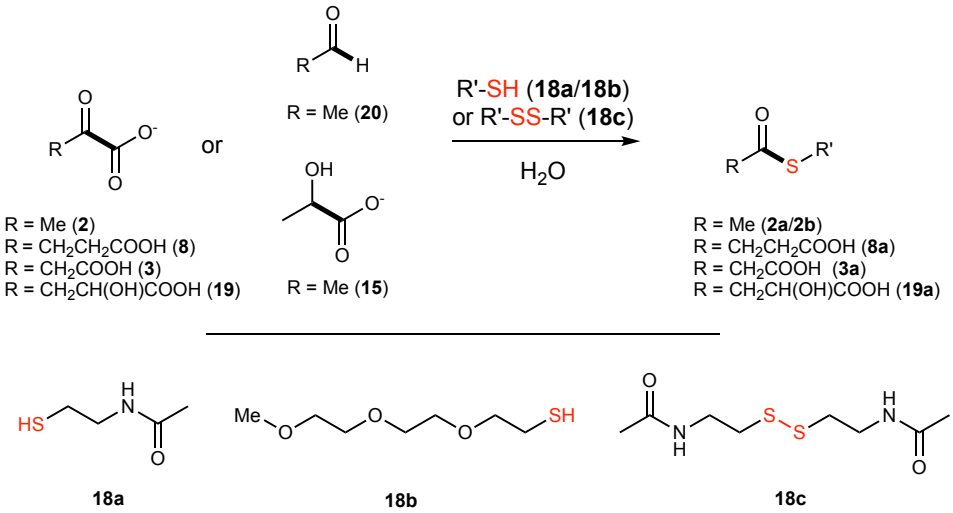

Entry	Substrate *(0.5 mmol)*	Thio-compd. *(0.1 mmol)*	Product	Product Yield (%) ± SD‡			
				Method A[a]	Method B[b]	Method C[c]	Method D[d]
1	Pyruvate **2**	**18a**	**2a**	26.6 ± 0.7	31.2 ± 0.4	5.1 ± 0.1	22.1 ± 0.4
2	Pyruvate **2**	**2b**	**2b**	14.6 ± 0.3	24.1 ± 0.6	5.6 ± 0.2	17.6 ± 1.0
3	Pyruvate **2**	**2c**[e]	**2&**	32.9 ± 0.9	31.9 ± 1.7	0.5 ± 0.1	4.9 ± 0.2
4	α-ketoglutarate **8**	**18a**	**8a**	9.5 ± 1.9	24.5 ± 1.8	/	13.1 ± 0.9
4'			**19a**	11.4 ± 0.5	3.8 ± 0.2	/	< 0.5
5	Oxaloacetate **3**	**18a**	**3a**	6.7 ± 0.4	23.6 ± 1.6	/	7.9 ± 1.7
5'			**2a**	2.6 ± 0.3	2.4 ± 0.3	/	< 0.5
6	Hydroxyketoglutarate **19**[f]	**18a**	**19a**	2.0 ± 0.1	9.9 ± 0.8	/	3.5 ± 0.2
7	Acetaldehyde **20**[g]	**18a**	**2a**	14.7 ± 1.4	12.9 ± 2.1	1.7 ± 0.2	19.6 ± 1.6
8	Lactate **15**	**18a**	**2a**	3.6 ± 0.1	3.5 ± 0.2	0.8 ± 0.1	0 ± 0.0

‡ Reported values were determined by GC-FID after an extraction procedure or by LCMS and represent the average of at least three runs. SD = standard deviation. Unless otherwise noted, 0.5 mmol of the substrate and 0.1 mmol of the thio compound were employed. [a] $K_2S_2O_8$ (2.0 equiv), FeS (0.5 equiv) in H_2O, 3 h, 70 °C. [b] $K_2S_2O_8$ (2.0 equiv), FeS (0.5 equiv) in H_2O, 6 h, UV-A. [c] $Fe(ClO_4)_3$ (2.0 equiv) in H_2O, 6 h, UV-A. [d] $KHSO_4$ (3 M) in H_2O, 6 h, UV-A. [e] 0.05 mmol of N-acetyl cysteamine disulfide was used instead of N-acetyl cysteamine. [f] Hydroxyketoglutarate was freshly prepared from glyoxylate and oxaloacetate without isolation. [g] 1.0 mmol of the substrate were used.

3.5.3.1. GC-Fid chromatograms of thioester under various conditions

Table 11, Entry 1, Method A

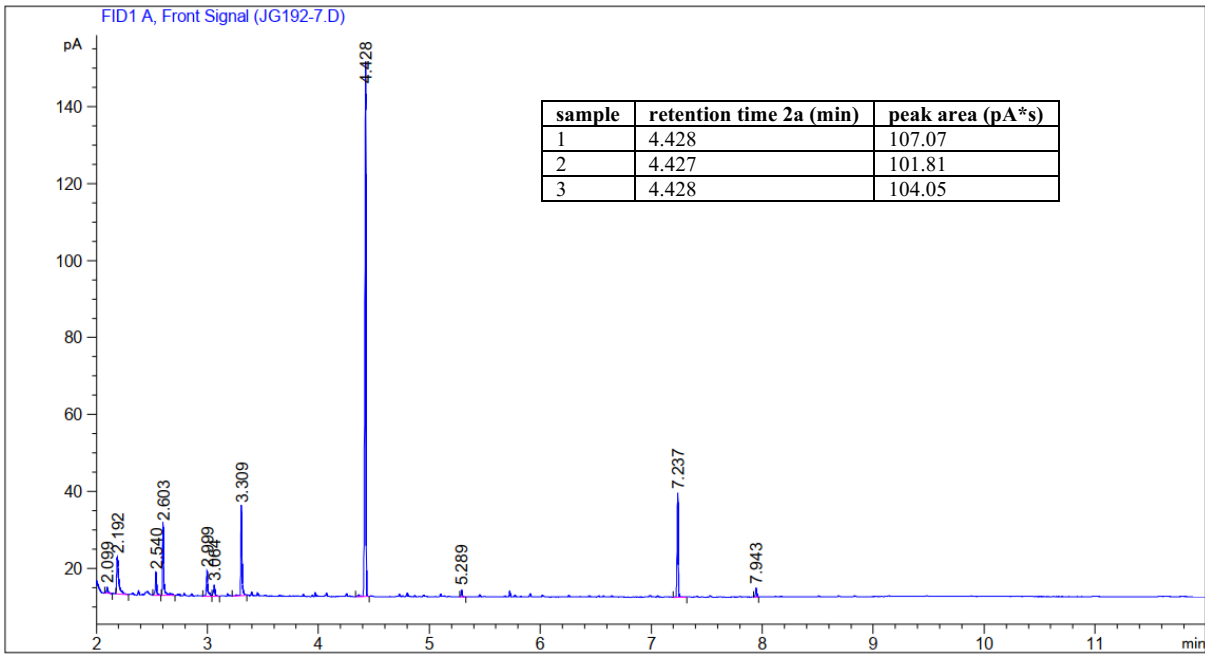

sample	retention time 2a (min)	peak area (pA*s)
1	4.428	107.07
2	4.427	101.81
3	4.428	104.05

Table 11, Entry 1, Method B

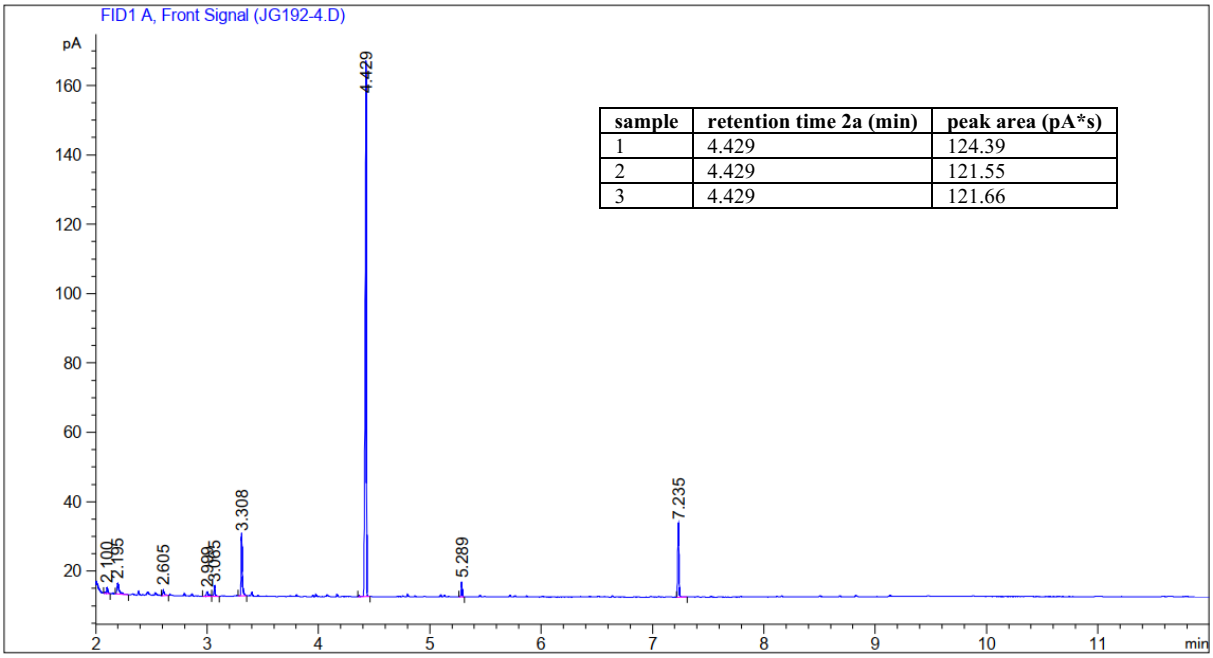

sample	retention time 2a (min)	peak area (pA*s)
1	4.429	124.39
2	4.429	121.55
3	4.429	121.66

Table 1, Entry 1, Method C

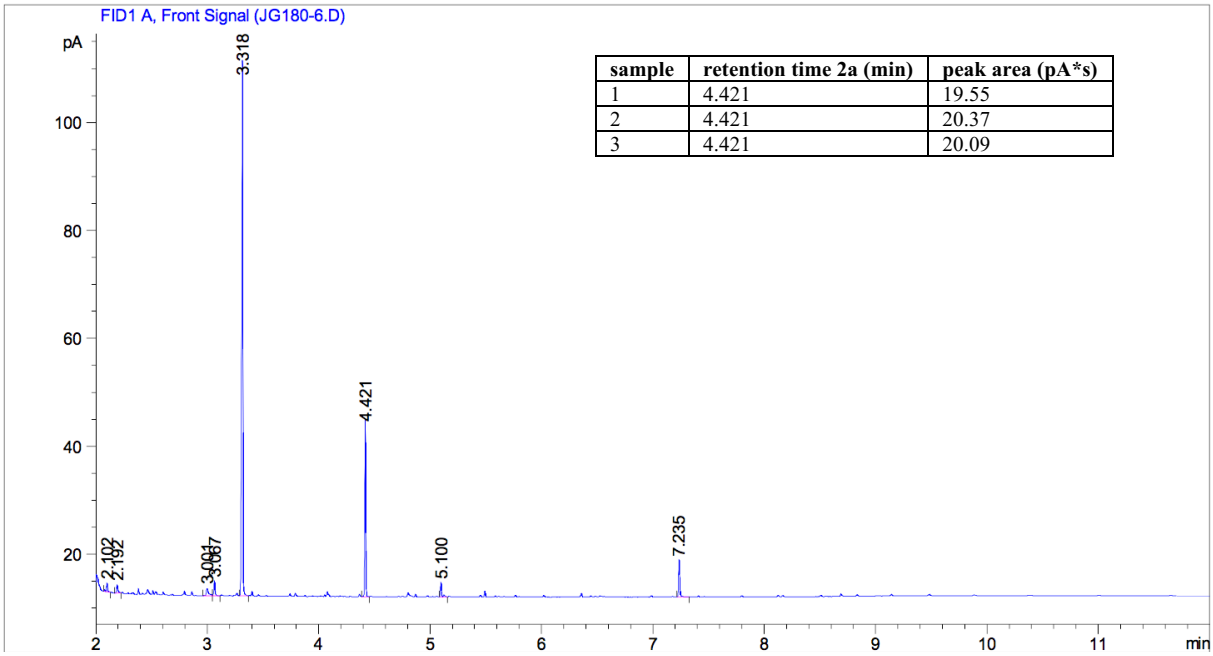

sample	retention time 2a (min)	peak area (pA*s)
1	4.421	19.55
2	4.421	20.37
3	4.421	20.09

Table 1, Entry 1, Method D

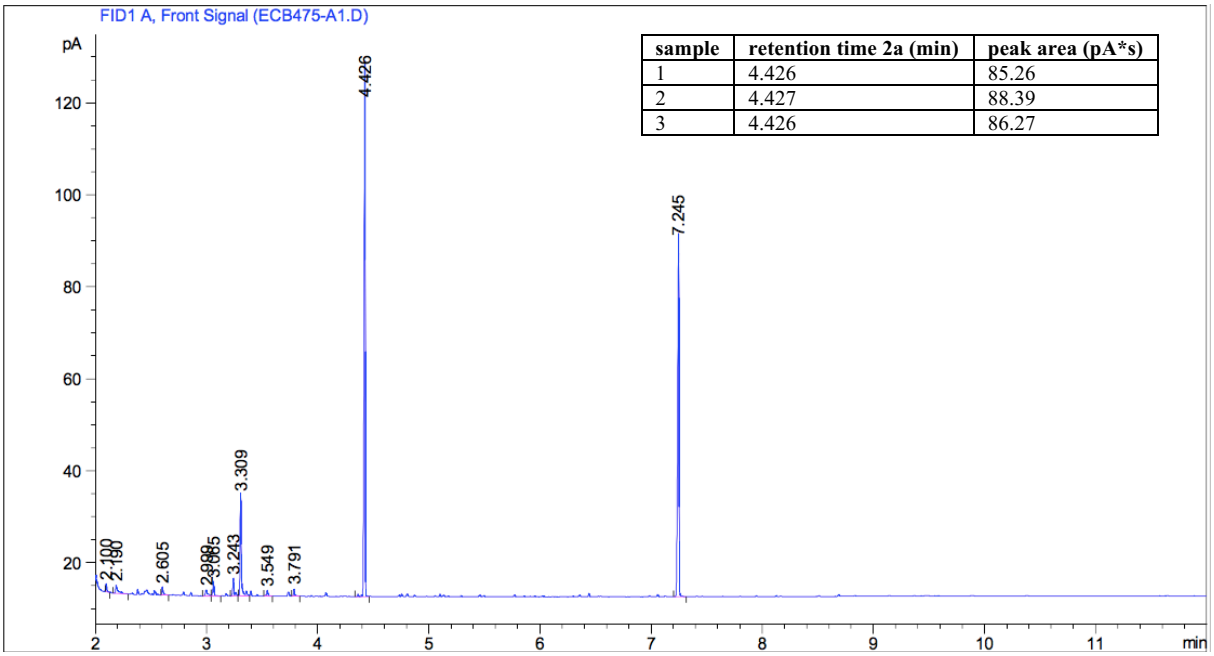

sample	retention time 2a (min)	peak area (pA*s)
1	4.426	85.26
2	4.427	88.39
3	4.426	86.27

Table 11, Entry 2, Method A

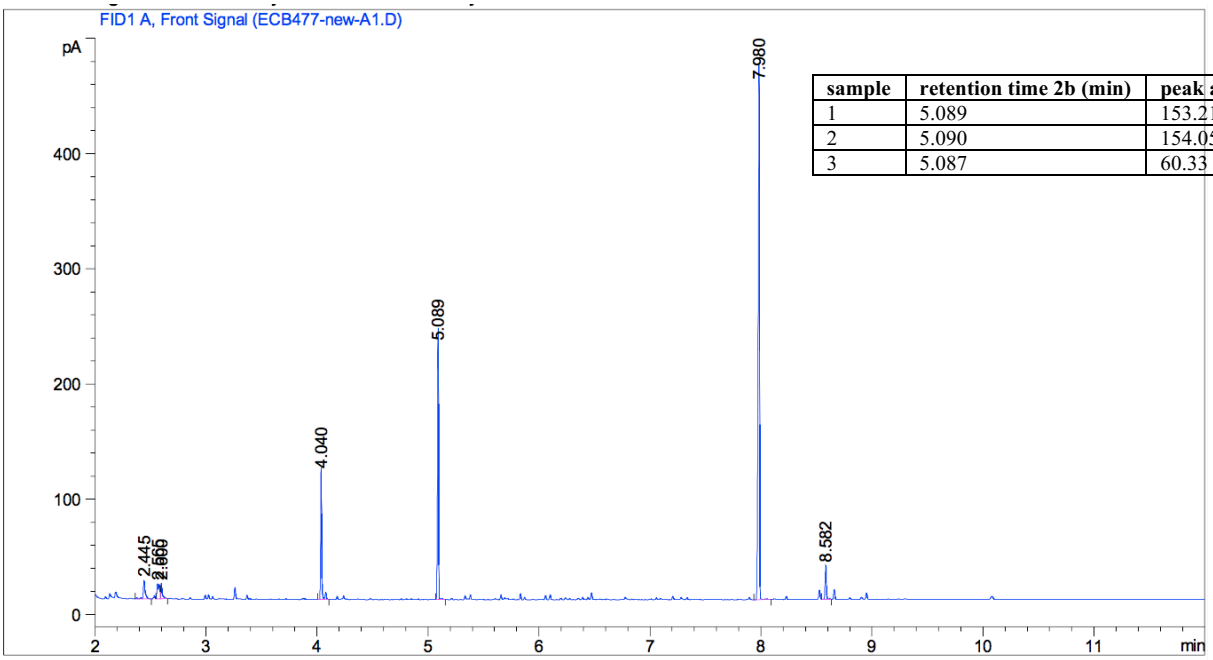

sample	retention time 2b (min)	peak area (pA*s)
1	5.089	153.21
2	5.090	154.05
3	5.087	60.33

Table 11, Entry 2, Method B

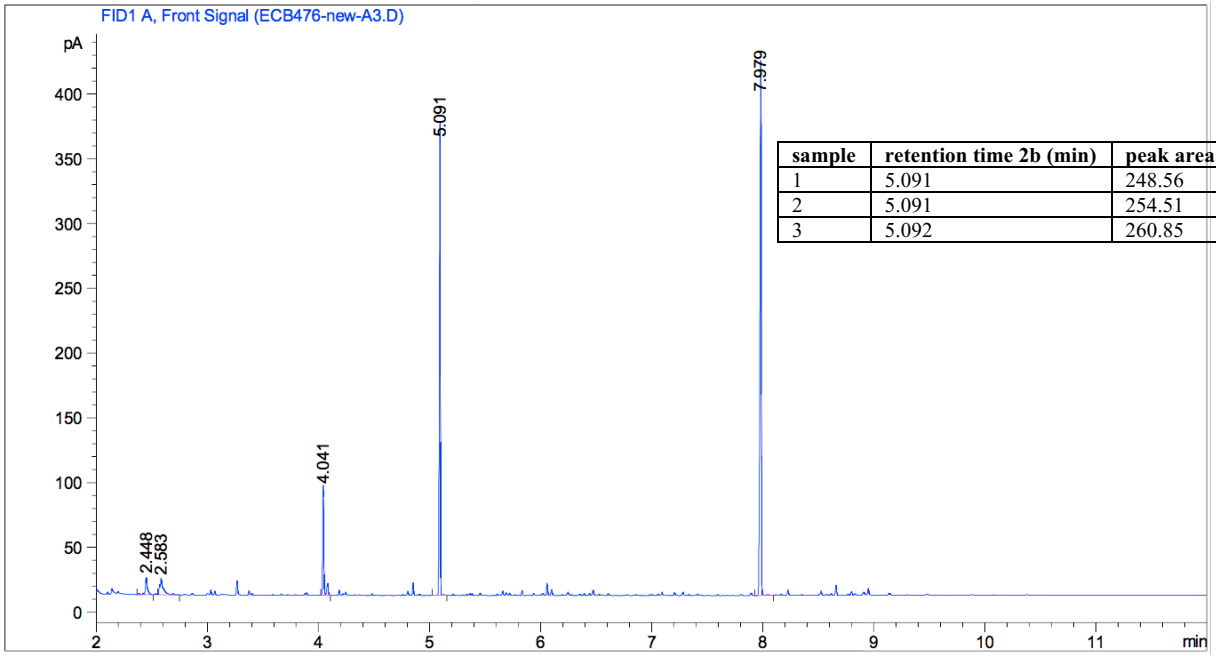

sample	retention time 2b (min)	peak area (pA*s)
1	5.091	248.56
2	5.091	254.51
3	5.092	260.85

Table 11, Entry 2, Method C

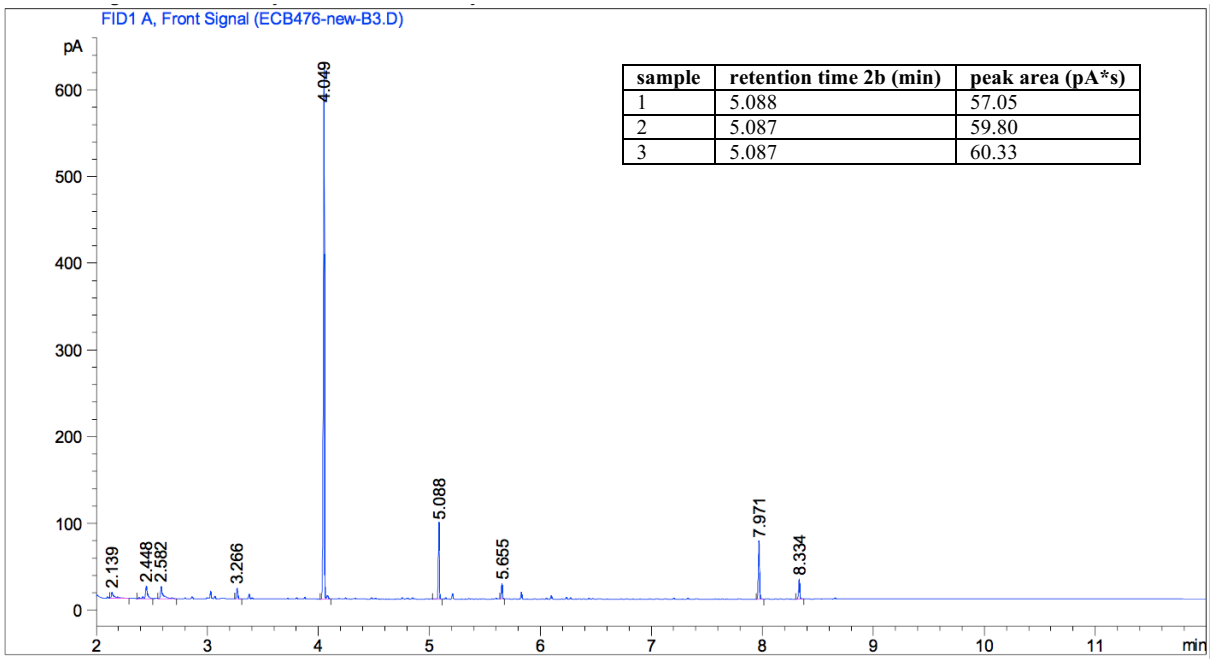

sample	retention time 2b (min)	peak area (pA*s)
1	5.088	57.05
2	5.087	59.80
3	5.087	60.33

Table 11, Entry 2, Method D

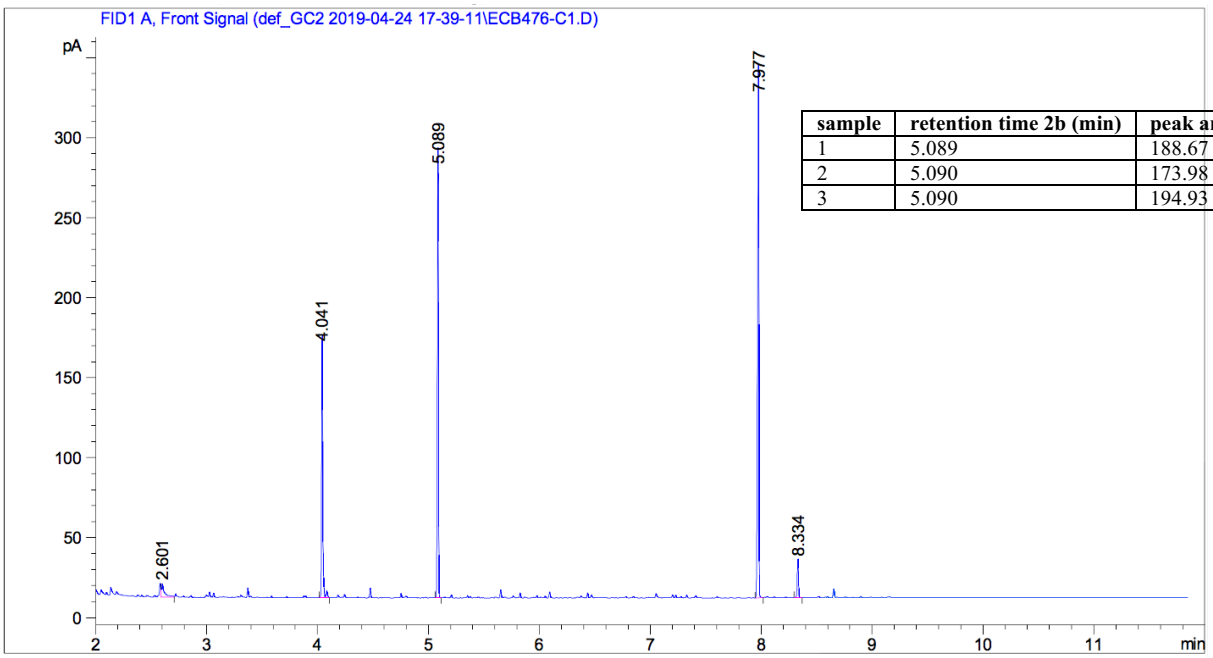

sample	retention time 2b (min)	peak area (pA*s)
1	5.089	188.67
2	5.090	173.98
3	5.090	194.93

Table 11, Entry 3, Method A

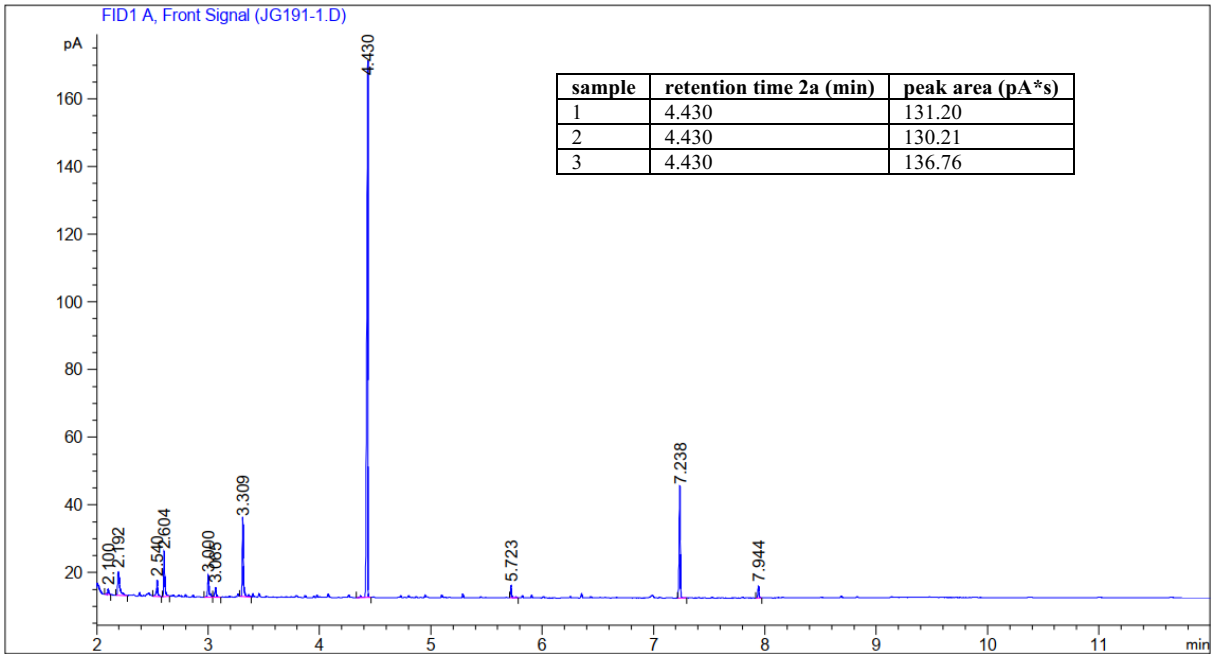

sample	retention time 2a (min)	peak area (pA*s)
1	4.430	131.20
2	4.430	130.21
3	4.430	136.76

Table 11, Entry 3, Method B

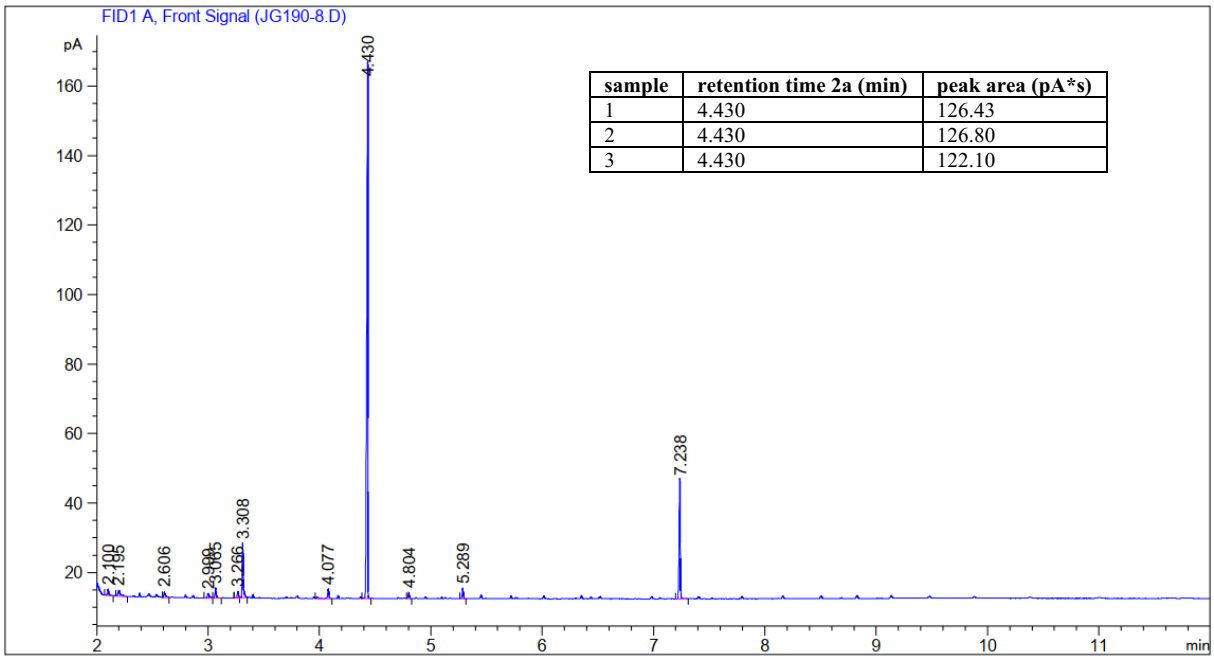

sample	retention time 2a (min)	peak area (pA*s)
1	4.430	126.43
2	4.430	126.80
3	4.430	122.10

Table 11, Entry 3, Method C

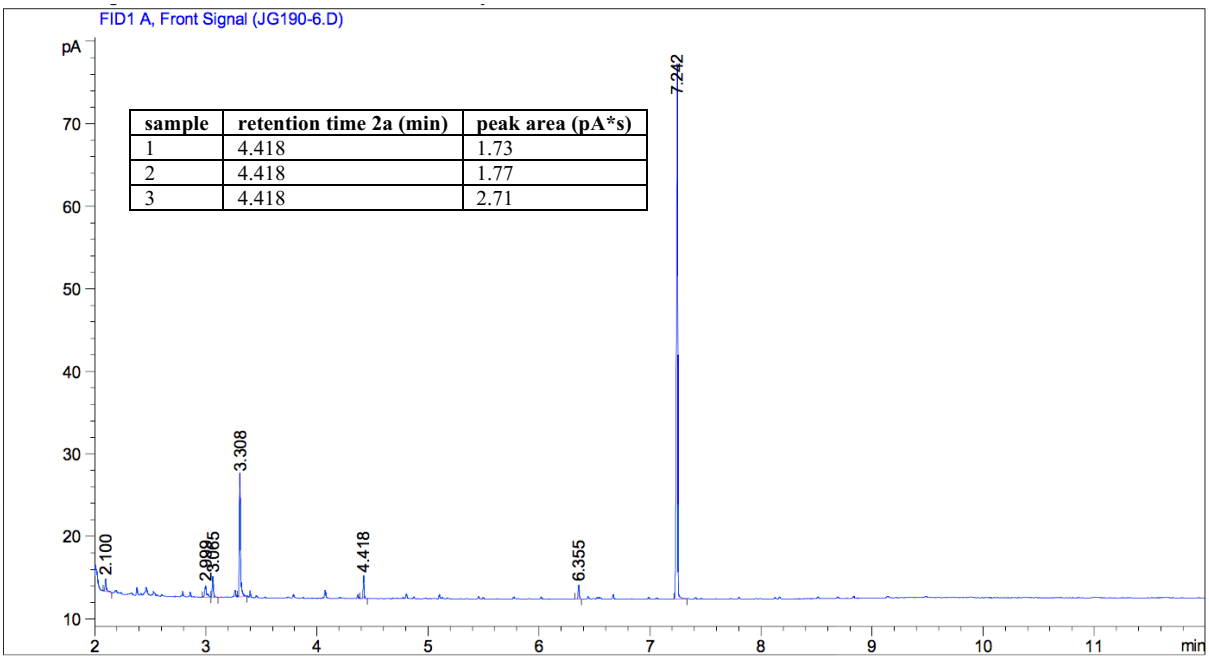

sample	retention time 2a (min)	peak area (pA*s)
1	4.418	1.73
2	4.418	1.77
3	4.418	2.71

Table 11, Entry 3, Method D

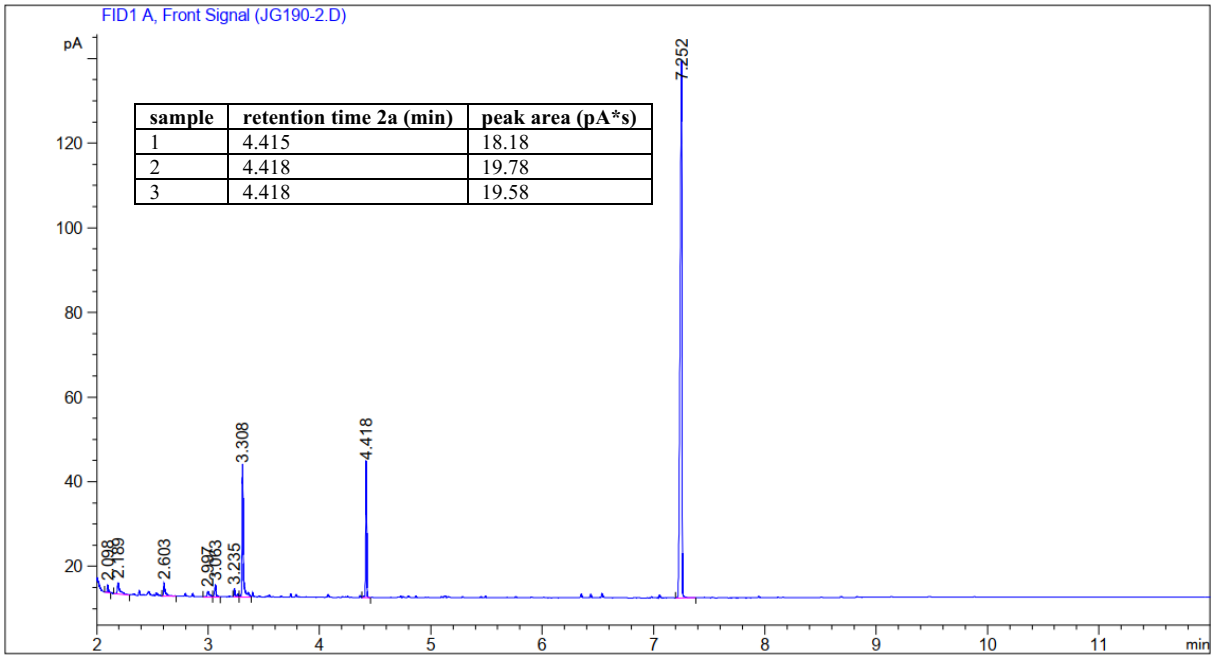

sample	retention time 2a (min)	peak area (pA*s)
1	4.415	18.18
2	4.418	19.78
3	4.418	19.58

Table 11, Entry 7, Method A

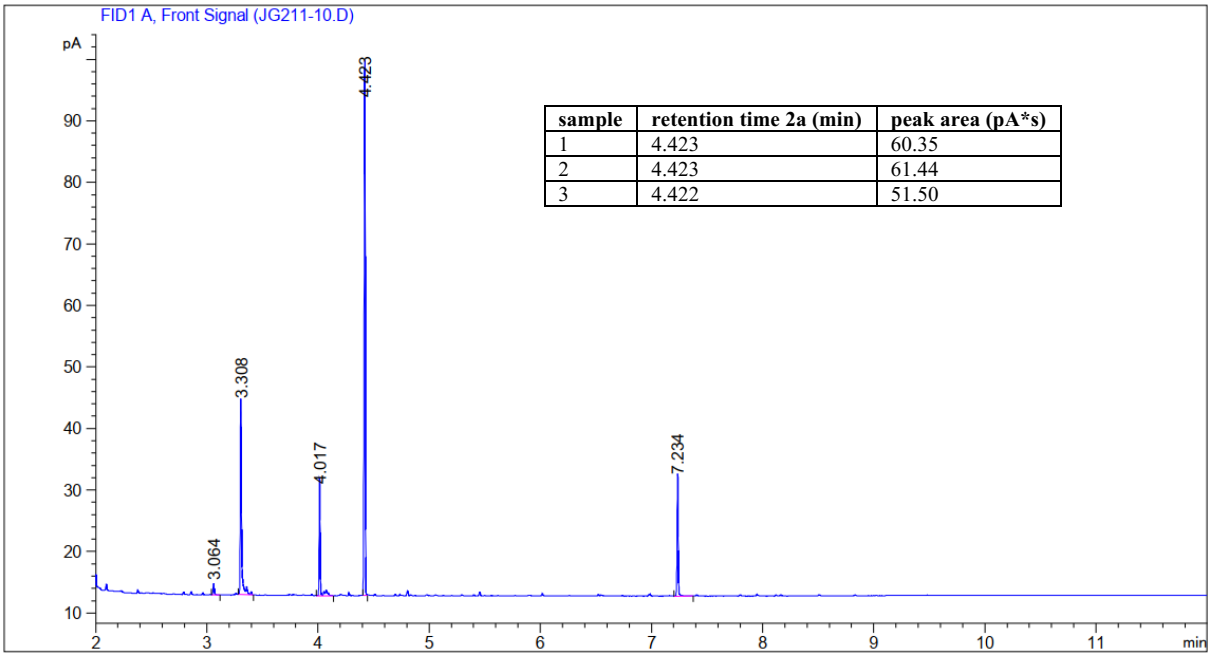

sample	retention time 2a (min)	peak area (pA*s)
1	4.423	60.35
2	4.423	61.44
3	4.422	51.50

Table 11, Entry 7, Method B

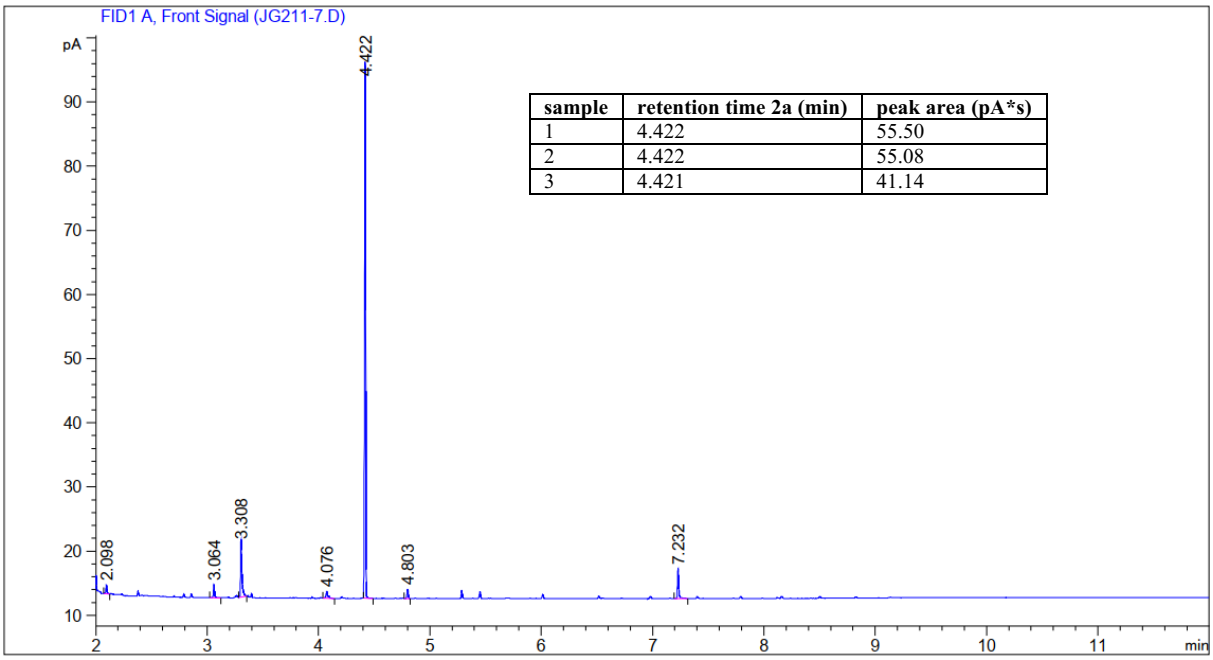

sample	retention time 2a (min)	peak area (pA*s)
1	4.422	55.50
2	4.422	55.08
3	4.421	41.14

Table 11, Entry 7, Method C

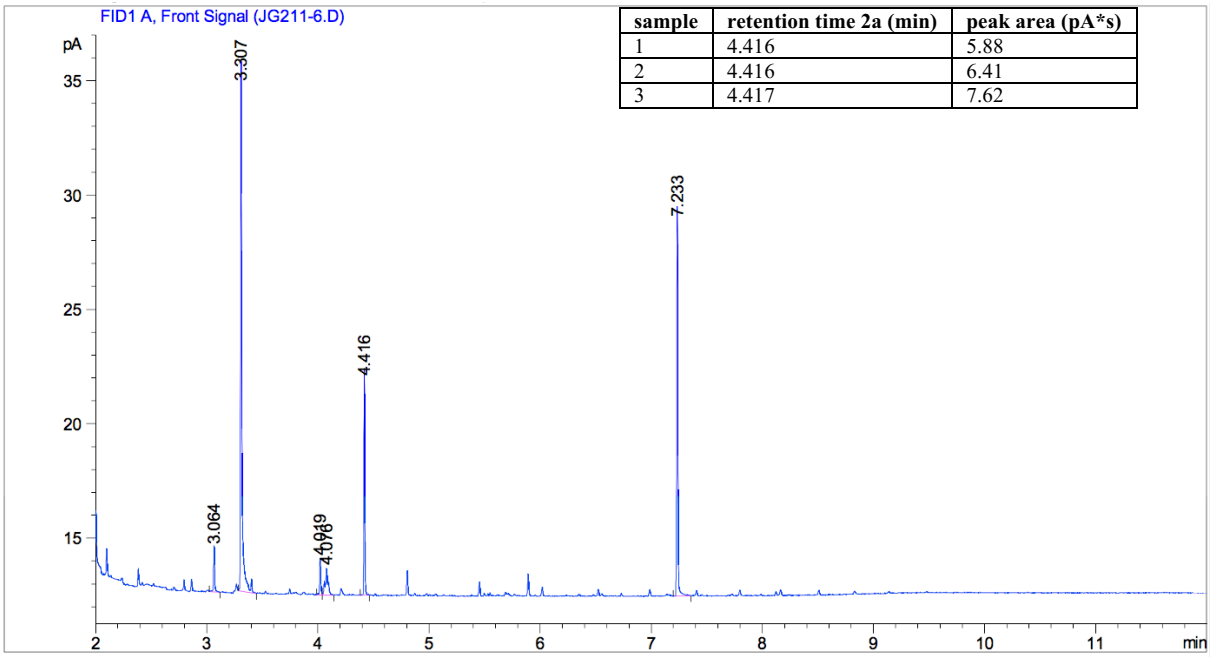

sample	retention time 2a (min)	peak area (pA*s)
1	4.416	5.88
2	4.416	6.41
3	4.417	7.62

Table 11, Entry 7, Method D

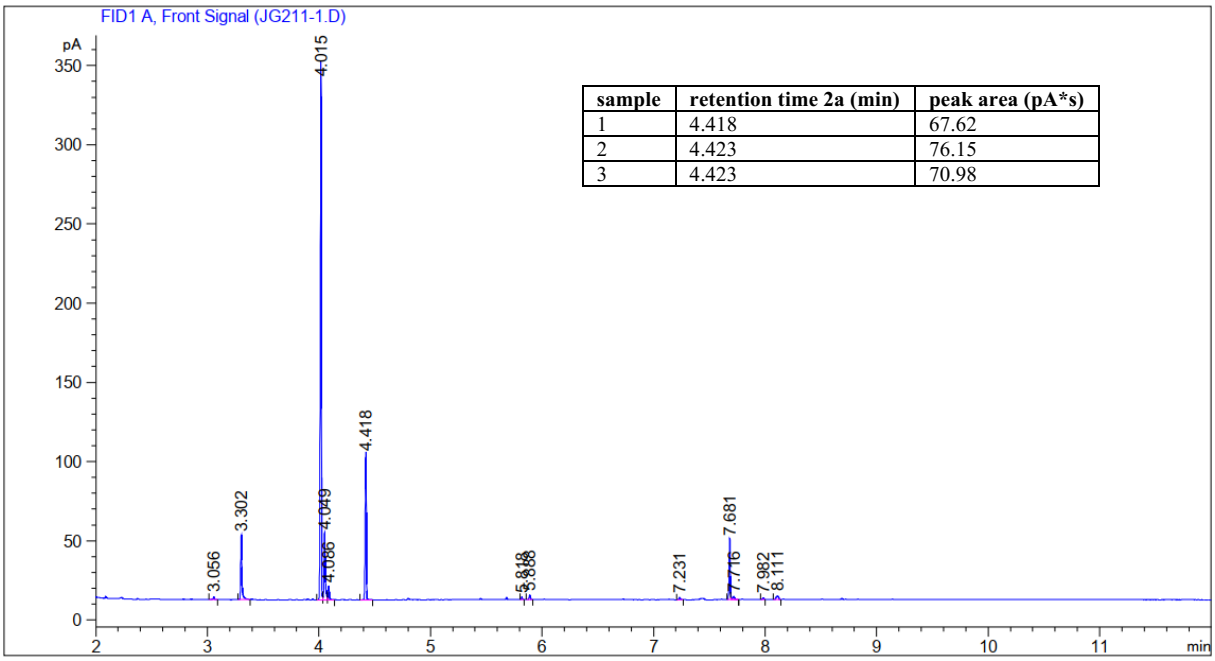

sample	retention time 2a (min)	peak area (pA*s)
1	4.418	67.62
2	4.423	76.15
3	4.423	70.98

Table 11, Entry 8, Method A

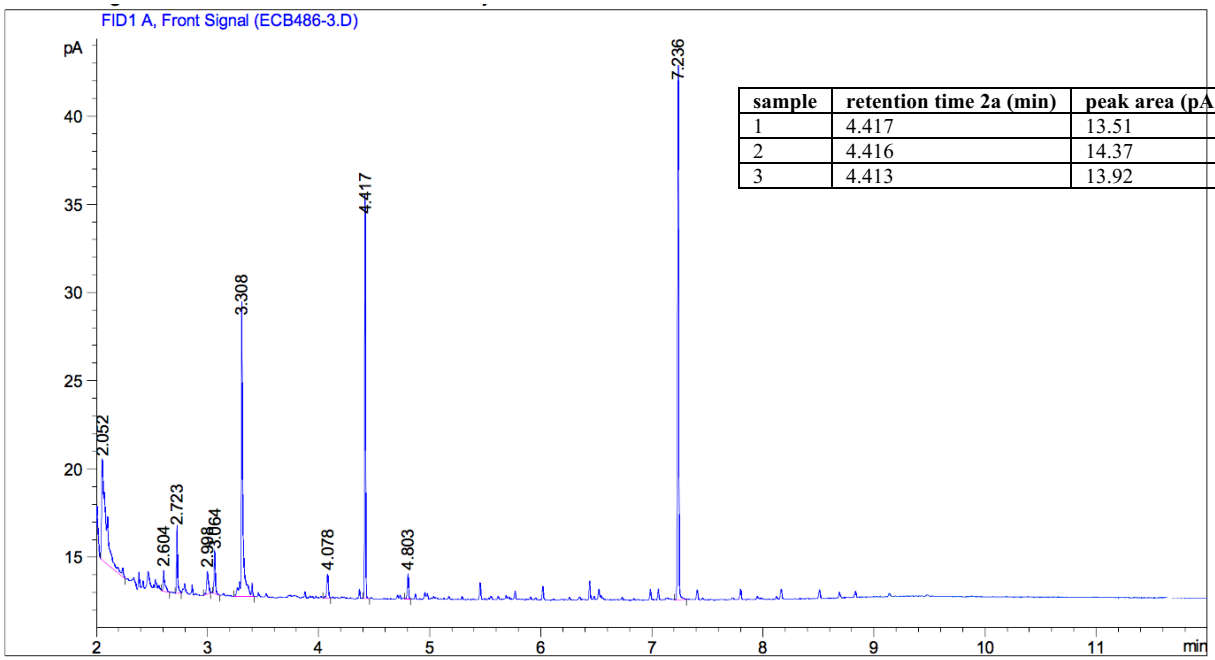

sample	retention time 2a (min)	peak area (pA*s)
1	4.417	13.51
2	4.416	14.37
3	4.413	13.92

Table 11, Entry 8, Method B

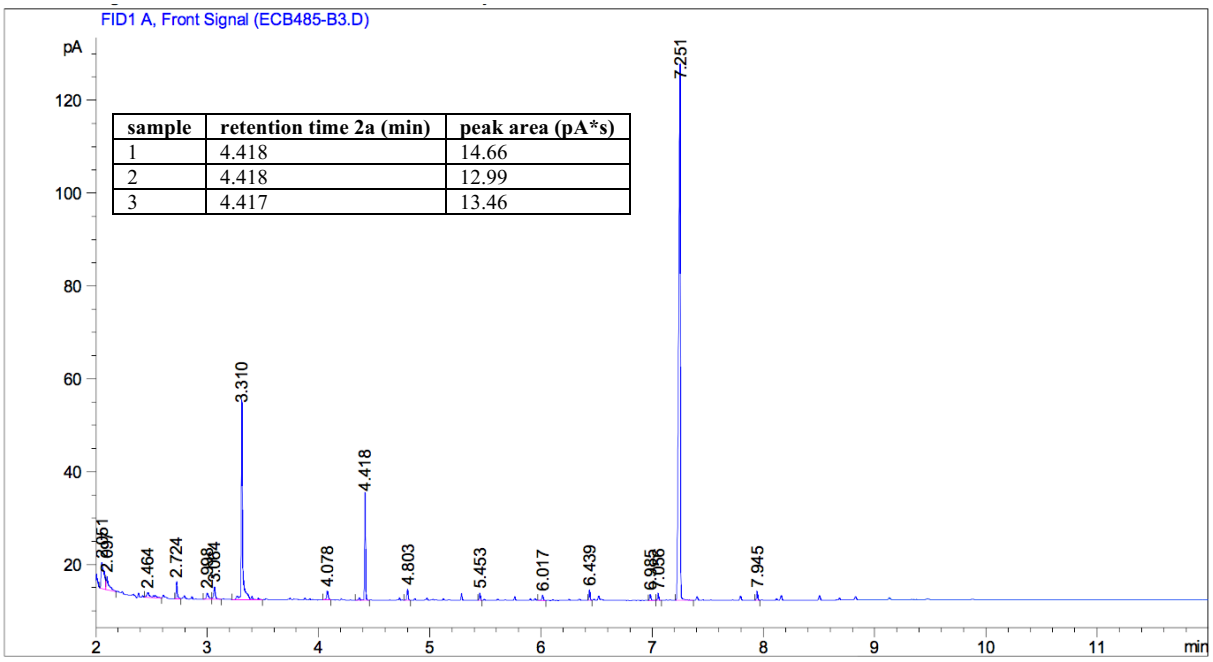

sample	retention time 2a (min)	peak area (pA*s)
1	4.418	14.66
2	4.418	12.99
3	4.417	13.46

Table 11, Entry 8, Method C

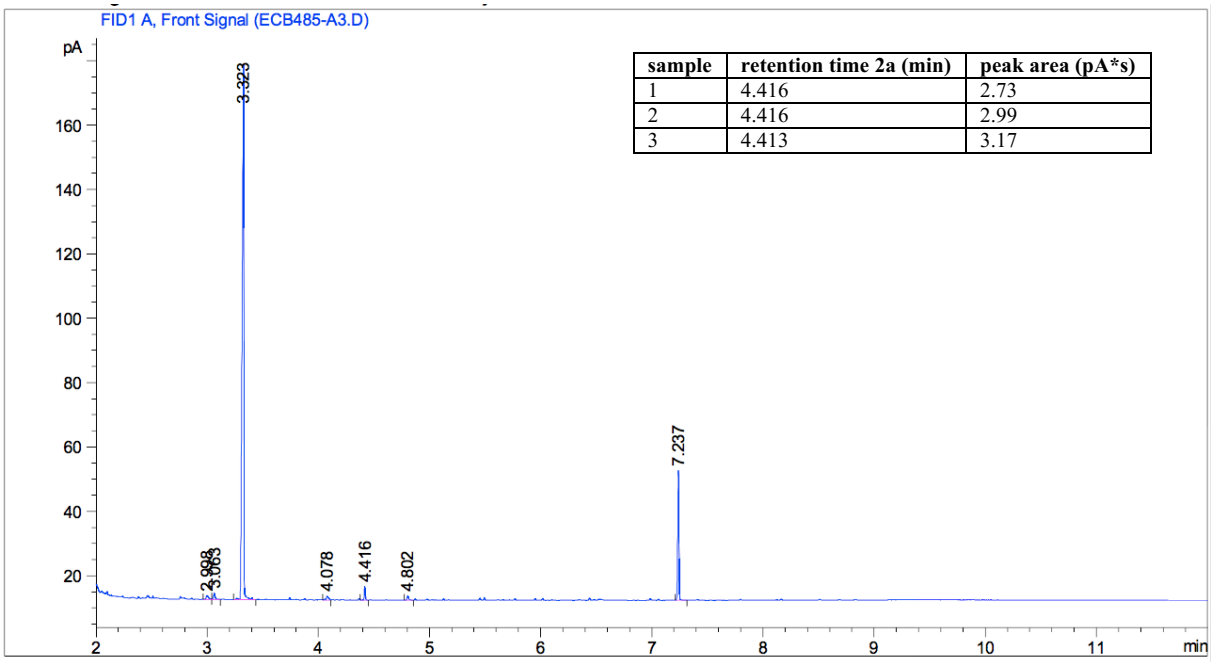

sample	retention time 2a (min)	peak area (pA*s)
1	4.416	2.73
2	4.416	2.99
3	4.413	3.17

3.5.3.2. LC-MS chromatograms of thioester under various conditions

Table 11, Entry 4, Method A (**8a**)

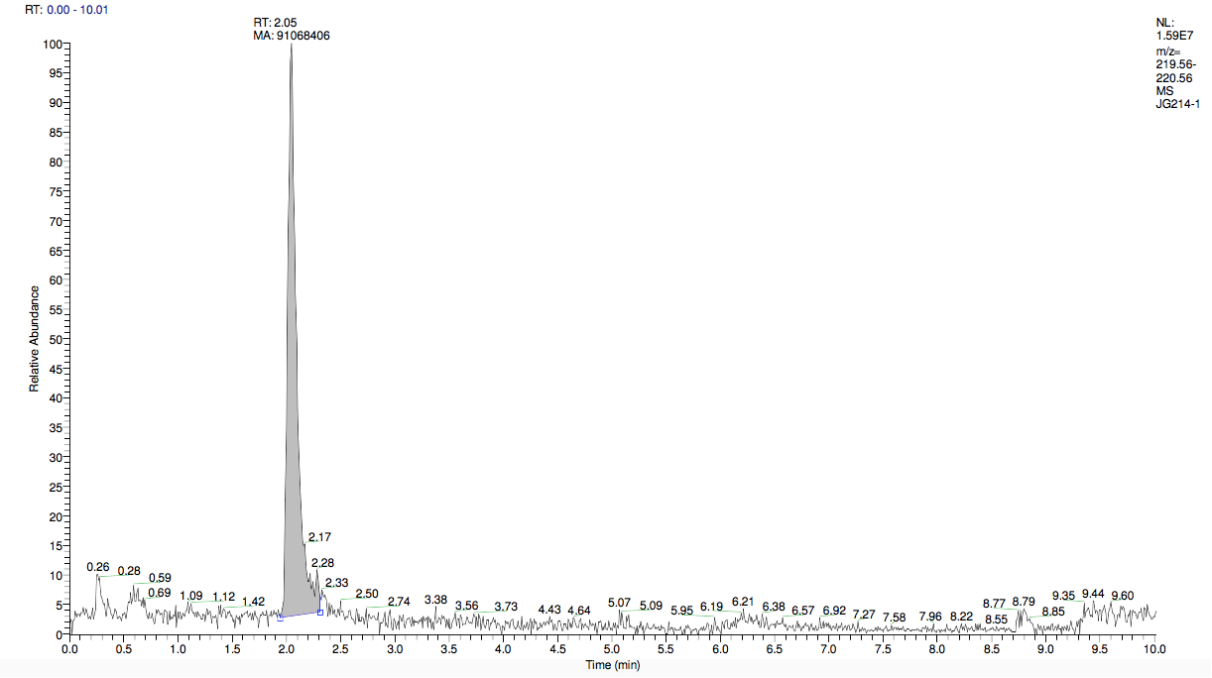

Table 11, Entry 4, Method B (**8a**)

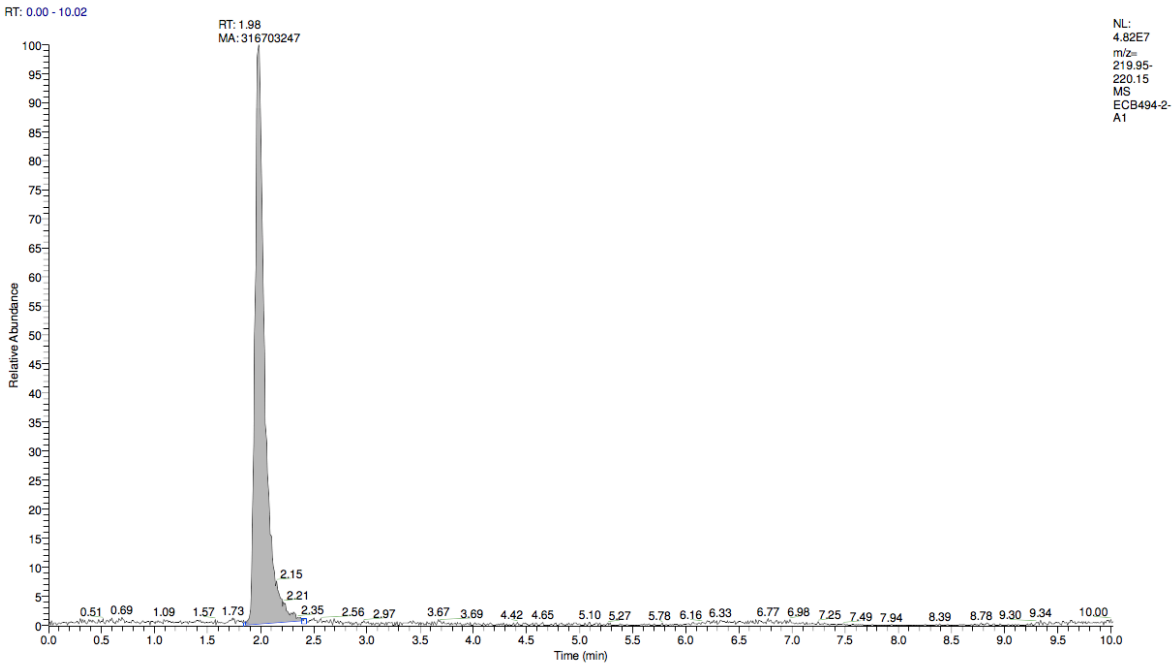

Table 11, Entry 4, Method D (**8a**)

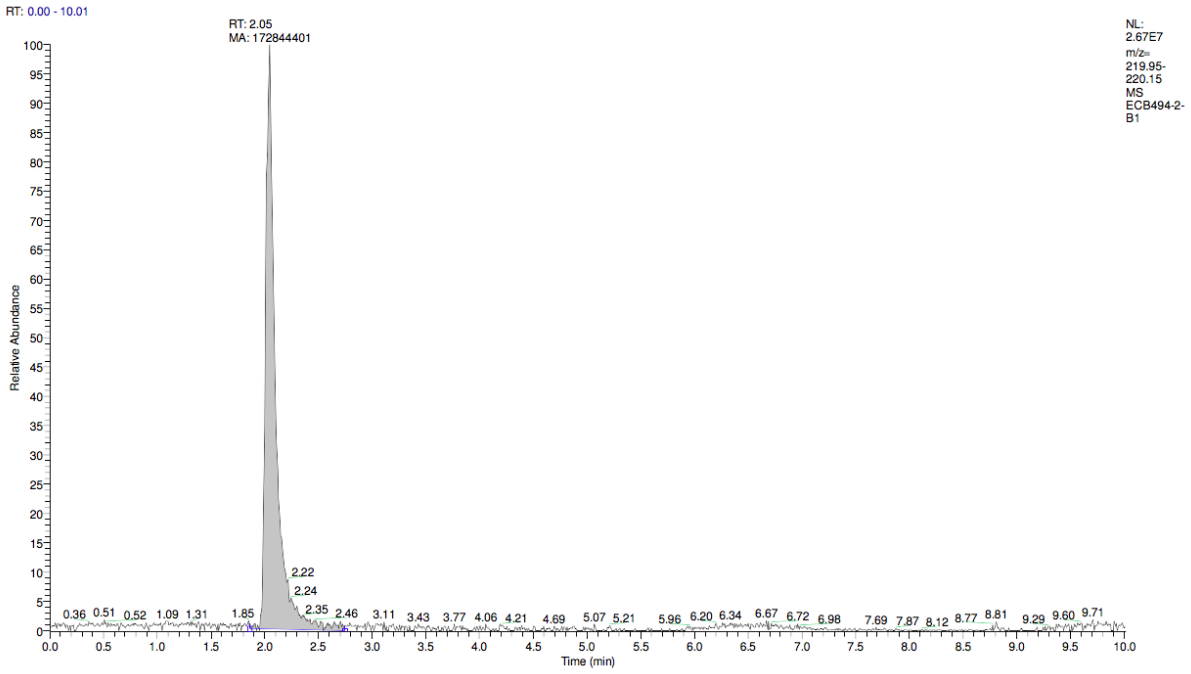

Table 11, Entry 4', Method A (19a)

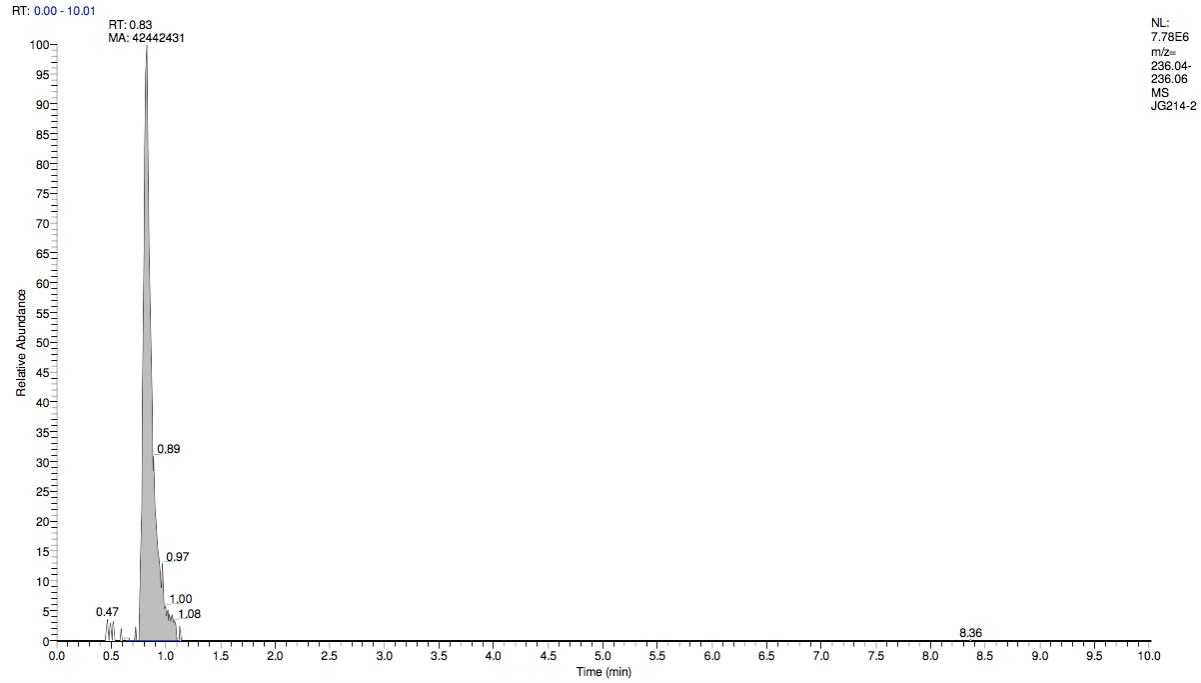

Table 11, Entry 4', Method B (**19a**)

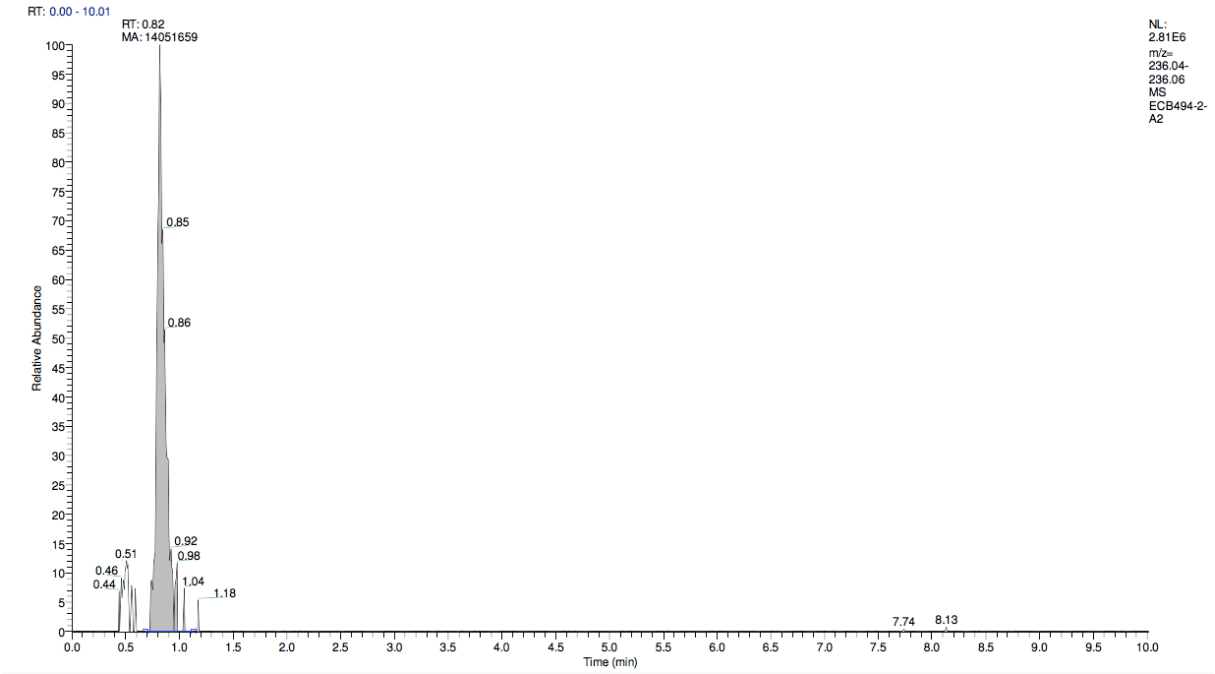

Table 11, Entry 5, Method A (**3a**)

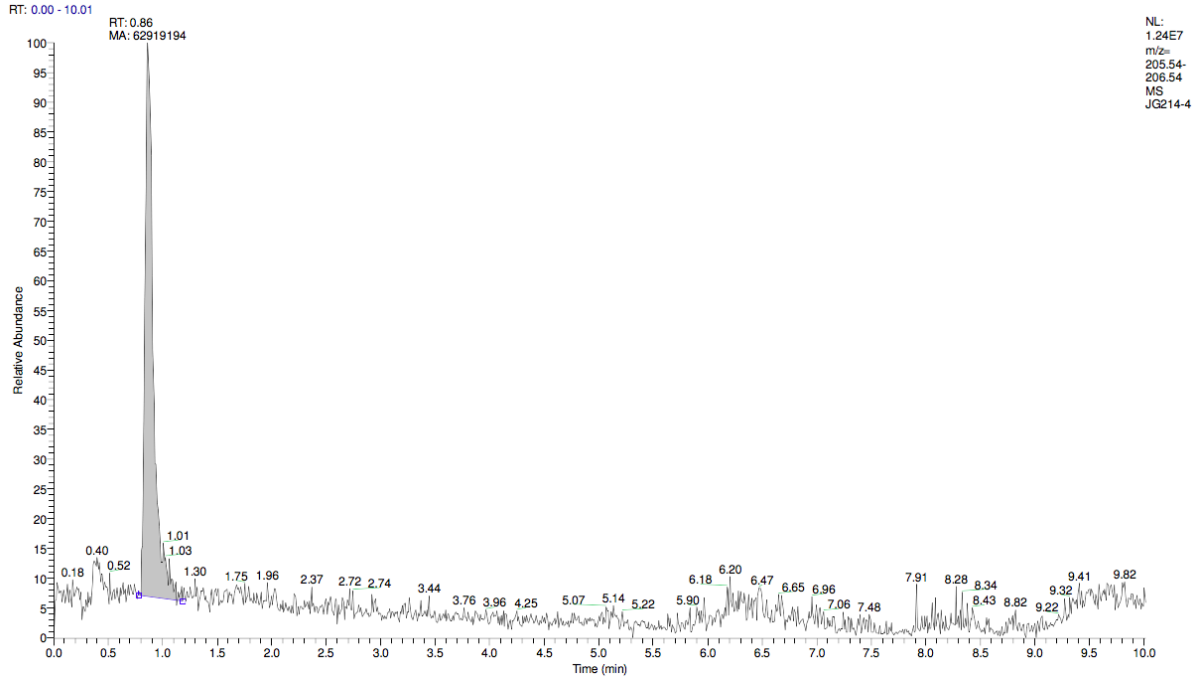

Table 11, Entry 5, Method B (**3a**)

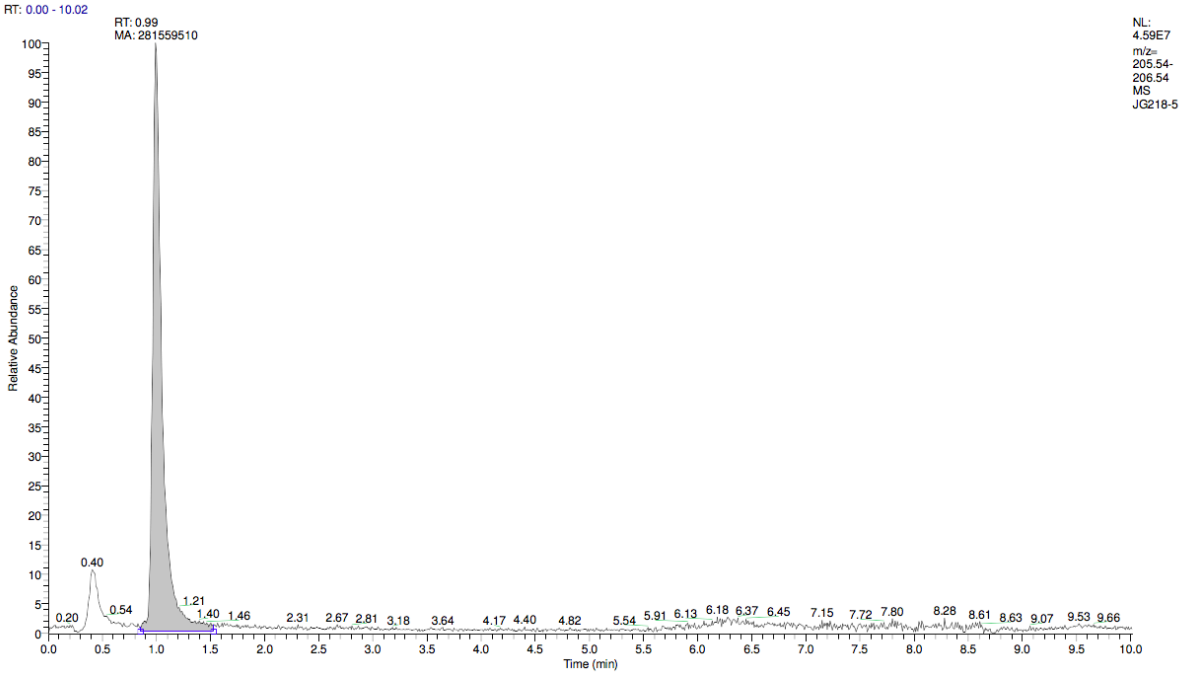

Table 11, Entry 5, Method D (**3a**)

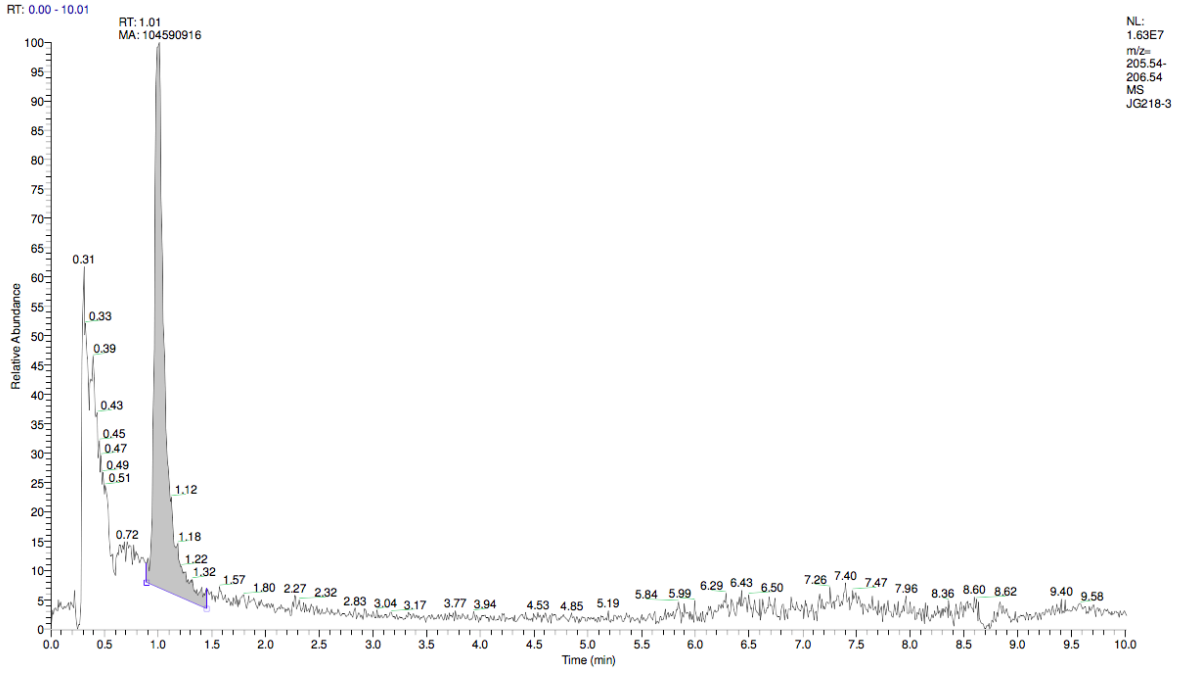

Table 11, Entry 5′, Method A (**2a**)

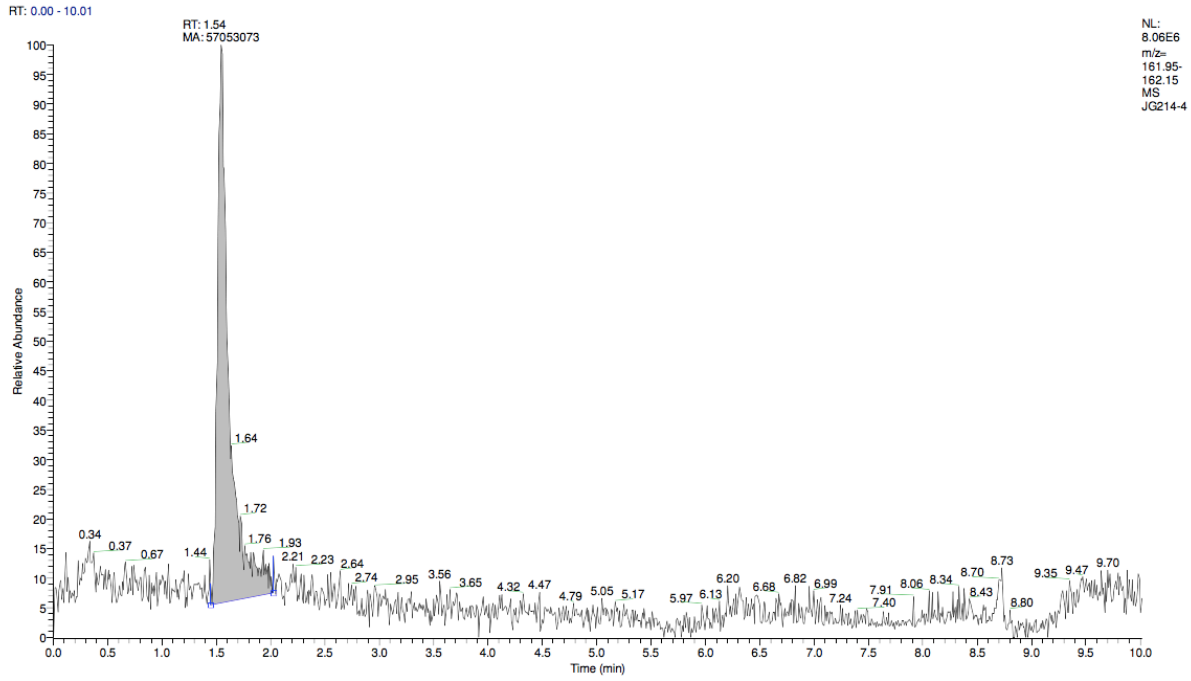

Table 11, Entry 5′, Method B (**2a**)

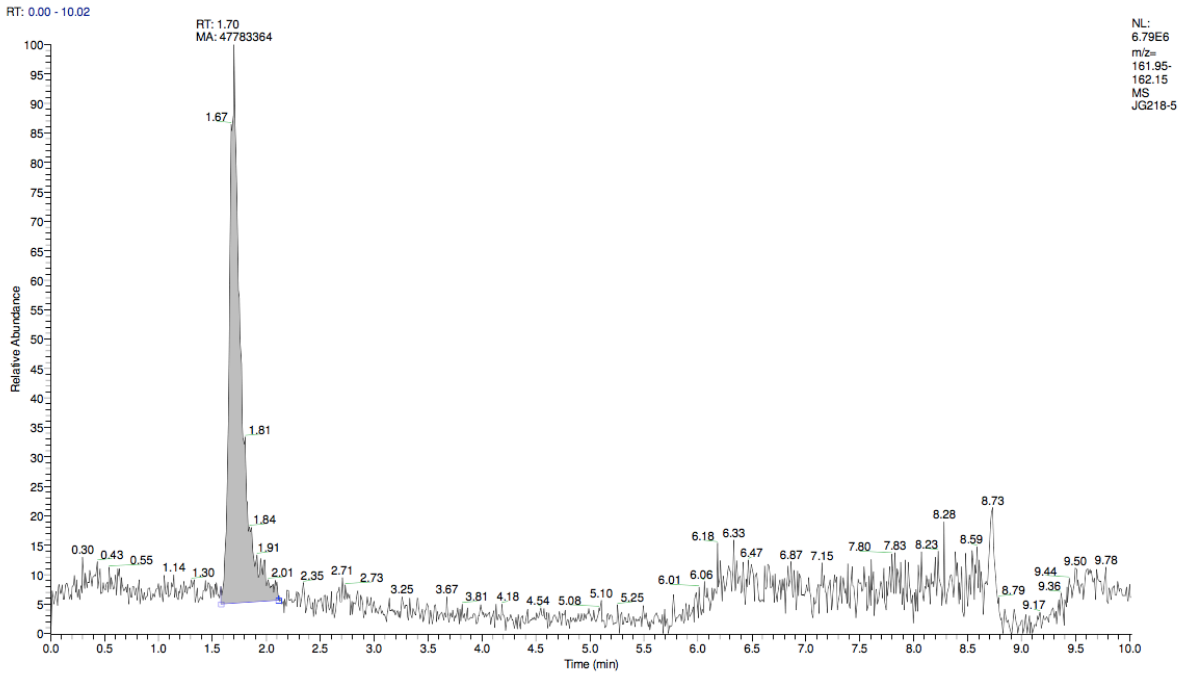

Table 11, Entry 6, Method A (**19a**)

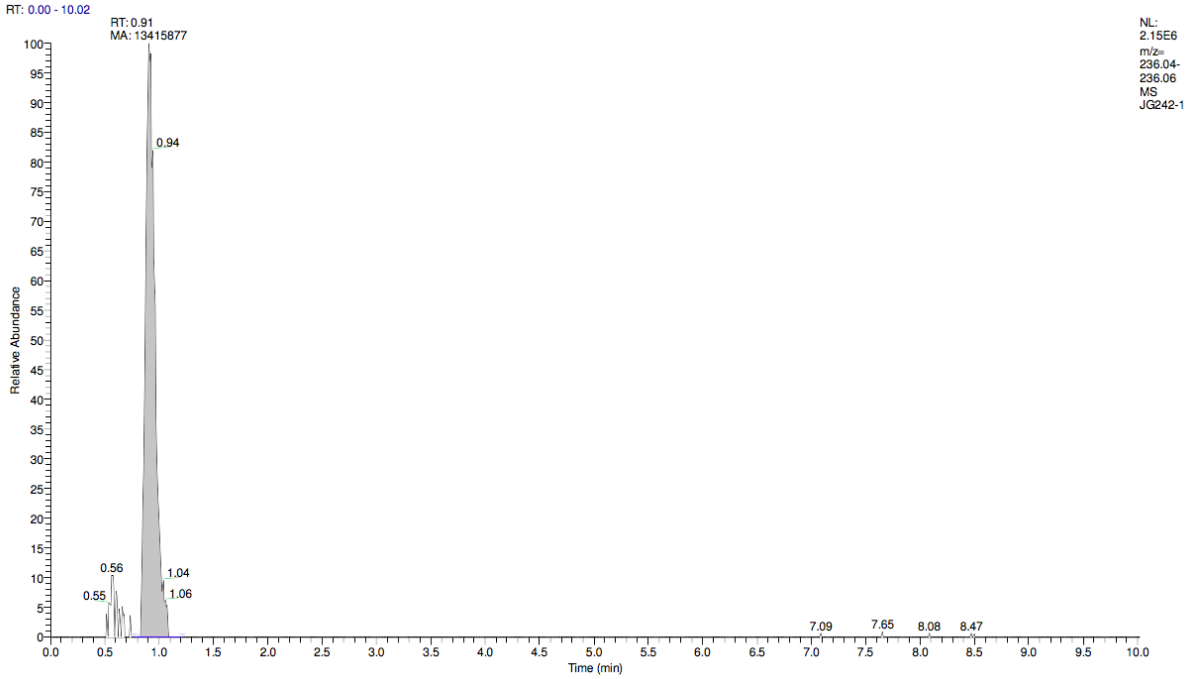

Table 11, Entry 6, Method B (**19a**)

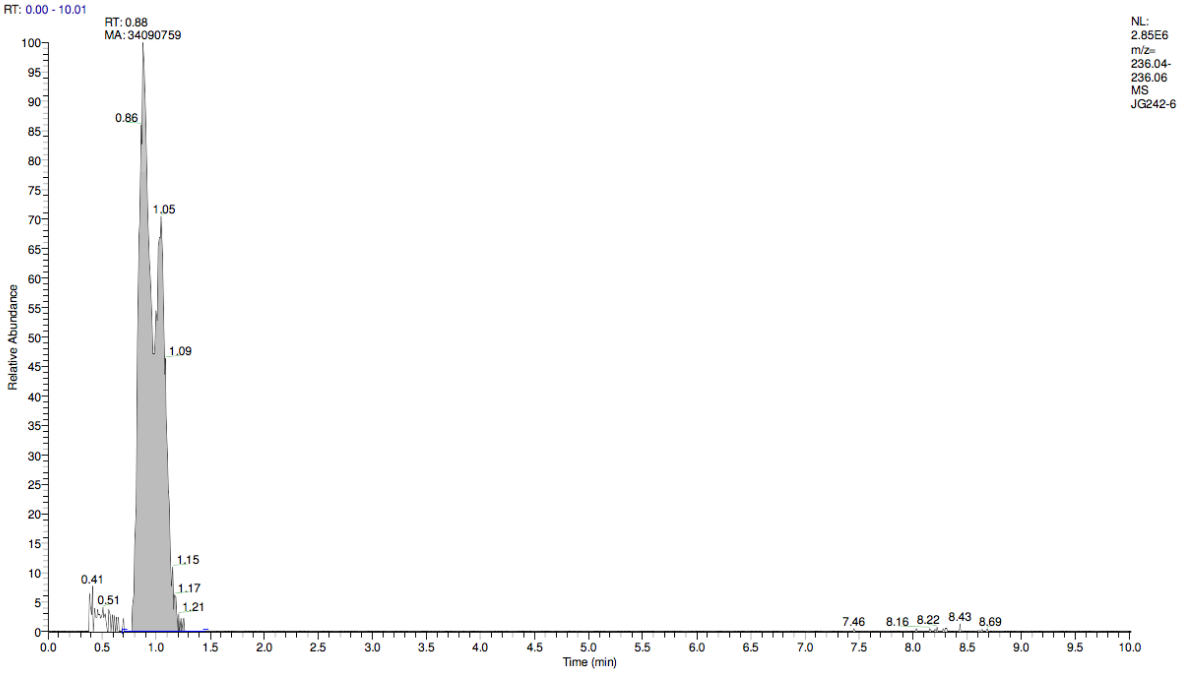

Table 11, Entry 6, Method D (**19a**)

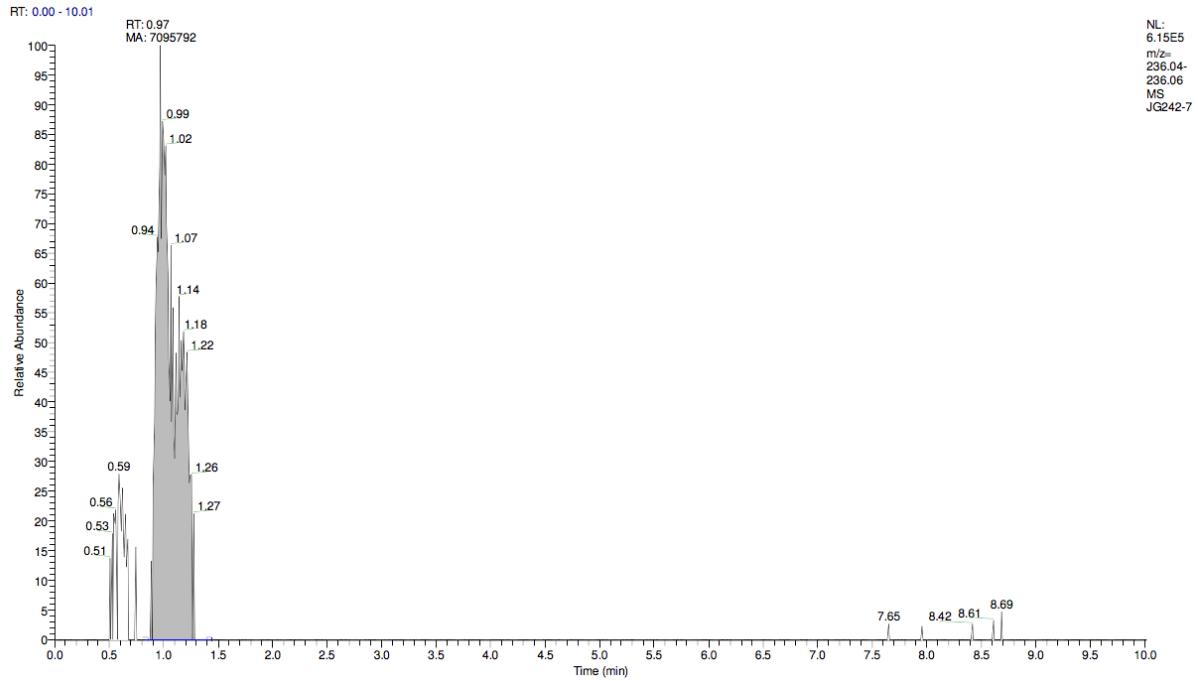

3.5.3.1. NMR spectra of thioester under various conditions

Table 11, Entry 1, Method A

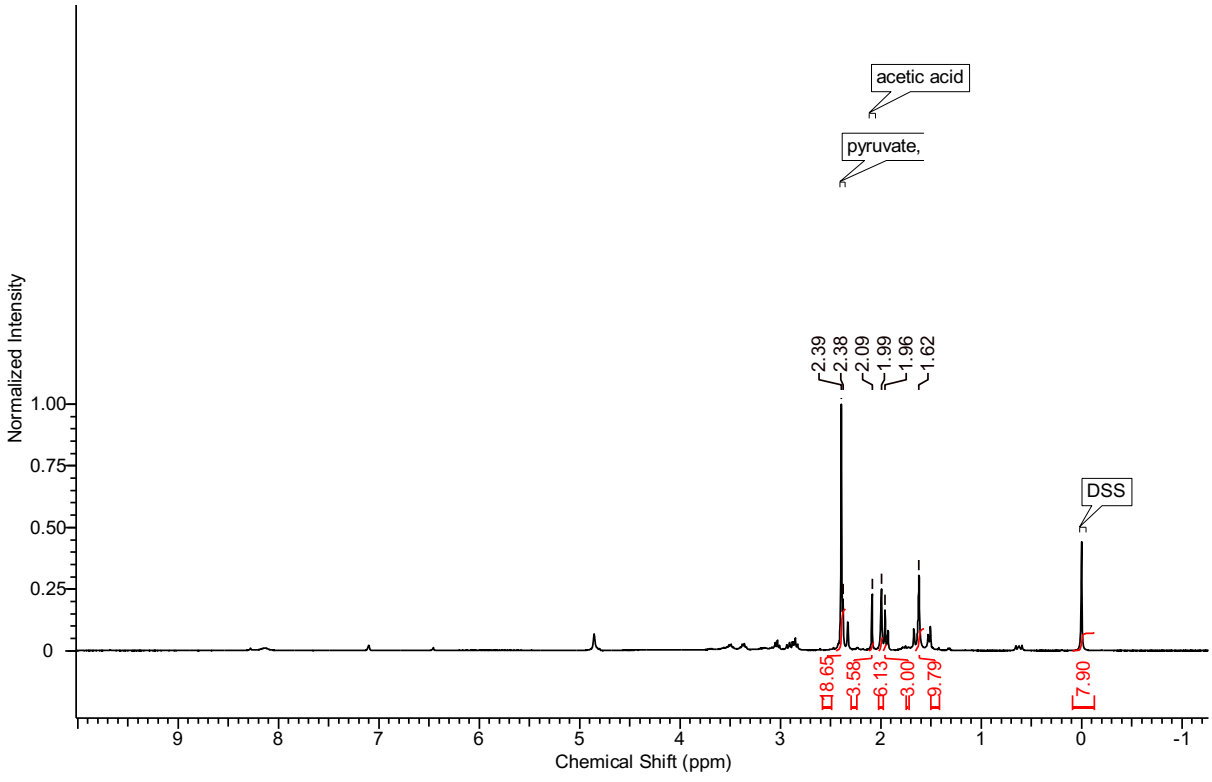

Table 11, Entry 1, Method B

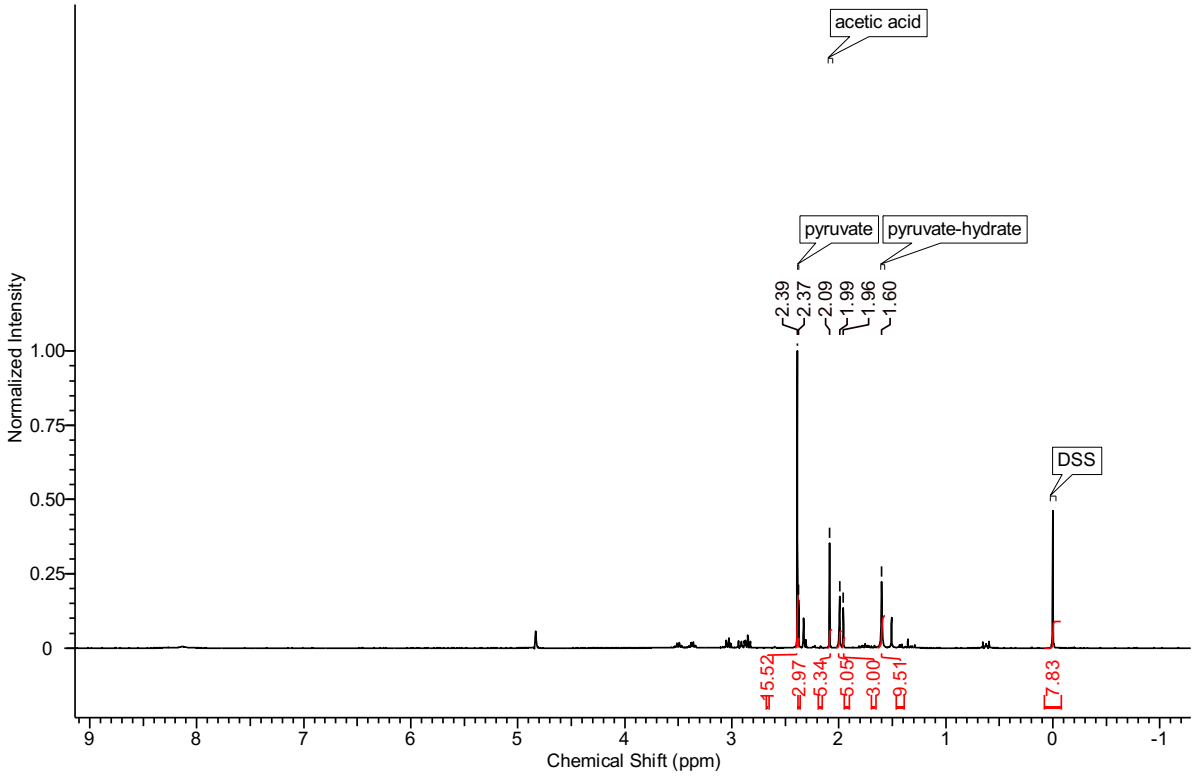

Table 11, Entry 1, Method C

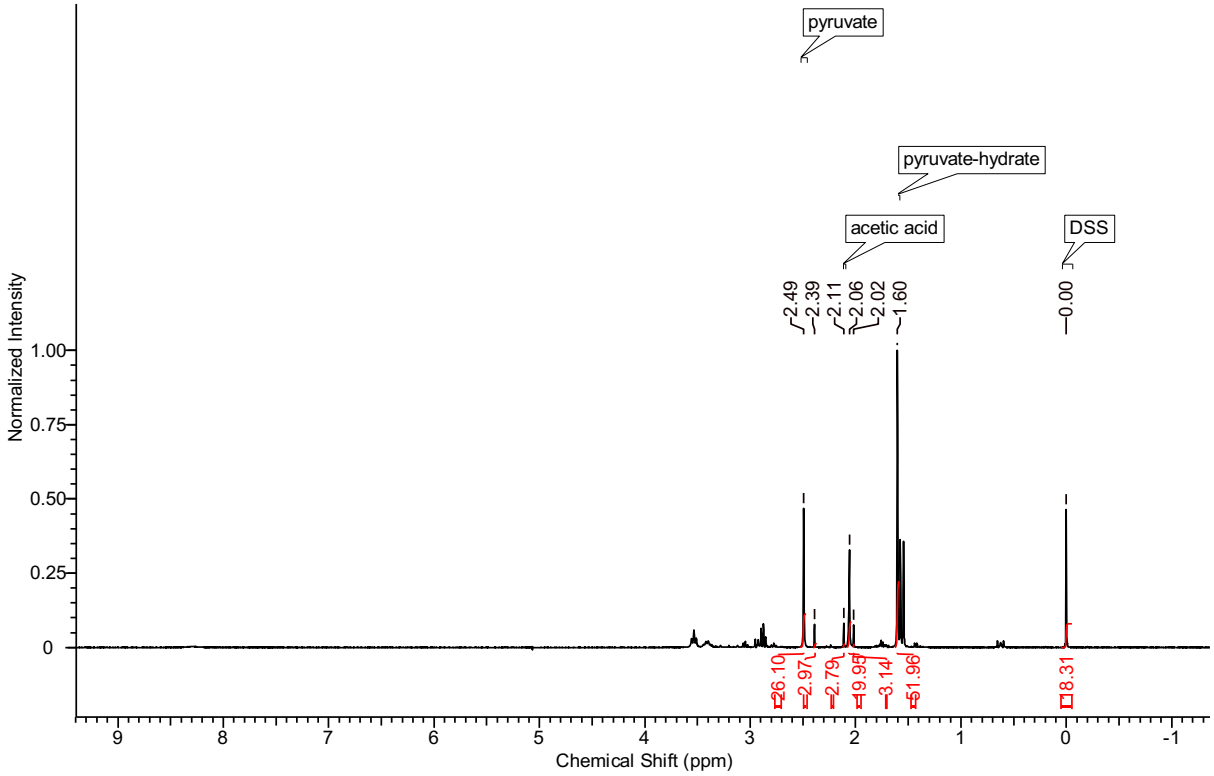

Table 11, Entry 3, Method A

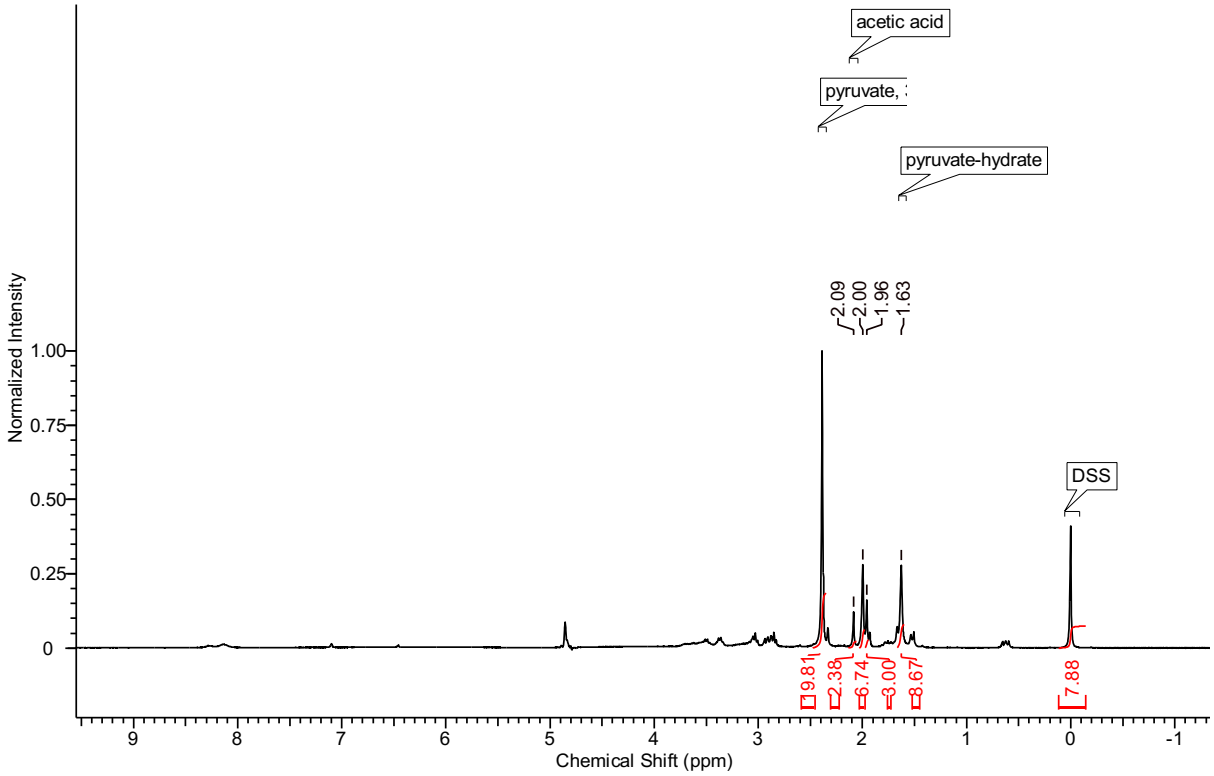

Table 11, Entry 3, Method B

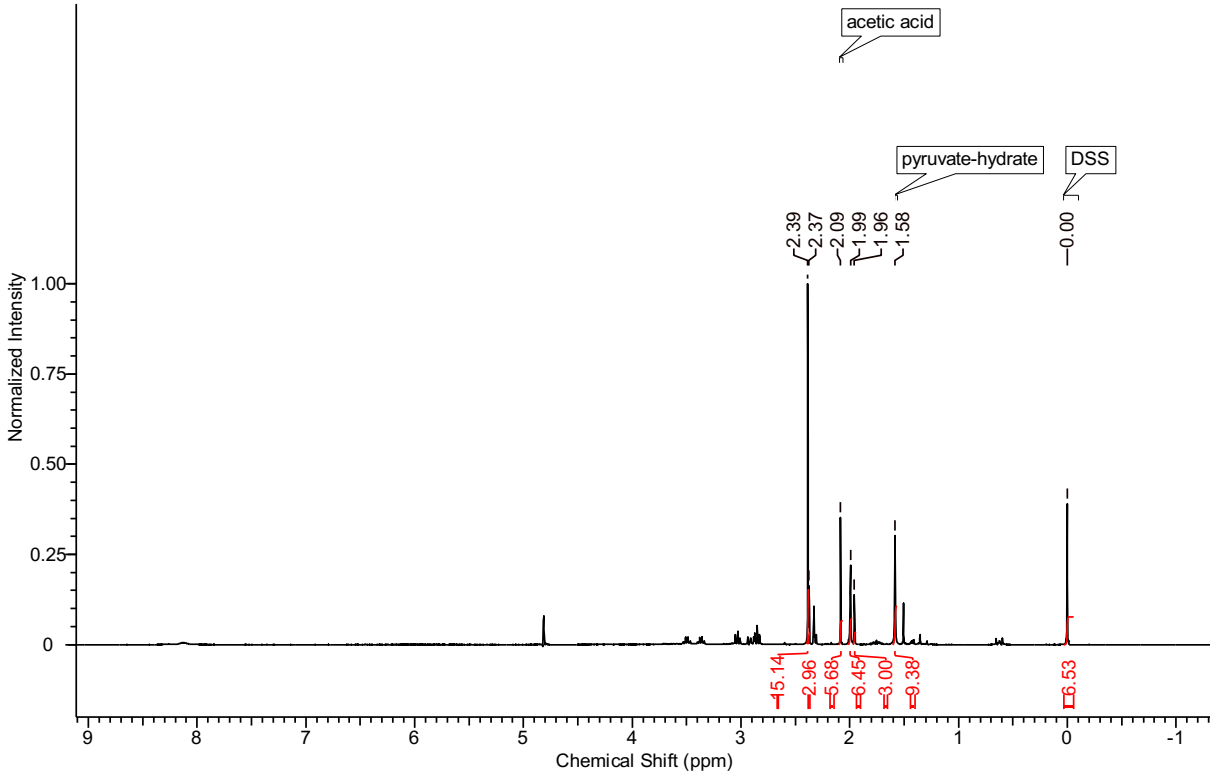

Table 11, Entry 3, Method C

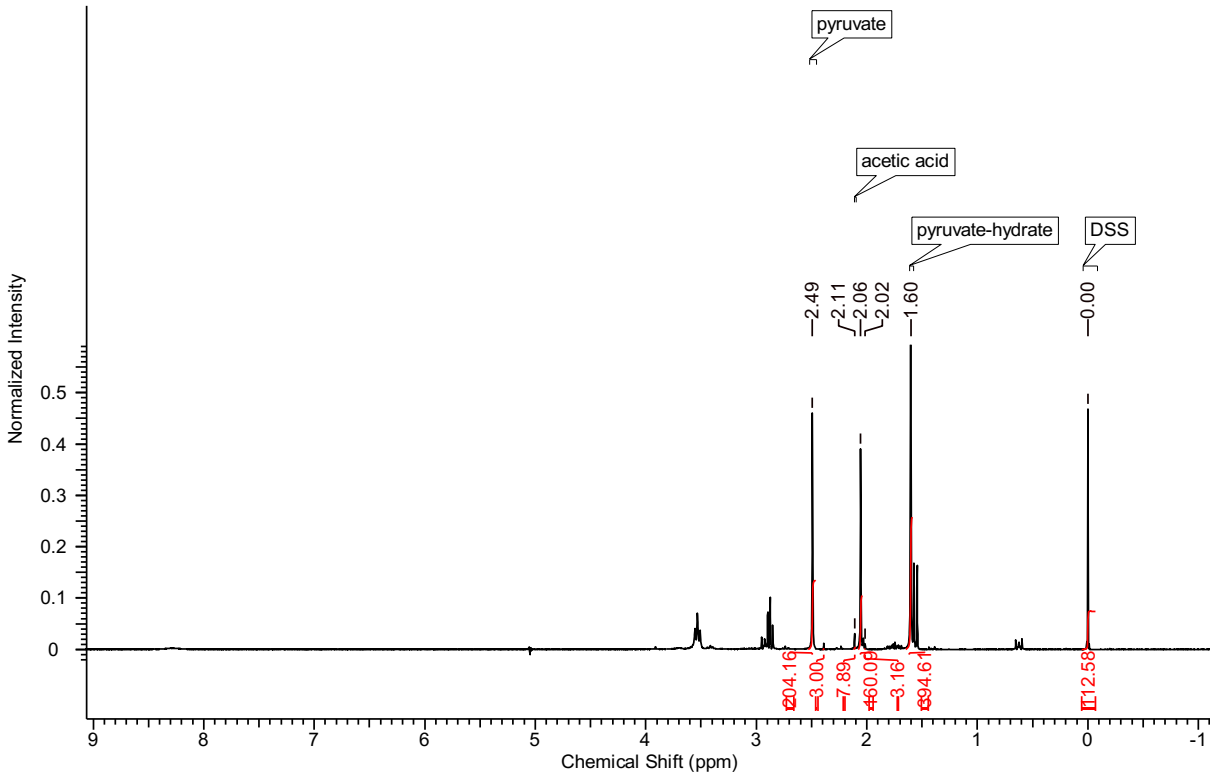
pyruvate
acetic acid
pyruvate-hydrate
DSS
2.49
2.11
2.06
2.02
1.60
0.00
Normalized Intensity
0.5
0.4
0.3
0.2
0.1
0
9
8
7
6
5
4
3
2
1
0
-1
Chemical Shift (ppm)

3.5.4. Thioester formation from a non-enzymatic reaction network

Table 12. Thioester formation from a non-enzymatic reaction network

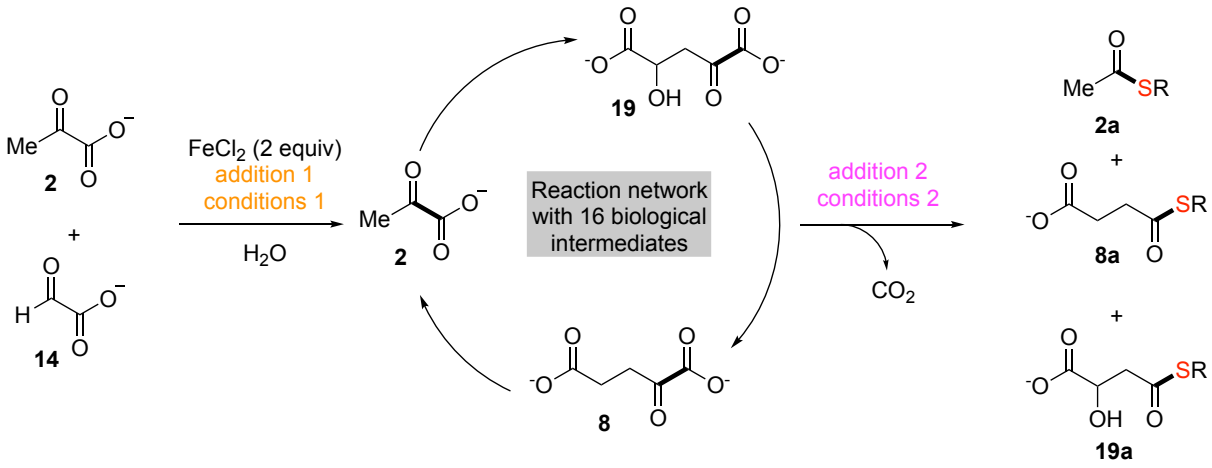

Entry	Pyruvate **2** equiv	addition 1 (equiv)	conditions 1	addition 2 (equiv)	conditions 2	Concentration (mM) Acetyl thioester **2a**[a]	Succinyl thioester **8a**[b]	Malyl thioester **19a**[b]
1	2		70 °C, 1 h	Thiol **18a** (1) $KHSO_4$ (3 M)	UVA, 3 h	0.11 ± 0.01	0.19 ± 0.04	0.06 ± 0.00
2	2	Thiol **18a** (1)	70 °C, 1 h	$K_2S_2O_8$ (2)	70 °C, 3 h	1.41 ± 0.11	0.11 ± 0.01	3.60 ± 0.30
3	2	Thiol **18a** (1)	70 °C, 3 h	$K_2S_2O_8$ (2)	70 °C, 3 h	1.11 ± 0.14	0.11 ± 0.02	3.63 ± 0.28
4	1	Thiol **18a** (1) $KHSO_4$ (3 M)	UVA, 3 h	-	-	0.06 ± 0.05	-	-
5	2	Thiol **18a** (1) $KHSO_4$ (3 M)	UVA, 6 h	-	-	0.16 ± 0.02	-	-
6	1	Thiol **2a** (1) $KHSO_4$ (3 M)	UVA, 3 h	-	-	0.11 ± 0.05	-	-
7	2	Thiol **18a** (1) $KHSO_4$ (3 M)	UVA, 6 h	-	-	0.31 ± 0.05	-	-
8	2	Thiol **18a** (1)	UVA, 1 h	$KHSO_4$ (3M)	UVA, 3 h	0.22 ± 0.02		
9	2	Thiol **18a** (1)	70 °C, 1 h	$KHSO_4$ (3M)	UVA, 3 h	0.12 ± 0.01	-	-
10	2	Thiol **18a** (1)	70 °C, 1 h	$KHSO_4$ (3M)	UVA, 6 h	0.15 ± 0.01	-	-

[a]Determined by GC-Fid analysis after extraction with ethyl acetate [b]Determined by LC-MS analysis. For the network experiments 0.5µL instead of 0.1µL were injected, the resulting value calculated using the calibration curves was divided by 5 afterwards. See section 3.5.4.3 for GC-MS chromatograms of the network products.

3.5.4.1. GC-Fid chromatograms of thioester from network

Table 12, Entry 1

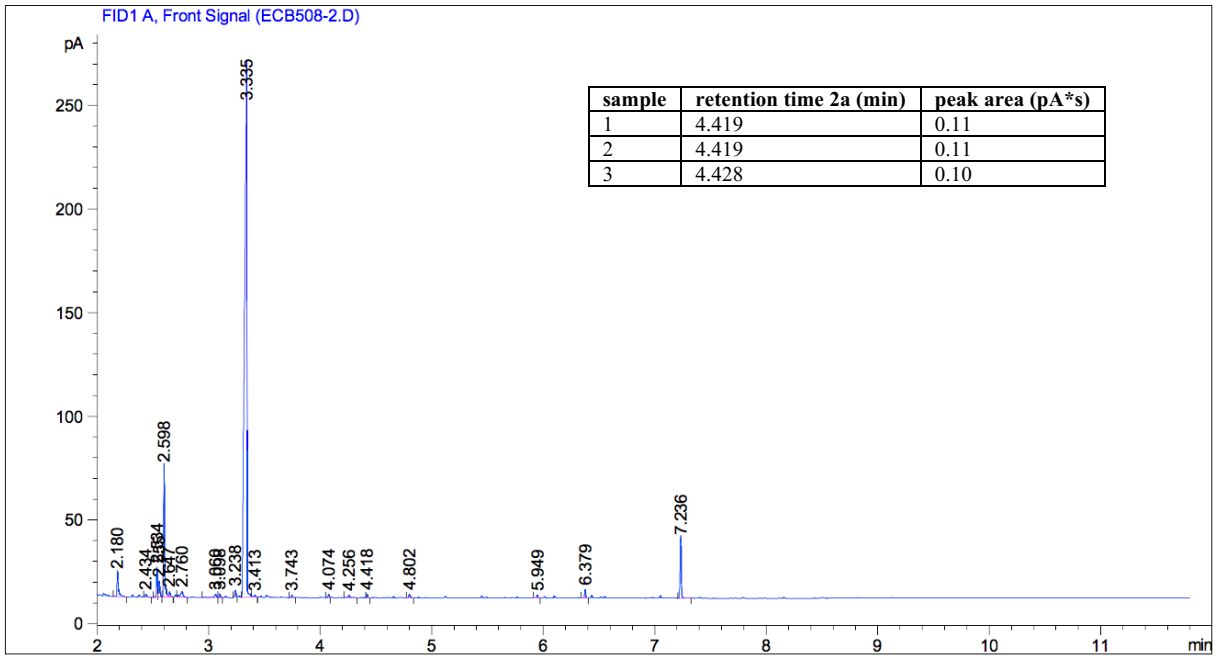

sample	retention time 2a (min)	peak area (pA*s)
1	4.419	0.11
2	4.419	0.11
3	4.428	0.10

Table 12, Entry 2

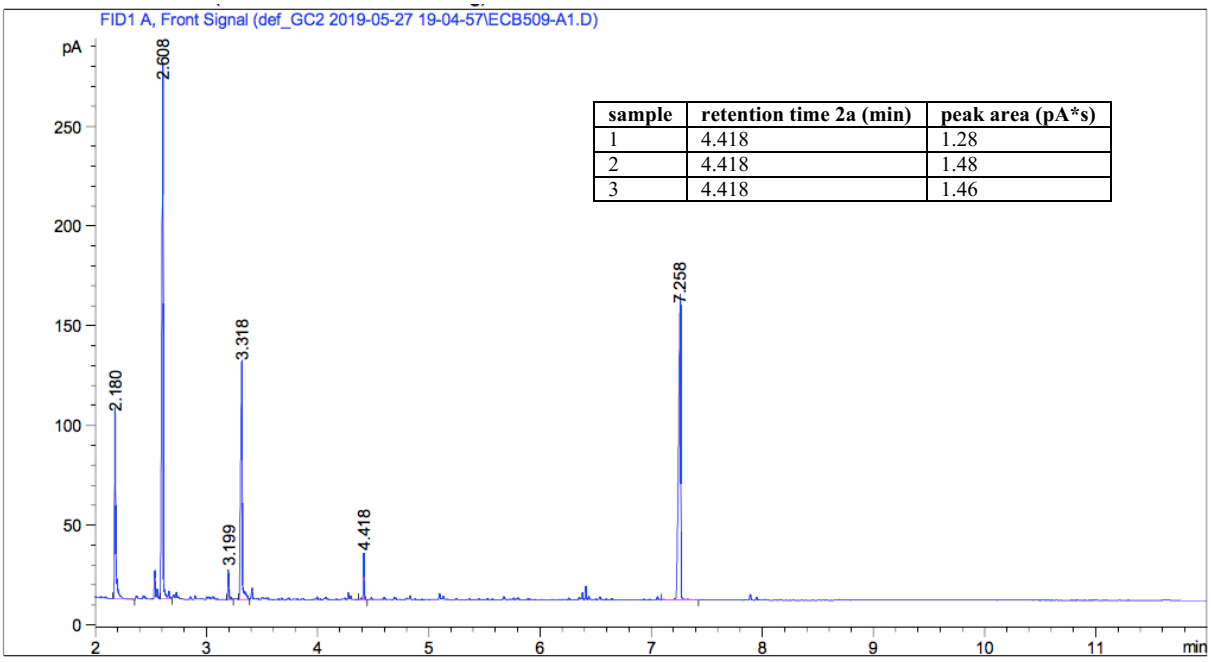

sample	retention time 2a (min)	peak area (pA*s)
1	4.418	1.28
2	4.418	1.48
3	4.418	1.46

Table 12, Entry 3

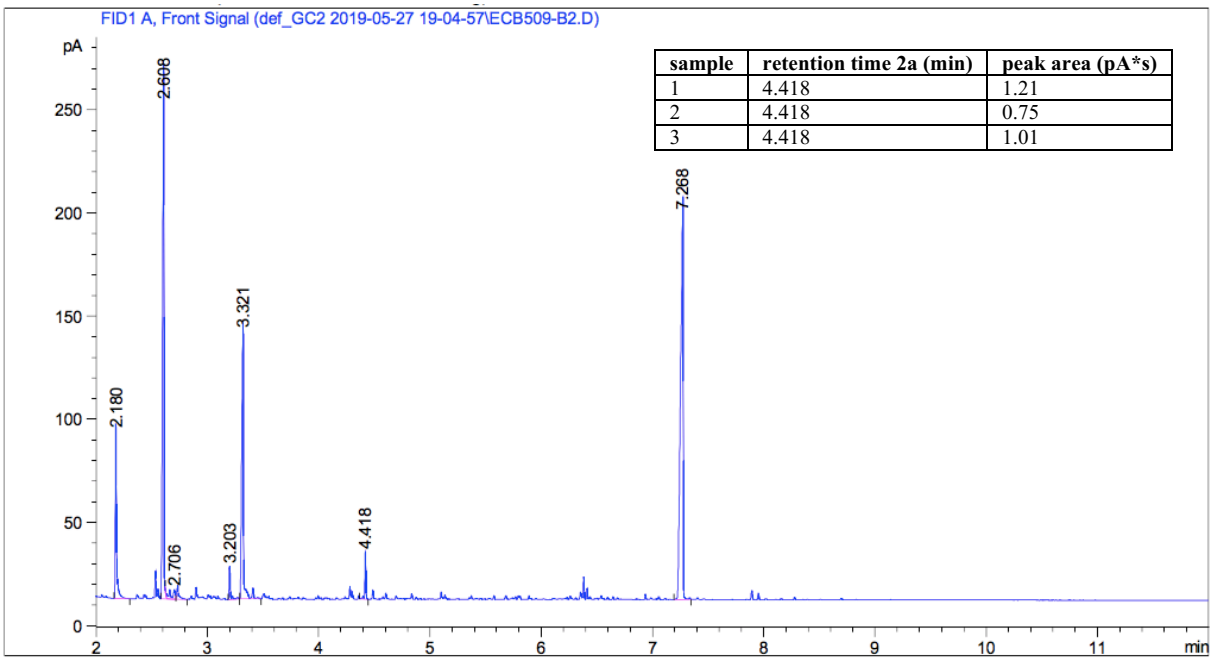

sample	retention time 2a (min)	peak area (pA*s)
1	4.418	1.21
2	4.418	0.75
3	4.418	1.01

3.5.4.2. LC-MS chromatograms of thioester from network

Table 12, Entry 1

8a

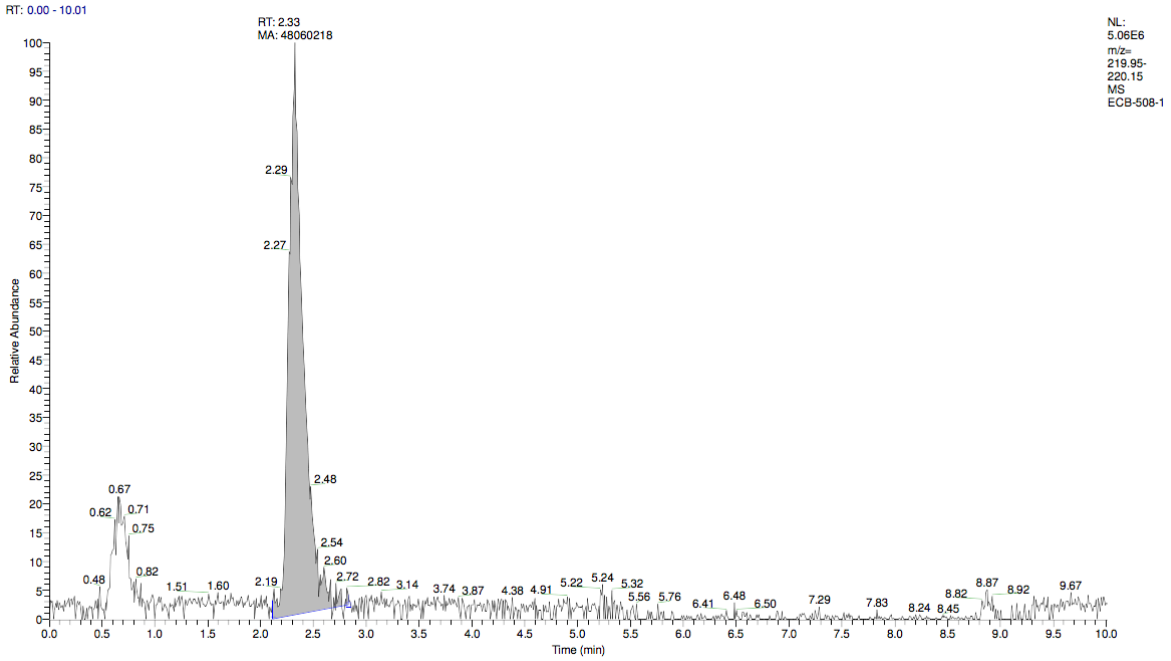

19a

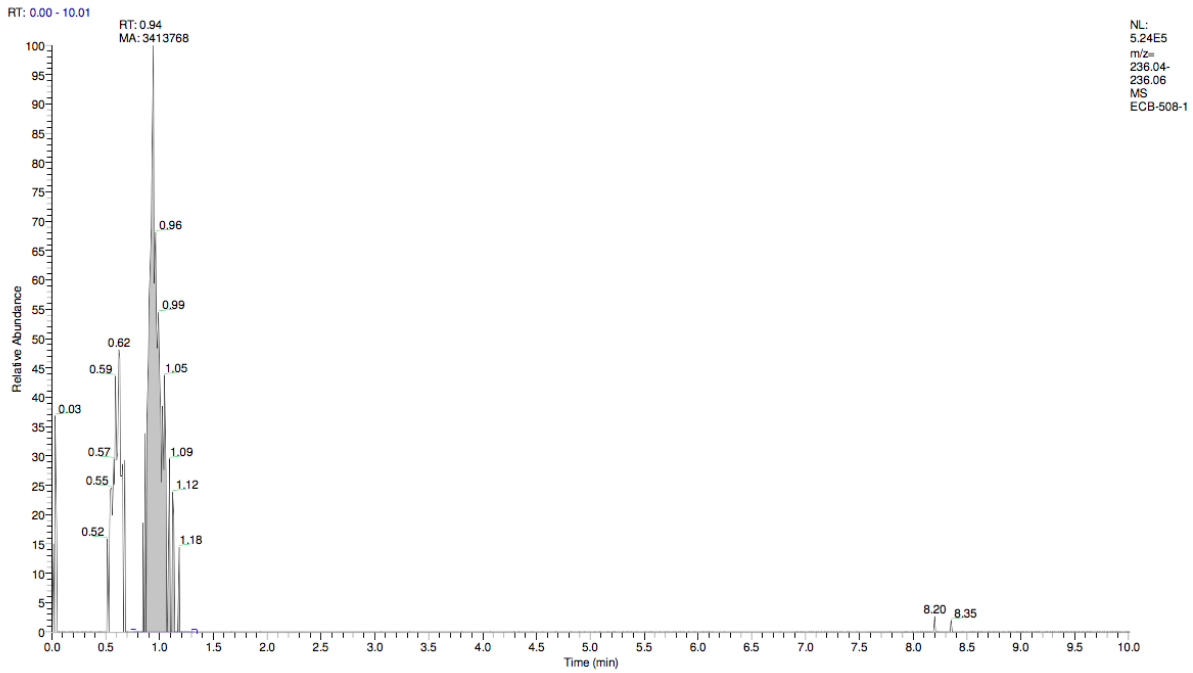

Table 12, Entry 2

8a

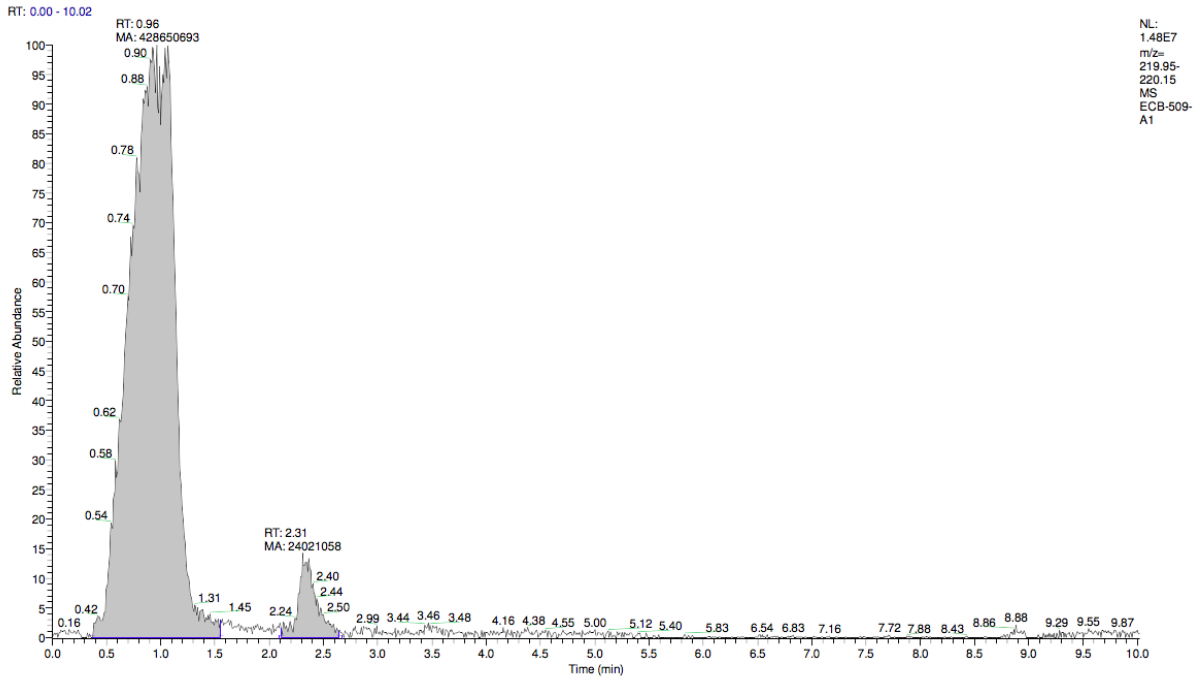

19a

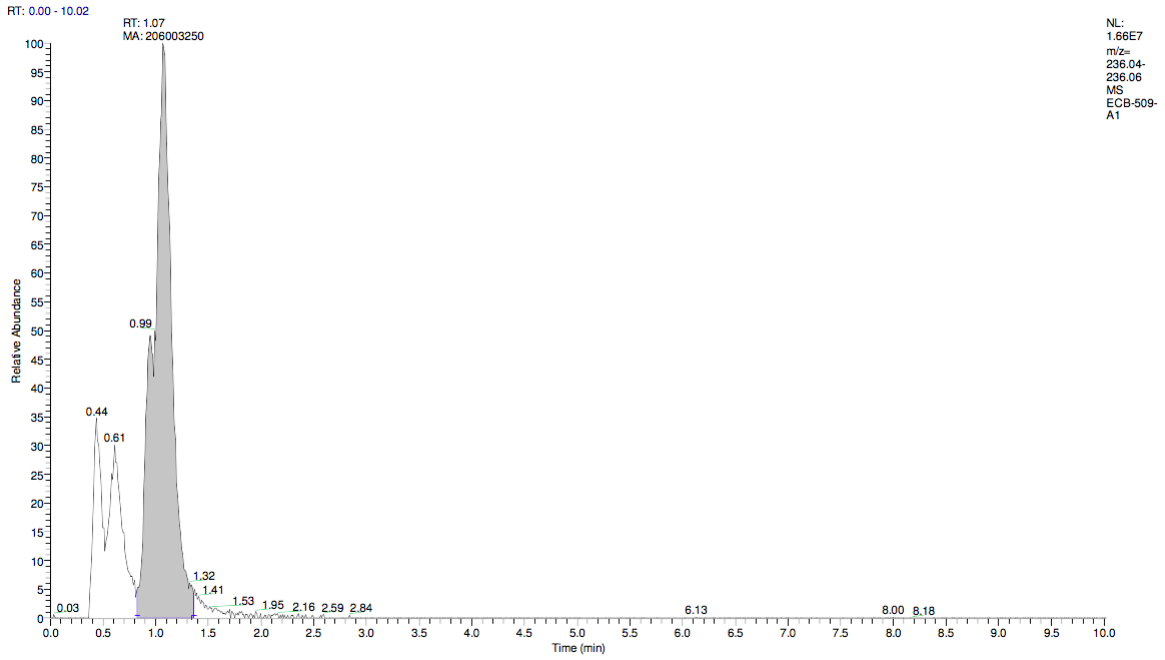

Table 12, Entry 3

8a

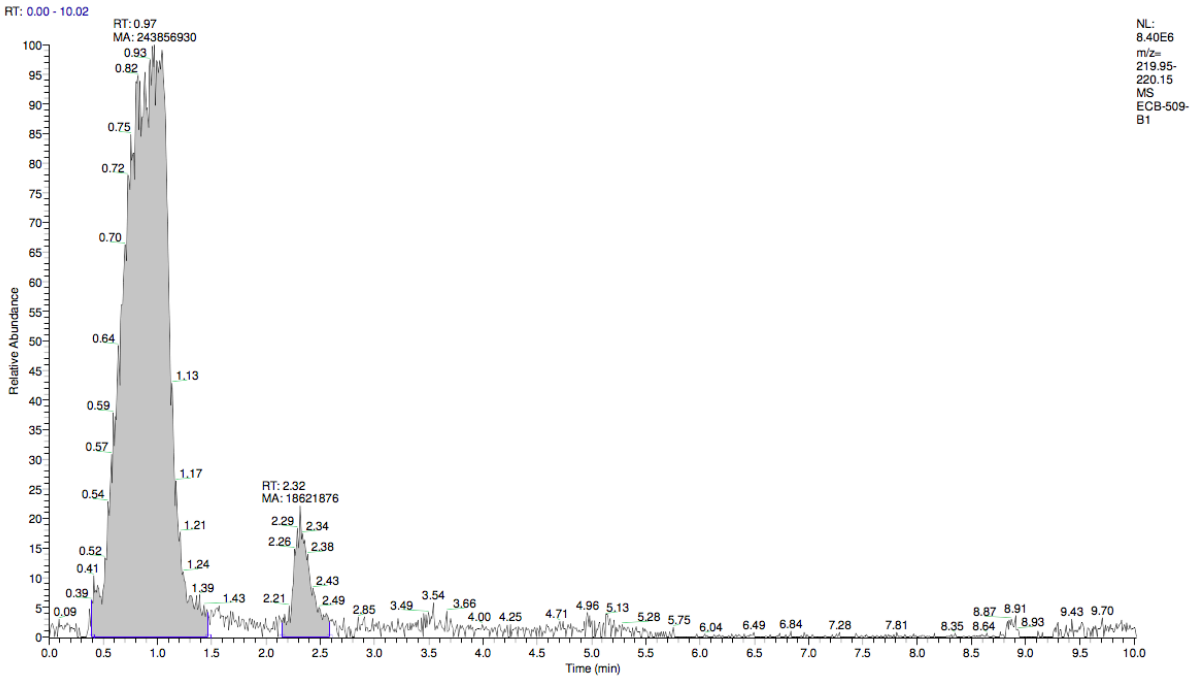

19a

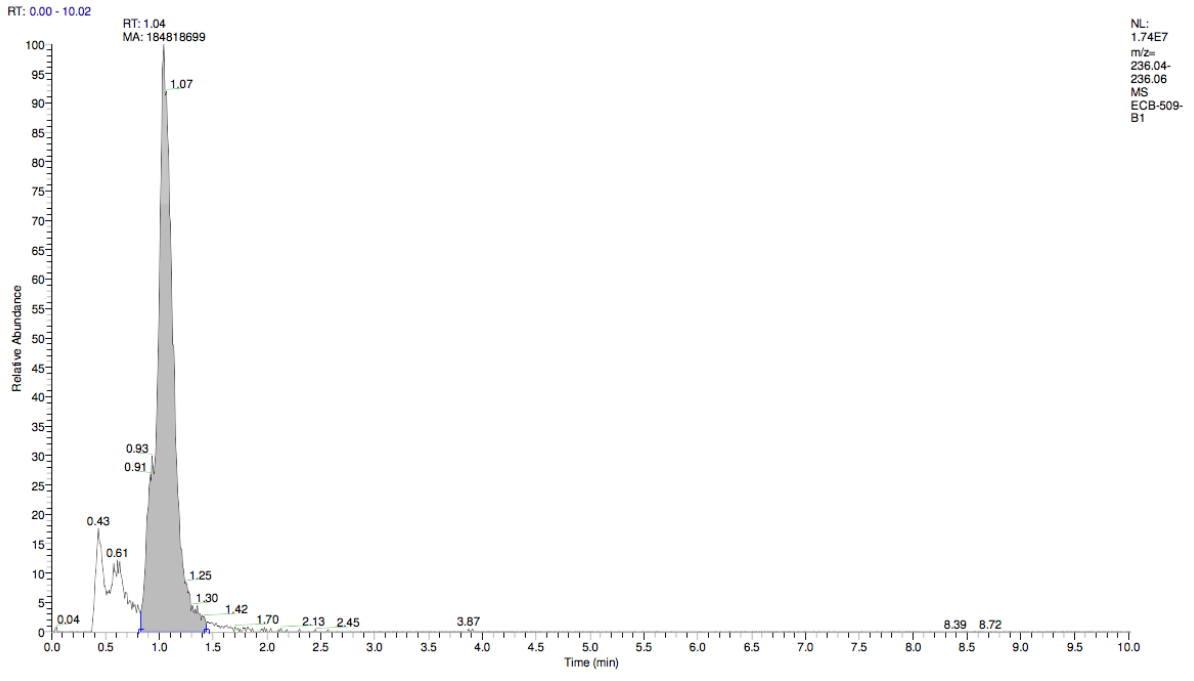

3.5.4.3. GC-MS chromatograms of thioester from network

Table 12, Entry 1

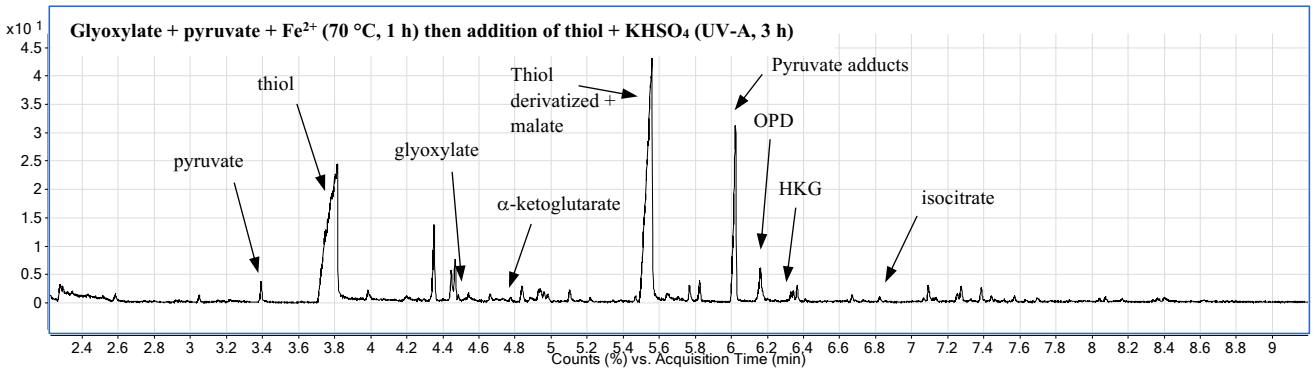

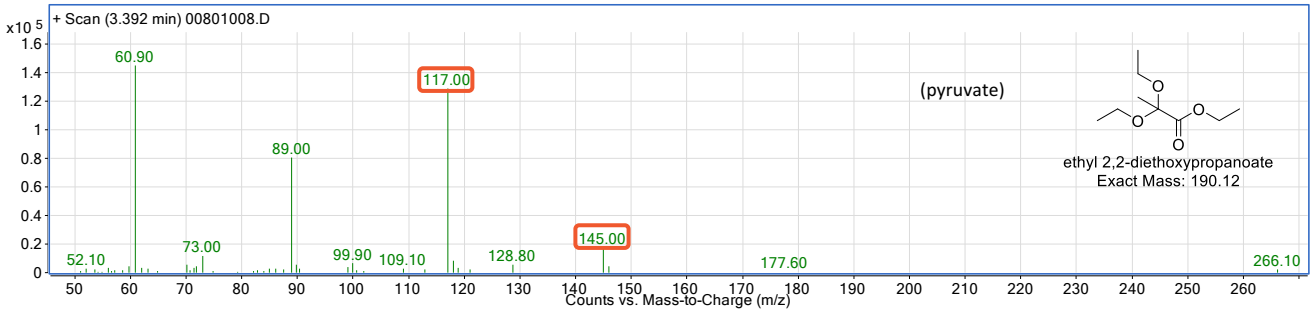

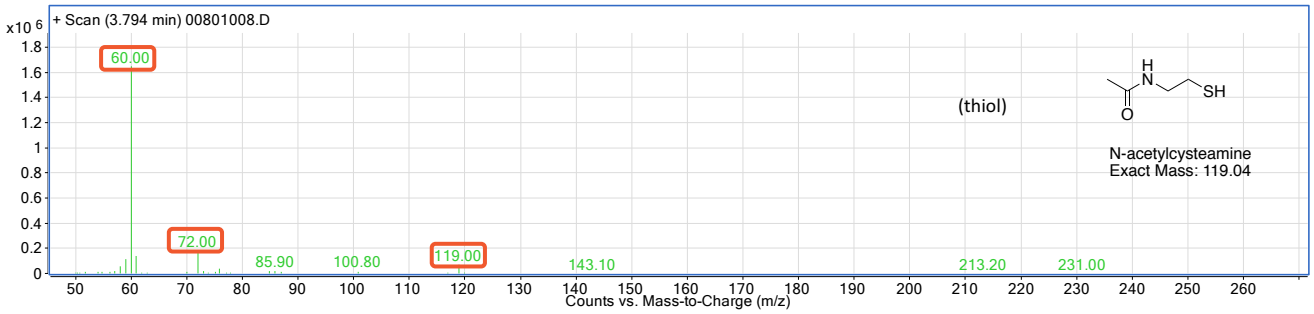

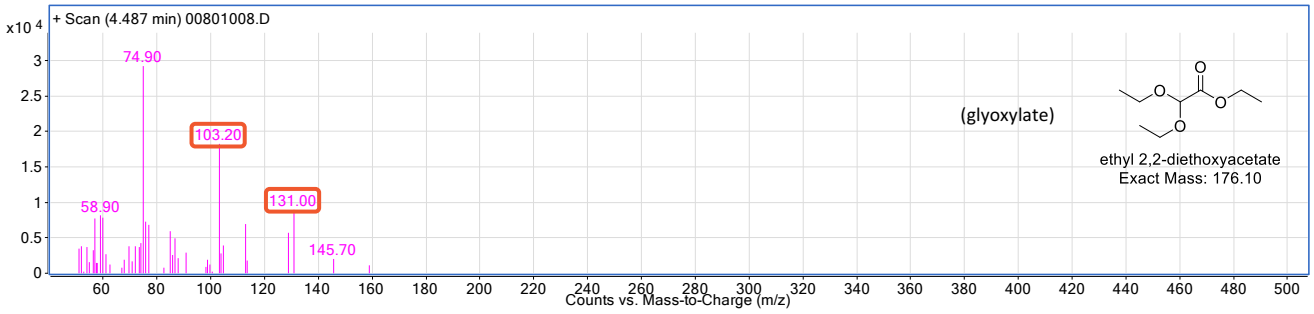

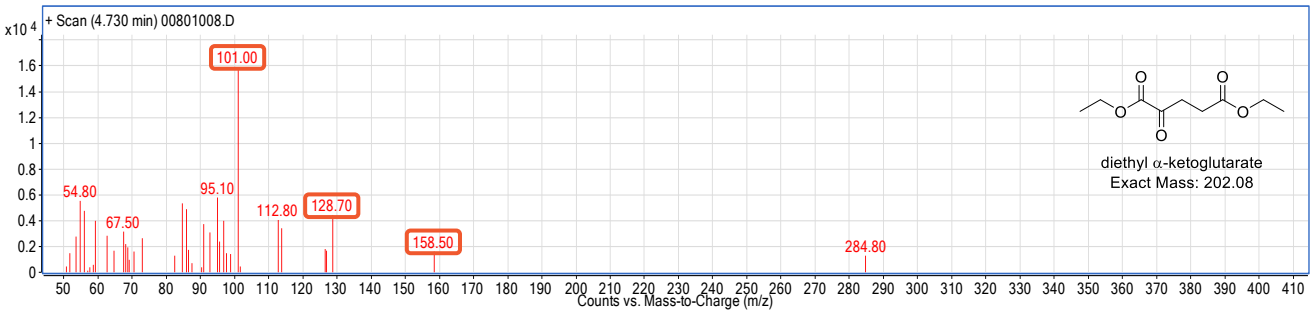

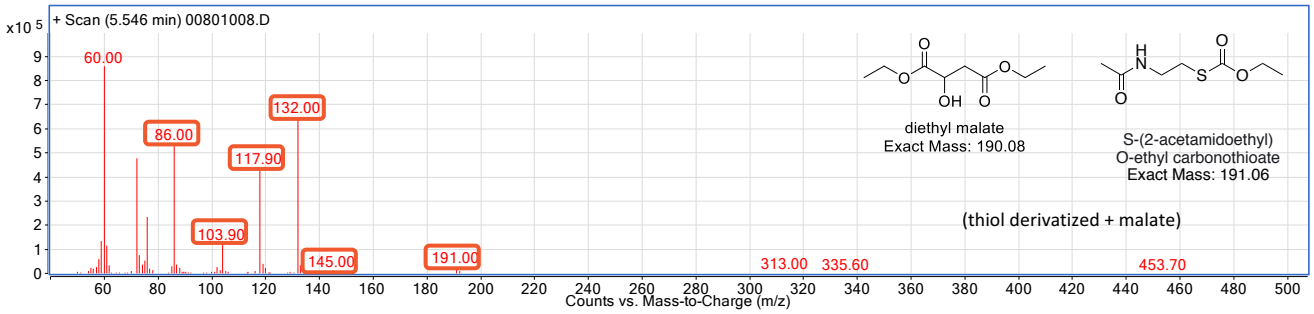
+ Scan (5.546 min) 00801008.D
x10 5
60.00
86.00
117.90
132.00
103.90
145.00
191.00
313.00
335.60
453.70
diethyl malate
Exact Mass: 190.08
S-(2-acetamidoethyl)
O-ethyl carbonothioate
Exact Mass: 191.06
(thiol derivatized + malate)
Counts vs. Mass-to-Charge (m/z)

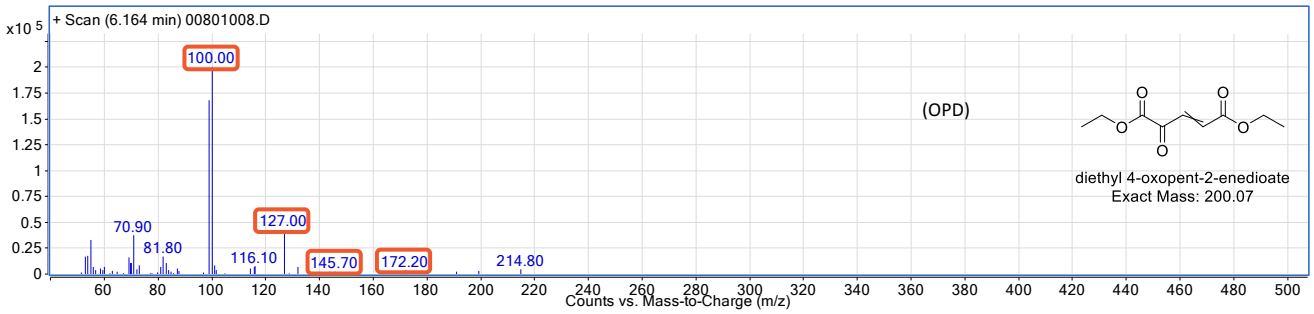
+ Scan (6.164 min) 00801008.D
x10 5
100.00
70.90
81.80
127.00
116.10
145.70
172.20
214.80
(OPD)
diethyl 4-oxopent-2-enedioate
Exact Mass: 200.07
Counts vs. Mass-to-Charge (m/z)

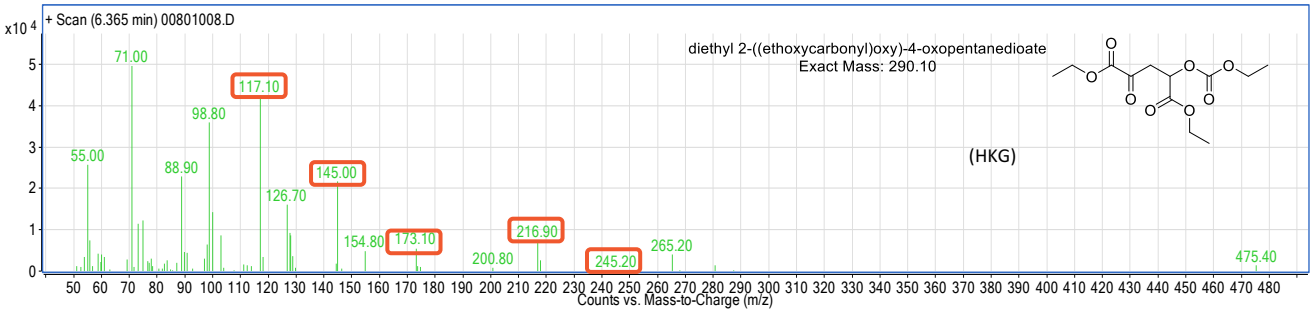
+ Scan (6.365 min) 00801008.D
x10 4
71.00
117.10
98.80
55.00
88.90
145.00
126.70
154.80
173.10
216.90
200.80
245.20
265.20
475.40
diethyl 2-((ethoxycarbonyl)oxy)-4-oxopentanedioate
Exact Mass: 290.10
(HKG)
Counts vs. Mass-to-Charge (m/z)

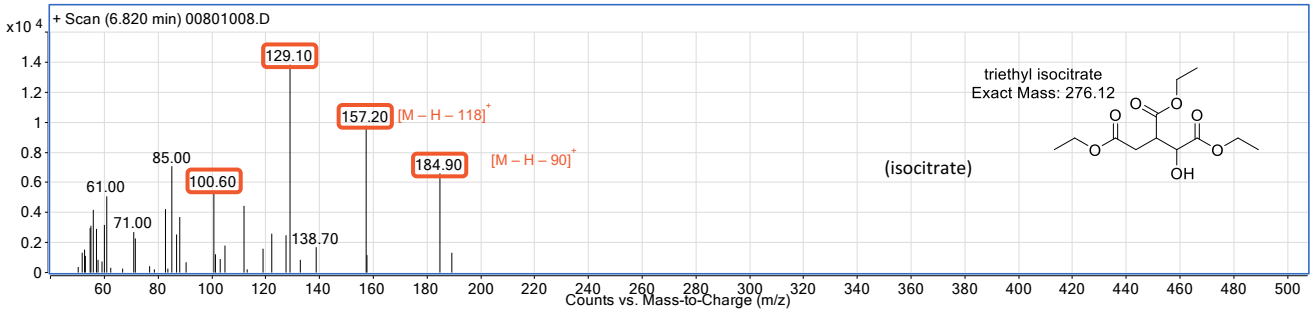
+ Scan (6.820 min) 00801008.D
x10 4
129.10
157.20
[M – H – 118]+
184.90
[M – H – 90]+
85.00
100.60
61.00
71.00
138.70
triethyl isocitrate
Exact Mass: 276.12
(isocitrate)
Counts vs. Mass-to-Charge (m/z)

Table 12, Entry 2

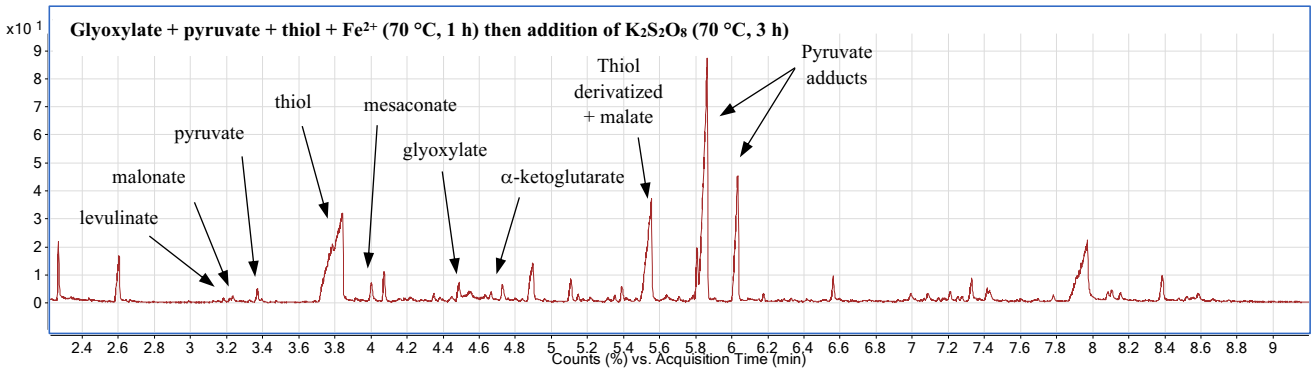

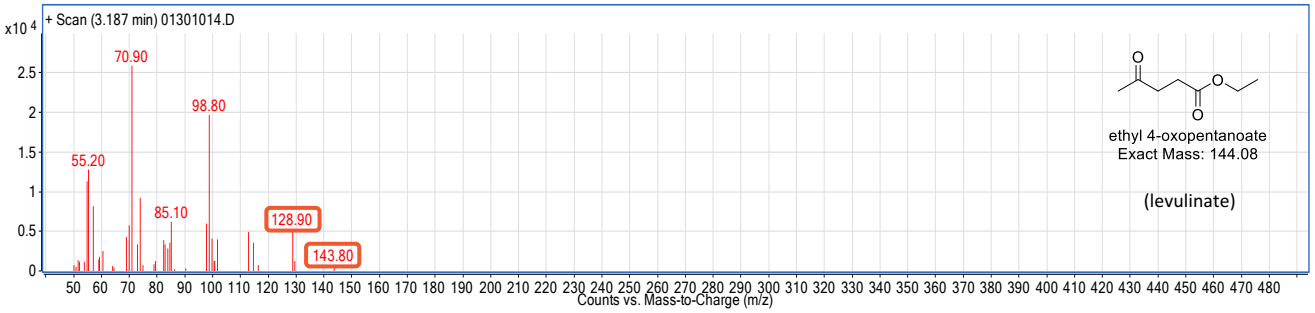

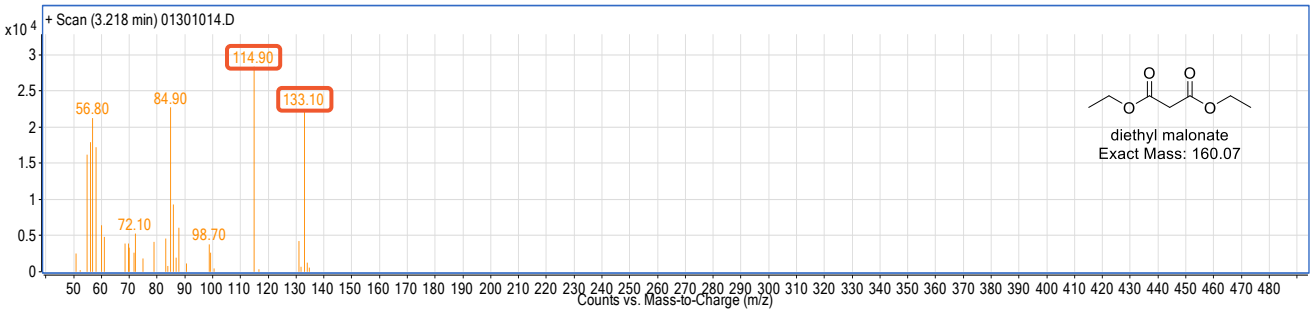

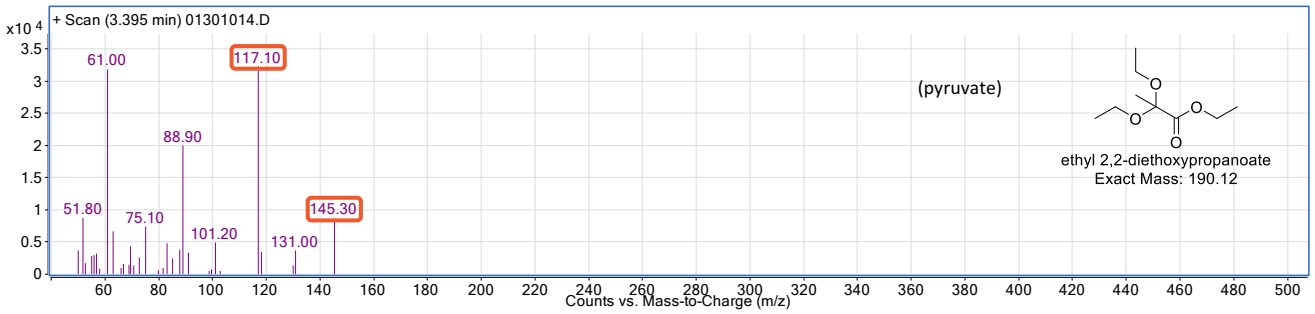

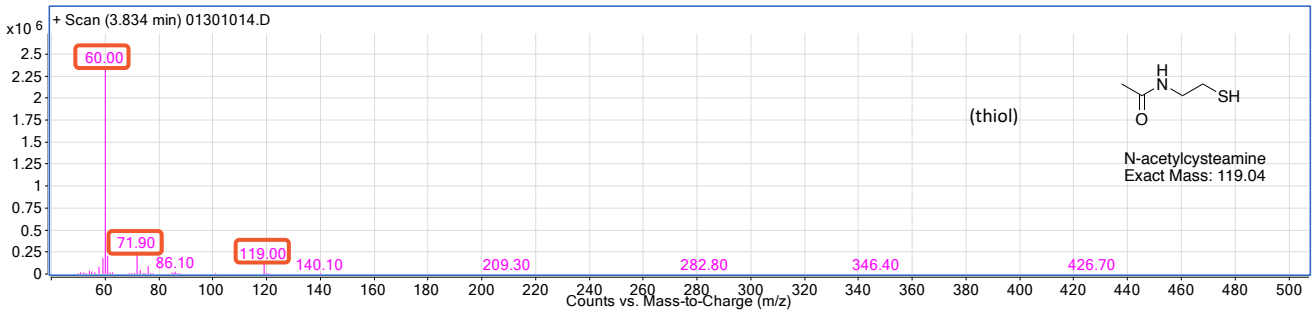

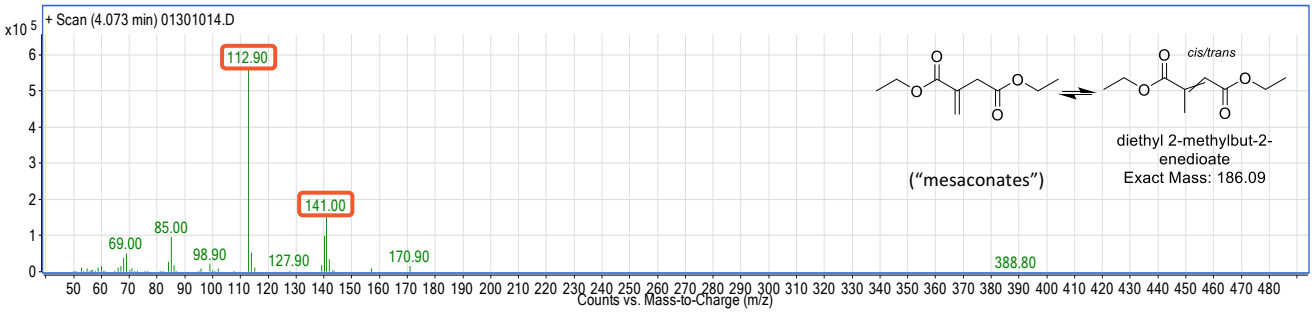
+ Scan (4.073 min) 01301014.D
x10 5
112.90
141.00
85.00
69.00
98.90
127.90
170.90
388.80
cis/trans
("mesaconates")
diethyl 2-methylbut-2-enedioate
Exact Mass: 186.09
Counts vs. Mass-to-Charge (m/z)

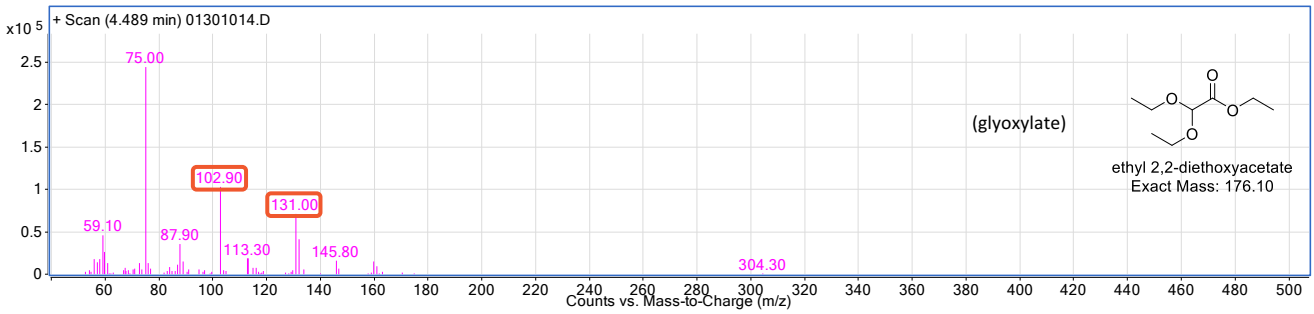
+ Scan (4.489 min) 01301014.D
x10 5
75.00
102.90
131.00
59.10
87.90
113.30
145.80
304.30
(glyoxylate)
ethyl 2,2-diethoxyacetate
Exact Mass: 176.10
Counts vs. Mass-to-Charge (m/z)

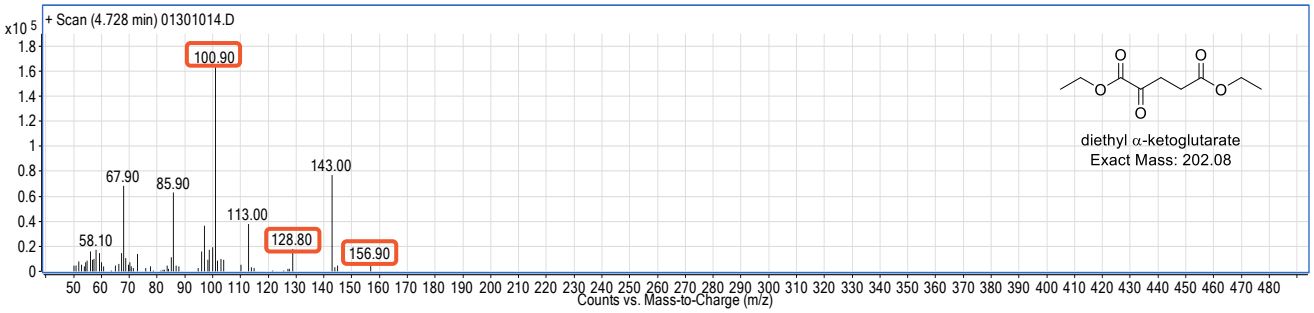
+ Scan (4.728 min) 01301014.D
x10 5
100.90
67.90
85.90
143.00
113.00
58.10
128.80
156.90
diethyl α-ketoglutarate
Exact Mass: 202.08
Counts vs. Mass-to-Charge (m/z)

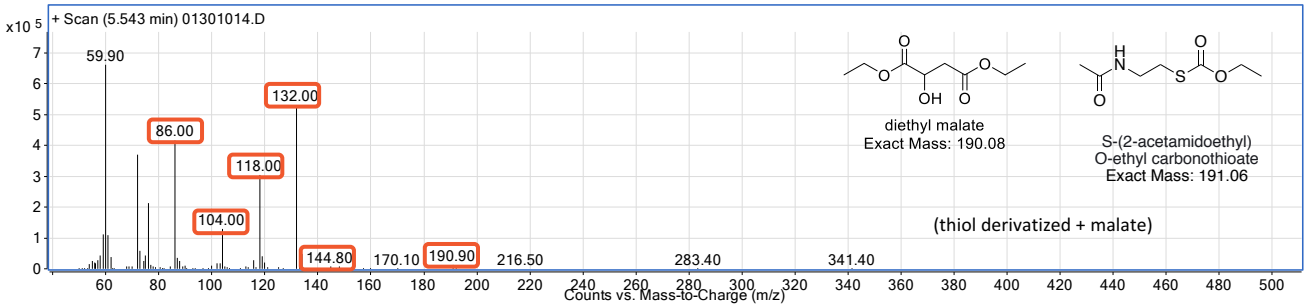
+ Scan (5.543 min) 01301014.D
x10 5
59.90
132.00
86.00
118.00
104.00
144.80
170.10
190.90
216.50
283.40
341.40
diethyl malate
Exact Mass: 190.08
S-(2-acetamidoethyl) O-ethyl carbonothioate
Exact Mass: 191.06
(thiol derivatized + malate)
Counts vs. Mass-to-Charge (m/z)

Table 12, Entry 3

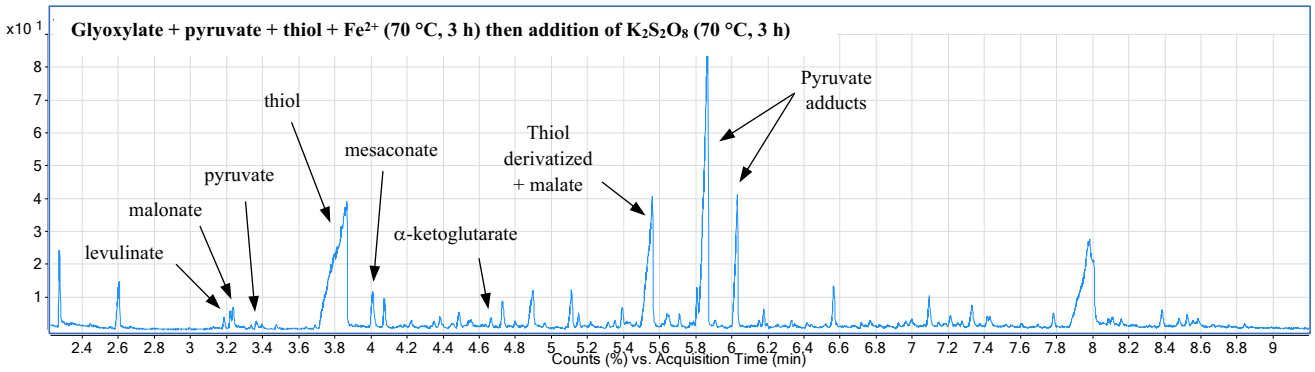

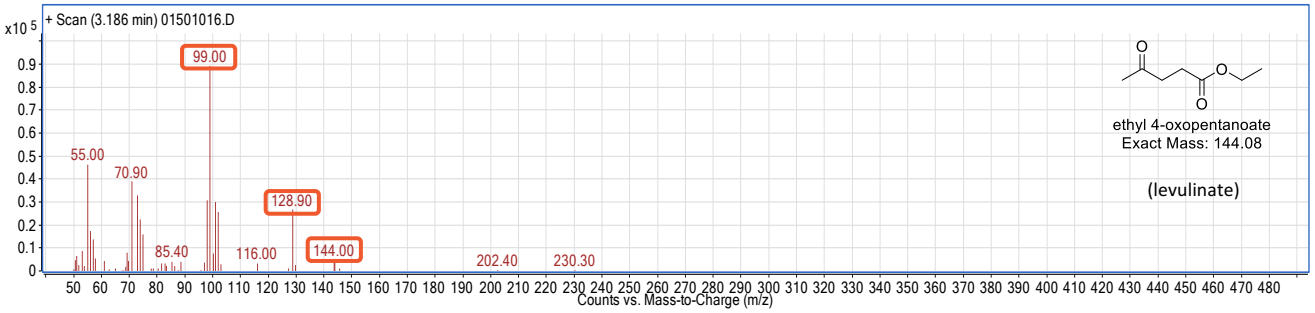

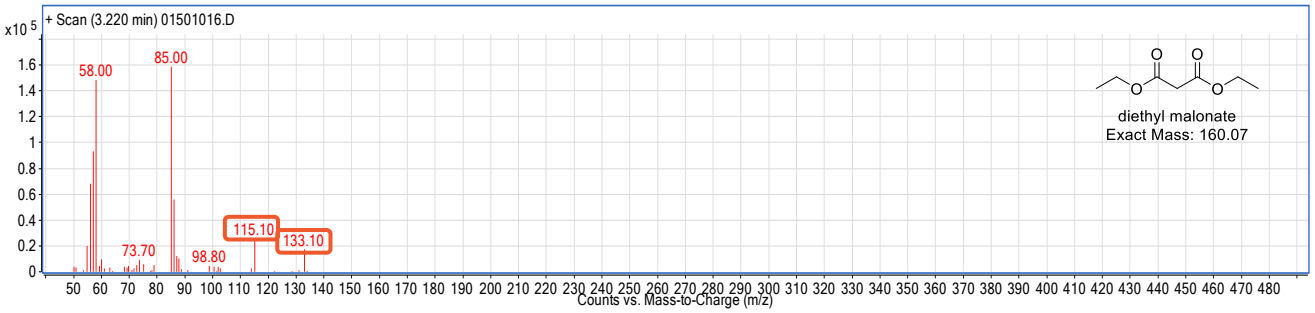

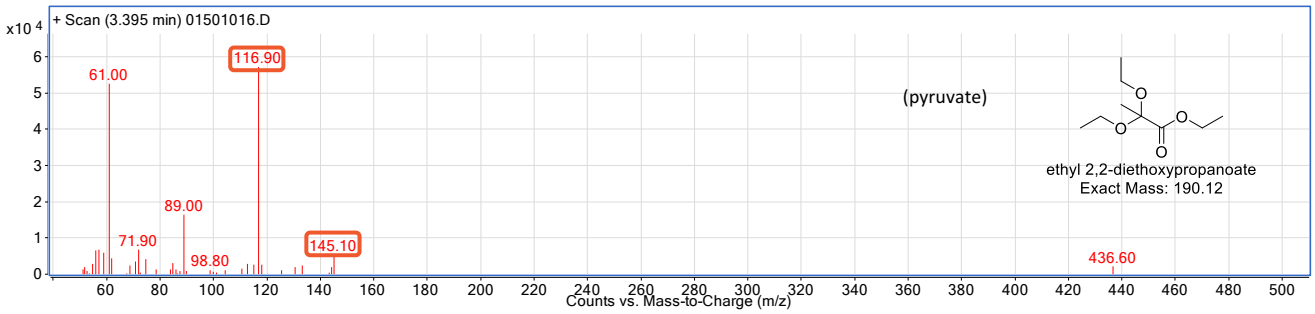

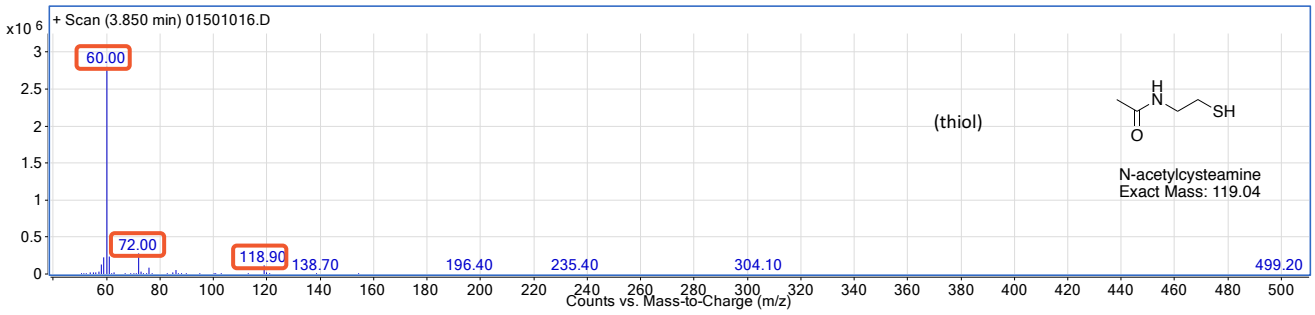

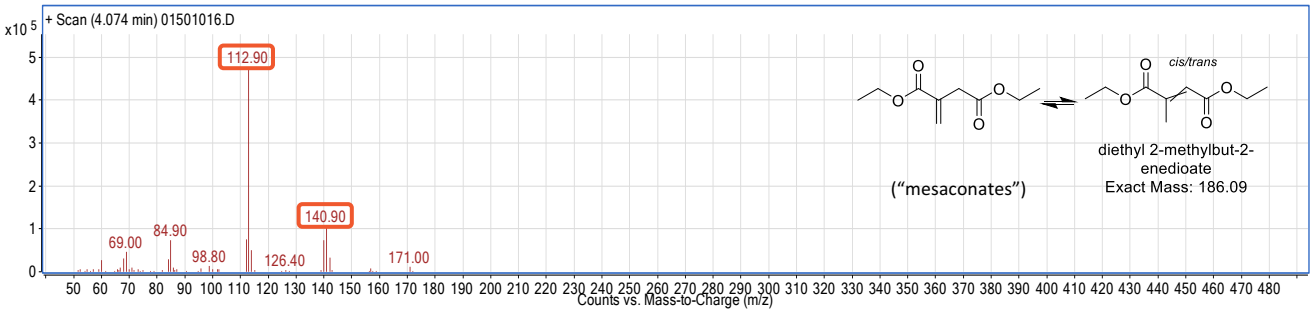
+ Scan (4.074 min) 01501016.D
x10 5
112.90
140.90
69.00
84.90
98.80
126.40
171.00
cis/trans
("mesaconates")
diethyl 2-methylbut-2-enedioate
Exact Mass: 186.09
Counts vs. Mass-to-Charge (m/z)

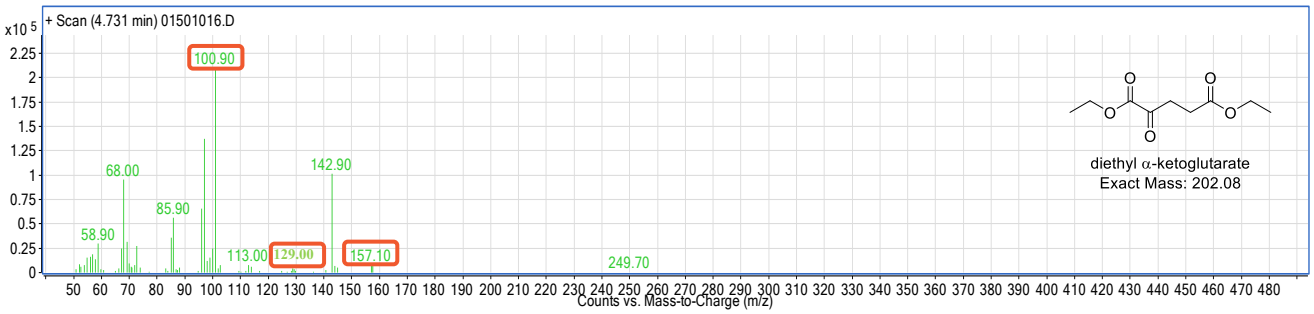
+ Scan (4.731 min) 01501016.D
x10 5
100.90
68.00
142.90
85.90
58.90
113.00
129.00
157.10
249.70
diethyl α-ketoglutarate
Exact Mass: 202.08
Counts vs. Mass-to-Charge (m/z)

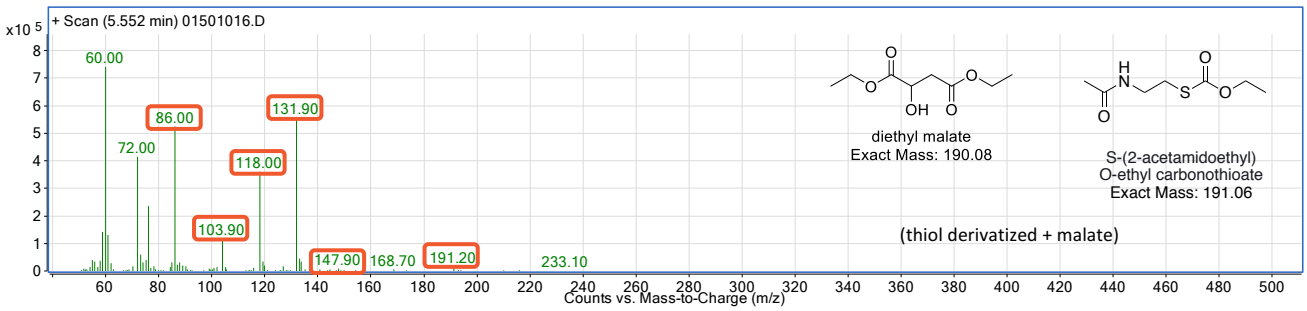
+ Scan (5.552 min) 01501016.D
x10 5
60.00
86.00
131.90
72.00
118.00
103.90
147.90
168.70
191.20
233.10
diethyl malate
Exact Mass: 190.08
S-(2-acetamidoethyl) O-ethyl carbonothioate
Exact Mass: 191.06
(thiol derivatized + malate)
Counts vs. Mass-to-Charge (m/z)

General conclusion

Many changes must have happened during the transition from a primitive non-enzymatic metabolism to the emergence of the LUCA, but prebiotic reactions must eventually give rise to biochemistry as we know it, accounting for why life has acquired its present chemical characteristics.[168] In this context, our group is trying to evaluate how much of biochemistry's characteristics can be explained with only geochemical support.

In my first section, I reported our success to promote two three-steps sequences of the rTCA cycle, found in deep-branching organisms and containing five standard universal precursors to all anabolic reactions.[13] This study reveals that a reducing and acidic medium (Fe^0, 1M HCl) in presence of metal irons (Zn^{2+} and Cr^{3+}) enables the reduction, hydration and dehydration steps of the cycle, which are carried out by 5 different enzymes in living systems. The study of parasitic reactions, one of the main criticisms of the hypothesis of non-enzymatic metabolic cycles due to its potential to inhibit the self-sufficient property of an autocatalytic cycle, reveal only a few proportions of off-cycle products. Although this supports the idea of a prebiotic rTCA cycle using only geochemistry, as part of a larger prebiotic network, the steps requiring ATP are still missing, which has made us skeptical about its emergence at the very earliest stage of prebiotic chemistry.

In my second section, I briefly described a finding from our group where Fe is reported to enable the production of acetate from CO_2, a chemical transformation that greatly resembles the Wood-Ljungdahl pathway. The chemistry could even go one step further, to produce pyruvate.[16] A surface mechanism has been proposed in response of other intermediates found after basic treatment (methanol and formate). For my part, I have tried to propose a better understanding of the mechanism of this reaction by different studies: spectroscopic studies report the presence of iron carbonate at the end of the reaction but did not provide us information on other trace intermediates that might be formed on the surface of iron. In the face of electrochemical results that are not easily reproducible, one hypothesis has been postulated: iron oxide, rather than Fe^0, was responsible for the reaction. The potential required for CO_2 reduction does not allow to keep iron oxides at the surface of the cathode, which could explain our impossibility to reproduce by electrochemistry our previous results with Fe^0 powder. Then, different iron oxides were tested in the presence of CO_2 and H_2.

Higher concentration of acetate and pyruvate were observed with magnetite (Fe_3O_4), a mix of Fe^{2+} and Fe^{3+}. From these results, a new mechanism has been proposed for the initial reaction with Fe^0: H_2 is produced from water reduction by Fe^0, which can reduce CO_2. This reaction required iron oxides as catalyst, which are produced from oxidation of Fe^0. However, there are still uncertainties concerning fairly similar results obtained in the absence of H_2. More studies are ongoing in the laboratory.

In my last section, I propose a simple way to promote non-enzymatic thioester synthesis from α-ketoacids or aldehydes. Using a simple inorganic oxidant ($K_2S_2O_8$) or $KHSO_4$ in the presence of light or heat (UV-A or 70 °C), a good conversion is observed. A mixture of multiple ketoacids can be converted to thioesters in one pot, prompting us to integrate this reaction with a ketoacid-generating chemical reaction network recently published by our laboratory.[9] In this experiment, pyruvate and glyoxylate in the presence of Fe^{2+} react to form a dynamic complex system, where many intermediates of the TCA and glyoxylate cycles can be observed, and which bypasses our failure to observe non-enzymatic ATP-dependent reactions of the rTCA cycle. Conditions for making thioesters have been integrated with the iron-catalyzed reaction network, and three biological analogs of thioesters were detected in a one-pot experiment after cycling with oxidant or light. Starting from only three organic molecules (pyruvate, glyoxylate and thiol), nine are formed, including three thioesters under prebiotic conditions. Moving forward, we suspect that under the right conditions, thioesters can further react to give access to fatty acids and similar structures.

Efforts in our laboratory to recreate large fragments of metabolism without enzymes, combined with advances from other groups in the world, like Ralser and colleagues showing glycolysis and steps of gluconeogenesis[169–171], support the hypothesis that the catalytic cores of some modern enzymes represent evolved variants of simple geochemical available prebiotic catalysts like transition metals, iron-sulfur clusters or organic cofactors.[172] However, the road to life is still long, and much more work is required to expand the scope of possible prebiotic chemical networks before the availability of proteinaceous enzymes.

One question remains in mind: will the greatest mystery of life ever be uncovered?

References

1. Morowitz, H. J. Beginnings of cellular life: Metabolism recapitulates biogenesis. *Yale University Press* (2004).
2. Gilbert, W. Origin of life: The RNA world. *Nature* **319**, 618–618 (1986).
3. Wachtershauser, G. Evolution of the first metabolic cycles. *Proc. Natl. Acad. Sci.* **87**, 200–204 (1990).
4. Shapiro, R. A simpler origin for life. *Sci. Am.* **296** 46–53 (2007).
5. Smith, E. & Morowitz, H. J. The origin and nature of life on earth: the emergence of the fourth geosphere. *Cambridge University Press* (2016).
6. Powner, M. W., Gerland, B. & Sutherland, J. D. Synthesis of activated pyrimidine ribonucleotides in prebiotically plausible conditions. *Nature* **459**, 239–242 (2009).
7. Fuchs, G. Alternative pathways of carbon dioxide fixation: Insights into the early evolution of life? *Annu. Rev. Microbiol.* **65**, 631–658 (2011).
8. Smith, E. & Morowitz, H. J. Universality in intermediary metabolism. *Proc. Natl. Acad. Sci.* **101**, 13168–13173 (2004).
9. Muchowska, K. B., Varma, S. J. & Moran, J. Synthesis and breakdown of universal metabolic precursors promoted by iron. *Nature* **569**, 104–107 (2019).
10. Glasfeld, A. Biochemistry: The chemical reactions of living cells. *J. Chem. Educ.* **81**, 646 (2004).
11. Duve, C. D. Clues from present-day biology: the thioester world. *Cambridge University Press* 219–236 (1998).
12. Zhang, X. V. & Martin, S. T. Driving parts of krebs cycle in reverse through mineral photochemistry. *J. Am. Chem. Soc.* **128**, 16032–16033 (2006).
13. Muchowska, K. B. *et al.* Metals promote sequences of the reverse Krebs cycle. *Nat. Ecol. Evol.* **1**, 1716–1721 (2017).
14. Sousa, F. L. & Martin, W. F. Biochemical fossils of the ancient transition from geoenergetics to bioenergetics in prokaryotic one carbon compound metabolism. *Biochim. Biophys.* **1837**, 964–981 (2014).
15. Ragsdale, S. W. Enzymology of the Wood-Ljungdahl pathway of acetogenesis. *Ann. N. Y. Acad. Sci.* **1125**, 129–136 (2008).
16. Varma, S. J., Muchowska, K. B., Chatelain, P. & Moran, J. Native iron reduces CO_2 to intermediates and end-products of the acetyl-CoA pathway. *Nat. Ecol. Evol.* **2**, 1019–1024 (2018).
17. Goldford, J. E., Hartman, H., Smith, T. F. & Segrè, D. Remnants of an ancient metabolism without phosphate. *Cell* **168**, 1126-1134.e9 (2017).
18. Yan, K. *et al.* Catalyst-free direct decarboxylative coupling of α-keto acids with thiols: a facile access to thioesters. *Org. Biomol. Chem.* **13**, 7323–7330 (2015).
19. Keller, M. A., Kampjut, D., Harrison, S. A. & Ralser, M. Sulfate radicals enable a non-enzymatic Krebs cycle precursor. *Nat. Ecol. Evol.* **1**, 0083 (2017).
20. Tirard S. Abiogenesis. *Encyclopedia of Astrobiology* (2014).
21. Pasteur, L. Mémoire sur la fermentation appelée lactique. *Compt. Rend.* 913–916 (1857).
22. Wallace, A. R. Contributions to the theory of natural selection: a series of essays. *Cambridge University Press* (1859).
23. Peretó, J., Bada, J. L. & Lazcano, A. Charles Darwin and the origin of life. *Orig. Life Evol. Biospheres* **39**, 395–406 (2009).
24. Bailey, C. H. The origin of life. *J. Chem. Educ.* **15**, 399 (1938).
25. Miller, S. L. A production of amino acids under possible primitive earth conditions. *Science* **117**, 528–529 (1953).
26. Danger, G., Plasson, R. & Pascal, R. Pathways for the formation and evolution of peptides in prebiotic environments. *Chem. Soc. Rev.* **41**, 5416 (2012).

27. Harada, K. & Fox, S. W. The thermal condensation of glutamic acid and glycine to linear peptides. *J. Am. Chem. Soc.* **80**, 2694–2697 (1958).
28. Orò, J. Synthesis of adenine from ammonium cyanide. *Biochem. Biophys. Res. Commun.* **2**, 407–412 (1960).
29. Orgel, L. E. Evolution of the genetic apparatus. *J. Mol. Biol.* **38**, 381–393 (1968).
30. Kruger, K. *et al.* Self-splicing RNA: Autoexcision and autocyclization of the ribosomal RNA intervening sequence of tetrahymena. *Cell* **31**, 147–157 (1982).
31. Altman, S. *et al.* Cleavage of RNA by RNase P from Escherichia coli. *Molecular Biology of RNA,* 3–15 (1987).
32. Ferris, J. P. Mineral Catalysis and prebiotic synthesis: Montmorillonite-catalyzed formation of RNA. *Elements* **1**, 145–149 (2005).
33. Pitsch, S., Wendeborn, S., Jaun, B. & Eschenmoser, A. Why pentose- and not hexose-nucleic acids? *Helv. Chim. Acta* **76**, 2161–2183 (1993).
34. Darwin, C. On the origin of species, by means of natural selection, or the preservation of favoured races in the struggle for life. (1859).
35. Fox, G. *et al.* The phylogeny of prokaryotes. *Science* **209**, 457–463 (1980).
36. Theobald, D. L. A formal test of the theory of universal common ancestry. *Nature* **465**, 219–222 (2010).
37. Williams, T. A., Foster, P. G., Cox, C. J. & Embley, T. M. An archaeal origin of eukaryotes supports only two primary domains of life. *Nature* **504**, 231–236 (2013).
38. Weiss, M. C. *et al.* The physiology and habitat of the last universal common ancestor. *Nat. Microbiol.* **1**, 16116 (2016).
39. Corliss, J. B. *et al.* Submarine thermal springs on the galápagos rift. *Science* **203**, 1073–1083 (1979).
40. Spiess, F. N. *et al.* East pacific rise: Hot springs and geophysical experiments. *Science* **207**, 1421–1433 (1980).
41. Russell, M. J., Hall, A. J. & Turner, D. In vitro growth of iron sulphide chimneys: possible culture chambers for origin-of-life experiments. *Terra Nova* **1**, 238–241 (1989).
42. Wächtershäuser, G. Before enzymes and templates: theory of surface metabolism. *Microbiol. Rev.* **52**, 452–484 (1988).
43. Blochl, E., Keller, M., Wachtershauser, G. & Stetter, K. O. Reactions depending on iron sulfide and linking geochemistry with biochemistry. *Proc. Natl. Acad. Sci.* **89**, 8117–8120 (1992).
44. Martin, W. & Russell, M. J. On the origin of biochemistry at an alkaline hydrothermal vent. *Philos. Trans. R. Soc. B Biol. Sci.* **362**, 1887–1926 (2007).
45. Martin, W., Baross, J., Kelley, D. & Russell, M. J. Hydrothermal vents and the origin of life. *Nat. Rev. Microbiol.* **6**, 805–814 (2008).
46. Cairns-Smith, A., G. & Wlaker, G., L. Primitive metabolism. *BioSystems* **5**, 173–186 (1974).
47. Richert, C. Prebiotic chemistry and human intervention. *Nat. Commun.* **9**, 5177 (2018).
48. Patel, B. H., Percivalle, C., Ritson, D. J., Duffy, C. D. & Sutherland, J. D. Common origins of RNA, protein and lipid precursors in a cyanosulfidic protometabolism. *Nat. Chem.* **7**, 301–307 (2015).
49. Kun, Á., Papp, B. & Szathmáry, E. Computational identification of obligatorily autocatalytic replicators embedded in metabolic networks. *Genome Biol.* **9**, R51 (2008).
50. Orgel, L. E. The implausibility of metabolic cycles on the prebiotic earth. *PLoS Biol.* **6**, e18 (2008).
51. Ruiz-Mirazo, K., Briones, C. & De la Escosura, A. Prebiotic Systems Chemistry: New Perspectives for the Origins of Life. *Chem. Rev.* **114**, 285–366 (2014).
52. Peretó, J. Out of fuzzy chemistry: from prebiotic chemistry to metabolic networks. *Chem. Soc. Rev.* **41**, 5394 (2012).

53. Pross, A. & Pascal, R. The origin of life: what we know, what we can know and what we will never know. *Open Biol.* **3**, 120190–120190 (2013).
54. Pross, A. Seeking the chemical roots of darwinism: Bridging between chemistry and biology. *Chem. - Eur. J.* **15**, 8374–8381 (2009).
55. Pross, A. & Khodorkovsky, V. Extending the concept of kinetic stability: toward a paradigm for life. *J. Phys. Org. Chem.* **17**, 312–316 (2004).
56. Pascal, R. Suitable energetic conditions for dynamic chemical complexity and the living state. *J. Syst. Chem.* **3**, 3 (2012).
57. Pross, A. The evolutionary origin of biological function and complexity. *J. Mol. Evol.* **76**, 185–191 (2013).
58. Pascal, R., Pross, A. & Sutherland, J. D. Towards an evolutionary theory of the origin of life based on kinetics and thermodynamics. *Open Biol.* **3**, 130156–130156 (2013).
59. Zahnle, K., Schaefer, L. & Fegley, B. Earth's earliest atmospheres. *Cold Spring Harb. Perspect. Biol.* **2**, a004895–a004895 (2010).
60. Kasting, J., F. Earth's early atmosphere. *Science* **259**, 920–926 (1993).
61. Ralser, M. An appeal to magic? The discovery of a non-enzymatic metabolism and its role in the origins of life. *Biochem. J.* **475**, 2577–2592 (2018).
62. Gutekunst, K. Hypothesis on the synchronistic evolution of autotrophy and heterotrophy. *Trends Biochem. Sci.* **43**, 402–411 (2018).
63. Sadownik, J. W., Mattia, E., Nowak, P. & Otto, S. Diversification of self-replicating molecules. *Nat. Chem.* **8**, 264–269 (2016).
64. Braakman, R. & Smith, E. The compositional and evolutionary logic of metabolism. *Phys. Biol.* **10**, 011001 (2012).
65. Braakman, R. & Smith, E. The emergence and early evolution of biological carbon-fixation. *PLoS Comput. Biol.* **8**, e1002455 (2012).
66. Figueroa, I. A. *et al.* Metagenomics-guided analysis of microbial chemolithoautotrophic phosphite oxidation yields evidence of a seventh natural CO_2 fixation pathway. *Proc. Natl. Acad. Sci.* **115**, E92–E101 (2018).
67. Berg, I. A. Ecological aspects of the distribution of different autotrophic CO_2 fixation pathways. *Appl. Environ. Microbiol.* **77**, 1925–1936 (2011).
68. Evans, M. C., Buchanan, B. B. & Arnon, D. I. A new ferredoxin-dependent carbon reduction cycle in a photosynthetic bacterium. *Proc. Natl. Acad. Sci.* **55**, 928–934 (1966).
69. Corliss, J., B., Baross, J., A. & Hoffman, S., E. Submarine hydrothermal systems: a probable site for the origin of life. *School of Oceanography* (1980).
70. Krebs, H. A. & Johnson, W. A. Metabolism of ketonic acids in animal tissues. *Biochem. J.* **31** (1937).
71. Lane, N. & Martin, W. F. The origin of membrane bioenergetics. *Cell* **151**, 1406–1416 (2012).
72. Ljungdahl, L., Irion, E. & Wood, H. G. Total synthesis of acetate from CO_2. I. Co-methylcobyric acid and Co-(Methyl)-5-methoxybenzimidazolylcobamide as intermediates with Clostridium thermoaceticum. *Biochemistry* **4**, 2771–2780 (1965).
73. Buckel, W. & Thauer, R. K. Energy conservation via electron bifurcating ferredoxin reduction and proton/Na+ translocating ferredoxin oxidation. *Biochim. Biophys. Acta.* **1827**, 94–113 (2013).
74. Dybas, M. & Konisky, J. Energy transduction in the methanogen Methanococcus voltae is based on a sodium current. *J. Bacteriol.* **174**, 5575–5583 (1992).
75. Poehlein, A. *et al.* An ancient pathway combining carbon dioxide fixation with the generation and utilization of a sodium ion gradient for ATP synthesis. *PLoS ONE* **7**, e33439 (2012).
76. Ferry, J. G. Enzymology of one-carbon metabolism in methanogenic pathways. *FEMS Microbiol. Rev.* **23**, 13–38 (1999).

77. Zhu, X. & Tan, X. Metalloproteins/metalloenzymes for the synthesis of acetyl-CoA in the Wood-Ljungdahl pathway. *Sci. China Ser. B Chem.* **52**, 2071–2082 (2009).
78. Ragsdale, S. W. Pyruvate ferredoxin oxidoreductase and its radical intermediate. *Chem. Rev.* **103**, 2333–2346 (2003).
79. Kluger, R. & Tittmann, K. Thiamin diphosphate catalysis: enzymic and nonenzymic covalent intermediates. *Chem. Rev.* **108**, 1797–1833 (2008).
80. Zhang, Q., Iwasaki, T., Wakagi, T. & Oshima, T. 2-Oxoacid:Ferredoxin Oxidoreductase from the Thermoacidophilic Archaeon, Sulfolobus sp. Strain 7. *J. Biochem.* **120**, 587–599 (1996).
81. Kai, Y., Matsumura, H. & Izui, K. Phosphoenolpyruvate carboxylase: three-dimensional structure and molecular mechanisms. *Arch. Biochem. Biophys.* **414**, 170–179 (2003).
82. Aoshima, M. & Igarashi, Y. A novel oxalosuccinate-forming enzyme involved in the reductive carboxylation of 2-oxoglutarate in Hydrogenobacter thermophilus TK-6. *Mol. Microbiol.* **62**, 748–759 (2006).
83. Aoshima, M., Ishii, M. & Igarashi, Y. A novel biotin protein required for reductive carboxylation of 2-oxoglutarate by isocitrate dehydrogenase in Hydrogenobacter thermophilus TK-6: Biotin protein required for carboxylation by ICDH. *Mol. Microbiol.* **51**, 791–798 (2003).
84. Barnes, L. D., McGuire, J. J. & Atkinson, D. E. Yeast diphosphopyridine nucleotide specific isocitrate dehydrogenase. Regulation of activity and unidirectional catalysis. *Biochemistry* **11**, 4322–4329 (1972).
85. Miura, A., Kameya, M., Arai, H., Ishii, M. & Igarashi, Y. A soluble NADH-dependent fumarate reductase in the reductive tricarboxylic acid cycle of hydrogenobacter thermophilus TK-6. *J. Bacteriol.* **190**, 7170–7177 (2008).
86. Maklashina, E. *et al.* Differences in protonation of ubiquinone and menaquinone in fumarate reductase from Escherichia coli. *J. Biol. Chem.* **281**, 26655–26664 (2006).
87. Neilson, N., E. The aconitase of Aspergillus niger. *Biochim. Biophys. Acta* **17**,139–140 (1955).
88. Broderick, J. B. Iron–Sulfur clusters in enzyme catalysis. *Comprehensive Coordination Chemistry II,* 739–757 (2003).
89. Yogev, O., Naamati, A. & Pines, O. Fumarase: a paradigm of dual targeting and dual localized functions: Fumarase: dual targeting and dual localized functions. *FEBS J.* **278**, 4230–4242 (2011).
90. Kanao, T., Fukui, T., Atomi, H. & Imanaka, T. Kinetic and biochemical analyses on the reaction mechanism of a bacterial ATP-citrate lyase: ATP-citrate lyase from Chlorobium limicola. *Eur. J. Biochem.* **269**, 3409–3416 (2002).
91. Schmid, M., Wild, M. R., Dahinden, P. & Dimroth, P. Subunit γ of the oxaloacetate decarboxylase Na^{+} Pump: Interaction with other subunits/domains of the complex and binding site for the Zn^{2+} metal ion. *Biochemistry* **41**, 1285–1292 (2002).
92. Wiegand, G. & Remington, S. J. Citrate synthase: Structure, control, and mechanism. *Annu. Rev. Biophys. Chem.* **15**, 97-117 (1986).
93. Yankovskaya, V. Architecture of cuccinate dehydrogenase and reactive oxygen species generation. *Science* **299**, 700–704 (2003).
94. Voet, D., Voet, J. G. & Pratt, C. W. Fundamentals of biochemistry: Life at the molecular level. *Wiley* 574-575 (2015).
95. Zhou, Z. H., McCarthy, D. B., O'Connor, C. M., Reed, L. J. & Stoops, J. K. The remarkable structural and functional organization of the eukaryotic pyruvate dehydrogenase complexes. *Proc. Natl. Acad. Sci.* **98**, 14802–14807 (2001).
96. McCartney, R. G. *et al.* Evidence for direct association of the α-ketoglutarate dehydrogenase and dihydrolipoamide dehydrogenase components. *J. Biol. Chem.* **273**, 24158-24164 (1998).

97. Kondrashov, F. A., Koonin, E. V., Morgunov, I. G., Finogenova, T. V. & Kondrashova, M. N. Evolution of glyoxylate cycle enzymes in Metazoa: evidence of multiple horizontal transfer events and pseudogene formation. *Biol. Direct* **1**, 31 (2006).
98. Lorenz, M. C. & Fink, G. R. Life and death in a macrophage: Role of the glyoxylate cycle in virulence. *Eukaryot Cell* **1**, 6 (2002).
99. Kaschke, M., Russell, M. J. & Cole, W. J. [FeS/FeS2]. A redox system for the origin of life: some experiments on the pyrite-hypothesis. *Orig. Life Evol. Biosph.* **24**, 43–56 (1994).
100. Guynn, R. W., Gelberg, H. J. & Veech, R. L. Equilibrium constants of the malate dehydrogenase, citrate synthase, citrate lyase, and acetyl coenzyme A hydrolysis reactions under physiological conditions. *J. Biol. Chem.* **248**, 6957–6965 (1973).
101. Rosing, J. & Slater, E. C. The value of G degrees for the hydrolysis of ATP. *Biochim. Biophys. Acta* **267**, 275–290 (1972).
102. Kamerlin, S. C. L., Sharma, P. K., Prasad, R. B. & Warshel, A. Why nature really chose phosphate. *Q. Rev. Biophys.* **46**, 1–132 (2013).
103. Westheimer, F. Why nature chose phosphates. *Science* **235**, 1173–1178 (1987).
104. Goldford, J. E., Hartman, H., Marsland, R. & Segre, D. Boundary conditions for early life converge to an organo-sulfur metabolism. *bioRxiv* (2018).
105. Fraser, M. E. *et al.* A detailed structural description of escherichia coli succinyl-CoA synthetase. *J. Mol. Biol.* 285, 1633-1653 (1999).
106. Aoshima, M., Ishii, M. & Igarashi, Y. A novel enzyme, citryl-CoA lyase, catalysing the second step of the citrate cleavage reaction in Hydrogenobacter thermophilus TK-6: Citryl-CoA lyase in H. thermophilus. *Mol. Microbiol.* **52**, 763–770 (2004).
107. Pelley, J. W. Glycolysis and pyruvate oxidation. *Elsevier's Integrated Biochemistry* 47–53 (2007).
108. Armstrong, C. T., Anderson, J. L. R. & Denton, R. M. Studies on the regulation of the human E1 subunit of the 2-oxoglutarate dehydrogenase complex, including the identification of a novel calcium-binding site. *Biochem. J.* **459**, 369–381 (2014).
109. Soukri, A. Role of the histidine 176 residue in glyceraldehyde-3-phosphate dehydrogenase as probed by site-directed mutagenesist. *Biochem.* **28**, 2586-2592 (1989).
110. Carbonell, P., Lecointre, G. & Faulon, J.-L. Origins of specificity and promiscuity in metabolic networks. *J. Biol. Chem.* **286**, 43994–44004 (2011).
111. Hartman, H. Speculations on the origin and evolution of metabolism. *J. Mol. Evol.* **4**, 359–370 (1975).
112. Gahan, L. R. *et al.* Metal ion promoted hydration of pendant alkenes and its possible relationship to aconitase. *J. Am. Chem. Soc.* **107**, 6231–6242 (1985).
113. Rozelle, L. T. & Alberty, R. A. Kinetics of the acid catalysis of the hydration of fumaric acid to malic acid. *J. Phys. Chem.* **61**, 1637–1640 (1957).
114. Olson, M. V. & Taube, Henry. Hydration and isomerization of coordinated maleate. *J. Am. Chem. Soc.* **92**, 3236–3237 (1970).
115. Cody, G. D. Primordial carbonylated iron-sulfur compounds and the synthesis of pyruvate. *Science* **289**, 1337–1340 (2000).
116. Pokhodenko, V. D., Kosheehko, V. G., Titov, V. E. & Lopushanskaja, V. A. A convenient electrochemical synthesis of α-oxoacids. *Tetrahedron Lett.* **38**, 3277-3278 (1995).
117. Cody, G. D. *et al.* Geochemical roots of autotrophic carbon fixation: hydrothermal experiments in the system citric acid, H_2O-(±FeS)−(±NiS). *Geochim. Cosmochim. Acta* **65**, 3557–3576 (2001).
118. Wang, W., Yang, B., Qu, Y., Liu, X. & Su, W. FeS/S/FeS_2 redox system and its oxidoreductase-like chemistry in the iron-sulfur world. *Astrobiology* **11**, 471–476 (2011).
119. Ross, D. S. The viability of a nonenzymatic deductive citric acid cycle – Kinetics and thermochemistry. *Orig. Life Evol. Biospheres* **37**, 61–65 (2007).

120.Bernàt, I. The distribution of iron in nature. *Iron Metabolism,* 9–13 (1983).
121.Mulkidjanian, A. Y. & Galperin, M. Y. On the origin of life in the Zinc world. 2. Validation of the hypothesis on the photosynthesizing zinc sulfide edifices as cradles of life on Earth. *Biol. Direct* **4**, 27 (2009).
122.Zerkle, A. L. Biogeochemical signatures through time as inferred from whole microbial genomes. *Am. J. Sci.* **305**, 467–502 (2005).
123.Lipshutz, B. H. *et al.* TPGS-750-M: A second-generation amphiphile for metal-catalyzed cross-couplings in water at room temperature. *J. Org. Chem.* **76**, 4379–4391 (2011).
124.Russell, M. J. & Hall, A. J. The emergence of life from iron monosulphide bubbles at a submarine hydrothermal redox and pH front. *J. Geol. Soc.* **154**, 377–402 (1997).
125.Ragsdale, S. W. & Pierce, E. Acetogenesis and the Wood–Ljungdahl pathway of CO_2 fixation. *Biochim. Biophys. Acta* **1784**, 1873–1898 (2008).
126.Huber, C. Activated acetic acid by carbon fixation on (Fe,Ni)S under primordial conditions. *Science* **276**, 245–247 (1997).
127.Takahashi, H. *et al.* CO_2 reduction using hydrothermal method for the selective formation of organic compounds. *J. Mater. Sci.* **41**, 1585–1589 (2006).
128.He, C., Tian, G., Liu, Z. & Feng, S. A mild hydrothermal route to fix carbon dioxide to simple carboxylic acids. *Org. Lett.* **12**, 649–651 (2010).
129.Liu, Y., Chen, S., Quan, X. & Yu, H. Efficient electrochemical reduction of carbon dioxide to acetate on nitrogen-doped nanodiamond. *J. Am. Chem. Soc.* **137**, 11631–11636 (2015).
130.Roldan, A. *et al.* Bio-inspired CO_2 conversion by iron sulfide catalysts under sustainable conditions. *Chem. Commun.* **51**, 7501–7504 (2015).
131.Moore, E. K., Jelen, B. I., Giovannelli, D., Raanan, H. & Falkowski, P. G. Metal availability and the expanding network of microbial metabolisms in the Archaean eon. *Nat. Geosci.* **10**, 629–636 (2017).
132.Wachtershauser, G. Before enzymes and templates: theory of surface metabolism. *Microbiol. Rev.* **52**, 33 (1988).
133.Hori, Y., Kikuchi, K. & Suzuki, S. Production of CO and CH_4 in electrochemical reduction of CO_2 at metal electrodes in aqueous hydrogencarbonate solution. *Chem. Lett.* **14**, 1695–1698 (1985).
134.Mistry, H. *et al.* Highly selective plasma-activated copper catalysts for carbon dioxide reduction to ethylene. *Nat. Commun.* **7**, 12123 (2016).
135.Hori, Y., Murata, A. & Takahashi, R. Formation of hydrocarbons in the electrochemical reduction of carbon dioxide at a copper electrode in aqueous solution. *J. Chem. Soc. Faraday Trans. 1* **85**, 2309-2326 (1989).
136.Kuhl, K. P., Cave, E. R., Abram, D. N. & Jaramillo, T. F. New insights into the electrochemical reduction of carbon dioxide on metallic copper surfaces. *Energy Environ. Sci.* **5**, 7050 (2012).
137.Yang, X., Fugate, E. A., Mueanngern, Y. & Baker, L. R. Photoelectrochemical CO_2 reduction to acetate on iron–copper oxide catalysts. *ACS Catal.* **7**, 177–180 (2017).
138.Genovese, C. *et al.* Operando spectroscopy study of the carbon dioxide electro-reduction by iron species on nitrogen-doped carbon. *Nat. Commun.* **9**, (2018).
139.Sawyer, D. T. & Interrante, L. V. Electrochemistry of dissolved gases. *J. Electroanal. Chem.* **2**, 310–327 (1961).
140.Preiner, M. *et al.* A hydrogen dependent geochemical analogue of primordial carbon and energy metabolism. *bioRxiv* (2019).
141.White, L. M., Bhartia, R., Stucky, G. D., Kanik, I. & Russell, M. J. Mackinawite and greigite in ancient alkaline hydrothermal chimneys: Identifying potential key catalysts for emergent life. *Earth Planet. Sci. Lett.* **430**, 105–114 (2015).
142.Mcenaney, B. & Smith, D. C. The reductive dissolution of γ-FeOOH in corrosion scales formed on cast iron in near-neutral water. *Corros. Sci.* **20**, 873-886 (1980).

143. Weber, A. L. Prebiotic formation of 'energy-rich' thioesters from glyceraldehyde and N-acetylcysteine. *Orig. Life Evol. Biosph.* **15**, 17–27 (1984).
144. Weber, A. L. Formation of pyrophosphate on hydroxyapatite with thioesters as condensing agents. *Biosystems* **15**, 183–189 (1982).
145. Keefe, A. D., Newton, G. L. & Miller, S. L. A possible prebiotic synthesis of pantetheine, a precursor to coenzyme A. *Nature* **373**, 683–685 (1995).
146. Liu, R. & Orgel, L. E. Oxidative acylation using thioacids. *Nature* **389**, 52–54 (1997).
147. Rong, G. *et al.* Formation of $C(sp^2)$–S bonds through decarboxylation of α-oxocarboxylic acids with disulfides or thiophenols. *RSC Adv.* **5**, 26461–26464 (2015).
148. Abenante, L. *et al.* Ultrasound-enhanced Ag-catalyzed decarboxylative coupling between α-keto acids and disulfides for the synthesis of thioesters. *Ultrason. Sonochem.* **49**, 41–46 (2018).
149. Rice, G., Yerabolu, J., Krishnamurthy, R. & Springsteen, G. The abiotic oxidation of organic acids to malonate. *Synlett* **28**, 98–102 (2016).
150. Lopalco, A. *et al.* Mechanism of decarboxylation of pyruvic acid in the presence of hydrogen peroxide. *J. Pharm. Sci.* **105**, 705–713 (2016).
151. Zhu, X., Shi, Y., Mao, H., Cheng, Y. & Zhu, C. Tetraethylammonium bromide-catalyzed oxidative thioesterification of aldehydes and alcohols. *Adv. Synth. Catal.* **355**, 3558–3562 (2013).
152. Zeng, J.-W. *et al.* Metal-free cross-coupling reaction of aldehydes with disulfides by using DTBP as an oxidant under solvent-free conditions. *Green Chem* **16**, 2644–2652 (2014).
153. Huang, Y.-T., Lu, S.-Y., Yi, C.-L. & Lee, C.-F. Iron-catalyzed synthesis of thioesters from thiols and aldehydes in water. *J. Org. Chem.* **79**, 4561–4568 (2014).
154. Yi, C.-L., Huang, Y.-T. & Lee, C.-F. Synthesis of thioesters through copper-catalyzed coupling of aldehydes with thiols in water. *Green Chem.* **15**, 2476 (2013).
155. Mandal, S., Bera, T., Dubey, G., Saha, J. & Laha, J. K. Uses of $K_2S_2O_8$ in metal-catalyzed and metal-free oxidative transformations. *ACS Catal.* **8**, 5085–5144 (2018).
156. Wacey, D., Kilburn, M. R., Saunders, M., Cliff, J. & Brasier, M. D. Microfossils of sulphur-metabolizing cells in 3.4-billion-year-old rocks of Western Australia. *Nat. Geosci.* **4**, 698–702 (2011).
157. Barrett, J., Fox, M. F. & Mansell, A. L. The photochemistry of aqueous sulfate oon. *J. Phys. Chem.* **69**, 2996–3000 (1965).
158. Karam, P. A. Inconstant sun: How solar evolution has affected cosmic and ultraviolet radiation exposure over the history of life on earth. *Health Phys.* **84**, 322–333 (2003).
159. Hartman, H. Photosynthesis and the origin of life. *Origins Life Evol. Biosphere* **28**, 515-521 (1998).
160. Blankenship, R. E. & Hartman, H. The origin and evolution of oxygenic photosynthesis. *Trends Biochem. Sci.* **23**, 94–97 (1998).
161. Benkelberg, H.-J. & Warneck, P. Photodecomposition of iron(III) hydroxo and sulfato complexes in aqueous solution: wavelength dependence of OH and SO4- quantum yields. *J. Phys. Chem.* **99**, 5214–5221 (1995).
162. David, F. & David, P. G. Photoredox chemistry of iron(III) chloride and iron(III) perchlorate in aqueous media. A comparative study. *J. Phys. Chem.* **80**, 579-583 (1976).
163. Plasson, R. Chemical reaction network. *Encyclopedia of Astrobiology,* 287–288 (2011).
164. Rimmer, P. B. & Shorttle, O. Origin of life's building blocks in carbon and nitrogen rich surface hydrothermal vents. *Life* **9** (2019).
165. Smart, K. F., Aggio, R. B. M., Van Houtte, J. R. & Villas-Bôas, S. G. Analytical platform for metabolome analysis of microbial cells using methyl chloroformate derivatization followed by gas chromatography–mass spectrometry. *Nat. Protoc.* **5**, 1709–1729 (2010).
166. Lu, Q. & Jiao, F. Electrochemical CO_2 reduction: Electrocatalyst, reaction mechanism, and process engineering. *Nano Energy* **29**, 439–456 (2016).

167.David R. Lide. *CRC Handbook of Chemistry and Physics*. (2007).
168.Goldford, J. E. & Segrè, D. Modern views of ancient metabolic networks. *Curr. Opin. Syst. Biol.* **8**, 117–124 (2018).
169.Keller, M. A., Turchyn, A. V. & Ralser, M. Non-enzymatic glycolysis and pentose phosphate pathway-like reactions in a plausible Archean ocean. *Mol. Syst. Biol.* **10**, 725–725 (2014).
170.Keller, M. A. *et al.* Conditional iron and pH-dependent activity of a non-enzymatic glycolysis and pentose phosphate pathway. *Sci. Adv.* **2**, e1501235 (2016).
171.Messner, C. B., Driscoll, P. C., Piedrafita, G., De Volder, M. F. L. & Ralser, M. Nonenzymatic gluconeogenesis-like formation of fructose 1,6-bisphosphate in ice. *Proc. Natl. Acad. Sci.* **114**, 7403–7407 (2017).
172.Keller, M. A., Piedrafita, G. & Ralser, M. The widespread role of non-enzymatic reactions in cellular metabolism. *Curr. Opin. Biotechnol.* **34**, 153–161 (2015).

Appendix – Oxidation project

I had the opportunity to work in collaboration with Dr. Mameri on complex clusters, I was in charge of testing the catalytic properties of different clusters, to a selective oxidation of benzyl alcohol by O_2. (DOI: 10.1039/C8DT04807J)

Synthesis of New Mn_{19} Analogues and their Structural, Electrochemical and Catalytic Properties

Elodie Chevallot-Beroux,[a†] Ayuk M. Ako,[b†] Wolfgang Schmitt,[b] Brendan Twamley,[b] Joseph Moran,[a] Corinne Boudon,[c] Laurent Ruhlmann[c] and Samir Mameri*[d]

We report the synthesis and structural characterisation of new Mn_{19} and $Mn_{18}M$ analogues, $[Mn^{III}_{12}Mn^{II}_{7}(\mu_4\text{-}O)_8(\mu_3\text{-}OCH_3)_2(\mu_3\text{-}Br)_6(HL^{Me})_{12}(MeOH)_6]Br_2$ (**2**) and $[Mn^{III}_{12}Mn^{II}_{6}Sr(\mu_4\text{-}O_8(\mu_3\text{-}Cl)_8(HL^{Me})_{12}(MeCN)_6]Cl_2$ cluster (**3**), where H_3L^{Me} is 2,6-bis(hydroxymethyl)-p-cresol. The electrochemistry of **2** and **3** have been investigated and their activity as catalysts in the oxidation of benzyl alcohol has been evaluated. Selective oxidation of benzyl alcohol to benzaldehyde by O_2 was achieved using 1 mol% of catalyst with conversions of 74 % (**2**) and 60 % (**3**) at 140 °C using TEMPO as a co-catalyst. No partial conversion of benzaldehyde to benzoic acid was observed. The results obtained revealed that different operative parameters - such as catalyst loading, temperature, time, solvent and the presence of molecular oxygen - played an important role in the selective oxidation of benzyl alcohol.

[a.] Laboratory of Chemical Catalysis, University of Strasbourg, ISIS UMR 7006, 8 allée Gaspard Monge, Strasbourg 67083, France.

[b.] School of Chemistry & CRANN, University of Dublin, Trinity College, Dublin 2, Ireland.

[c.] Laboratoire d'Electrochimie et de Chimie Physique du Corps Solide, Institut de Chimie, UMR CNRS 7177, Université de Strasbourg, 4 rue Blaise Pascal, CS 90032, Strasbourg 67081, France.

[d.] Dr. S. Mameri: IUT Robert Schuman, Département Chimie, 72 route du Rhin, BP 70028, Illkirch 67411, France. Tel: +33-695-981-651. E-mail: mameri@unistra.fr

† Both authors contributed equally to this work.

Electronic Supplementary Information (ESI) available: Experimental section, Single-crystal X-ray crystallographic measurements, X-ray powder diffraction, electrochemical studies, Chemical oxidation studies, Infrared spectral analysis, Mass spectrometry. See DOI: 10.1039/x0xx00000x

Introduction

Manganese-based coordination clusters continue to attract intense research interest because they serve as models for various metalloenzymes,[1] and sometimes show interesting magnetic properties.[2,3] For some time now, we have developed a variety of homo- and hetero-metallic Mn clusters using phosphonate ligands,[4-8] and the H_3L^R ligand system based on 2,6-bis(hydroxymethyl)-4-R-phenol (where R is the substituent at the 4-position).[9-14] Among others, we are particularly interested in the coordination chemistry of the H_3L^R ligand system because of the variable modes (μ_2 or μ_3) of coordination provided by this oxido-rich molecule that leads to the isolation of organic-inorganic hybrid architectures with multiple metal centers. To this end, we have successfully developed reproducible routes for the syntheses of homometallic Mn_{19}(R) (R = H, Me, I, F, OMe, SMe)[9-12] and/or heterobimetallic $Mn_{18}M$ (M = Cd, Sr, Dy, Lu, Y) aggregates[13,14] using this ligand system. The Mn_{19} and $Mn_{18}M$ systems represent a family of materials with attractive structural and magnetic properties which may open new gateways to coordination complexes exhibiting a broad range of physicochemical properties appropriate for developing applications in data storage,[15] catalysis,[16] piezoelectricity,[17] and superconductivity.[18] Experimental and theoretical studies have revealed that the achievement of the maximum possible ground spin state of S_T = 83/2 for the mixed-valence Mn_{19} system is insensitive to replacement of its eight μ_3-N_3 ligands of the original Mn_{19} aggregate $[Mn^{III}_{12}Mn^{II}_7(\mu_4\text{-}O)_8(\mu_3\text{-}N_3)_8(HL^{Me})_{12}(MeCN)_6]Cl_2$ (1) by μ_3-Cl, μ_3-Br, μ_3-OH or μ_3-OMe, substantiating that the ferromagnetic interactions are mediated mainly by the internal (μ_4-O) ligands. Indeed, ESI-MS studies have further demonstrated the robustness of the inorganic $\{Mn^{III}_{12}Mn^{II}_7(\mu_4\text{-}O)_8\}$ core in the Mn_{19} and $Mn_{18}Y$ species as these maintain their integrity even in relatively reactive solvents ($MeOH/H_2O$).[12] While structural studies on these systems have focused on the modification of peripheral organic ligands, the manipulation of the face-bridging ligands as well as the selective incorporation of heterometals in view of assessing their influence on the magnetic properties of the resulting compounds,[9-14] their potential as catalysts has not been explored, despite their structural (core robustness, labile apical ligands, ease of functionalization) and electronic (mixed-valence Mn) attributes. Manganese species have been shown to function as catalysts for

organic and water oxidations in the presence of a variety of oxidants,[19] and have also been used as electrocatalysts.[20,21]

A variety of catalytic methods have been developed to harness molecular oxygen for the partial oxidation of alcohols to aldehydes, or for their complete oxidation to yield carboxylic acids.[22] Along these lines, the partial oxidation of benzyl alcohol to benzaldehyde with molecular oxygen has been particularly well-studied, due to the role of the latter as a versatile intermediate in the pharmaceutical and agrochemical industries.[23-26] A great many factors such as catalyst, temperature, solvent and oxidant play an important role in the reaction.[27-33] Homometallic Mn and heterometallic Mn/M (M = Ce) complexes and many other metal-oxo complexes have also been widely used as oxidants in chemical transformations such as the partial dehydrogenation of primary alcohols into their corresponding aldehydes.[33-37] To this end, we have chosen the partial oxidation of benzyl alcohol as a model substrate to study the catalytic activity of new analogues of the structural robust Mn_{19} and $Mn_{18}Sr$ coordination clusters, namely, $[Mn^{III}_{12}Mn^{II}_{7}(\mu_4\text{-}O_8(\mu_3\text{-}OCH_3)_2(\mu_3\text{-}Br)_6(HL^{Me})_{12}(MeOH)_6]Br_2$ (**2**) and $[Mn^{III}_{12}Mn^{II}_{6}Sr(\mu_4\text{-}O_8(\mu_3\text{-}Cl)_8(HL^{Me})_{12}(MeCN)_6]Cl_2$ (**3**). Compounds **2** and **3** are mixed-valent, comprising multiple Mn^{II}/Mn^{III} centres and thus have the ability to transfer (multiple) electrons. Moreover, the core features labile solvent molecules that may facilitate the coordination of incoming substrates. The electrochemical properties of **2** and **3** have been investigated, and their catalytic activity in the oxidation of benzyl alcohol has been evaluated, to test the potential of these compounds in molecular catalysis.

Experimental

Reagents and analytical methods

All chemicals and solvents were of reagent grade and purchased from Sigma-Aldrich and used without further purification. Infrared spectra were recorded on a PerkinElmer Spectrum One FT-IR spectrometer using either a universal ATR sampling accessory or a diffuse reflectance sampling accessory. Data were collected and processed using Spectrum v5.0.1 (2002 PerkinElmer Instrument LLC) software. The scan rate was 16 scans per minute with a resolution of 4 scans in the range 4000-500 cm ^{1}(ATR measurements were performed on an ATR IRAffinity-1 instrument (Shimadzu Scientific Instruments). The analyzed samples were

prepared by deposition of powder or crystals directly onto the sample plate surface). The standard abbreviations were used to describe the intensities: s, strong; m, medium; w, weak; br, broad. Elemental analyses (CHN) were performed at the School of Chemistry and Chemical Biology, University College Dublin (Ireland), using Exeter Analytical CE 440 elemental analyser. GC-MS analysis was performed on a GC System 7820A (G4320) connected to an MSD block 5977E (G7036A), using Agilent High Resolution Gas Chromatography Column: PN 19091S – 433UI, HP – 5MS UI, 28 m×0.250 mm, 0.25 Micron, SN USD 489634H. All samples were prepared in ethyl acetate (200 µL sample volume). The analysis was carried out on a splitless 1 µL injection volume with an injection port temperature 250 °C. Column oven temperature program was as follows: 60 °C for 1 min, ramped at 30 °C/min to 310 °C with 3 min hold, with a total running time of 12.33 min. The mass spectrometer was turned on after 2 min and was operated at the electron ionization mode with quadrupole temperature of 150 °C. Data acquisition was performed in the full-scan mode (50-500). Hydrogen (99.999 % purity) was used as carrier gas at a constant flow rate of 1.5 mL/min.

Synthesis

Synthesis of $[Mn^{III}_{12}Mn^{II}_{7}(\mu_4\text{-}O)_8(\mu_3\text{-}OCH_3)_2(\mu_3\text{-}Br)_6(HL^{Me})_{12}(MeOH)_6]Br_2$ (2)

$MnCl_2{\cdot}4H_2O$ (0.2 g, 1 mmol, 1.0 equiv), Et_3N (0.1 g, 1 mmol, 1.0 equiv) and 2,6-bis(hydroxymethyl)-4-methylphenol (0.17 g, 1 mmol, 1.0 equiv) were respectively added, under stirring, to a MeCN/MeOH solution (25 mL/5 mL). The resulting slurry was stirred for 1 h at RT, before being heated at reflux for 2 h, to afford a dark brown solution, which was cooled and filtered. Dark brown crystals of **2** were obtained after 48 h slow evaporation at RT. The crystals were filtered, washed and dried. Yield: 30 % (based on Mn). Elemental analysis (%) calc. for $C_{137}H_{184}Br_8Mn_{19}N_{10}O_{53}$: C 36.55; H 4.12; N 3.11; found: C 36.62; H 4.23; N 3.25. Selected IR data (KBr pellet, cm ^{1}) 600 (s), 800 (s), 1050 (m), 1100 (m), 1211 (s), 1409 (s), 1610 (m), 2800 (w), 3300 (w,br).

Synthesis of $[Mn^{III}_{12}Mn^{II}_{6}Sr(\mu_4\text{-}O_8(\mu_3\text{-}Cl)_8(HL^{Me})_{12}(MeCN)_6]Cl_2$ (3)

A slurry of $MnCl_2{\cdot}4H_2O$ (0.2 g, 1 mmol, 1.0 equiv), Et_3N (0.1 g, 2 mmol, 2.0 equiv), 2,6-bis(hydroxymethyl)-4-methylphenol (0.17 g, 1 mmol, 1.0 equiv) in a solvent mixture of MeCN and MeOH (25 mL/5 mL) was stirred for 30 min at RT, and $Sr(NO_3)_2$ (0.11 g, 0.5 mmol, 0.5 equiv) was added. The resulting mixture was further stirred for an additional 1 h, then heated at reflux for 2 h. The dark brown mixture was cooled and filtered. After a 24 h slow evaporation at RT, dark brown crystals of **3** suitable for X-ray diffraction analysis were obtained. Yield: 40 % (based on Mn). Elemental analysis (%) calc. for $C_{127}H_{154}Cl_8Mn_{18}N_6O_{51}Sr$ (3): C 38.71; H 3.94; N 2.13; found: C 38.62; H 3.63; N 2.25. FT-IR (cm^{-1}): 610 (s), 740 (s), 990 (s), 1050 (s), 1248 (s), 1495 (s), 1600 (m), 2812(w), 3300(s,br).

Single-crystal X-ray crystallographic measurements

X-ray structural analyses for crystals of **2** (TCD304) and **3** (TCD 716) were performed on at 100K on a Bruker APEX DUO CCD and Bruker D8 Quest ECO diffractometer respectively (Mo-K_α **λ** = 0.71073 Å). The maximum resolution for data collection was 0.77 Å with data collected using **ω** and **φ** scans for **2** and 0.80 Å using **ω** scans only for **3**.

The data were reduced and processed using the Bruker APEX suite of programs.[38] Multi-scan absorption corrections were applied using SADABS.[39] Using Olex2,[40] the structure was solved with the XT[41] structure solution program using Intrinsic Phasing and refined with the XL[42] refinement package using Least Squares minimisation. All non-hydrogen atoms were refined anisotropically. Hydrogen atoms were placed in calculated positions and refined with a riding model, with isotropic displacement parameters equal to either 1.2 or 1.5 times the isotropic equivalent of their carrier atoms.

The data were solved in the monoclinic space group $P2_1/n$ (**2**) trigonal space group $R\bar{3}$ (**3**). In the structure of **2**, uncoordinated MeOH was refined with restraints (DFIX, ISOR) and modelled as half occupied. Hydroxide hydrogen atoms on all MeOH (coordinated and uncoordinated) as well as ligand OH moieties were located and refined with restraints (DFIX). Two acetonitrile solvates were also modelled with restraints (ISOR). In **3**, all MeOH molecules were modelled as half occupied with restraints (DFIX, ISOR). One MeOH (C32-O33) is on the three fold axis and the hydrogens are modelled with an occupancy of 0.16667. Large voids

are present in **3** of ca. 227 Å^3, with a total of 689Å^3 per unit cell. SQUEEZE[43] was used to verify that the void volume does not contain any electron density.

Crystal data and details of data collection and refinement of compounds **2** and **3** are summarized in Table S1. Crystallographic data, CCDC 1882361-1882362, can be obtained free of charge from the Cambridge Crystallographic Data Centre via www.ccdc.cam.ac.uk/data_request/cif.

Electrochemistry

Electrochemical measurements were carried out in DMF containing 0.1 M Bu_4NPF_6 in a classical three-electrode cell by cyclic voltammetry (CV) and rotating-disk voltammetry (RDV). The working electrode was a glassy carbon disk (GC, 3 mm in diameter), the auxiliary electrode a Pt wire, and the pseudo reference electrode a Pt wire. The cell was connected to an Autolab PGST, AT30 potentiostat (Eco Chemie, Holland) driven by a GPSE software running on a personal computer. All potentials are given vs. Fc^+/Fc used as internal reference and are uncorrected from ohmic drop.

Chemical Oxidation

Optimization of oxidation of benzyl alcohol to benzaldehyde

All reactions were carried out in 1 mL glass vial under oxygen atmosphere, unless otherwise noted.

In a typical experiment: To a 1 mL glass vial containing a Teflon-coated magnetic stir bar was added cluster catalyst (2.3 mg, 0.60 μmol, 1.0 mol%), TEMPO (2.1 mg, 0.013 mmol, 22 mol%), benzyl alcohol (6.4 μL, 0.060 mmol, 1.0 equiv), followed by the addition of DMF (300 μL). The contents of the vial were flushed with oxygen for ca. 2 minutes. The vial was then quickly sealed, and the reaction mixture magnetically stirred for 24 h in sand bath that was maintained at an internal temperature of 140 °C using an electronic thermocouple. The reaction vial was then removed from the sand bath and allowed to cool to RT. 500 μL of ethyl acetate was added to the mixture, and the solution was centrifuged until separation of the solid catalyst was achieved. A sample for GC-MS analysis was prepared by removing 10 μL of the liquid phase from the reaction, followed by dilution with ethyl acetate (190 μL).

Results and Discussion

Previously, we have demonstrated that depending on the reactants, the face-bridging ligands of the Mn_{19} system can either be N_3, Br, Cl, OMe or OH.[9-14] Herein, refluxing a mixture of H_3L^{Me} and $MnBr_2{\cdot}4H_2O$ in the presence of Et_3N in MeCN/MeOH (5/1, v/v) afforded $[Mn^{III}_{12}Mn^{II}_7(\mu_4\text{-}O_8(\mu_3\text{-}OCH_3)_2(\mu_3\text{-}Br)_6(HL^{Me})_{12}(MeOH)_6]Br_2$ (**2**). When a similar reaction was carried out with $MnCl_2{\cdot}4H_2O$ as source of Mn and in the additional presence of $Sr(NO_3)_2$, the compound $[Mn^{III}_{12}Mn^{II}_6Sr(\mu_4\text{-}O_8(\mu_3\text{-}Cl)_8(HL^{Me})_{12}(MeCN)_6]Cl_2$ (**3**) was obtained. Single crystal X-ray analyses revealed that the compounds crystallize in the monoclinic $P2_1/n$ (**2**) and the trigonal R-3 (**3**) space groups, with two and three molecules, respectively in the unit cell. The results of the X-ray structural analysis are summarized in Table S1. The crystal structure of **2** and **3** are given in Fig. 1.

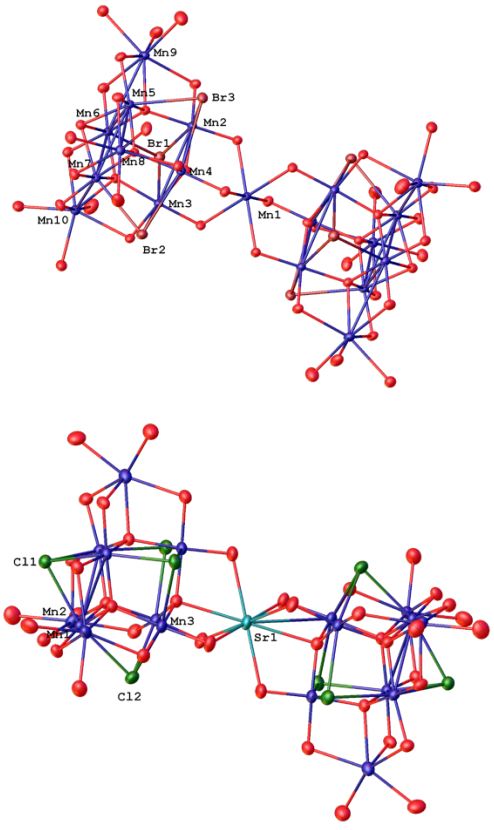

Fig. 1. Symmetry unique metal/halide labelled core only diagrams of 2 (upper) and 3 (lower). All solvents, hydrogen, carbon and nitrogen atoms omitted for clarity. A full diagram of each molecule is given in the SI. Atomic displacement shown at 50% probability.

The core of **2** and **3** are isostructural to the topology of the previously reported $\{Mn_{19}\}$ and $\{Mn_{18}M\}$ complexes[9-14] and can be considered as consisting of two supertetrahedral $\{Mn^{III}_6Mn^{II}_4\}$ units sharing a common Mn^{II} vertex (**2**) or two supertetrahedral $\{Mn^{III}_6Mn^{II}_3Sr\}$ units sharing a common Sr vertex (**3**). Compounds **2** and **3** slightly differ from the previously reported analogues. For instance, compound **2** differs from the original Mn_{19} aggregate (**1**)[9], as well as the analogous compound $[Mn^{III}_{12}Mn^{II}_7(\mu_4\text{-}O)_8(HL^{Me})_{12}(\mu_3\text{-}Br)_7(\mu_3\text{-}OH)(MeCN)_6]Br_2$ (**4**)[12], in terms of their μ_3-face-bridging ligands. In **2**, the two face-bridging ligands on the molecular threefold axis are both (μ_3-OMe) unlike in compound **1** and **4** where these are made up of μ_3-N_3 (**1**) or μ_3-Br and μ_3-OH (**4**) ligands, respectively. Compound **2** also differs from **4** in the composition of the six terminal ligands on the outer Mn^{II} vertices of the supertetrahedron. In **2**, these are MeOH while in **4** these are exclusively MeCN as in compound **1**. It should be pointed out here that while similar solvent mixtures (MeCN/MeOH, 5/1, vol/vol) were employed for these reactions, the reason for the observed differences in structural composition is unclear. Moreover, all attempts to completely substitute the face-bridging ligands with μ_3-Br by using excess bromide source were unsuccessful. We have also previously reported a Mn_{19} aggregate, $[Mn^{III}_{12}Mn^{II}_7(\mu_4\text{-}O)_8(HL^{Me})_{12}(\mu_3\text{-}Cl)_6(\mu_3\text{-}OMe)_2(MeOH)_5(MeCN)]Cl_2$ (**5**),[12] where the two face-bridging ligands on the molecular threefold axis are both μ_3-OMe as observed in **2**. In **5**, six of the face-bridging ligands are chlorides, hence compound **2** is a new analogue of the Mn_{19} system.

Electrochemistry

Investigations of the species were carried out by cyclic voltammetry and rotating disk voltammetry (RDV) in DMF + 0.1 M Bu_4NPF_6. The electrochemical data for compound **2** and **3** are shown in Table 1.

Table 1. Electrochemical data for 2 and 3 in DMF (+ 0.1 M Bu_4NPF_6 against Fc^+/Fc).

Species	CV			RDV
	$E°$ [a]	ΔEp [b]	Ep [c]	$E_{1/2}$ [d]
	$V/_{Fc+/Fc}$	mV	$V/_{Fc+/Fc}$	$V/_{Fc+/Fc}$
Mn_{19} (2)			0.42	0.33
			-1.29	[d]
			-1.89	[d]
	-2.25	90		
$Mn_{18}Sr$ (3)			0.25	0.29
			-1.20	-1.20
			-1.75	-1.75
			-2.10	-2.16

[a] $E° = (E_{pc} + E_{pa})/2$, where E_{pc} and E_{pa} correspond to the cathodic and anodic peak potentials, respectively.

[b] $\Delta E_p = E_{pa} - E_{pc}$.

[c] E_p = irreversible peak potential.

[d] Due to important adsorption at the electrode, the RDV in the cathodic domain is ill defined and is not exploitable.

In oxidation, cyclic voltammetry (CV) of **2** showed two successive irreversible peaks measured at -0.12 V and 0.42 V vs. Fc^+/Fc measured without Fc after the reduction of Mn_{19} (**2**) (Fig. 2, red curve with initial scanning direction to negative potential, explicitly reduction followed by the oxidation) while RDV presented only one wave at 0.33 V vs. Fc^+/Fc (Fig. S3, left). It should be pointed out that, the first peak detected from CV at -0.12 V was not measured in the case of the initial scanning direction to positive potential (Fig. 2, black curve), namely oxidation followed by the reduction. The potential of the only irreversible peak observed was measured at 0.27 V (measured in the absence of Fc), a value close to the potential obtained from RDV (Fig. S3). Thus, the first peak may be due to the re-oxidation of the reduced compound **2**, which might evolve after reduction to give a different oxidation potential for the Mn(III/II) redox couple. Alternatively, the first signal might be due to adsorption of the reduced compound **2** at the GC electrode, which renders the Mn atoms easier to oxidize. Because of such adsorption the coulometry is difficult to be done and give important variability of the value for the number of electrons exchanged measured. The wave from CV at 0.27 V corresponds to the irreversible oxidation of the seven Mn(II) atoms to Mn(III) according the molecular structure of $[Mn^{III}_{12}Mn^{II}_7(\mu_4\text{-}O_8(\mu_3\text{-}OCH_3)_2(\mu_3\text{-}Br)_6(HL^{Me})_{12}(MeOH)_6]Br_2$

(**2**). Controlled potential coulometry under continuous argon bubbling and stirring at applied potential of 0.4 V has been conducted several times and consumes between 6.8 to 7.4 electrons per molecule. Indeed, we have done two exhaustive oxidations giving 6.8, and 7.4 electrons exchanged. The fluctuation of the number of electrons exchanged is probably due to the adsorption of compound (**2**) at the electrode which strongly alter the measurements.

For the $Mn_{18}Sr$ cluster (**3**), in oxidation, cyclic voltammogram (CV) showed only one irreversible peaks at 0.25 V vs. Fc^+/Fc. RDV presented also only one wave at 0.29 V vs. Fc^+/Fc (Fig. S4). The first peak detected might be due to the oxidation of the six Mn(II) atoms to Mn(III). Such behavior is similar to **2** compound except that the six Mn(II) are easier to be oxidized (0.25 V versus 0.43 V).

In the cathodic domain, CV showed three successive reductions. The first two reductions are irreversible and ill-defined at -1.29 V and -1.89 V, while the last reduction was reversible at -2.25 V (ΔE_p = 90 mV) vs. Fc^+/Fc peaks. Due to significant adsorption at the electrode, the RDV in the cathodic domain is ill-defined and is not exploitable (Fig. S3). Thus, for compound **3**, the presence of the Sr atom does not affect strongly the redox behavior in reduction. In oxidation, the oxidation of the Mn(II) are 180 mV easier to be oxidized than for **2**. The redox behavior in reduction is also similar to 2 showing three successive steps but 90, 140 and 150 mV easier to be reduced than for **2**, respectively.

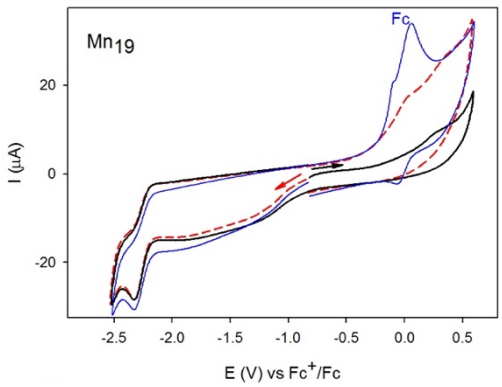

Fig. 2. Cyclic voltammetry of Mn_{19} (2) at a scan rate of 0.1 Vs^{-1} in DMF 0.1 M $TBAPF_6$ with Fc (blue curve) and without Fc (black and red curves), c = 1 mM. The arrow as well as the color of the curves (black or red) indicate the beginning and sweep direction of the voltammetric scan. Black curve: initial scanning direction to negative potential [reduction of Mn_{19} (**2**)] followed by a reverse sweep back in order to join the oxidation wave. Red curve: initial scanning direction to positive potential [oxidation of Mn_{19} (**2**)].

Catalytic Oxidation

The ability of compounds **2** and **3** to act as catalysts for the partial chemical oxidation of benzyl alcohol to benzaldehyde was investigated. In analogy with previous catalytic oxidations using manganese clusters,[33] our initial investigations employed **2** (typically 1 mol%) with benzyl alcohol (1 equiv) and TEMPO (22 mol%) in DMF under an oxygen atmosphere (1 atm). GC-MS analysis of reactions carried out in a variety of solvents after 18 h at 100 °C indeed confirmed that DMF was the most efficient, likely due to the high solubility of the catalyst in that solvent (see Table S2). After optimization of temperature and time, it was found that after 24 h at 140 °C, 74% conversion to benzaldehyde was achieved without observable accompanying over-oxidation to benzoic acid (Table 2, entry 1). Further optimisation and control experiments were carried out to better understand the reaction. Catalyst **2** was indeed required (entry 2). Lower reaction temperatures were not suitable (entries 3-4). A catalyst loading of 1 mol% was found to be optimal, with higher or lower loadings leading to poorer yields (entries 5-7). Leaving out TEMPO does not completely stop the reaction but leads to lower yields (entry 8). In the presence of TEMPO, using air instead of O_2 or even conducting the reaction under an Ar atmosphere still does not completely inhibit the reaction (entries 9-10), showing that the ultimate source of oxidant is flexible. However, an oxidant is nonetheless required, since omitting TEMPO and using air instead of O_2 at the same time leads to a drastic drop in yield (entry 11).

The oxidation of benzyl alcohol was also evaluated with $Mn_{18}Sr$ (**3**) under the same conditions (Table 3). The $Mn_{18}Sr$ catalyst gives slightly lower yields compared to Mn_{19} and overoxidation is again not observed. No reaction occurs in the absence of **3** (entry 2). One notable observation is that the $Mn_{18}Sr$ catalyst works best in the absence of TEMPO (entry 3), in departure from oxidation reactions catalyzed by $CeMn_6$ clusters previously reported by Christou and co-workers.[33] In that prior report, the Ce atom was found to be the active component in the catalytic oxidation, and served to oxidize TEMPO, which in turn oxidizes the alcohol. The presence of TEMPO was thus found to be essential to catalytic oxidation. In the present work, the observation that the $Mn_{18}Sr$ catalyst **3** is optimal in the absence of TEMPO indicates a change in mechanism, such that the catalyst itself is capable of oxidizing

the alcohol with catalytic turnover. As expected, the yield drastically decreases if TEMPO, O_2 or both are removed (entries 4-6).

Table 2. Influence of conditions on the chemical oxidation of benzyl alcohol catalyzed by Mn_{19} **2**.

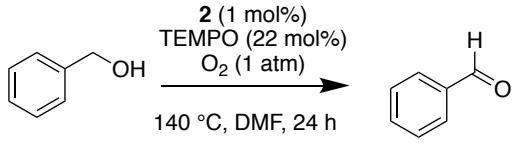

Entry	Deviation from standard conditions[a,b]	Alcohol (%)	Aldehyde (%)
1	None	26	74
2	No **2**	99	1
3	120 °C instead of 140 °C	70	30
4	100 °C instead of 140 °C	95	5
5[c]	5 mol% 2 instead of 1% mol%	80	20
6[c]	10 mol% 2 instead of 1 mol%	100	0
7[c]	0.1 mol% 2 instead of 1 mol%	79	21
8[c]	No TEMPO	48	52
9	Air instead of O_2	53	47
10	Ar instead of O_2	54	46
11[c]	No TEMPO and air instead of O_2	89	11

[a] Reaction conditions: oxygen (1 atm), benzyl alcohol (0.06 mmol), TEMPO (22 mol%), Mn_{19} **2** (1 mol%) in 1 mL of DMF, at 140 °C; 48 h. [b] PhCHO was the only product; no $PhCO_2H$ acid was detected by GC-MS. [c] Reaction run for 48 h.

Table 3. Influence of various conditions in the chemical oxidation of benzyl alcohol by $Mn_{18}Sr$ **3**.

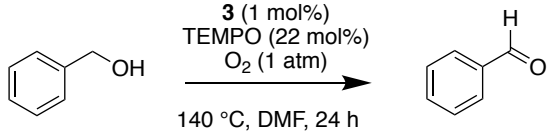

Entry	Deviation from standard conditions[a]	Alcohol (%)	Aldehyde (%)[b]
1	None	54	46
2	No **3**	99	1
3	No TEMPO	35	65
4	Air instead of O_2	49	51
5	Ar instead of O_2	55	45
6	No TEMPO and air instead of O_2	65	35

[a] Reaction condition: oxygen (1 atm), benzyl alcohol (0.06 mmol), TEMPO (22 mol%), $Mn_{18}Sr$ 3 (1 mol%) in 1 mL of DMF, at 140 °C; 24 h. [b]PhCHO was the only product; no $PhCO_2H$ acid was detected by GC-MS.

To determine whether the catalysts employed in the present study are stable under the reaction conditions, the solid catalyst was analysed by IR spectroscopy. The IR spectra of **2** and **3** before and after the reaction show some discrepancy (Fig. S9, new bands appearing at 1300-1600 cm [1]), suggesting that the catalyst might have undergone some modification under the catalytic conditions. This is expected as we previously observed that the system undergoes ligand exchange and/or scrambling under certain conditions.[12]

Conclusions

We have reported new analogues of the {Mn_{19}} and {$Mn_{18}Sr$} aggregates, compounds **2** and **3** and demonstrated their catalytic activity in the selective oxidation of benzyl alcohol to benzaldehyde in up to 74 and 65 % yields, respectively. These values are comparable to those obtained by Christou et al for similar cluster compounds.[33] The attractiveness of the {Mn_{19}} system is that it can be further tuned to access a variety of functionalized Mn_{19}(R) aggregates, where the interplay of the electronic contribution of the substituent R can be investigated, where R = the substituent at the 4-positon of the H_3L^R ligand system). Moreover {$Mn_{18}M$} (where M is a heterometals), are readily accessible and could be suitable candidates to explore the influence of heterometals on the redox-potential of the system and hence catalysis, even in the absence of organic co-catalysts. Linking these species to form one-, two- and three-dimensional extended arrays and evaluation of these compounds towards photo-catalytic water splitting (oxygen evolution) is also envisaged.

Acknowledgements

This project has received funding from the European Research Council (ERC) under the European Union's Horizon 2020 research and innovation programme (grants agreements n° 639170 and n°647719), from ANR LabEx "Chemistry of Complex Systems", and from Science Foundation Ireland (13/IA/1896).

Conflicts of interest

There are no conflicts to declare.

Notes and references

1 C.S. Mullins, V.L. Pecoraro, Coord. Chem. Rev., 2008, 252, 416.
2 F. Troiani, M. Affronte, Chem. Soc. Rev., 2011, 40, 3119.
3 G. Aromí, D. Aguila, P. Gamez, F. Luis, O. Roubeau, Chem. Soc. Rev., 2012, 41, 537.
4 L. Zhang, R. Clérac, C.I. Onet, M. Venkatesan, P. Heijboer, W. Schmitt, Chem. Eur. J., 2012, 18, 13984.
5 L. Zhang, R. Clérac, P. Heijboer, W. Schmitt, Angew. Chem., Int. Ed., 2012, 51, 3007.
6 L. Zhang, B. Marzec, R. Clérac, Y. Chen, H. Zhang, W. Schmitt, Chem. Commun., 2013, 49, 66.
7 T.O. Chimamkpam, R. Clérac, D. Mitcov, B. Twamley, M. Venkatesan, W. Schmitt, Dalton Trans., 2016, 45, 1349.
8 L. Zhang, T. Chimamkpam, C.I. Onet, N. Zhu, R. Clérac, W. Schmitt, Dalton Trans., 2016, 45, 17705.
9 A.M. Ako, I.J. Hewitt, V. Mereacre, R. Clérac, W. Wernsdorfer, C.E. Anson, A.K. Powell, Angew. Chem., Int. Ed., 2006, 45, 4926.
10 A.M. Ako, M.S. Alam, S. Mameri, Y. Lan, M. Hibert, M. Stocker, P. Müller, C.E. Anson, A.K. Powell, Eur. J. Inorg. Chem., 2012, 26, 4131.
11 S. Mameri, A.M. Ako, F. Yesil, M. Hibert, Y. Lan, C.E. Anson, A.K. Powell, Eur. J. Inorg.Chem., 2014, 26, 4326.
12 A.M. Ako, Y. Lan, O. Hampe, E. Cremades, E. Ruiz, C.E. Anson, A.K. Powell, Chem. Commun., 2014, 50, 5847.
13 A.M. Ako, V. Mereacre, R. Clérac, I.J. Hewitt, W. Wernsdorfer, C.E. Anson, A.K Powell, Chem. Commun., 2009, 544.
14 A.M. Ako, B. Burger, Y. Lan, V. Mereacre, R. Clérac, G. Buth, S. Gómez-Coca, E. Ruiz, C.E. Anson, A.K. Powell, Inorg. Chem., 2013, 52, 5764.
15 L. Bogani, W. Wernsdorfer, Nat. Mater., 2008, 7, 179.
16 W. Zhou, X. Zhao, Y. Wang, J. Zhang, Appl. Catal., A, 2004, 260, 19.
17 B. Noheda, Curr. Opin. Solid State Mater. Sci., 2002, 6, 27.
18 S. Yonezawa, Y. Maeno, Phys. Rev. B, 2005, 72, 180504(R).
19 T.G. Carrell, S. Cohen, G.C. Dismukes, J. Mol. Catal. A: Chem., 2002, 187, 3.
20 R. Tagore, R.H. Crabtree, G.W Brudvig, Inorg. Chem., 2008, 47, 1815.
21 M.M. Najafpour, T. Ehrenberg, M. Wiechen, P. Kurz, Angew. Chem., Int. Ed., 2010, 49, 2233.
22 Z. Shi, C. Zhang, C. Tanga, N. Jiao, Chem. Soc. Rev., 2012, 41, 3381.
23 G. Zhan, Y. Hong, V.T. Mbah, J. Huang, A.-R. Ibrahim, M. Du, Q. Li, Appl. Catal., A, 2012, 439, 179.
24 B. Wang, M. Lin, T.P. Ang, J. Chang, Y. Yang, A. Borgna, Catal. Commun., 2012, 25, 96.
25 J. Zhu, J.L. Figueiredo, J.L. Faria, Catal. Commun., 2008, 9, 2395.
26 C. Zhou, Z. Guo, Y. Dai, X. Jia, H. Yu, Y. Yang, Appl. Catal., B, 2016, 181, 118.
27 C.Y. Ma, J. Cheng, H.L. Wang, Q. Hu, H. Tian, C. He, Z.P. Hao, Catal. Today, 2010, 158, 246.
28 Q. Tang, X. Gong, P. Zhao, Y. Chen, Y. Yang, Appl. Catal., A, 2010, 389, 101.
29 M. Yang, Q. Ling, R. Rao, H. Yang, Q. Zhang, H. Liu, A. Zhang, J. Mol. Catal. A: Chem., 2013, 380, 61.
30 M. Ilyas, M. Saeed, Int. J. Chem. React. Eng., 2010, 8, A77.
31 J. Zhu, K. Kailasam, A. Fischer, A. Thomas, ACS Catal., 2011, 1, 342.
32 L. Yao, L. Zhang, Y. Liu, L. Tian, J. Xu, T. Liu, D. Liud, C. Wang, **CrystEngComm**, 2016,**18**, 8887.
33 G. Maayan, G. Christou, Inorg. Chem. 2011, 50, 7015.
34 D. Sengupta, R. Bhattacharjee, R. Pramanick, S.P. Rath, N.S. Chowdhury, A. Datta, S. Goswami, Inorg. Chem., 2016, 55, 9602.
35 A. S. Borovik, Chem. Soc. Rev., 2011, 40, 1870.
36 G. Yin, Coord. Chem. Rev., 2010, 254, 1826.
37 K.P. Bryliakov, E.P. Talsi, Coord. Chem. Rev., 2014, 276, 73.
38 APEX-3 v. 2016.9-0, Bruker-AXS Inc., Madison, WI, 2016.
39 SADABS v. 2016/2, Bruker-AXS Inc., Madison, WI, 2016.
40 O.V. Dolomanov, L.J. Bourhis, R.J. Gildea, J.A.K. Howard, H.J. Puschmann, Appl. Cryst., 2009, 42, 339.
41 G.M. Sheldrick, Acta Cryst., 2015, A71, 3.
42 G.M. Sheldrick,. Acta Cryst., 2008, A64, 112.
43 A.L. Spek, J.Appl.Cryst., 2003, 36, 7.

Elodie CHEVALLOT-BEROUX

Non-enzymatic metabolic processes to understand the origin of life

Résumé

L'origine de la vie est l'un des plus grands mystères non résolus, sur lequel se sont penché de très nombreux scientifiques et philosophes. Aujourd'hui, deux hypothèses majeures se sont développées : la première porte sur la synthèse de molécules complexes (semblables à l'ARN), qui aurait permis par la suite l'apparition des différentes fonctions biologiques. La seconde porte sur le développement d'un métabolisme primitif, ensemble de réactions chimiques à partir de molécules très simples, qui aurait permis la naissance d'une première forme de vie sans enzymes. Ce travail de thèse supporte cette deuxième hypothèse, démontrant le possible développement de deux voies métaboliques, le cycle de Krebs inverse (ou rTCA) et la voie de Wood-Ljungdahl (ou AcCoA), considérés comme primitives et permettant la synthèse d'intermédiaires universelle pour la biochimie, dans un environnement prébiotique à partir de CO_2 et de métaux. De plus, une méthode permettant la synthèse de thioesters, intermédiaires supposés nécessaire à l'évolution du métabolisme, est présenté ainsi que son intégration dans un réseau réactionnel complexe semblable au métabolisme.

Mots clés : Chimie prébiotique, Métabolisme, Cycle de Krebs inverse (ou rTCA), Voie de Wood-Ljungdahl (ou AcCoA), Thioesters.

Abstract

The origin of life is one of the greatest unsolved mysteries, which has been studied by many scientists and philosophers. Today, two major hypotheses have been developed: the first concerns the synthesis of complex molecules (similar to RNA), which would have subsequently led to the appearance of the various biological functions. The second is the development of a primitive metabolism, a set of chemical reactions based on very simple molecules, which would have allowed the emergence of a first life form without enzymes. This thesis work supports this second hypothesis, demonstrating the possible development of two metabolic pathways, the reverse Krebs cycle (or rTCA) and the Wood-Ljungdahl pathway (or AcCoA), considered primitive and allowing the synthesis of universal intermediates for biochemistry, in a prebiotic environment from CO_2 and metals. In addition, a method for the synthesis of thioesters, intermediates presumed necessary for the evolution of metabolism, is presented as well as its integration into a complex reaction network similar to metabolism.

Keys words: Prebiotic chemistry, Metabolism, Reverse Krebs cycle (or rTCA), Wood-Ljungdahl pathway (or AcCoA), Thioesters.